Università degli Studi di Ferrara

DOTTORATO DI RICERCA IN SCIENZE DELL'INGEGNERIA

CURRICULUM MATEMATICA

COORDINATORE PROF. SSA EVELINA LAMMA

MODELING AND NUMERICAL METHODS FOR MULTISCALE HYPERBOLIC AND KINETIC EQUATIONS

DOTTORANDO
DOTT. ING. GIACOMO DIMARCO

TUTORE
PROF. LORENZO PARESCHI

XX° CICLO

ANNI 2005 - 2007

Alla mia famiglia e Federica

Ringraziamenti

Ringrazio innanzitutto il mio tutore di Dottorato, Prof. Lorenzo Pareschi, per avermi insegnato e motivato nel corso di questi anni, ma soprattutto per aver avuto fiducia in me. Grazie a lui ho avuto la possibilità di partecipare a conferenze e scuole, di conoscere e collaborare con membri della comunità scientifica internazionale, di trarre esperienza da altre realtà di ricerca in Europa e nel mondo e di imparare i rudimenti dell'analisi e della modellistica numerica. Mi ha lasciato libero di pensare e di esprimermi, guidandomi e corregendomi ogni volta che ve ne sia stata necessità.

Un ringraziamento particolare al Prof. Pierre Degond e al Dott. Luc Mieussens che mi hanno accolto al MIP di Tolosa nel loro gruppo di ricerca e con i quali ho avuto il piacere di discutere e collaborare. Grazie anche al Prof. Caflisch e al Dott. Richard Wang del dipartimento di matematica di UCLA che mi hanno dato la possibilità di lavorare con loro a progetti per me molto stimolanti, al Prof. Bruce Cohen e al Dott. Andris Dimits del Livermore National Laboratory. Ognuno di loro ha fatto tutto il possibile per farmi sentire e lavorare come a casa.

Grazie ai miei colleghi di dottorato, ai professori del dipartimento di matematica dell' Università di Ferrara e a tutte le persone con cui ho avuto il piacere di interagire in questi tre anni scientificamente e personalmente. Grazie a Marcello, Elisa, Alessia, Marco per aver condiviso con me lo studio borsisti a cui auguro sinceramente di trovare presto una posizione permanente e appagante.

Grazie a tutti i miei amici, alcuni vicini, molti ormai lontani che ho avuto il piacere di incontrare, conoscere e frequentare in questi trent'anni. Infine, vorrei davvero ringraziare la mia famiglia, i miei genitori, mia sorella e Federica per il loro costante sostegno, senza il quale ogni cosa sarebbe stata impossibile.

Acknowledgments

First of all, I wish to thank my PhD supervisor, Prof. Lorenzo Pareschi, who taught and motivated me during these years and above all because he trusted me. Thanks to him I could attend schools and conferences, meet and work with important members of the international scientific community, gain experience from other research centers in Europe and in the world and finally to learn the basics of numerical analysis and modeling. He leaved me free to think and follow my ideas, driving and rectifying every time I need it.

A particular thanks to Prof. Pierre Degond and Dott. Luc Mieussens who kindly welcomed me in their research group in MIP Laboratory of Toulouse, with them I had important discussions and collaborations. Thanks also to Prof. Russell Caflisch and to Dott. Richard Wang of the mathematics department of UCLA, they gave me the possibility to work together on very stimulating projects, to Prof. Bruce Cohen and to Dott. Andris Dimits of the Livermore National Laboratory. They all did everything to make me feel comfortable.

Thanks to all my PhD colleagues, to the Professors of the Mathematics department of the University of Ferrara and to all the people I had the pleasure to interact scientifically and personally in this three years. Thanks to Marcello, Elisa, Alessia e Marco who sheared with me the office, I sincerely wish them to find quickly a permanent and fulfilling position.

Thanks to all my friends, some close, many now far that I had the fortune to meet, know and spend time in these thirty years. At least, I would like to truly thank my family, my parents, my sister and Federica for their constant support, without them everything would have been impossible.

Contents

Introduction

Nature involves different space and time scale phenomena. Things are made up of atoms and electrons and, at the same time, are characterized by their natural geometric dimensions which are usually several order of magnitude larger. In the same way, atomic processes occur at time scales which are much more faster respect events in our life. Normally, we refer to the macroscopic scale as the particular scale that we are interested in, all smaller scales are referred to as microscopic scales. The first approach, to deal with such problems, is to ignore the details of the microscopic interactions obtaining, analytically or empirically, explicit models for the scale of interest by ignoring the rest. Unfortunately, this is not always possible and sometimes, to correctly describe a macroscopic physical phenomena, microscopic information turn out to be necessary. Many examples could depict this situation, dislocation in plastic deformation, turbulence in fluid, molecular reaction in biology simulations or microscopic charge perturbations in macroscopic neutral plasmas. In all the above examples, we are obliged to introduce and numerically solve different laws which presumably govern processes at different scales. However, the simulation of large physical systems through the solution of microscopic deterministic model is computationally highly prohibitive and in future it is not imaginable that computers technology is able to change radically this situation.

An intermediate step between the microscopic and the macroscopic description is given by the so-called kinetic or mesoscopic models. These models deal with a quantity, the distribution function, which represent the density of particles in phase-space. As a consequence, one possibilities to round on the high cost of microscale models, is to use particles schemes or other stochastic numerical methods [80, 28, 18] based on the kinetic equations, which are known to be very fast, but at the same time, solutions computed with such schemes are affected by lot of fluctuations. The other possibility is to construct algorithms which are able to face the particular nature of multiscale problems like heterogeneous or hybrid methods

[48, 49, 50], wavelets [67], domain decomposition [10, 11, 37], or adaptive mesh refinement methods [22, 105].

Scope of this PhD thesis is the development of efficient algorithms for the numerical simulation of multiscale phenomena in the case of problems described by hyperbolic and/or kinetic equations. In the sequel, we will follow two different and complementary methodologies, one in the field of domain decomposition methods and the other in the field of hybrid methods. We remark the generality of the formulation of the methods presented, in fact both approaches described are easily adaptable to different situations as showed in the different parts of this dissertation.

In the following, we will briefly summarize the contents of the different chapters of the thesis. In the first part we discuss how to deal with multiscale hyperbolic equations. In the second part we generalize the hybrid method to kinetic equations, and we introduce two different domain decomposition methods. All the schemes proposed in that part are designed with the scope of reducing the computational cost of the simulation of the Boltzmann equation together with more accurate solutions respect the one furnished by particles schemes, in regimes close to the thermodynamical equilibrium. In the last part we tackle the difficult problem of the multiscale description of plasma physics phenomena, first we analyze how to deal with Coulomb collisions and after we describe an algorithm which can accelerate Monte Carlo methods for the simulations of plasma problems.

I Multiscale Hyperbolic Equations

Hyperbolic systems of conservation laws with stiff relaxation terms are often used to describe physical systems. The effect of the relaxation term is to lead the system to a reduced one of parabolic or hyperbolic type, when the limit of small value for the relaxation number is reached. Such systems are normally used to describe turbulence [74], phase transition [53], water waves [130], viscoelasticity [111], reacting flow [31] and gas flow [125]. These problems could represent a challenge for numerical methods due to the presence of different time and/or space scales. However, because the characteristic of these systems is to present a natural dimension reduction of the model due to a large variation of some parameters [30, 91], we could try to take advantage designing the scheme in such a way that is able to catch this reduction.

A methodology, that can be applied to design new hybrid methods for the numerical solution of a wide class of hyperbolic problems that involve different

scales, is presented in this first chapter. We consider hyperbolic systems with relaxation of the form [30]

$$\partial_t U + \partial_x F(U) = \frac{1}{\varepsilon} R(U), \quad x \in \mathbb{R}, \tag{I.1}$$

where $U = U(x,t) \in \mathbb{R}^N$, $F : \mathbb{R}^N \to \mathbb{R}^N$, the Jacobian matrix $F'(U)$ has real eigenvalues and $\varepsilon > 0$ is the relaxation time. Here we consider one dimensional system for sake of simplicity, however extension to multi dimensional situations are straightforward and showed in the numerical tests at the end of the chapter.

The operator $R : \mathbb{R}^N \to \mathbb{R}^N$ is called relaxation operator, and consequently (I.1) defines a relaxation system in the sense of Whitham and Liu [81], thus, if there exists a constant $n \times N$ matrix Q with $\text{rank}(Q) = n < N$ such that

$$QR(U) = 0 \quad \forall\, U \in \mathbb{R}^N. \tag{I.2}$$

this gives n independent conserved quantities $v = QU$. Moreover such conserved quantities uniquely determine a local equilibrium value

$$U = \mathcal{E}(v) \;\text{ such that }\; R(\mathcal{E}(v)) = 0. \tag{I.3}$$

Using (I.2) in (I.1) we obtain a system of n conservation laws which is satisfied by every solution of (I.1)

$$\partial_t(QU) + \partial_x(QF(U)) = 0. \tag{I.4}$$

For small values of the relaxation parameter ε from (I.1) we get $R(U) = 0$ which by (I.3) implies $U = \mathcal{E}(v)$. In this case system (I.1) is well approximated by the reduced system

$$\partial_t v + \partial_x G(v) = 0, \tag{I.5}$$

where $G(v) = QF(\mathcal{E}(v))$.

For these systems we consider the following general representation

$$U(x,t) = \underbrace{\tilde{U}(x,t)}_{nonequilibrium} + \underbrace{W(x,t)\mathcal{E}(v(x,t))}_{equilibrium}, \tag{I.6}$$

where $W(x,t) = \text{diag}(w_1(x,t), w_2(x,t), \ldots, w_N(x,t))$, $0 \le w_i(x,t) \le 1$ is a $N \times N$ matrix that characterizes the equilibrium fraction and $\tilde{U}(x,t)$ the non equilibrium part of the solution.

The idea is based on the use of probabilistic Monte Carlo methods for the solution of the micro scale model $\tilde{U}(x,t)$, combined with deterministic high order kinetic techniques for the macro scale model $W(x,t)\mathcal{E}(v(x,t))$. The parameter which measure the distance between the two models is the ratio of the equilibrium function $\mathcal{E}(v(x,t))$ (which is a function of the macroscopic variables) respect to the probabilistic distribution function $U(x,t)$ (which is the microscopic variable).

Thus, far from equilibrium regimes the solution is furnished by the stochastic component, while close to equilibrium regimes the solution is given by the deterministic scheme, in intermediate regimes the solution is obtained as a combination of the two. In order to better explain the structure of the schemes, in this first application, we considered problems which concern simple relaxation systems. The performance of the new methods is tested at the end of the chapter in the case of Jin-Xin relaxation system in one and two space dimension and for the Broadwell model. Results show the schemes ability to merge correctly the probabilistic and the deterministic fraction of the solution. However, the methods here presented are based on a kinetic solver for the relaxed part of the solution, thus we wish to include a more general fluid solver. This extension and extensions of the present methods to kinetic equations is performed in the next chapter.

II Multiscale Kinetic Equations

The great interest that kinetic models have in applied sciences is due to their ability in describing many different applications as rarefied gases [28, 7], electron and ions transport in plasmas [8, 123], granular flows [104], reacting gases [31], quantum gases [83], but also car traffic flows [70], tumor immune cells competition [6], market economies [32]. In this context, the Boltzmann equation represent the paradigm of kinetic equations and his validity to describe different physical systems has been proven in many different situations. Here we focus on the gas dynamic interpretation of the Boltzmann equation, extension of the methods presented to other applications are possible and in progress. For an overview on the Boltzmann equation and its applications we remind to [26]. We consider the non linear kinetic equation of the form

$$\frac{\partial f}{\partial t} + v \cdot \nabla_x f = \frac{1}{\varepsilon} Q(f,f) \tag{II.1}$$

with the initial condition

$$f(x,v,t=0) = f_0(x,v), \tag{II.2}$$

where $f = f(x, v, t)$ is a non negative function describing the time evolution of the distribution of particles which move with velocity $v \in \mathbb{R}^3$ in the position $x \in \Omega \subset \mathbb{R}^3$ at time $t > 0$. The bilinear operator $Q(f, f)$ describes the details of binary interactions between particles, while ε represent the so called Knudsen number and it is proportional to the mean free path between particles.

In the present part we work with the BGK relaxation form of the Boltzmann equation. This simplified model is known to be accurate in describing system close to the thermodynamical equilibrium, which are the main subject of our research, however we stress that the methods here introduced can be extended to others collision kernel without changing the structure of the algorithms, one example is showed in the third part of the present dissertation, while Boltzmann kernel of rarefied gas dynamic can be treated thanks to the Time Relaxed methods described in [94]. In the BGK simplified model, collisions are mimic by a relaxation towards the equilibrium, thus the operator takes the form

$$Q(f, f) = (M_f - f) \tag{II.3}$$

the local Maxwellian function is defined by

$$M_f(\varrho, u, T)(v) = \frac{\varrho}{(2\pi T)^{3/2}} \exp\left(\frac{-|u - v|^2}{2T}\right), \tag{II.4}$$

where ϱ, u, T are the density, mean velocity and temperature of the gas

$$\varrho = \int_{\mathbb{R}^3} f dv,\ u = \int_{\mathbb{R}^3} v f dv,\ T = \frac{1}{3\varrho} \int_{\mathbb{R}^3} |v - u|^2 f dv, \tag{II.5}$$

while the energy E is defined as

$$E = \frac{1}{2} \int_{\mathbb{R}^3} |v|^2 f dv, \tag{II.6}$$

The Maxwellian M_f can be characterized as the unique solution of the following entropy minimization problem

$$H(M_f) = \min\{H(f),\ f \geq 0\ s.t. \int_{\mathbb{R}^3} \mathbf{m} f\, dv = \boldsymbol{\varrho}\} \tag{II.7}$$

where the following inequality expresses the dissipation of entropy:

$$\partial_t \left(\int f \log f\, dv \right) + \nabla_x \cdot \left(\int v f \log f\, dv \right) \leq 0. \tag{II.8}$$

and $\mathbf{m}$ and $\boldsymbol{\varrho}$ are the vectors of the collision invariants and of the first three moments of f respectively:

$$\mathbf{m}(v) = (1, v, \frac{1}{2}|v|^2),\ \boldsymbol{\varrho} = (\varrho, \varrho u, E) \tag{II.9}$$

This is the well-known Boltzmann *H-theorem*, and it means that the local equilibrium state minimizes the entropy of all the possible states leading to the same macroscopic properties.

The numerical solution of this equation has encountered and still encounter many difficulties mainly due to a dimensionality problem: the distribution function depends on seven independent variables: time, physical space and velocity space. Moreover the necessity of physical conservation properties, positivity and entropy inequality are very important since they characterize the steady states, the significant velocity range that may vary strongly with space position (steady states may not be compactly supported in velocity space), the stiffness of the problem for small mean free paths and/or large velocities yields the problem hard to solve in practice.

Observe, anyway, that in many situations it is not necessary to solve the full Boltzmann equation, instead same results can be obtained through the solution of macroscopic transport equations, which describe the temporal and spatial variation of relevant macroscopic parameters, obtained averaging collective behavior of large number of particles and directly linked to the moments of the distribution function. To that aim considering the BGK equation (II.2), multiply it by the collision invariants, and integrate wit respect to v, we obtain the following set of balance laws:

$$\begin{aligned}
&\frac{\partial \varrho}{\partial t} + \nabla_x \cdot (\varrho u) = 0,\\
&\frac{\partial \varrho u}{\partial t} + \nabla_x \cdot (\varrho u \otimes u + P) = 0,\\
&\frac{\partial}{\partial t} E + \nabla_x \cdot (Eu + Pu + q) = 0,
\end{aligned} \tag{II.10}$$

which express the conservation of mass, momentum and energy, in which $P = \int (v-u) \otimes (v-u) f\, dv$ is the pressure tensor while $q = \int \frac{1}{2}(v-u)|v-u|^2\, dv$ is the heat flux. System (II.10) is not closed, since it involves other moments of the distribution function than just ϱ, ϱu and E.

Formally as $\varepsilon \to 0$ the function f tends to Maxwellian. In this limit, it is possible to compute the moments P and q of f in terms of ϱ, ϱu and E. In this way, one can close the system of balance laws (II.10) and get the Euler system of

compressible gas dynamics equations

$$\begin{aligned} &\frac{\partial \varrho}{\partial t} + \nabla_x \cdot (\varrho u) = 0, \\ &\frac{\partial \varrho u}{\partial t} + \nabla_x \cdot (\varrho u \otimes u + pI) = 0, \\ &\frac{\partial E}{\partial t} + \nabla_x \cdot ((E+p)u) = 0, \\ &p = \varrho\theta, \quad E = \frac{3}{2}\varrho\theta + \frac{1}{2}\varrho|u|^2. \end{aligned} \tag{II.11}$$

The rigorous passage from the Boltzmann equation to the compressible Euler equations for more general collision kernels has been investigated by several authors. Among them we mention references [20, 92]. Higher order fluid models, such as the Navier-Stokes model, can be considered using the Chapmann-Enskog and the Hilbert expansions, we refer to [78] for a mathematical setting of the problem.

Thus, in general if we are just interested to macroscopic variables can be unnecessary to afford the simulation of microscopic kinetic equations, unfortunately this is not always true, it happens that macroscopic equations fails to give correct results and a more detailed analysis becomes essential. Commonly the Knudsen number permits to switch from one model to the other, when it is sufficiently large a kinetic description becomes necessary. Anyway, we will see also that, taking in to account only the Knudsen number, leads to an overestimate of the necessity of micro model inside computational domains. In this part we develop different schemes to try to overcome the difficulties just described.

In the second chapter we present an automatic domain decomposition method for the solution of gas dynamics problems which require a localized resolution of the kinetic scale. The basic idea is to couple the macroscopic hydrodynamics model and the microscopic kinetic model through a buffer zone in which both equations are solved [37]. Discontinuities or sharp gradients of the solution are responsible for locally strong departures to local equilibrium which require the resolution of the kinetic model. The buffer zone is drawn around the kinetic region by introducing a cut-off function, which takes values between zero and one and which is identically zero in the fluid zone and one in the kinetic zone. Denoting the buffer interval by $[a, b]$, and introducing a cut-off function $h(x, t)$ such that

$$h(x,t) = \begin{cases} 1, & \text{for} \quad x \le a \\ 0, & \text{for} \quad x \ge b \\ 0 \le h(x,t) \le 1, & \text{for} \quad x \in [a,b] \end{cases} \tag{II.12}$$

we define two distribution functions such that $f_R = hf$ while $f_L = (1-h)f$. Looking now for an evolution equation for f_R and for f_L, we write

$$\partial_t f_R = \partial_t(hf) = f\,\partial_t h + h\partial_t f,$$
$$\partial_t f_L = \partial_t((1-h)f) = -f\,\partial_t h + (1-h)\partial_t f.$$

which after some computations leads to the following system for f_L and f_R:

$$\partial_t f_R + hv\partial_x f_R + hv\partial_x f_L = \frac{h}{\tau}(M_f - f) + f\partial_t h, \tag{II.13}$$
$$\partial_t f_L + (1-h)v\partial_x f_L + (1-h)v\partial_x f_R = \frac{1-h}{\tau}(M_f - f) - f\partial_t h, \tag{II.14}$$
$$f = f_R + f_L \tag{II.15}$$

It is now possible to derive the following set of equations, replacing f_L by M_{f_L} in the interval $x \leq b$:

$$\begin{aligned}
&\frac{\partial \varrho_L}{\partial t} + (1-h)\partial_x(\varrho_L u_L) = -(1-h)\partial_x\left(\int_{\mathbb{R}} v f_R\,dv\right) - \varrho\partial_t h,\\
&\frac{\partial \varrho_L u_L}{\partial t} + (1-h)\partial_x(\varrho_L u_L^2 + p_L) = -(1-h)\partial_x\left(\int_{\mathbb{R}} v^2 f_R\,dv\right) - \varrho u\partial_t h,\\
&\frac{\partial E_L}{\partial t} + (1-h)\partial_x((E_L + p_L)u_L) = -(1-h)\partial_x\left(\int_{\mathbb{R}} v\frac{|v|^2}{2} f_R\,dv\right) - E\partial_t h,
\end{aligned} \tag{II.16}$$

Under some assumptions reported in details in the chapter, we are able to prove that $f = f_R + M_{f_L}$, where f_R is a solution of:

$$\partial_t f_R + hv\partial_x f_R + hv\partial_x M[\varrho_L, u_L, \theta_L] = \frac{h}{\tau}(M_f - f) + f\partial_t h, \tag{II.17}$$

in the interval $x \geq a$. Thus the coupling model consists of system (II.16) for the hydrodynamic moments in the region $x \leq b$ and eq. (II.17) for the kinetic distribution function in the region $x \geq a$.

We specifically consider the possibility of moving the kinetic region or creating new kinetic regions, by evolving the cut-off function with respect to time. We present algorithms which perform this task by taking into account indicators which characterize the non-equilibrium state of the gas. The method is shown to be highly flexible as it relies on the time evolution of the buffer cut-off function rather than on the geometric definition of a moving interface which requires

remeshing, by contrast to many previous methods and to allow large speedup without loosing accuracy in the solutions. At the end of the chapter several numerical examples are shown in order to prove the validity and efficiency of the new method.

In the third chapter we extend the hybrid methods developed for hyperbolic problems with relaxations to kinetic equations. This procedure involves some generalizations to afford the new complications that arise in the simulations of multiscale gas dynamics like the lack of a compact support for the probability distribution function in velocity space. Consider the normalized distribution

$$f(v) \geq 0,\ \varrho = \int_{-\infty}^{+\infty} f(v)dv = 1, \tag{II.18}$$

and the following definition of hybrid representation:

Given a probability density $f(v)$, and a probability density $M(v)$, called equilibrium density, we define $w(v) \in [0,1]$ and $\tilde{f} \geq 0$ in the following way

$$w(v) = \begin{cases} \dfrac{f(v)}{M(v)}, & f(v) \leq M(v) \neq 0 \\ 1, & f(v) \geq M(v) \end{cases} \tag{II.19}$$

and

$$\tilde{f}(v) = f(v) - w(v)M(v). \tag{II.20}$$

Thus $f(v)$ can be represented as

$$f(v) = \tilde{f}(v) + w(v)M(v). \tag{II.21}$$

If we take now

$$\beta = \min_v\{w(v)\}, \tag{II.22}$$

and

$$\tilde{f}(v) = f(v) - \beta M(v), \tag{II.23}$$

we have

$$\int_v \tilde{f}(v)dv = 1 - \beta. \tag{II.24}$$

Let us define for $\beta \neq 1$ the probability density

$$f^p(v) = \frac{\tilde{f}(v)}{1-\beta}.$$

The case $\beta = 1$ is trivial since it implies $f(v) = M(v)$. Thus the probability density $f(v)$, can be written as a convex combination of two probability densities in the form [16, 17]

$$f(v) = (1-\beta)f^p(v) + \beta M(v). \tag{II.25}$$

Instead, if we need to restrict the deterministic part of the schemes to compactly supported function in velocity space, the following representations are particular useful. Consider for $R > 0$

$$w_R(v) = \begin{cases} w(v), & |v| \le R \\ 0, & |v| > R \end{cases} \tag{II.26}$$

and

$$\tilde{f}_R(v) = \begin{cases} \tilde{f}(v), & |v| \le R \\ f(v), & |v| > R \end{cases} \tag{II.27}$$

we have the representation

$$f(v) = \tilde{f}_R(v) + w_R(v)M(v). \tag{II.28}$$

In this case taking

$$\beta_R = \min_v\{w_R(v)\} \ge \beta, \tag{II.29}$$

and

$$\tilde{f}_R(v) = f(v) - \beta_R E(v), \tag{II.30}$$

where $E(v) = M(v)\Psi(|v| \le R)$ and $\Psi(\cdot)$ is the indicator function, we have

$$\int_v \tilde{f}_R(v)dv = 1 - \rho_E\beta_R, \qquad \rho_E = \int E(v)dv \le 1. \tag{II.31}$$

Let us define the probability density

$$f_R^p(v) = \frac{\tilde{f}_R(v)}{1-\rho_E\beta_R}.$$

Again $f(v)$, can be written as a convex combination of two probability densities in the form

$$f(v) = (1-\rho_E\beta_R)f_R^p(v) + \rho_E\beta_R\frac{E(v)}{\rho_E}. \tag{II.32}$$

More in general we consider the following representation

$$f(x,v,t) = \underbrace{\tilde{f}(x,v,t)}_{nonequilibrium} + \underbrace{w(x,v,t)M(x,v,t)}_{equilibrium},$$

where $w(x,v,t)$ is a continuum function (which may or may not be compactly supported in v) that characterizes the equilibrium fraction and $\tilde{f}(x,v,t)$ the non equilibrium part of the distribution function. Once the problem is defined the idea is the same of the first chapter, thus we solve the evolution of the perturbation by Monte Carlo methods, and we solve the evolution of the equilibrium fraction by deterministic kinetic methods.

Moreover in the present chapter we propose to solve the tails of the density function with Monte Carlo scheme no matter if they are in thermodynamical equilibrium or not. That choice combined with the hybrid treatment of the interactions term leads to a faster and more accurate solution of the Boltzmann equation respect to classical discrete velocity model, that needs the computations at each time step of a compact supported equilibrium function to mimic the real Maxwellian distribution. The chapter ends with several numerical tests in which the results of the simulations are showed in different test cases and for different values of the Knudsen number.

The next chapter represent a generalization of the kinetic hybrid methods presented before. Here we develop an algorithm which is easy to implement and form-fitting with any type of finite volume or finite difference methods of kinetic or fluid nature. Thanks to the coupling of Monte Carlo techniques for the solution of the Boltzmann equations with deterministic methods for the compressible Euler equations, we are able to treat the multiscale nature of fluid dynamic phenomena faster respect to traditional discrete velocity model or spectral model for kinetic equations with solutions affected by less fluctuations respect to Monte Carlo schemes. We could estimate the total computational time for this algorithm as

$$CT_{TOT} = CT_E + \alpha CT_{MC} \tag{II.33}$$

where CT_{TOT} is the total computational time, CT_E the time to compute the solution for fluid equations, while CT_{MC} is the time we need to perform a particles simulation for Boltzmann equations, finally α is a scalar function that contains the information related to the equilibrium/nonequilibrium character of the distribution function f. If we are in a thermodynamical state $\alpha = 0$, to the other part if we are in a completely non equilibrium situation $\alpha = 1$.

The results achieved in this chapter represent an important step forward in the numerical solution of the Boltzmann equation, although, the main gain of the method described is due to the possibility of determining the equilibrium fraction remained in each cell after the convection of the distribution function. The intensive research on that problem is the subject of future works, here we only introduce and test some ideas. In the second part of the chapter we shows how a set of domain decomposition methods can be obtained as a subset of the fluid independent hybrid method described. In this part, to overcome the problem of determining the fraction of equilibrium we use the knowledge of regions in which commonly the kinetic equations are necessary, thus we construct deriving directly from the above methods a new class of schemes simply imposing the value of the Knudsen number equal to zero in some regions of the computational domain. In that way, where the solution furnished by the macroscopic compressible Euler equations are sufficiently accurate, we impose artificially the relaxation number to zero. One dimensional numerical tests are showed for the fluid independent hybrid method together with some time comparisons between different methods, while some applications to the two-dimensional BGK equation are presented to show the performance of the domain decomposition method.

III Multiscale Plasma Modeling and Simulation

The term *plasma* is used to describe a wide variety of macroscopically neutral substances containing many interacting free electrons, ionized atoms or molecules, which exhibit collective behavior due to the long-range Coulomb forces [8]. Plasma draw the attention of the scientific community both for its extremely large occurrence in nature and for the challenging applications like the controlled thermonuclear fusion.

The fundamental properties of a plasma depend on the particles interactions. Collisions can be distinguished in to long-range interactions and short-range interactions, many efficient numerical methods exist for short-range forces, while how treat long-range forces is still not clear. The Boltzmann bilinear operator $Q(f,f)$ describes binary collisions between particles

$$Q(f,f) = \int_{\mathbb{R}^3}\int_{S^2} B\left(|q|, \frac{q\cdot n}{|q|}\right)[f(v')f(v'_*) - f(v)f(v_*)]dndv_* \qquad \text{(III.1)}$$

where S^2 is the unit sphere in $\mathbb{R}^3$, $q = v - v_*$, $n \in S^2$ the unit normal. The collision kernel $B(|q|, q\cdot n/|q|)$, which characterize the detail of the interaction,

is defined as

$$B(|q|, \cos\theta) = |q|\sigma(|q|, \theta),\ (0 \leq \theta \leq \pi) \tag{III.2}$$

Here $\cos\theta = q \cdot n/|q|$ and $\sigma(q, \theta)$ is the collision cross section at the scattering angle θ, in the case of Coulomb interactions the Rutherford formula holds

$$\sigma(|q|, \theta) = \frac{b_0^2}{4\sin^4(\theta/2)} \tag{III.3}$$

where $b_0 = e^2/(4\pi\epsilon_0 m_r|v - v_*|^2)$, with e the charge of the particle, ϵ_0 the vacuum permittivity and m_r the reduced mass, which corresponds to $m/2$, if the interacting particles are of the same species, with m equal to the mass. Observe that from the above formula follows that the scattering cross section tends to infinity as the angle θ tends to zero, thus in order to obtain finite and meaningful values for the total and the momentum cross section is necessary to introduce a cut-off value for the impact parameter.

The Boltzmann operator takes into account only binary collisions, while in plasmas each charged particle interacts simultaneously with a large number of neighboring particles. However, considering Coulomb interactions as a series of consecutive weak binary collisions it is possible to derive the Landau-Fokker-Planck collision term (see [42] for details), which is known to correctly describe these phenomena

$$Q^L(f, f) = \frac{1}{8}\frac{\partial}{\partial v_i}\int_{\mathbb{R}^3} |q|\sigma_m(|q|)((|q|^2)\delta_{ij} - q_i q_j) \times \left(\frac{\partial}{\partial v_j} - \frac{\partial}{\partial v_{*j}}\right) f(v) f(v_*) dv_* \tag{III.4}$$

In 2000 Bobylev [9] proposed an approximate version of the Boltzmann integral

$$Q(f, f) = \frac{1}{\tau}\int_{\mathbb{R}^3} (\exp(\tau J) - \widehat{I}) F(U, q) dv_* + 0(\tau) \tag{III.5}$$

with $U = (v + v_*)/2$ denotes the center of mass velocity, and

$$F(U, q) \equiv f(U + q/2) f(U - q/2) = f(v) f(v_*) \tag{III.6}$$

and where the operator $\exp(\tau J)$ can be written as

$$\exp(\tau J)\psi(\omega) = \int_{S^2} B_\tau(\omega \cdot n, |q|)\psi(n) dn \tag{III.7}$$

with $\psi(\omega)$ is an arbitrary function and

$$B_\tau(\omega \cdot n, |q|) = \sum_{l=0}^{\infty} \frac{2l+1}{4\pi} \exp(-\lambda_l(|q|)\tau) P_l(\omega \cdot n) \tag{III.8}$$

is the Green function, with $P_l(\omega \cdot n)$ the Legendre polynomial and $\lambda_l(|q|)$ equal to

$$\lambda_l(|q|) = 2\pi \int_{-1}^{1} B(\mu, |q|)(1 - P_l(\mu))d\mu \tag{III.9}$$

where $\mu = \omega \cdot n,\ -1 \leq \mu \leq 1$.

This approximated operator is showed to represent also a first order approximation ($0(\tau)$) of the Landau-Fokker-Planck equations in the case of small angle scattering between particles

$$Q(f,f) = \frac{1}{\tau}\left(\int_{\mathbb{R}^3 \times S^2} D\left(\frac{q \cdot n}{|q|}, \frac{\tau}{2\varrho\tau_1}\right) f(v')f(v'_*)dndv_* - \varrho f(v)\right) \tag{III.10}$$

where

$$\frac{1}{\tau_1} = 4\pi \left(\frac{e^2}{4\pi\epsilon_0 m_r}\right)^2 \frac{\varrho \ln \Lambda}{|q|^3} \tag{III.11}$$

with $\Lambda = \frac{1}{\sin(\theta^{min}/2)}$ and

$$D(\mu, \tau_0) = \sum_{l=0}^{\infty} \frac{2l+1}{4\pi} P_l(\mu) \exp(-l(l+1)\tau_0) \tag{III.12}$$

Starting from Bobylev results in chapter 5 we try to give a contribution to the understanding of the link between binary and multiple simultaneously collisions, through the construction of a series of direct Monte Carlo methods based on the commonly used schemes of rarefied gas dynamic like the Bird scheme. In particular we show the non intuitive nature of the methods, which permit to obtain, with the same computational price, more accurate solution with algorithms in which, not all the particles collide in one time step and some particles collide more than once, respect to algorithms in which all particles collide at least once each time step.

In the last chapter we open the way to the hybrid simulations of plasma phenomena, through the construction of an algorithm for Coulomb collisions based both on the binary collision model of Nanbu [88] or of Takizuka & Abe [120]. In

fact, we observe that if the collisional time scale for Coulomb collisions is comparable to the characteristic time scales for a plasma, then simulation of Coulomb collisions may be important for computation of kinetic plasma dynamics. This can be a computational bottleneck because of the large number of simulated particles and collisions (or phase-space resolution requirements in continuum algorithms), as well as the wide range of collision rates over the velocity distribution function. Thus, in the scheme proposed the velocity distribution function is represented as a combination of a thermal component and a kinetic component , i.e.

$$f(v) = m(v) + k(v). \tag{III.13}$$

the thermal component is a Maxwellian distribution

$$m(v) = n_m(2\pi T_m)^{-3/2} \exp\left(-|v - u_m|^2/2T_m\right). \tag{III.14}$$

while the kinetic component will be simulated using a set of discrete particles:

$$g(v) = \sum_{i=1}^{n_k} \delta(v - v_i). \tag{III.15}$$

Because of the (expected) slow interaction of the thermal component m with the kinetic component k, the average density, velocity and temperature n_m, u_m and T_m of m are not assumed to be those of the full distribution f. Now, collisions between particles from the thermal component preserve the Maxwellian; collisions between particles from the kinetic component are performed using the method of or Nanbu. Collisions between the kinetic and thermal components are performed by sampling a particle from the thermal component and selecting a particle from the kinetic component. Particles are also transferred between the two components according to thermalization and dethermalization probabilities, which are functions of phase space. Some computational results are showed at the end of the chapter to prove the validity of the method.

Finally in the appendix, because of the large use of Monte Carlo techniques in all the dissertation, we inserted a remark about some precautions that are necessary to have when dealing with conservative Monte Carlo methods. We emphasized some of the side effects due to the use of conservative methods over a finite number of statistical samples (particles) in the simulation. The most relevant aspect is that the steady states of the system are compactly supported and thus they cannot be Maxwellian (or any other non compactly supported statistics) unless the number of particles goes to infinity. We stressed the difference between working with many or few samples, especially in the simulation of steady problems in

which averages are often used to eliminate fluctuations. These aspects are studied numerically with the help of a simple one-dimensional space homogeneous kinetic model.

Part I

Multiscale Hyperbolic Equations

Chapter 1

Hybrid Multiscale Methods I. Hyperbolic Relaxation Problems

This Chapter is based on the work [43] published in **Communication in Mathematical Sciences Vol. 4, No. 1, pp. 155-177** in collaboration with Prof. Lorenzo Pareschi of the Department of Mathematics and Center for Modeling Computing and Statistics (CMCS) of University of Ferrara.

1.1 Introduction

Hyperbolic systems with relaxation are used to describe many physical problems that involve both convection and nonlinear interaction [30, 81]. In the Boltzmann equation from the kinetic theory of rarefied gas dynamics, the collision (relaxation) term describes the interaction of particles [27]. Relaxations also occur in several other problems ranging from water waves to traffic flow. In such systems, when the nonlinear interactions are strong, the relaxation rate is large. In kinetic theory, for example, this occurs when the mean free path between collisions is small (i.e., the Knudsen number is small). Within this regime, which is referred to as the fluid dynamic limit, the gas flow is well described by the Euler or Navier Stokes equations of fluid mechanics, except in shock layers and boundary layers.

These problems represent a challenge for numerical methods due to the presence of different time and/or space scales. In these systems, besides conventional deterministic discretizations, a probabilistic approach is highly desirable. Monte Carlo methods or probabilistic techniques at different levels are widely used to simulate complex systems [18, 80]. They have many advantages in terms of com-

putational cost for problems with high dimensions, simplicity in preserving some physical properties of the underlying problem (typically using a particle interpretation of the statistical sample) and great flexibility when dealing with complicate geometries.

A characteristic of relaxation-like systems is to present a natural dimension reduction of the model due to a large variation of some parameters [30, 81, 66, 91]. Domain decomposition techniques are then used in order to better adapt the modelling strategy and the design of the numerical schemes. However this multi-modelling approach, which at the mathematical level is a consequence of asymptotic approximations, requires the a-priori knowledge of some of the scales in the problem which are typically hard to know in practice [10, 75].

A complementary strategy would be to use the full model in the whole computational domain and to design the numerical method in such a way that it is capable to take advantage of the model reduction induced by the presence of small scales [21, 62, 64, 65, 90, 95]. Off course this would involve the development of heterogeneous numerical methods which hybridize different numerical approaches of probabilistic and deterministic nature.

Often, the design of such hybrid methodology involves not only the use hybrid numerical methods but also their efficient coupling with suitable multi-modelling strategies. Clearly the details of the schemes are rather problem dependent [19, 35, 16, 17, 71, 114, 117]. We quote the recent works by Weinan E and Bjorn Engquist for a general approach to heterogeneous multiscale methods in scientific computing [48, 49, 50, 51].

In this work we describe a methodology that can be applied to design new hybrid methods for the numerical solution of a wide class of hyperbolic problems that involve different scales. The main components of the schemes is the use of probabilistic Monte Carlo methods for the full model (far from equilibrium regimes) combined with deterministic shock capturing techniques for the reduced one (close to equilibrium regimes). An essential aspect in the development of the algorithms is the choice of a suitable hybrid representation of the solution. The main features of the schemes can be summarized as follows

- In non stiff regions, where the solution of the full dimensional model is required, the schemes provide a probabilistic Monte Carlo approximation of the solution.

- In stiff regions, where the reduced equilibrium model is valid, the schemes provide a deterministic high order finite volume (differences) approximation without any time step restrictions induced by the small relaxation rate.

- In intermediate regions, the approximated solution is generated automatically by the schemes as a suitable blending of a nonequilibrium probabilistic component and an equilibrium deterministic components.

The rest of the article is organized as follows. First we introduce the model problems we are considering. Then we present the different schemes in the case of Jin-Xin relaxation system. Next we apply the method to the more realistic case of the Broadwell model. Some final considerations and future developments are discussed in the last section.

1.2 Hyperbolic relaxation systems

We will consider here one-dimensional hyperbolic systems with relaxation of the form [30]

$$\partial_t U + \partial_x F(U) = \frac{1}{\varepsilon} R(U), \quad x \in \mathbb{R}, \tag{1.2.1}$$

where $U = U(x,t) \in \mathbb{R}^N$, $F : \mathbb{R}^N \to \mathbb{R}^N$, the Jacobian matrix $F'(U)$ has real eigenvalues and $\varepsilon > 0$ is the relaxation time.

The operator $R : \mathbb{R}^N \to \mathbb{R}^N$ is said a relaxation operator, and consequently (1.2.1) defines a relaxation system in the sense of Whitham and Liu [81], if there exists a constant $n \times N$ matrix Q with rank$(Q) = n < N$ such that

$$QR(U) = 0 \quad \forall\, U \in \mathbb{R}^N. \tag{1.2.2}$$

This gives n independent conserved quantities $v = QU$. Moreover such conserved quantities uniquely determine a local equilibrium value

$$U = \mathcal{E}(v) \;\text{ such that }\; R(\mathcal{E}(v)) = 0. \tag{1.2.3}$$

The image of $\mathcal{E}$ represents the manifold of local equilibria of the relaxation operator R. Using (1.2.2) in (1.2.1) we obtain a system of n conservation laws which is satisfied by every solution of (1.2.1)

$$\partial_t(QU) + \partial_x(QF(U)) = 0. \tag{1.2.4}$$

For small values of the relaxation parameter ε from (1.2.1) we get $R(U) = 0$ which by (1.2.3) implies $U = \mathcal{E}(v)$. In this case system (1.2.1) is well approximated by the reduced system

$$\partial_t v + \partial_x G(v) = 0, \tag{1.2.5}$$

where $G(v) = QF(\mathcal{E}(v))$.

Remark 1.2.1 *Following the terminology introduced in [48, 49, 50] the macroscale process is described by the conserved quantities v whereas the microscopic process is described by the variables U. The two processes and state variables are related to each other by compression and reconstruction operators, characterized respectively by the matrices Q and M such that $QU = v$ and $Mv = U$, with the property $QM = I$, where I is the n-dimensional identity matrix. The compression operator is in general a local/ensemble average (projection to low order moments). The reconstruction operator does the opposite and in general it is under-determined, except close to the local equilibrium state when $R(U) = 0$ implies $U = \mathcal{E}(v)$.*

1.2.1 Jin-Xin relaxation system

A simple prototype example of relaxation system in the case $N = 2$ is given by the Jin-Xin system [66]

$$\begin{aligned} &\partial_t u + \partial_x v = 0, \\ &\partial_t v + \partial_x a u = -\frac{1}{\varepsilon}(v - F(u)), \end{aligned} \tag{1.2.6}$$

which corresponds to take $U = (u, v)^T$, $F(U) = (v, au)^T$ and $R(U) = (0, F(u) - v)^T$.

For small values of ε from the second equation in (1.2.6) we get the local equilibrium

$$v = F(u) \tag{1.2.7}$$

and under Liu's subcharacteristic condition $a > F'(u)^2$ solutions to (1.2.6) converges to the solution of the scalar conservation law

$$\partial_t u + \partial_x F(u) = 0. \tag{1.2.8}$$

1.2.2 Broadwell model

A simple discrete velocity kinetic model for a gas was introduced by Broadwell [13]. It describes a fictitious gas composed of particles with only six (four) veloc-

ities in the 3D (2D) velocity space. In one space dimension these models reads

$$\begin{aligned}
&\partial_t f + \partial_x f = \frac{1}{\varepsilon}(h^2 - fg),\\
&\partial_t g + \partial_x g = \frac{1}{\varepsilon}(h^2 - fg),\\
&\partial_t h = -\frac{1}{\alpha\varepsilon}(h^2 - fg),
\end{aligned} \tag{1.2.9}$$

where ε is the mean free path, f, h, and g denote the mass densities of gas particles with speed 1, 0, and -1, respectively, and $\alpha = 1$ for the 2D model and $\alpha = 2$ for the 3D one. The fluid dynamic moment variables are density ϱ , momentum m, and velocity u defined by

$$\varrho = f + 2\alpha h + g, \;\; m = f - g, \;\; u = \frac{m}{\varrho} \tag{1.2.10}$$

In addition define

$$z = f + g \tag{1.2.11}$$

Then the Broadwell equations can be rewritten as

$$\begin{aligned}
&\partial_t \varrho + \partial_x m = 0,\\
&\partial_t m + \partial_x z = 0,\\
&\partial_t z + \partial_x m = -\frac{1}{2\alpha^2\varepsilon}(\varrho^2 + (1-\alpha^2)z^2 + \alpha^2 m^2 - 2\varrho z).
\end{aligned} \tag{1.2.12}$$

Note that if the fluid variables ϱ , m, and z are known then f, g, and h can be recovered as

$$f = \frac{1}{2}(z+m), \;\; g = \frac{1}{2}(z-m), \;\; h = \frac{1}{2\alpha}(\varrho - z) \tag{1.2.13}$$

A *local equilibrium* is obtained when the state variables satisfy

$$\varrho^2 + (1-\alpha^2)z^2 + \alpha^2 m^2 - 2\varrho z = 0, \tag{1.2.14}$$

which gives

$$z = z_E(\varrho, u) = \begin{cases} \dfrac{\varrho}{3}(2\sqrt{3u^2+1} - 1), & \alpha = 2,\\ \dfrac{1}{2}\varrho(1+u^2), & \alpha = 1. \end{cases} \tag{1.2.15}$$

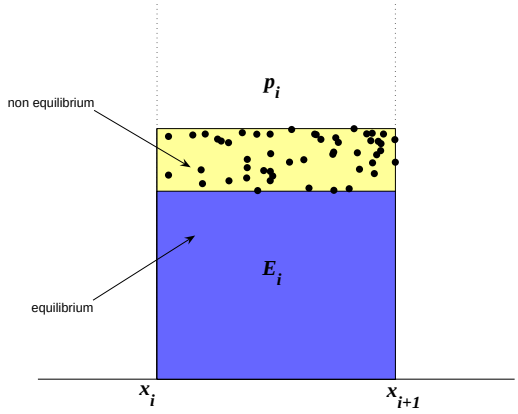

Figure 1.1: Hybrid representation of a cell value.

Thus as $\varepsilon \to 0$ one gets the fluid dynamic limit described by the set of Euler equations

$$\begin{aligned} &\partial_t \varrho + \partial_x(\varrho u) = 0, \\ &\partial_t(\varrho u) + \partial_x z_E(\varrho, u) = 0. \end{aligned} \tag{1.2.16}$$

To the next order, a model Navier-Stokes equation can be derived via the Chapmann-Enskog expansion. For a description of the Broadwell model and its fluid dynamic limit see, for example [13].

1.3 Hybrid methods

The starting point in the construction of the methods is the following definition of hybrid representation of a discrete probability density.

Definition 1.3.1 *Given a discrete probability density p_i, $i = 1, \ldots, N$ (i.e. $p_i \geq 0$, $\sum_i p_i = 1$) and a discrete probability density E_i, $i = 1, \ldots, N$ called equilibrium density, we define $w_i \in [0, 1]$ and $\tilde{p}_i \geq 0$ in the following way*

$$w_i = \begin{cases} \dfrac{p_i}{E_i}, & p_i \leq E_i \neq 0 \\ 1, & p_i \geq E_i \end{cases} \tag{1.3.1}$$

and

$$\tilde{p}_i = p_i - w_i E_i. \tag{1.3.2}$$

Thus p_i can be represented as

$$p_i = \tilde{p}_i + w_i E_i. \tag{1.3.3}$$

Remark 1.3.1 *If we take*

$$\beta = \min_i \{w_i\}, \tag{1.3.4}$$

and

$$\tilde{p}_i = p_i - \beta E_i, \tag{1.3.5}$$

we have

$$\sum_i \tilde{p}_i = 1 - \beta. \tag{1.3.6}$$

Let us define for $\beta \neq 1$ the discrete probability density

$$p_i^p = \frac{\tilde{p}_i}{1-\beta}.$$

The case $\beta = 1$ is trivial since it implies $p_i = E_i$, $i = 1, \ldots, N$. Thus the discrete probability density p_i, $i = 1, \ldots, N$ can be written as a convex combination of two probability densities in the form [16, 17]

$$p_i = (1-\beta) p_i^p + \beta E_i. \tag{1.3.7}$$

Clearly the above representation is a particular case of (1.3.3).

In the case of an hyperbolic system with relaxation we recall that $U(x,t) \in \mathbb{R}^N$ denotes the solution of the system whereas $\mathcal{E}(v(x,t)) \in \mathbb{R}^N$ denotes the equilibrium state where $v(x,t) \in \mathbb{R}^n$ are the conserved variables.

Thus we consider the following general representation

$$U(x,t) = \underbrace{\tilde{U}(x,t)}_{nonequilibrium} + \underbrace{W(x,t)\mathcal{E}(v(x,t))}_{equilibrium},$$

where $W(x,t) = \mathrm{diag}(w_1(x,t), w_2(x,t), \ldots, w_N(x,t))$, $0 \leq w_i(x,t) \leq 1$ is a $N \times N$ matrix that characterizes the equilibrium fraction and $\tilde{U}(x,t)$ the non equilibrium part of the solution.

The general methodology consist in

- Solve the evolution of the non equilibrium part by Monte Carlo methods. Thus $\tilde{U}(x,t)$ will be represented by a set of samples in the computational domain.
- Solve the evolution of the equilibrium part by deterministic methods. Thus $W(x,t)\mathcal{E}(v(x,t))$ will be represented on a suitable grid in the computational domain.

In the sequel, we will describe the different schemes in the case of Jin-Xin relaxation system (1.2.6) although our treatment extends far beyond this simple system. In order to introduce the reader to the main tools used we start the section by describing a simple Monte Carlo approach where the entire solution is represented by samples [100].

1.3.1 Monte Carlo methods (MCM)

First we rewrite the system in diagonal form

$$\begin{aligned}
\partial_t f + \sqrt{a}\partial_x f &= -\frac{1}{\varepsilon}(f - E_f(u)) \\
\partial_t g - \sqrt{a}\partial_x g &= -\frac{1}{\varepsilon}(g - E_g(u)).
\end{aligned}$$

$$f = \frac{\sqrt{a}u + v}{2\sqrt{a}}, \quad g = \frac{\sqrt{a}u - v}{2\sqrt{a}},$$

$$E_f(u) = \frac{\sqrt{a}u + F(u)}{2\sqrt{a}}, \quad E_g(u) = \frac{\sqrt{a}u - F(u)}{2\sqrt{a}}.$$

We assume $-u\sqrt{a} \leq F(u) \leq u\sqrt{a}$ and $u \geq 0$ so that $f, g \geq 0$. This is guaranteed by the subcharacteristic condition if $F(0) = 0$.

We start by splitting the system in the two separate steps, a relaxation step represented by a system of stiff ordinary differential equations

$$\begin{aligned}
\partial_t f^r &= -\frac{1}{\varepsilon}(f^r - E_f(u^r)) \\
\partial_t g^r &= -\frac{1}{\varepsilon}(g^r - E_g(u^r))
\end{aligned}$$

and a convection step

$$\begin{aligned}
\partial_t f^c + \sqrt{a}\partial_x f^c &= 0 \\
\partial_t g^c - \sqrt{a}\partial_x g^c &= 0
\end{aligned}$$

Note that, given an initial data $f(x,0)$ and $g(x,0)$, we can easily compute the exact solution of the relaxation step as

$$f^r(x,t) = e^{-t/\varepsilon} f(x,0) + (1-e^{-t/\varepsilon}) E_f(u(x,0)), \tag{1.3.8}$$
$$g^r(x,t) = e^{-t/\varepsilon} g(x,0) + (1-e^{-t/\varepsilon}) E_g(u(x,0)), \tag{1.3.9}$$

this solution is then used as initial data for the transport step to get the approximate solution at time t. We recall that $u^r(x,t) = u(x,0)$ during the relaxation step.

In the case of nonnegative initial data and if $E_f, E_g \geq 0$, the solution of our problem can be sought in the form of a discrete probability density at each space point

$$p(x,v,t) = \begin{cases} \dfrac{f(x,t)}{u(x,t)}, & v = \sqrt{a}, \\ \dfrac{g(x,t)}{u(x,t)}, & v = -\sqrt{a}. \end{cases} \tag{1.3.10}$$

Let us define with $\{\nu_1, \nu_2, \ldots, \nu_N\}$ the initial samples from $p(x,v,0)$ at a given space point x, we know that $\nu_k = \pm\sqrt{a}$, $k = 1, \ldots, N$. Hence a Monte Carlo method to obtain samples from $p^r(x,v,t)$ with $f^r(x,t)$ and $g^r(x,t)$ solutions of the relaxation step is

Algorithm 1.3.1 (Simple Monte Carlo for Jin-Xin relaxation system)

1. *Given a sample ν_k*
   - (a) *with probability $e^{-t/\varepsilon}$ the sample is unchanged*
   - (b) *with probability $1 - e^{-t/\varepsilon}$ the sample is replaced with an equilibrium sample. To extract an equilibrium sample proceed as follows*
     - i. *with probability $\dfrac{E_f(u(x,0))}{u(x,0)}$ take $\nu_k = \sqrt{a}$*
     - ii. *with probability $\dfrac{E_g(u(x,0))}{u(x,0)}$ take $\nu_k = -\sqrt{a}$.*

Note that the above procedure requires the exact knowledge of $u(x,0)$ which we can only estimate from the samples at the given point x.

In practice we can integrate equations (1.3.8-1.3.9) over the cell I_j and write, up to second order accuracy in space, the time evolution of the cell averages

$$f^r_{j+1/2}(t) = e^{-t/\varepsilon} f_{j+1/2}(0) + (1-e^{-t/\varepsilon}) E_f(u_{j+1/2}(0)), \tag{1.3.11}$$
$$g^r_{j+1/2}(t) = e^{-t/\varepsilon} g_{j+1/2}(0) + (1-e^{-t/\varepsilon}) E_g(u_{j+1/2}(0)). \tag{1.3.12}$$

Thus we can apply Algorithm 1.3.1 on the whole set of samples in the space interval interested by the reconstruction of $u_{j+1/2}(0)$. The simplest method, which produces a piecewise constant reconstruction, is based on evaluating the histogram of the samples on the grid. Given a set of N samples $p_1, p_2, \ldots, p_N$ we define the discrete probability density at the cell centers

$$p(x_{j+1/2}) = \frac{1}{N}\sum_{k=1}^{N} \Psi_{\Delta x}(p_k - x_{j+1/2}), \quad j = \ldots, -2, -1, 0, 1, 2, \ldots \quad (1.3.13)$$

where $\Psi_{\Delta x}(x) = 1/\Delta x$ if $|x| \leq \Delta x/2$ and $\Psi_{\Delta x}(x) = 0$ elsewhere.

Let us denote by the index k the sample ν_k and its position χ_k. If we use equations (1.3.13) then $u_{j+1/2}$ is given by the number of samples N_j belonging to the cell I_j

$$u_{j+1/2} = \frac{1}{N\Delta x}\sum_{x_k \in I_j} 1 = \frac{N_j}{N\Delta x}$$

and the Monte Carlo procedure is applied on such set of samples $\{\nu_k \,|\, \chi_k \in I_j\}$. In this case, when we extract a new equilibrium sample ν_k in the cell I_j its position χ_k is taken as uniformly distributed in the cell. We refer the reader to [99] (and the references therein) for an introduction to basic sampling and different reconstruction techniques in Monte Carlo methods.

Finally the transport step does not present any difficulty and can be applied without any need of meshes or reconstructions. In fact, from the exact expression of the solution $f^c(x,t) = f^r(x - \sqrt{a}t, t)$, $g^c(x,t) = g^r(x + \sqrt{a}t, t)$ we simply need to shift the position of the samples accordingly to the law

$$\chi_k = \chi_k + \nu_k t, \quad \forall k. \quad (1.3.14)$$

In the sequel we will use the terminology "particle" to denote the pair (χ_k, ν_k) characterizing the sample ν_k and its position χ_k.

The method described above deserves some remarks.

Remark 1.3.2

- *One important aspect in the method is that we do not need to reconstruct the functions f and g but only the conserved quantity u. This is of paramount relevance when dealing with very large systems, as in kinetic equations.*
- *The Monte Carlo scheme is conservative and preserve positivity of the solution without any time step limitation. Note that as $\varepsilon \to 0$ the method*

becomes a Monte Carlo algorithm for the limiting scalar conservation law. This limiting method is the analogue of a kinetic particle method for the scalar conservation law [100].

- *The simple splitting method we have described here is first order in time. Second order Strang splitting can be implemented similarly.*

1.3.2 The hybrid method (HM)

The standard hybrid method is based on the hybrid representation (1.3.7). Thus we assume our solution of the form

$$f(x,t) = (1-\beta(x,t))f_p(x,t) + \beta(x,t)E_f(u(x,t)), \tag{1.3.15}$$
$$g(x,t) = (1-\beta(x,t))g_p(x,t) + \beta(x,t)E_g(u(x,t)). \tag{1.3.16}$$

From the exact solution of the relaxation step (1.3.8) if we consider that initially

$$\begin{aligned} f(x,0) &= (1-\beta(x,0))f_p(x,0) + \beta(x,0)E_f(u(x,0)), \\ g(x,0) &= (1-\beta(x,0))g_p(x,0) + \beta(x,0)E_g(u(x,0)) \end{aligned}$$

we obtain the identities

$$\begin{aligned} f^r(x,t) &= (1-\beta^r(x,t))f_p^r(x,t) + \beta^r(x,t)E_f(u^r(x,t)) \\ &= e^{-t/\varepsilon}[(1-\beta(x,0))f_p(x,0) + \beta(x,0)E_f(u(x,0))] + \\ &+ (1-e^{-t/\varepsilon})E_f(u(x,0)), \\ g^r(x,t) &= (1-\beta^r(x,t))g_p^r(x,t) + \beta^r(x,t)E_g(u^r(x,t)) \\ &= e^{-t/\varepsilon}[(1-\beta(x,0))g_p(x,0) + \beta(x,0)E_g(u(x,0))] + \\ &+ (1-e^{-t/\varepsilon})E_g(u(x,0)). \end{aligned}$$

By equating the equilibrium terms and the non equilibrium ones in the above equations and using the fact that $u^r(x,t) = u(x,0)$ we obtain the evolution for the unknowns $f_p^r(x,t)$, $g_p^r(x,t)$ and $\beta^r(x,t)$

$$f_p^r(x,t) = f_p(x,0), \quad g_p^r(x,t) = g_p(x,0). \tag{1.3.17}$$
$$\beta^r(x,t) = e^{-t/\varepsilon}\beta(x,0) + 1 - e^{-t/\varepsilon}. \tag{1.3.18}$$

Note that $\beta^r(x,t) \to 1$ as $\varepsilon \to 0$. If we start from $\beta(x,0) = 0$ (all particles) at the end of the relaxation a fraction $1 - e^{-t/\varepsilon}$ of the particles is discarded by the

method as the effect of the relaxation to equilibrium. Thus particles will represent the fractions $f_p^r(x,t) = (1-\beta^r(x,t))f_p^r(x,t)$ and $(1-\beta^r(x,t))g_p^r(x,t)$. Moreover the hybrid representation is naturally kept by the relaxation.

After relaxation the exact solution of the transport step reads

$$\begin{aligned} f^c(x,t) &= (1-\beta^c(x,t))f_p^c(x,t) + \beta^c(x,t)E_f(u^c(x,t)) = f^r(x-\sqrt{a}t,t) \\ &= (1-\beta^r(x-\sqrt{a}t,t))f_p^r(x-\sqrt{a}t,t) + \\ &+ \beta^r(x-\sqrt{a}t,t)E_f(u(x-\sqrt{a}t,0)) \\ g^c(x,t) &= (1-\beta^c(x,t))g_p^c(x,t) + \beta^c(x,t)E_f(u^c(x,t)) = g^r(x+\sqrt{a}t,t) \\ &= (1-\beta^r(x+\sqrt{a}t,t))g_p^r(x+\sqrt{a}t,t) + \\ &+ \beta^r(x+\sqrt{a}t,t)E_g(u(x+\sqrt{a}t,0)). \end{aligned} \tag{1.3.19}$$

To simplify notations let us set

$$\begin{aligned} f_p^*(x,t) &= (1-\beta^r(x-\sqrt{a}t,t))f_p^r(x-\sqrt{a}t,t), \\ E_f^*(x,t) &= \beta^r(x-\sqrt{a}t,t)E_f(u(x-\sqrt{a}t,0)), \\ g_p^*(x,t) &= (1-\beta^r(x+\sqrt{a}t,t))g_p^r(x+\sqrt{a}t,t), \\ E_g^*(x,t) &= \beta^r(x+\sqrt{a}t,t)E_g(u(x+\sqrt{a}t,0)). \end{aligned}$$

Unfortunately now the hybrid structure of the solution is not kept since $E_f^*(x,t)$ and $E_g^*(x,t)$ are not equilibrium states. For example the above set of equations can be solved taking

$$\beta^c(x,t) = 0, \tag{1.3.20}$$

and

$$f^c(x,t) = f_p^*(x,t) + E_f^*(x,t), \tag{1.3.21}$$

$$g^c(x,t) = g_p^*(x,t) + E_g^*(x,t). \tag{1.3.22}$$

Thus we need to resample the whole deterministic fraction $E_f^*(x,t)$ and $E_g^*(x,t)$.

Note however that if we move one step t_1 further in the relaxation using $f^c(x,t)$ and $g^c(x,t)$ defined above as initial data we have $\beta^r(x,t+t_1) = 1-e^{-t_1/\varepsilon}$

and

$$\begin{aligned} f^r(x,t+t_1) &= (1-\beta^r(x,t+t_1))f_p^r(x,t+t_1)+ \\ &+ \beta^r(x,t+t_1)E_f(u^r(x,t+t_1)) \\ &= e^{-t_1/\varepsilon}f^c(x,t)+(1-e^{-t_1/\varepsilon})E_f(u^c(x,t)) \qquad (1.3.23) \\ &= e^{-t_1/\varepsilon}(f_p^*(x,t)+E_f^*(x,t))+(1-e^{-t_1/\varepsilon})E_f(u^c(x,t)), \\ g^r(x,t+t_1) &= (1-\beta^r(x,t+t_1))g_p^r(x,t+t_1)+ \\ &+ \beta^r(x,t+t_1)E_g(u^r(x,t+t_1)) \\ &= e^{-t_1/\varepsilon}g^c(x,t)+(1-e^{-t_1/\varepsilon})E_g(u^c(x,t)) \qquad (1.3.24) \\ &= e^{-t_1/\varepsilon}(g_p^*(x,t)+E_g^*(x,t))+(1-e^{-t_1/\varepsilon})E_g(u^c(x,t)). \end{aligned}$$

Thus, in practice, we can avoid to resample particles after the convection and apply the resampling only on a fraction $e^{-t_1/\varepsilon}$ of the deterministic fraction as needed by the relaxation. More precisely taking cell averages of (1.3.23)-(1.3.24) as in a standard Monte Carlo method, and using equations (1.3.13) for the reconstruction as shown later, the algorithm to compute the particles that represent the fractions $e^{-t_1/\varepsilon}f^c_{j+1/2}(t)$ and $e^{-t_1/\varepsilon}g^c_{j+1/2}(t)$ reads as follows

Algorithm 1.3.2 (Hybrid Monte Carlo for Jin-Xin relaxation)

1. *Given* $m = \dfrac{\Delta x}{N}\sum_j u^c_{j+1/2}(t)$

2. *for each interval* I_j, $j = \ldots,-2,-1,0,1,2,\ldots$

   (a) *set* $\beta_j = 1-e^{-t_1/\varepsilon}$

   (b) *set* $N_j = \text{Iround}\left((1-\beta_j)\dfrac{\Delta x}{m}u^c_{j+1/2}(t)\right)$

   (c) *set* $P_j = \dfrac{u^*_{p,j+1/2}(t)}{u^*_{p,j+1/2}(t)+u^*_{E,j+1/2}(t)}$,
   with $u^*_{p,j+1/2}(t) = f^*_{p,j+1/2}(t)+g^*_{p,j+1/2}(t)$
   and $u^*_{E,j+1/2}(t) = E^*_{f,j+1/2}(t)+E^*_{g,j+1/2}(t)$

   (d) *for* $k = 1,\ldots,N_j$
   with probability P_j *take* (ν_k,χ_k) *as one of the advected particles.*
   with probability $1-P_j$ *take one sample* ν_k *from the deterministic fraction. To extract such a sample do the following*

i. with probability $\dfrac{E^*_{f,j+1/2}(t)}{u^*_{E,j+1/2}}$ *take* $\nu_k = \sqrt{a}$

ii. with probability $\dfrac{E^*_{g,j+1/2}(t)}{u^*_{E,j+1/2}(t)}$ *take* $\nu_k = -\sqrt{a}$

iii. take χ_k *uniformly distributed in* I_j

After this the hybrid solution is computed simply adding the deterministic terms

$$\beta_j E_f(u^c_{j+1/2}(t)), \quad \beta_j E_g(u^c_{j+1/2}(t))$$

to the stochastic terms

$$(1-\beta_j) f^r_{p,j+1/2}(t) = \frac{m}{\Delta x} N_j^+, \quad (1-\beta_j) g^r_{p,j+1/2}(t) = \frac{m}{\Delta x} N_j^-$$

where N_j^+ and N_j^- are the number of samples in cell I_j equal to $\sqrt{a}$ and $-\sqrt{a}$ respectively.

This permits to avoid inefficient discard-resample procedures for small values of ε. For example, as $\varepsilon \to 0$ we do not perform any resampling at all, and we obtain a relaxation scheme for the limiting scalar conservation law.

Remark 1.3.3

- *The convection part corresponding to* $f^*_p(x,t)$ *and* $g^*_p(x,t)$ *is solved exactly by transport of particles as in a full Monte Carlo method. At variance the convection part corresponding to* $E^*_f(x,t)$ *and* $E^*_g(x,t)$ *can be solved by finite volumes or finite differences since it corresponds to solve the convection step with initial data* $f(x,0) = \beta^r(x,t) E_f(u(x,0))$ *and* $g(x,0) = \beta^r(x,t) E_g(u(x,0))$.

- *At variance with the simple Monte Carlo method positivity of the hybrid solution and presence of time step restrictions depend on the deterministic scheme used to solve the convection part for* $E^*_f(x,t)$ *and* $E^*_g(x,t)$.

- *Note that the effective value of* β_j *used in the above algorithm differs from* $1 - e^{-t_1/\varepsilon}$. *In fact if* N^c_j *denotes the number of particles in cell* j *after the convection step, during the relaxation we keep only an integer approximation* N^β_j *of* $(1-\beta_j)N^c_j$. *The effective value of* β_j *can then be computed at the end of the algorithm as*

$$\beta^E_j = 1 - \frac{N^\beta_j}{N^c_j}.$$

1.3.3 A Componentwise hybrid method (CHM)

A better approach would consist in finding the maximum value of $\beta^c(x,t) > 0$ in order to maximize the deterministic fraction in equations (1.3.19). In order to achieve this goal we consider the componentwise hybrid representation

$$f(x,t) = \tilde{f}(x,t) + w_f(x,t)E_f(u(x,t)), \tag{1.3.25}$$
$$g(x,t) = \tilde{g}(x,t) + w_g(x,t)E_g(u(x,t)). \tag{1.3.26}$$

The relaxation step now leads to

$$\begin{aligned} f^r(x,t) &= \tilde{f}^r(x,t) + w_f^r(x,t)E_f(u^r(x,t)) \\ &= e^{-t/\varepsilon}[\tilde{f}(x,0) + w_f(x,0)E_f(u(x,0))] + \\ &+ (1-e^{-t/\varepsilon})E_f(u(x,0)), \\ g^r(x,t) &= \tilde{g}^r(x,t) + w_g^r(x,t)E_g(u^r(x,t)) \\ &= e^{-t/\varepsilon}[\tilde{g}(x,0) + w_g(x,0)E_g(u(x,0))] + \\ &+ (1-e^{-t/\varepsilon})E_g(u(x,0)). \end{aligned}$$

Again by equating the equilibrium terms and the non equilibrium ones in the above equations we obtain the evolution for the unknowns $\tilde{f}^r(x,t)$, $\tilde{g}^r(x,t)$, $w_f^r(x,t)$ and $w_g^r(x,t)$

$$\tilde{f}^r(x,t) = e^{-t/\varepsilon}\tilde{f}(x,0), \quad w_f^r(x,t) = e^{-t/\varepsilon}w_f(x,0) + 1 - e^{-t/\varepsilon}, \tag{1.3.27}$$
$$\tilde{g}^r(x,t) = e^{-t/\varepsilon}\tilde{g}(x,0), \quad w_g^r(x,t) = e^{-t/\varepsilon}w_g(x,0) + 1 - e^{-t/\varepsilon}. \tag{1.3.28}$$

As before the hybrid representation is kept by the relaxation process. The only difference with respect to the HM method is that we discard particles from f and g with different ratios.

The convection destroys the structure of the solution and we get

$$\begin{aligned} f^c(x,t) &= \tilde{f}^c(x,t) + w_f^c(x,t)E_f(u^c(x,t)) = f^r(x-\sqrt{a}t,t) \\ &= \tilde{f}^r(x-\sqrt{a}t,t) + w_f^r(x-\sqrt{a}t,t)E_f(u(x-\sqrt{a}t,0)) \quad (1.3.29) \\ g^c(x,t) &= \tilde{g}^c(x,t) + w_g^c(x,t)E_f(u^c(x,t)) = g^r(x+\sqrt{a}t,t) \\ &= \tilde{g}^r(x+\sqrt{a}t,t) + w_g^r(x+\sqrt{a}t,t)E_g(u(x+\sqrt{a}t,0)) \quad (1.3.30) \end{aligned}$$

To simplify notations let us set

$$f_p^*(x,t) = \tilde{f}^r(x-\sqrt{a}t,t), \quad \tilde{E}_f(x,t) = w_f^r(x-\sqrt{a}t,t)E_f(u(x-\sqrt{a}t,0)),$$
$$g_p^*(x,t) = \tilde{g}^r(x+\sqrt{a}t,t), \quad \tilde{E}_g(x,t) = w_g^r(x+\sqrt{a}t,t)E_g(u(x+\sqrt{a}t,0)).$$

Here we do not assume $w_f^c(x,t) = 0$, $w_g^c(x,t) = 0$ since we want to take advantage of the componentwise hybrid representation in order to maximize the deterministic fraction of the solution. Thus, starting from the deterministic fractions $\tilde{E}_f(x,t)$ and $\tilde{E}_g(x,t)$ defined above we construct the new values of $w_f^c(x,t)$, $\tilde{f}^c(x,t)$, $w_g^c(x,t)$ and $\tilde{g}^c(x,t)$ using Definition 1.3.1.

More precisely we define

$$w_f^c(x,t) = \begin{cases} \dfrac{\tilde{E}_f(x,t)}{E_f(u^c(x,t))}, & \tilde{E}_f(x,t) \le E_f(u^c(x,t)) \neq 0 \\ 1, & \tilde{E}_f(x,t) \ge E_f(u^c(x,t)) \end{cases} \tag{1.3.31}$$

and

$$E_f^*(x,t) = \tilde{E}_f(x,t) - w_f^c(x,t) E_f(u^c(x,t)). \tag{1.3.32}$$

In this way we obtain

$$\tilde{f}^c(x,t) = f_p^*(x,t) + E_f^*(x,t). \tag{1.3.33}$$

Note that if $\tilde{E}_f(x,t) \le E_f(u^c(x,t)) \neq 0$ we have $\tilde{f}^c(x,t) = f_p^*(x,t)$ and thus we keep all the deterministic fraction. Similarly we compute $w_g^c(x,t)$ and $\tilde{g}_p^c(x,t)$.

The next relaxation step then applies straightforwardly using directly Algorithm 3.3.3 on cell averages. In fact moving one step further we have

$$\begin{aligned} f^r(x,t+t_1) &= \tilde{f}^r(x,t+t_1) + w_f^r(x,t+t_1) E_f(u^r(x,t+t_1)) \\ &= e^{-t_1/\varepsilon} f^c(x,t) + (1 - e^{-t_1/\varepsilon}) E_f(u^c(x,t)) \qquad (1.3.34) \\ &= e^{-t_1/\varepsilon}(f_p^*(x,t) + E_f^*(x,t) + w_f(x,t) E_f(x,t)) + \\ &+ (1 - e^{-t_1/\varepsilon}) E_f(u^c(x,t)) \\ g^r(x,t+t_1) &= \tilde{g}^r(x,t+t_1) + w_g^r E_g(u^r(x,t+t_1)) \\ &= e^{-t_1/\varepsilon} g^c(x,t) + (1 - e^{-t_1/\varepsilon}) E_g(u^c(x,t)) \qquad (1.3.35) \\ &= e^{-t_1/\varepsilon}(g_p^*(x,t) + E_g^*(x,t) + w_g(x,t) E_g(x,t)) + \\ &+ (1 - e^{-t_1/\varepsilon}) E_g(u^c(x,t)). \end{aligned}$$

The only difference is that now the final hybrid solution is recovered adding the deterministic terms

$$((1-\beta_j) w_f(x_{j+1/2},t) + \beta_j) E_f(u_{j+1/2}^c(t)),$$
$$((1-\beta_j) w_g(x_{j+1/2},t) + \beta_j) E_g(u_{j+1/2}^c(t))$$

in each cell.

Remark 1.3.4 *If we define after the convection step*

$$\beta^c(x,t) = \min\{w_f^c(x,t), w_g^c(x,t)\}, \tag{1.3.36}$$

we maximize the common value of β^c such that the standard hybrid method applies. This is particularly relevant in many applications where it is important that the hybrid decomposition is component independent. For example for more general relaxation terms.

1.4 Implementation and numerical tests

In this section we report some numerical results for the different schemes considered. We use the shorthand MCM, HM1, HM2 and CHM to denote the Monte Carlo Method, the Hybrid Method with the choices (1.3.20) and (1.3.36) respectively, and the Componentwise Hybrid Method.

1.4.1 High resolution scheme for the equilibrium component

In order to compute the evolution of the deterministic part of the solution in all the hybrid methods we use a second order MUSCL type scheme based on cell averages [76]. The second order scheme is defined taking as a flux

$$F_j(x_i) = \frac{f_j(x_{i-j+2}) - f_j(x_{i-j+1})}{\triangle x}\phi(\theta_j(x_i)) \tag{1.4.1}$$

where ϕ_j is the limiter function

$$\phi_j = \phi(\theta_j), \qquad \theta_j(x_i) = [\frac{f_j(x_i) - f_j(x_{i-1})}{f_j(x_{i+1}) - f_j(x_i)}]^{i_j}.$$

For example the so-called "superbee" of Roe

$$\phi(\theta) = \max(0, \min(1, 2\theta), \min(\theta, 2)).$$

Finally the scheme for the convection step is defined as

$$\begin{aligned} f_j^{n+1/2}(x_i) &= f_j^n(x_i) + \eta(f_j^n(x_{i+i_j}) - f_j^n(x_i)) - \\ &+ i_j\frac{\eta(1-\eta)}{2}[F_j^n(x_{i+i_j})\triangle x - F_j^n(x_{i_j})\triangle x], \quad j = 1,2 \end{aligned} \tag{1.4.2}$$

where $\eta = \frac{\triangle t}{\triangle x}$ and $i_j = (-1)^j$. As $\varepsilon \to 0$ the relaxation step becomes a projection step and thus we obtain a second order in space, first order in time relaxation scheme [66] for the limiting scalar conservation law. Extension to the multidimensional case can be done as usual dimension by dimension.

1.4.2 Jin-Xin system

In all tests we take initially the solution represented by samples and $F(u) = u^2/2$ (thus as $\varepsilon \to 0$ we have the Burgers equation). We consider the following test cases with periodic boundary conditions.

1D case

First we consider a one-dimensional test problem with initial data

$$u(x,0) = \frac{1}{4}(2 + \sin(2\pi x) - \sin(\pi x)), \quad x \in [-1,1], \quad t \in [0,1]. \tag{1.4.3}$$

We report the numerical solution for different values of the relaxation parameter $\varepsilon = 0.1,\ 0.01,\ 0.001$ with 200 grid points starting initially with $N = 10^3$ particles. The particle solution has been reconstructed using the simple formula (1.3.13). The final computing times are given in the figures captions (see Figure 1.2 and Figure 1.3). We also compute the L_1 norm of the error in time using a finite difference solution on a very fine mesh(six times the mesh of the methods) as a reference result (see Figure 1.4).

In the same figure the number of particles as a function of time is also given. The variance reduction of hybrid methods with respect to standard MCM is evident. In particular HM2 and CHM have the better efficiency and accuracy properties.

2D case

Next we consider the 2D case

$$\begin{aligned} &\partial_t u + \partial_x v + \partial_y w = 0, \\ &\partial_t v + \partial_x p(u) = -\frac{1}{\varepsilon}(v - F(u)), \\ &\partial_t w + \partial_y q(u) = -\frac{1}{\varepsilon}(w - G(u)), \end{aligned} \tag{1.4.4}$$

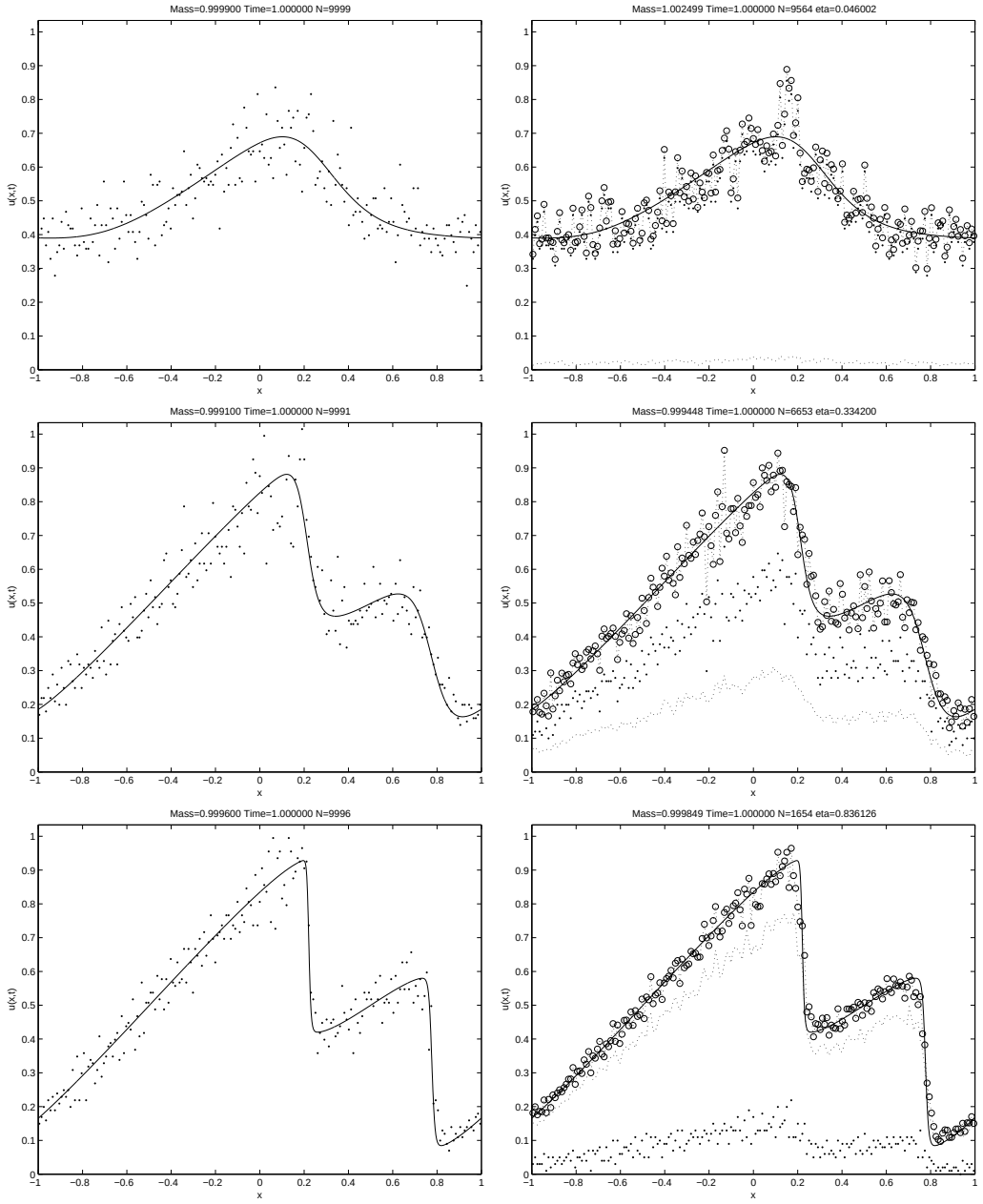

Figure 1.2: 1D case: Solution at $t = 1$ with $\varepsilon = 0.1$ (top), $\varepsilon = 0.01$ (middle) and $\varepsilon = 0.001$ (bottom) for MCM (left) and HM1 (right), with initial data (1.4.3). Particle solution ($\cdot$), equilibrium solution (dashed line) and hybrid solution ($\circ$).

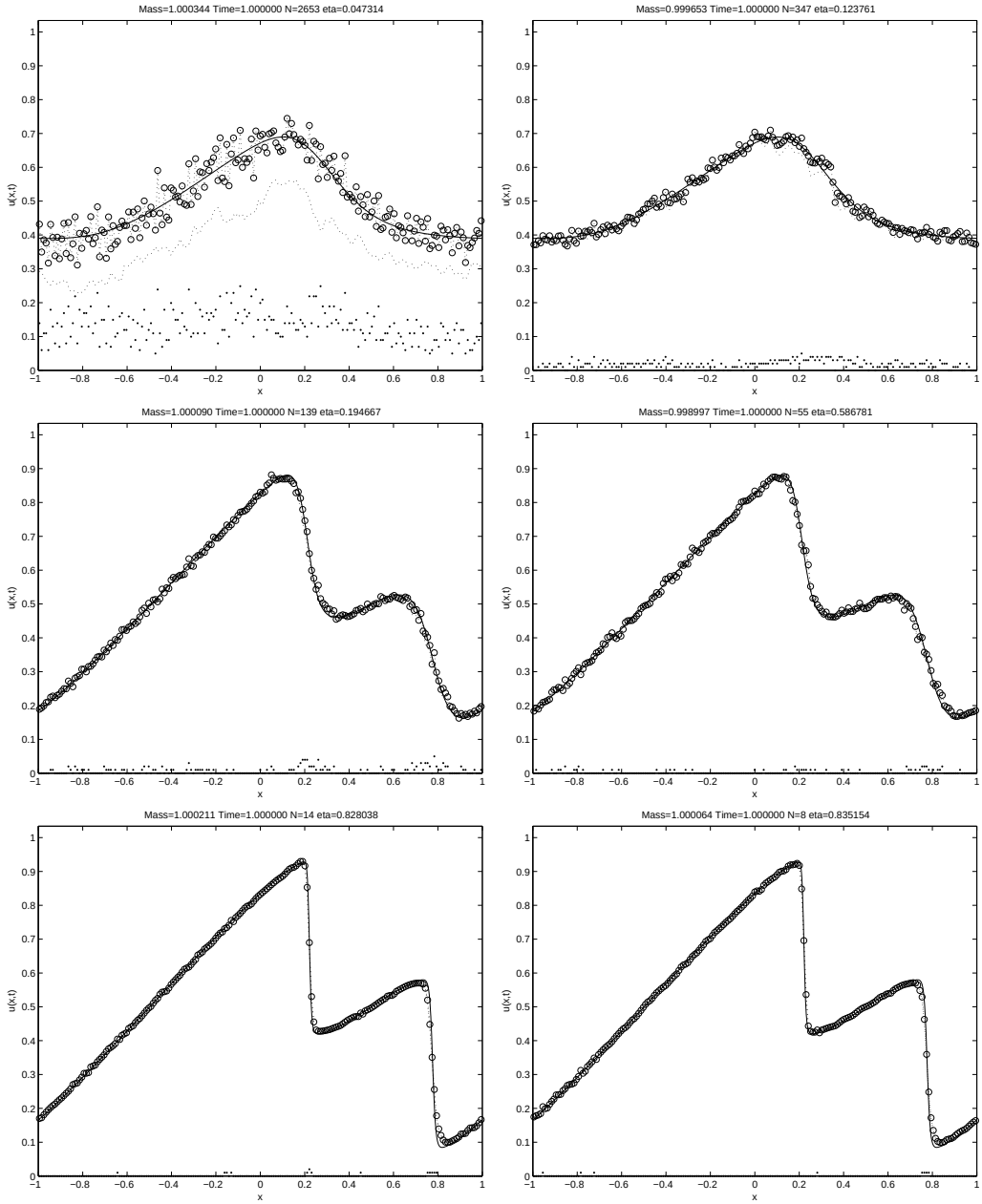

Figure 1.3: 1D case: Solution at $t = 1$ with $\varepsilon = 0.1$ (top), $\varepsilon = 0.01$ (middle) and $\varepsilon = 0.001$ (bottom) for HM2 (left) and CHM (right), with initial data (1.4.3). Particle solution ($\cdot$), equilibrium solution (dashed line) and hybrid solution ($\circ$).

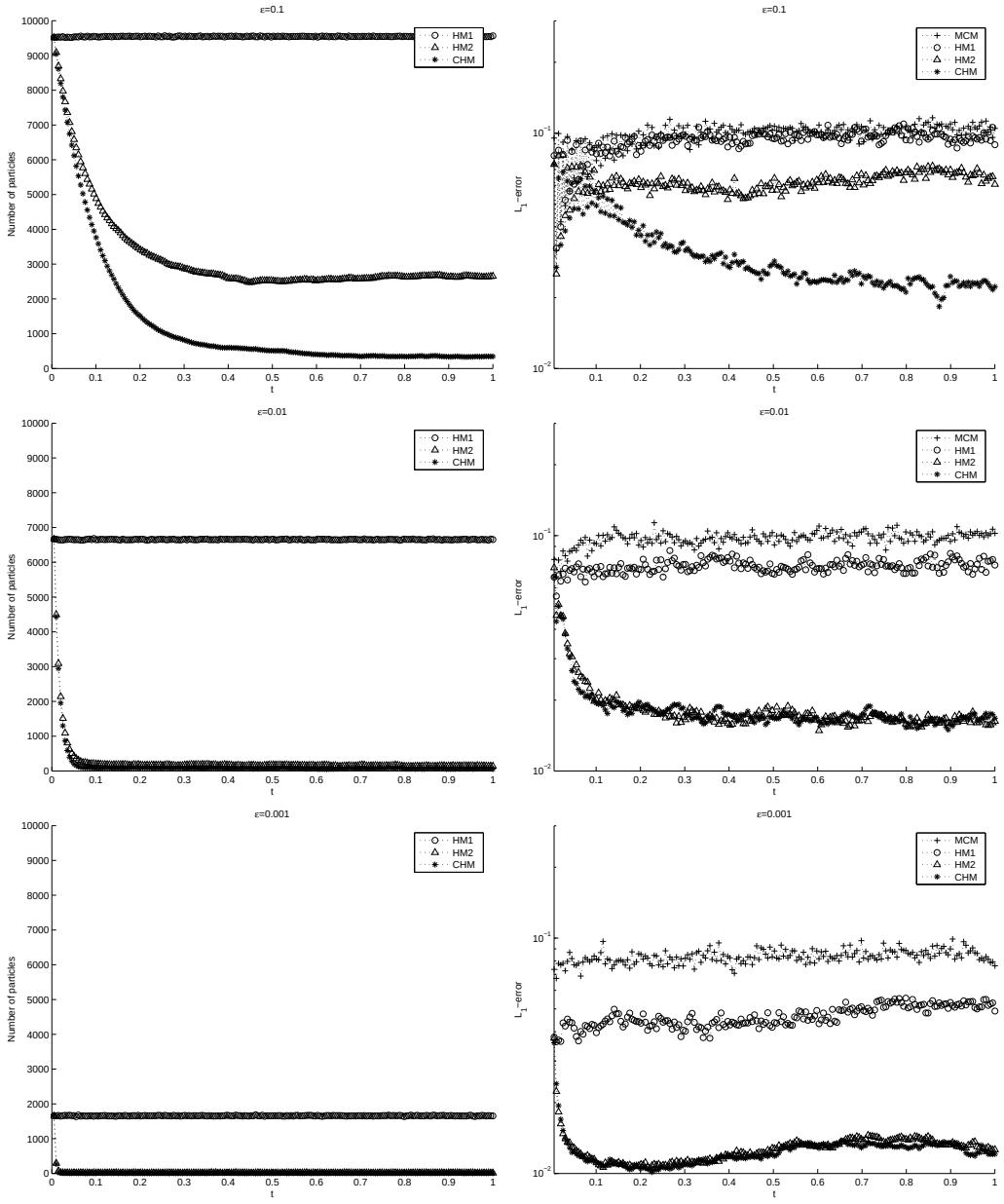

Figure 1.4: 1D case: Number of particles (left) and relative L_1-error in time (right) for $\varepsilon = 0.1$ (top), $\varepsilon = 0.01$ (middle) and $\varepsilon = 0.001$ (bottom), for (1.4.3) initial data.

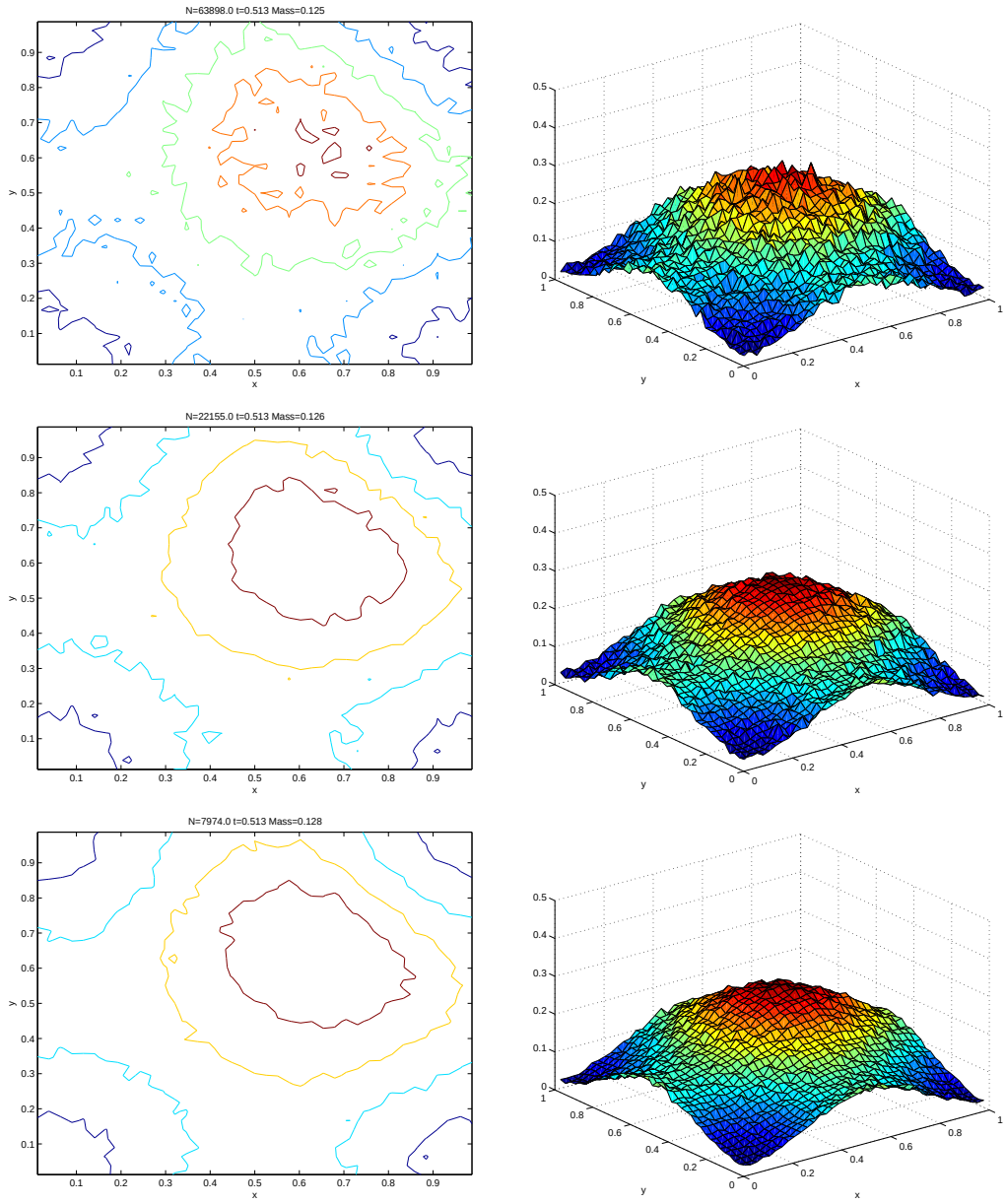

Figure 1.5: 2D case: Solution at $t = 0.5$ with $\varepsilon = 0.1$ for HM (top) HM1 (middle) and CHM (bottom).

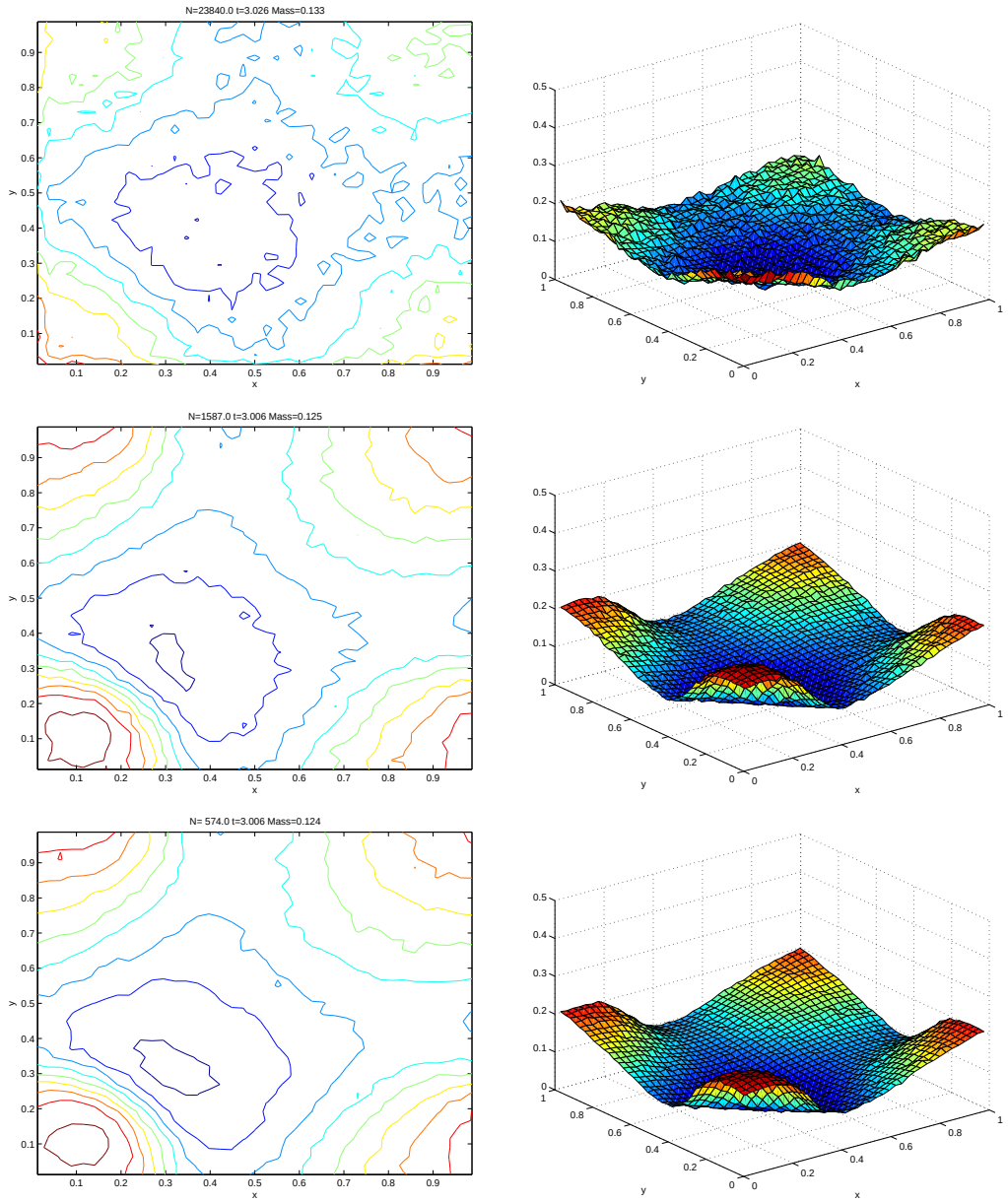

Figure 1.6: 2D case: Solution at $t = 3$ with $\varepsilon = 0.01$ for HM (top) HM1 (middle) and CHM (bottom).

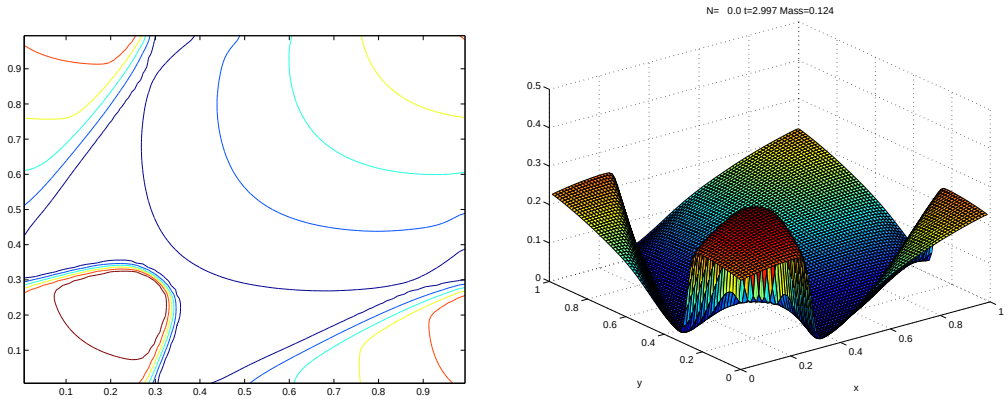

Figure 1.7: 2D case: Solution at $t = 3$ with $\varepsilon = 10^{-6}$ for HM methods.

with $F(u) = G(u) = u^2/2$. For $\varepsilon \to 0$ we obtain the 2D Burgers equation

$$\partial_t u + \partial_x \frac{u^2}{2} + \partial_y \frac{u^2}{2} = 0. \tag{1.4.5}$$

We consider periodic boundary conditions and initial data

$$u(x, y) = \sin(\pi x)^2 \sin(\pi y)^2, \quad (x, y) \in [0, 1]^2.$$

First we report the result for the three hybrid methods for $\varepsilon = 0.1$ and $\varepsilon = 0.01$ using a 40×40 mesh. The initial data is represented by $N = 8 \times 10^4$ particles. The results and the final computation times are shown in Figure 1.5 for $\varepsilon = 0.1$ and in Figure 1.6 for $\varepsilon = 0.01$. Finally we also report the result obtained for $\varepsilon = 10^{-6}$ with a 80×80 mesh (Figure 1.7). In this latter case, due to the small value of ε all hybrid methods yield essentially the same result corresponding to the second order relaxation scheme for the limiting equation.

1.4.3 Broadwell models

The extension of the above schemes to the case of the Broadwell model equations does not present any particular difficulty and we omit the details. We solve the Broadwell equations with $\alpha = 1$, corresponding to the four velocity reduced Broadwell model, with the following initial data

$$\rho(x, 0) = 2 \;\; m = 1 \;\; z = 1 \;\; x < 0,$$

$$\rho(x,0) = 1 \;\; m = 0.13692 \;\; z = 1 \;\; x > 0.$$

We integrate over the domain $[-1,1]$ with reflecting boundary condition. We use 100 grid points for $\varepsilon = 1$ and $\varepsilon = 0.02$ and 200 grid points for $\varepsilon = 0.001$ starting initially with $N = 3 * 10^3$ particles. The reference solution is obtained using a second order finite difference solver with six times the cells number of the computed hybrid solution. We report the results obtained with the different hybrid methods and the Monte Carlo method (MCM) depicted with the reference solution. Note that the initial datum for z is not a local equilibrium, which yields an initial layer. First we consider the case $\varepsilon = 1$ (Figure 1.8) corresponding to a non stiff (rarefied) regime where all the hybrid methods give a very similar result to MCM. In fact, we are far from the local thermal equilibrium and the solution is represented mostly by samples in all schemes. In the intermediate regime (Figure 1.9, where Δx, Δt and ε are of the same order, the methods give different results, in particular HM1 is very close to MCM, whereas HM2 and CHM provide a more accurate solution with less fluctuations due to the stochastic component of the solution.

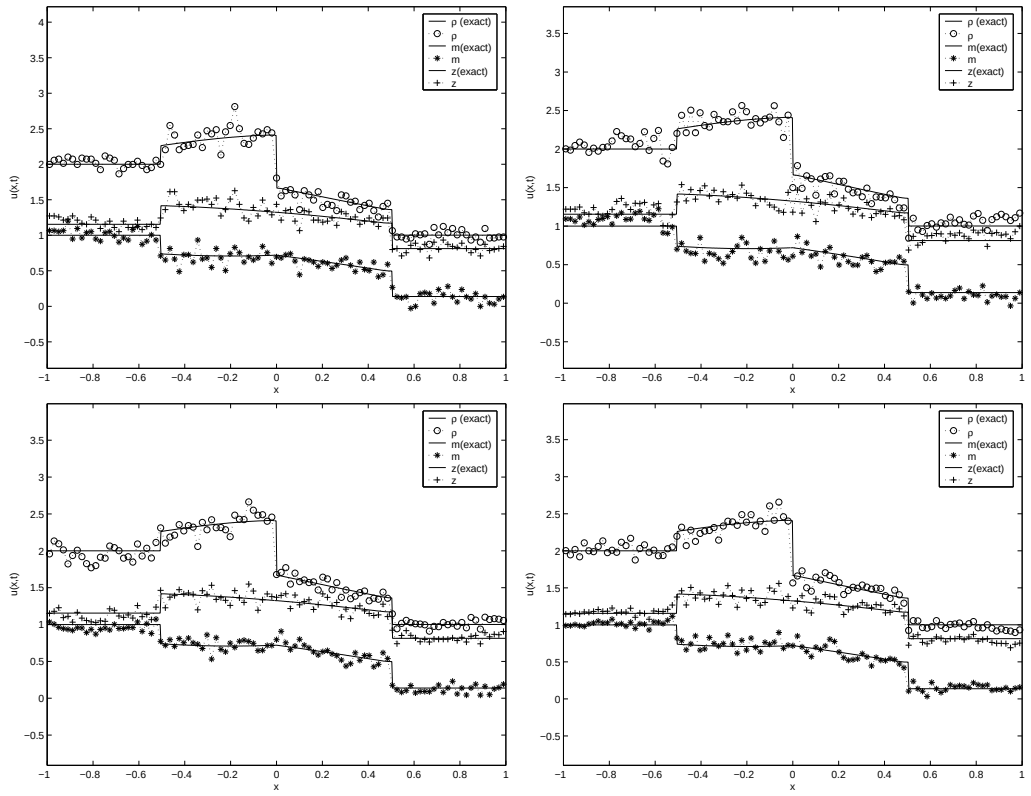

Figure 1.8: The numerical solutions of Broadwell equations for $\varrho = (\circ)$, $m = (+)$ and $z(*)$ with MCM (top left) HM1 (top right) HM2 (bottom left) CHM (bottom right) for $\varepsilon = 1$.

The small hump that is possible to notice near $x = -0.2$ is part of the exact solution. It is due to the fact that the initial condition represents an exact traveling shock wave for the relaxed system. Finally we consider the stiff regime $\varepsilon = 10^{-6}$ (Figure 1.10), corresponding to the Euler limit where the solution is a shock wave moving right with speed $s = 0.86038$ determined by the Rankine-Hugoniot jump condition. In this latter case all hybrid methods give essentially the same result due to the high resolution second order deterministic solver. The general methodology is based on a suitable blending of particles representation of the non equilibrium part of the solution with a finite difference or finite volume approximation of the equilibrium part.

1.5 Conclusion

In this paper we have considered the development of hybrid methods for multi-scale problems. Here we restricted our analysis to the case of hyperbolic systems with relaxation. In order to better explain the structure of the schemes we considered applications to simple relaxation systems. Several numerical results show the efficiency of the schemes and their ability to merge correctly the probabilistic and the deterministic fraction of the solution.

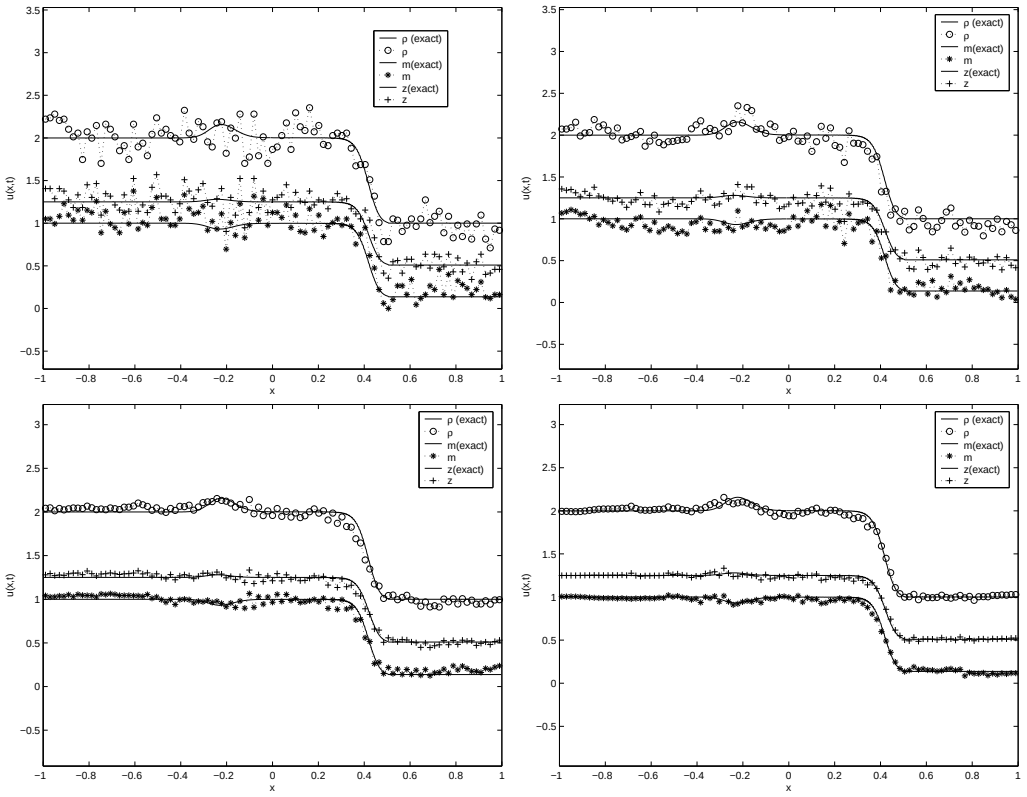

Figure 1.9: The numerical solutions of Broadwell equations for $\varrho = (\circ)$, $m = (+)$ and $z(*)$ with MCM (top left) HM1 (top right) HM2 (bottom left) CHM (bottom right) for $\varepsilon = 0.02$.

The schemes here presented rely on a relaxed scheme as deterministic solver and on a kinetic-like interpretation of the hyperbolic system for the Monte Carlo solver. Several interesting questions remain open among which we mention

- Inclusion in the schemes of a more general fluid solver.
- Extension of the present methods to kinetic equations and other multiscale problems such as diffusive limits.
- Convergence and error estimates for the hybrid schemes.

The prospects in these directions are encouraging and we hope to present more challenging results in the nearby future [44].

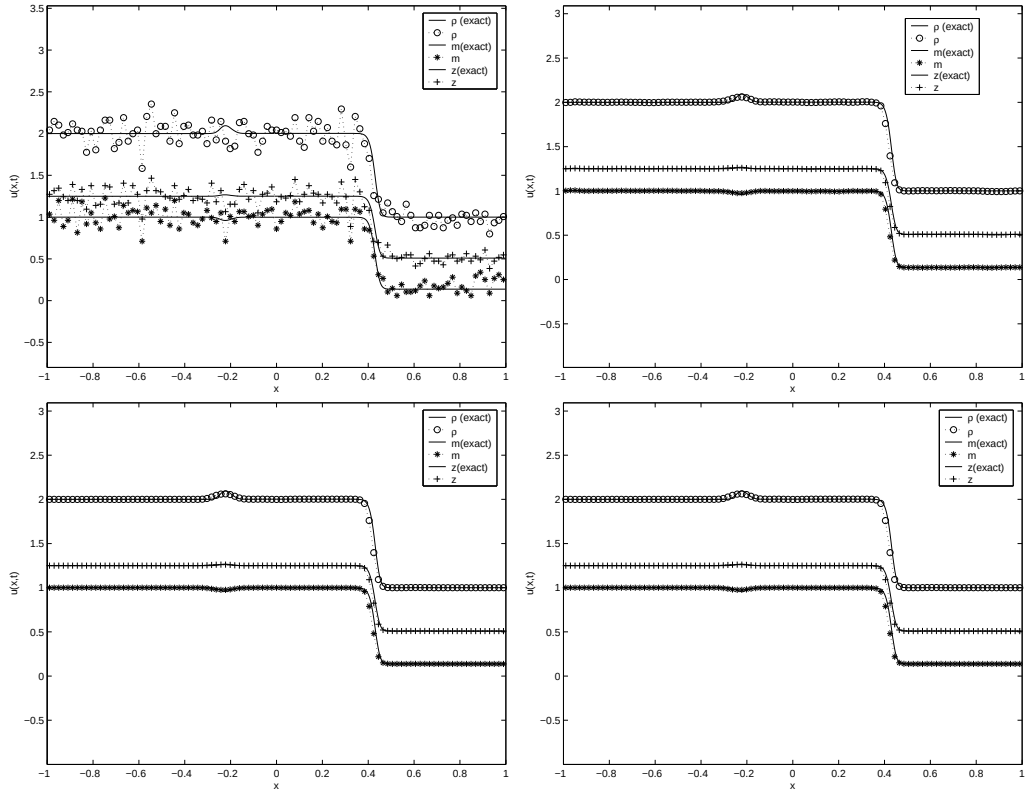

Figure 1.10: The numerical solutions of Broadwell equations for $\varrho = (\circ)$, $m = (+)$ and $z(*)$ with MCM (top left) HM1 (top right) HM2 (bottom left) CHM (bottom right) for $\varepsilon = 10^{-6}$.

Acknowledgements. The authors would like to thank Russ Caflisch for the many stimulating discussions.

Part II

Multiscale Kinetic Equations

Chapter 2

A Moving Interface Method for Dynamic Kinetic-Fluid Coupling

This Chapter is based on the work [40] published in **Journal of Computational Physics Vol. 227, pp. 1176-1208** in collaboration with Prof. Pierre Degond and Dott. Luc Mieussens of Université Paul Sabatier, Toulouse, France.

2.1 Introduction

In this work we consider the numerical simulation of fluid flows in rarefied regimes. In this situation the Navier-Stokes or the Euler equations do not provide a satisfactory description of the physical system and a kinetic description through the Boltzmann equation becomes necessary. In practice, we are primarily interested in the macroscopic scales of the problems but the solution of the microscopic model is necessary to obtain the correct representation of the physical phenomena. From the computational side, the numerical solution through such microscopic models remains nowadays too expensive even with the use of super-computers.

The most widely used numerical method for the Boltzmann equation is the Direct Simulation Monte-Carlo (DSMC) method (see [48], [50], [18] [16], [17], [44], [99]). It has many advantages in terms of computational cost for large dimensional problems, for enforcing physical properties such as conservation laws and in terms of flexibility when handling with complex geometries. On the other hand, these methods involve a significant level of numerical noise when the unsteady character of the problem does not permit averages on the solution. In these cases, if we want to preserve the efficiency in computational time, fluctuations can

be present as compared to deterministic methods. Moreover the convergence rate is in general quite slow.

In situations close to thermodynamical equilibrium, the cost of direct Monte Carlo simulations increases. For this reason, domain decomposition techniques have been proposed in the literature (see [10], [75], [71], [77], [38], [45], [128]). They allow a more efficient treatment of the regions close to thermodynamical equilibrium. Automatic domain decomposition methods have also been proposed, (see e.g. [73] or [122]). Indeed, in many situations, the resolution of the kinetic equations in the whole computational domain is unnecessary because the Euler or Navier-Stokes equations provide a sufficiently accurate solution, except in small zones like shock layers where departure from thermodynamical equilibrium is strong.

The present work is a contribution in this direction. We propose a numerical method for the resolution of the Boltzmann-BGK equation coupled with the compressible Euler equations through a domain decomposition technique. The validity of BGK model is sometimes questionnable. However it provides a cheaper model than the Boltzmann collision integral, in particular close to the fluid regime where the simulation of others models becomes extremely expensive. As a matter of convenience all the schemes and the algorithms are described in the one dimensional case in the paper, making it more readable. The extension to the multidimensional case do not introduce any difficulty in the schemes, only the definition of the different domains can create some trouble, which will be examined in a future work. We could also choose the Navier-Stokes model instead of the Euler model as a fluid model.

This paper is an extension of an earlier work [37], in which the domain decomposition technique is used to couple the BGK equation and the compressible Euler equations. In this earlier work, a buffer zone is introduced. In this buffer zone, the transition from the Boltzmann model to the hydrodynamic one and vice-versa is gradual. Therefore, in the buffer zone, both models are solved and the solution of the problem is obtained as the combination of the kinetic and fluid solutions. The buffer zone is materialized by a cut-off function which defines the gradual transition from one model to the other one. Additionally, the introduction of the cut-off makes each of the models degenerate at the boundary of the buffer zone. In this way, no interface condition is needed.

In the present work, we propose a methodology to allow for the time evolution of the buffer zone between the kinetic and fluid models. In this way, we can follow in time the regions where discontinuities or sharp gradients of the solution occur, and solve the microscopic model in these regions, while, in the rest of the domain,

we can use the macroscopic model. Thanks to this technique, it is possible to use as small a microscopic domain as possible, and to achieve considerable computational speedup compared with a steady interface coupling strategy. An important point in implementing this method is to use adequate criteria which allow to reliably identify the zones for which the microscopic model is necessary. Another novelty of the present work is to propose the use of a new indicator, the equilibrium fraction, which has been introduced in the works of Dimarco and Pareschi in [44].

The main features of the method can be summarized as follows:

- The domain is divided in regions where the solution is computed through kinetic equations and in regions where the solution is computed through Euler equations and in buffer zones where both model are used.
- During the simulation the zones move according to some equilibrium criteria in order to solve the kinetic model only where it is necessary.
- The utilized criteria are combinations of:
  - Checking the value of the Knudsen number against an adequate threshold value
  - Checking the values of the gradients of the macroscopic quantities (density, momentum) against an adequate threshold value
  - Measuring the equilibrium fraction in the kinetic zone.

The article is organized as follows. In section 2.2, we introduce the Boltzmann-BGK equations and its properties. In section 2.3, we present the coupling method and in section 2.4 the numerical schemes. Section 2.5 is devoted to the illustration of the equilibrium identification criteria. Several test problems which demonstrate the capabilities of the method are presented in section 2.6. Some final considerations and future developments are discussed in section 2.7.

2.2 Boltzmann-BGK Equation

2.2.1 The model

We consider the Boltzmann-BGK equation

$$\partial_t f + v \cdot \nabla_x f = \frac{1}{\tau}(M_f - f), \tag{2.2.1}$$

with the initial condition

$$f(x, v, t = 0) = f_0(x, v), \tag{2.2.2}$$

where $f = f(x, v, t)$ is a non negative function describing the time evolution of the distribution of particles which move with velocity $v \in \mathbb{R}^3$ in the position $x \in \Omega \subset \mathbb{R}^3$ at time $t > 0$. In the BGK equation the collisions are modeled by a relaxation towards the local thermodynamical equilibrium defined by the Maxwellian distribution function M_f. The local Maxwellian function is defined by

$$M_f = M_f[\varrho, u, T](v) = \frac{\varrho}{(2\pi\theta)^{3/2}} \exp\left(\frac{-|u - v|^2}{2\theta}\right), \tag{2.2.3}$$

where ϱ and u are the density and mean velocity while $\theta = RT$ with T the temperature of the gas and R the gas constant. The macroscopic values ϱ,u and T are related to f by:

$$\varrho = \int_{\mathbb{R}^3} f dv, \qquad u = \int_{\mathbb{R}^3} v f dv, \qquad \theta = \frac{1}{3\varrho} \int_{\mathbb{R}^3} |v - u|^2 f dv. \tag{2.2.4}$$

The energy E is defined as

$$E = \frac{1}{2} \int_{\mathbb{R}^3} |v|^2 f dv = \frac{1}{2}\varrho|u|^2 + \frac{3}{2}\varrho\theta. \tag{2.2.5}$$

The parameter $\tau > 0$ is the relaxation time. In this paper, we use the common choice $\tau = (\frac{\mu}{p})$ where $\mu = \mu_{ref} \cdot (\theta/\theta_{ref})^{\omega}$ is the viscosity and p is the pressure. We refer to section 2.6 for the numerical value of μ_{ref}, θ_{ref} and ω. Finally we define the kinetic entropy of f by

$$H(f) = \int_{\mathbb{R}^3} f \log f dv. \tag{2.2.6}$$

Now, if we consider the BGK equation (2.2.1), multiply it by 1, v, $\frac{1}{2}|v^2|$ (the so-called collision invariants), and integrate wit respect to v, we obtain the following balance laws:

$$\begin{aligned} &\frac{\partial \varrho}{\partial t} + \nabla_x \cdot (\varrho u) = 0, \\ &\frac{\partial \varrho u}{\partial t} + \nabla_x \cdot (\varrho u \otimes u + P) = 0, \\ &\frac{\partial}{\partial t} E + \nabla_x \cdot (Eu + Pu + q) = 0, \end{aligned} \tag{2.2.7}$$

which express the conservation of mass, momentum and energy, in which $P = \int (v-u) \otimes (v-u) f \, dv$ is the pressure tensor while $q = \int \frac{1}{2}(v-u)|v-u|^2 \, dv$ is the heat flux. Furthermore the following inequality expresses the dissipation of entropy:

$$\partial_t \left(\int f \log f \, dv \right) + \nabla_x \cdot \left(\int v f \log f \, dv \right) \leq 0. \tag{2.2.8}$$

System (2.2.7) is not closed, since it involves other moments of the distribution function than just ϱ, ϱu and E.

The Maxwellian M_f can be characterized as the unique solution of the following entropy minimization problem

$$H(M_f) = \min\{H(f),\ f \geq 0 \ s.t. \int_{\mathbb{R}^3} \mathbf{m} f \, dv = \boldsymbol{\varrho}\} \tag{2.2.9}$$

where $\mathbf{m}$ and $\boldsymbol{\varrho}$ are the vectors of the collision invariants and of the first three moments of f respectively:

$$\mathbf{m}(v) = (1, v, \frac{1}{2}|v|^2),\ \boldsymbol{\varrho} = (\varrho, \varrho u, E) \tag{2.2.10}$$

This is the well-known local Gibbs principle, and it expresses that the local thermodynamical equilibrium state minimizes the entropy, in the mathematical meaning, of all the possible states subject to the constraint that its moments $\boldsymbol{\varrho}$ are prescribed.

Formally as $\varepsilon \to 0$ the function f tends to Maxwellian. In this limit, it is possible to compute the moments P and q of f in terms of ϱ, ϱu and E. In this way, one can close the system of balance laws (2.2.7) and get the Euler system of compressible gas dynamics equations

$$\begin{aligned}
&\frac{\partial \varrho}{\partial t} + \nabla_x \cdot (\varrho u) = 0, \\
&\frac{\partial \varrho u}{\partial t} + \nabla_x \cdot (\varrho u \otimes u + pI) = 0, \\
&\frac{\partial E}{\partial t} + \nabla_x \cdot ((E+p)u) = 0, \\
&p = \varrho\theta, \quad E = \frac{3}{2}\varrho\theta + \frac{1}{2}\varrho|u|^2.
\end{aligned} \tag{2.2.11}$$

2.2.2 Boundary Conditions

Eq. (2.2.1) must be supplemented with boundary conditions for $x \in \partial\Omega$ and for $v \cdot n \geq 0$ where n denotes the unit normal, pointing inside the domain. The boundary conditions are expressed as follows:

$$|v \cdot n| f(v) = \int_{v_* \cdot n < 0} |v_* \cdot n| K(v_* \to v) f(v_*) dv_* \,, \tag{2.2.12}$$

where v_* is the particle velocity after its interaction with the boundary. The entering flux is described as a function of the outgoing flux modified by the boundary kernel K. Such a definition of the boundary condition preserve the mass if and only if

$$K(v_* \to v) \geq 0, \int_{v_* \cdot n \geq 0} K(v_* \to v) dv = 1. \tag{2.2.13}$$

Usually, the boundary condition is a convex combination of specular reflection and total accomodation. Specular reflection is the process by which the incoming velocity (i.e. after the interaction with the wall) is the symmetric of the outgoing velocity with respect to the tangent plane to the wall. Total accomodation instead means that the outgoing velocity loses the memory of the incoming velocity and is taken randomly according to a Maxwellian distribution at the wall temperature. Let α be the fraction of particles which suffer total accomodation and $1 - \alpha$ that of specularly reflected particles. With these assumptions, the boundary condition is written:

$$f(v) = (1 - \alpha) R f(v) \alpha M f(v), \; v \cdot n(x) \geq 0, \tag{2.2.14}$$

with

$$R f(v) = f(v - 2n(n \cdot v)), \quad M f(v) = \mu M_\omega(v). \tag{2.2.15}$$

If we denote by u_w and θ_w the wall velocity and temperature, M_w is given by

$$M_w[u_w, \theta_w](v) = \frac{1}{(2\pi\theta_w)^{3/2}} \exp\left(\frac{-|u_w - v|^2}{2\theta_w}\right), \tag{2.2.16}$$

and μ is determined by mass conservation

$$\mu \int_{v \cdot n \geq 0} M_w(v) |v \cdot n| dv = \int_{v \cdot n < 0} f(v) |v \cdot n| dv. \tag{2.2.17}$$

It is easy to show that this boundary condition enters the class of boundary conditions of the type (2.2.12), with a suitably defined (and possibly distributional)

kernel K. We note that for $\alpha = 0$ (pure specular reflection) the re-emitted particle have the same flow of mass, energy and tangential momentum as the incoming molecules, while as soon as $\alpha > 0$ (partial or full accommodation) the re-emitted particle partly or completely lose the memory of the incoming velocities. In particular, only mass is conserved.

2.3 The coupling method

2.3.1 Decomposition of the kinetic equation

For sake of simplicity we describe the method proposed in [37] in one space and velocity dimensions. It can be easily extended to a generic N-dimensional setting. Also different meshes for the cut-off function and for the other variables can be used.

We denote the buffer interval by $[a, b]$, and we introduce a cut-off function $h(x, t)$ such that

$$h(x,t) = \begin{cases} 1, & \text{for} \quad x \leq a \\ 0, & \text{for} \quad x \geq b \\ 0 \leq h(x,t) \leq 1, & \text{for} \quad x \in [a,b] \end{cases} \tag{2.3.1}$$

For instance, h can be chosen piecewise linear in $[a, b]$:

$$h(x,t) = \frac{x-b}{a-b} \quad \text{for} \quad x \in [a,b].$$

We define two distribution functions such that $f_R = hf$ while $f_L = (1-h)f$. We look now for an evolution equation for f_R and for f_L. We write

$$\begin{aligned} \partial_t f_R &= \partial_t(hf) = f\,\partial_t h + h\partial_t f, \\ \partial_t f_L &= \partial_t((1-h)f) = -f\,\partial_t h + (1-h)\partial_t f. \end{aligned}$$

Thus multiplying the Boltzmann-BGK equation (2.2.1) by h and $1-h$ respectively, (2.2.1) can be rewritten in the following form

$$\begin{aligned} \partial_t f_R &= f\,\partial_t h + h(-v\partial_x f + \frac{1}{\tau}(M_f - f)), \\ \partial_t f_L &= -f\,\partial_t h + (1-h)(-v\partial_x f + \frac{1}{\tau}(M_f - f)), \end{aligned}$$

which finally leads to the following system for f_L and f_R:

$$\partial_t f_R + hv\partial_x f_R + hv\partial_x f_L = \frac{h}{\tau}(M_f - f) + f\partial_t h, \tag{2.3.2}$$

$$\partial_t f_L + (1-h)v\partial_x f_L + (1-h)v\partial_x f_R = \frac{1-h}{\tau}(M_f - f) - f\partial_t h, \tag{2.3.3}$$

$$f = f_R + f_L \tag{2.3.4}$$

with initial data

$$f_R(x,v,0) = h(x,0)f(x,v,0)\,, \quad f_L(x,v,0) = (1-h(x,0))f(x,v,0). \tag{2.3.5}$$

It is important to note that if $f = f_L + f_R$ is the solution of (2.2.1) with initial data (2.2.2), then (f_L, f_R) is the solution of (2.3.2-2.3.3) with initial data (2.3.5) and conversely.

2.3.2 Kinetic-Hydrodynamic coupling

We refer to [37] for more detail about the derivation that follows. Let us assume that the domain can be subdivided in two regions: in one of the regions, the distribution function is close to a local Maxwellian while in the other, it is far from it. We choose to set $h = 0$ in the region where f is close to the Maxwellian. Therefore, $f_L = f$ is close to its associated Maxwellian $M_{f_L} = M_f$ and we can replace the Boltzmann equation by the Euler equations without making any significant error. We also suppose that in the buffer zone, f_L remains close to the equilibrium and thus, it can be replaced by M_{f_L} in the whole interval $x < b$.

Replacing f_L by M_{f_L} in (2.3.3) and taking the hydrodynamic moments (mass, momentum and energy), leads to the following modified Euler system defined in the interval $x \leq b$:

$$\begin{aligned}
&\frac{\partial \varrho_L}{\partial t} + (1-h)\partial_x(\varrho_L u_L) = -(1-h)\partial_x\left(\int_{\mathbb{R}} v f_R\, dv\right) - \varrho\partial_t h,\\
&\frac{\partial \varrho_L u_L}{\partial t} + (1-h)\partial_x(\varrho_L u_L^2 + p_L) = -(1-h)\partial_x\left(\int_{\mathbb{R}} v^2 f_R\, dv\right) - \varrho u\partial_t h,\\
&\frac{\partial E_L}{\partial t} + (1-h)\partial_x((E_L + p_L)u_L) = -(1-h)\partial_x\left(\int_{\mathbb{R}} v\frac{|v|^2}{2} f_R\, dv\right) - E\partial_t h,
\end{aligned} \tag{2.3.6}$$

with initial data

$$(\varrho_L, u_L, \theta_L)|_{(x,0)} = (1 - h|_{(x,0)})(\varrho, u, \theta)|_{(x,0)}.$$

Under these assumptions, we have $f = f_R + M_{f_L}$, where f_R is a solution of:

$$\partial_t f_R + hv\partial_x f_R + hv\partial_x M[\varrho_L, u_L, \theta_L] = \frac{h}{\tau}(M_f - f) + f\partial_t h, \tag{2.3.7}$$

in the interval $x \geq a$. The coupling model consists of system (2.3.6) for the hydrodynamic moments in the region $x \leq b$ and eq. (2.3.7) for the kinetic distribution function in the region $x \geq a$.

When $h = 0$, system (2.3.6) coincides with system (2.2.11) because $f_R = 0$ and $f_L = M_{f_L}$. Moreover no boundary condition is needed at the boudary $x = b$ because $h = 1$ at this point, and the factors in front of the spatial derivatives of (2.3.6) vanish (in other words, the spatial derivatives are degenerate at $x = b$ for the fluid model). A similar remark is true for f_R. Indeed, when $h = 0$, $f_R = 0$ and no boundary condition is needed for the kinetic equation at $x = a$ because $h = 0$ at this point and the factor in front of the spatial derivatives in (2.3.7) vanishes. In the buffer zone $[a, b]$, the solution of the full kinetic problem f is computed as the sum of the Maxwellian M_{f_L} and of the function f_R. To summarize, the solution of the full kinetic problem is given by f_R if $x > b$, by M_{f_L} if $x < a$ and by $M_{f_L} + f_R$ if $x \in [a, b]$.

An important feature of the method is that it is very easy to divide the domain in more than two zones. Thus we can define as many buffers and as many kinetic regions as necessary if the macroscopic model fails to give the correct solution in different parts of the domain which are far apart from each other. In this latter case, the function h is still a piecewise linear function but there are multiple buffer zones $[a_j, b_j]$. Additionally, we can create new buffer zones and new kinetic zones during the simulation. For this purpose, one can update the cut-off function h according to convenient criteria to a new value and reset $f_R = hf$ and $f_L = (1 - h)f$ at the time when h is changed. The way in which new zones are created is detailed in the next section. In the last section this technique will be tested on shock tube problems.

2.4 Numerical approximation of the coupled model

In this section we extend the simple numerical scheme proposed in [37] for the case of a steady buffer zone to the dynamical buffer zone case considered here. We also introduce a new scheme based on a time splitting of the equations which is able to circumvent some numerical problems that are observed with a direct discretization of the equations. Finally, we introduce a different, more efficient

kinetic scheme for the solution of the Euler equations. The scheme will be shown in the last section to dramatically increase the efficiency of the code.

2.4.1 Velocity discretization

We introduce a Cartesian grid $\mathcal{V}$ of N nodes $v_k = k\Delta v + a$, where k is a bounded index, Δv is the grid step, and a is a constant. We denote the discrete collision invariants by $\mathbf{m}_k = (1, v_k, \frac{1}{2}|v_k^2|)$. The continuous distribution function f is approximated by a discrete velocity model $(f_k(t,x))_k$, where $f_k(t,x) \approx f(x, v_k, t)$. The fluid quantities are obtained from f_k thanks to discrete summations on $\mathcal{V}$:

$$\boldsymbol{\varrho}(t,x) = \sum_k \mathbf{m}_k f_k(t,x)\,\Delta v. \tag{2.4.1}$$

The discrete velocity BGK model consists of a set of N evolution equations for f_k:

$$\partial_t f_k + v_k \cdot \nabla_x f_k = \frac{1}{\tau}(\mathcal{E}_k[\boldsymbol{\varrho}] - f_k), \tag{2.4.2}$$

where $\mathcal{E}_k[\boldsymbol{\varrho}]$ is an approximation of M_f such that (2.4.2) satisfies the same properties of conservation (2.2.7) and entropy (2.2.8) as the continuous model (2.2.1). Namely we have

$$\mathcal{E}_k[\boldsymbol{\varrho}] = \exp(\boldsymbol{\alpha}(\boldsymbol{\varrho}) \cdot \mathbf{m}_k), \tag{2.4.3}$$

where $\boldsymbol{\alpha}(\boldsymbol{\varrho})$ solves the nonlinear equation

$$\sum_k \mathbf{m}_k \exp(\boldsymbol{\alpha}(\boldsymbol{\varrho}) \cdot \mathbf{m}_k)\,\Delta v = \boldsymbol{\varrho}. \tag{2.4.4}$$

These equations can be solved by a Newton algorithm. In the velocity continuous case the parameters $\boldsymbol{\alpha}$ are

$$\boldsymbol{\alpha} = \left(\log\left(\frac{\varrho}{(2\pi\theta)^{\frac{1}{2}}} - \frac{|u|^2}{2\theta}\right), \frac{u}{\theta}, -\frac{1}{\theta}\right) \tag{2.4.5}$$

This discretization (existence, uniqueness, convergence) has been mathematically studied in [84, 86].

2.4.2 Space and time discretization of the kinetic part

According to the previous section, the velocity discretized version of (2.3.7) is

$$\partial_t f_{k,R} + h v_k \partial_x f_{k,R} + h v_k \partial_x \mathcal{E}_k[\boldsymbol{\varrho}_L] = \frac{h}{\tau}(\mathcal{E}_k[\boldsymbol{\varrho}] - f_k) + f_k \partial_t h, \tag{2.4.6}$$

where $f_{k,R}$ is an approximation of $f_R(t, x, v_k)$, and $\mathcal{E}_k[\boldsymbol{\varrho}_L]$ is an approximation of $M[\varrho_L, u_L, \theta_L]$ defined as in (2.4.3)–(2.4.4) with $\boldsymbol{\varrho}$ replaced by $\boldsymbol{\varrho}_L$. Finally, f_k is the global distribution defined as in the continuous case by $f_k = f_{k,R} + \mathcal{E}_k[\boldsymbol{\varrho}_L]$, and the corresponding global Maxwellian $\mathcal{E}_k[\boldsymbol{\varrho}]$ is defined accordingly with $\boldsymbol{\varrho}$ being the moments of f_k.

Consider a spatial Cartesian uniform grid defined by nodes $x_i = i\Delta x$ and a time discretization $t_n = n\Delta t$. If $f_i^n = (f_{k,i}^n)_k$ is an approximation of $(f_k(t_n, x_i))$, the moments of f_i^n are $\boldsymbol{\varrho}_i^n = \sum_k \mathbf{m}_k f_i^n \, \Delta v$. The corresponding discrete equilibrium is $\mathcal{E}_k[\boldsymbol{\varrho}_i^n]$ is defined as in (2.4.3)–(2.4.4)

Eq. (2.4.6) constitutes a set of linear hyperbolic equations with source terms. The transport part is simply a linear convection equation and can be approximated by any standard finite volume scheme. For the discretization in time we use an explicit Euler method. The scheme finally reads

$$\begin{aligned} f_{k,i,R}^{n+1} = f_{k,i,R}^n &- h_i^{n+1} \frac{\Delta t}{\Delta x} \left(\phi_{i+1/2}(f_{k,R}^n) - \phi_{i-1/2}(f_{k,R}^n) \right) \\ &- h_i^{n+1} \frac{\Delta t}{\Delta x} \left(\phi_{i+1/2}(\mathcal{E}_k[\boldsymbol{\varrho}_L^n]) - \phi_{i-1/2}(\mathcal{E}_k[\boldsymbol{\varrho}_L^n]) \right) \\ &+ h_i^{n+1} \frac{\Delta t}{\tau_i^n} \left(\mathcal{E}_k[\boldsymbol{\varrho}_i^n] - f_{k,i}^n \right) + f_{k,i}^n (h_i^{n+1} - h_i^n). \end{aligned} \tag{2.4.7}$$

For every grid function $(g_{k,i})_{k,i}$, the numerical fluxes are defined by

$$\phi_{i+1/2}(g_k) = \frac{1}{2} \left(v_k g_{k,i+1} + v_k g_{k,i} - |v_k|(g_{k,i+1} - g_{k,i}) \right). \tag{2.4.8}$$

The updated value of the function h_i^{n+1} is computed, with the criteria described in section 2.5, at the beginning of each time step. Thus at time step $n+1$, we compute h^{n+1} and next we compute the new value of f_R. The time step is computed through an estimate of the CFL number:

$$\Delta t \left(\max_i (\frac{1}{\tau_i^n}) + \max_k \left(\frac{|v_k|}{\Delta x} \right) \right) < 1. \tag{2.4.9}$$

2.4.3 Space and time discretization for the hydrodynamic part

A simple kinetic scheme for (2.3.6) is obtained by first discretizing (2.3.3) as we did for (2.3.2) in the section above. Then like in the continuous case, we take the moments of the corresponding discrete equation, and $f^n_{L,k,i}$ is replaced by $\mathcal{E}_k[\boldsymbol{\varrho}^n_{L,i}]$. This leads to

$$\begin{aligned}\boldsymbol{\varrho}^{n+1}_{i,L} = \boldsymbol{\varrho}^n_{i,L} &- (1-h_i^{n+1})\frac{\Delta t}{\Delta x}\sum_k \mathbf{m}_k \left(\phi_{i+1/2}(\mathcal{E}_k[\boldsymbol{\varrho}^n_L]) - \phi_{i-1/2}(\mathcal{E}_k[\boldsymbol{\varrho}^n_L])\right)\Delta v \\ &- (1-h_i^{n+1})\frac{\Delta t}{\Delta x}\sum_k \mathbf{m}_k \left(\phi_{i+1/2}(f^n_{k,R}) - \phi_{i-1/2}(f^n_{k,R})\right)\Delta v \\ &- (h_i^{n+1}-h_i^n)\boldsymbol{\varrho}^n_i.\end{aligned} \tag{2.4.10}$$

Again we first compute h^{n+1} at the beginning of the time step and afterwards, we advance $\boldsymbol{\varrho}_L$ in time. The severe time restrictions which occur with the kinetic scheme due to the relaxation parameter ε, do not occur with the hydrodynamic model. Thus, it would be possible to use different time steps for the fluid and kinetic parts of the model. We leave the implementation of this improvement to future work.

2.4.4 An alternative scheme: time splitting

We propose here an alternative to the previous scheme which consists of a time splitting scheme. With this scheme, the creation of new kinetic zones is simpler. It is based on a time splitting between the time evolution of h on the one hand and the transport and relaxation operators on the other hand. This splitting scheme reads:

First step: evolution of h:

$$f^{n+\frac{1}{2}}_{k,i,R} = f^n_{k,i,R} + f^n_{k,i}(h_i^{n+1}-h_i^n), \tag{2.4.11}$$

$$\boldsymbol{\varrho}^{n+\frac{1}{2}}_{i,L} = \boldsymbol{\varrho}^n_{i,L} - (h_i^{n+1}-h_i^n)\boldsymbol{\varrho}^n_i, \tag{2.4.12}$$

Second step: evolution of the kinetic and fluid eqs.

$$\begin{aligned} f_{k,i,R}^{n+1} = f_{k,i,R}^{n+\frac{1}{2}} &- h_i^{n+1}\frac{\Delta t}{\Delta x}\left(\phi_{i+1/2}(f_{k,R}^{n+\frac{1}{2}}) - \phi_{i-1/2}(f_{k,R}^{n+\frac{1}{2}})\right) \\ &- h_i^{n+1}\frac{\Delta t}{\Delta x}\left(\phi_{i+1/2}(\mathcal{E}_k[\boldsymbol{\varrho}_L^{n+\frac{1}{2}}]) - \phi_{i-1/2}(\mathcal{E}_k[\boldsymbol{\varrho_L}^{n+\frac{1}{2}}])\right) \\ &+ h_i^{n+1}\frac{\Delta t}{\tau_i^{n+\frac{1}{2}}}\left(\mathcal{E}_k[\boldsymbol{\varrho}_i^{n+\frac{1}{2}}] - f_{k,i}^{n+\frac{1}{2}}\right), \end{aligned} \tag{2.4.13}$$

$$\begin{aligned} \boldsymbol{\varrho}_{i,L}^{n+1} = \boldsymbol{\varrho}_{i,L}^{n+\frac{1}{2}} &- (1-h_i^{n+1})\frac{\Delta t}{\Delta x}\sum_k \mathbf{m}_k\left(\phi_{i+1/2}(\mathcal{E}_k[\boldsymbol{\varrho}_L^{n+\frac{1}{2}}]) - \phi_{i-1/2}(\mathcal{E}_k[\boldsymbol{\varrho}_L^{n+\frac{1}{2}}])\right)\Delta v \\ &- (1-h_i^{n+1})\frac{\Delta t}{\Delta x}\sum_k \mathbf{m}_k\left(\phi_{i+1/2}(f_{k,R}^{n+\frac{1}{2}}) - \phi_{i-1/2}(f_{k,R}^{n+\frac{1}{2}})\right)\Delta v. \end{aligned} \tag{2.4.14}$$

The first step of this scheme can be further simplified by using the following remark: since f^n and f_R^n are supposed to approximate $f(t_n)$ and $f_R(t_n)$, then we should have

$$f_R^n \approx f_R(t_n) = h(t_n)f(t_n) \approx h^n f^n. \tag{2.4.15}$$

Consequently, if we assume that f_R^n is **exactly** $h^n f^n$, then (2.4.11) reads

$$f_{k,i,R}^{n+\frac{1}{2}} = h_i^{n+1} f_{k,i}^n, \tag{2.4.16}$$

and in the same way we can obtain $\boldsymbol{\varrho}_{i,L}^{n+\frac{1}{2}} = (1-h_i^{n+1})\boldsymbol{\varrho}_i^n$.

Thus relation (2.4.13) now reads

$$\begin{aligned} f_{k,i,R}^{n+1} = h_i^{n+1}\Bigg\{ f_{k,i}^n &- \frac{\Delta t}{\Delta x}\left(\phi_{i+1/2}(f_{k,R}^{n+\frac{1}{2}}) - \phi_{i-1/2}(f_{k,R}^{n+\frac{1}{2}})\right) \\ &- \frac{\Delta t}{\Delta x}\left(\phi_{i+1/2}(\mathcal{E}_k[\boldsymbol{\varrho}_L^{n+\frac{1}{2}}]) - \phi_{i-1/2}(\mathcal{E}_k[\boldsymbol{\varrho}_L^{n+\frac{1}{2}}])\right) \\ &+ \frac{\Delta t}{\tau_i^{n+\frac{1}{2}}}\left(\mathcal{E}_k[\boldsymbol{\varrho}_i^{n+\frac{1}{2}}] - f_{k,i}^{n+\frac{1}{2}}\right)\Bigg\}. \end{aligned} \tag{2.4.17}$$

We recall that $f_{i,k}^{n+\frac{1}{2}} = f_{i,k,R}^{n+\frac{1}{2}} + \mathcal{E}_k[\boldsymbol{\varrho}_{i,L}^{n+\frac{1}{2}}]$. But, we have

$$\mathcal{E}_k[\boldsymbol{\varrho}_{i,L}^{n+\frac{1}{2}}] = \mathcal{E}_k[(1-h_i^{n+1})\boldsymbol{\varrho}_i^n] = (1-h_i^{n+1})\mathcal{E}_k[\boldsymbol{\varrho}_i^n],$$

because the equilibria are degree 1 homogeneous functions of $\boldsymbol{\varrho}$. Then, with (2.4.16), we have:

$$f_{i,k}^{n+\frac{1}{2}} = h_i^{n+1} f_{i,k}^n + (1 - h_i^{n+1}) \mathcal{E}_k[\boldsymbol{\varrho}_i^n]. \tag{2.4.18}$$

However, according to the derivation of the coupling model the kinetic distribution function in the buffer zone must be close to the equilibrium. Assume again an exact equality, we have $f_{i,k}^n = \mathcal{E}_k[\boldsymbol{\varrho}_i^n]$. Inserting this relation into (2.4.18), we deduce that

$$f_{i,k}^{n+\frac{1}{2}} = f_{i,k}^n. \tag{2.4.19}$$

Note that relation (2.4.19) is very natural, since it means that f is not changed by the evolution of the buffer zone. With this identity and the linearity of the fluxes with respect to the distribution function, we use (2.4.17) to rewrite $f_{k,i,R}^{n+1}$ as

$$\begin{aligned} f_{k,i,R}^{n+1} &= h_i^{n+1} \left(f_{k,i}^n - \frac{\Delta t}{\Delta x} \left(\phi_{i+1/2}(f_k^n) - \phi_{i-1/2}(f_k^n) \right) + \frac{\Delta t}{\tau_i^n} \left(\mathcal{E}_k[\boldsymbol{\varrho}_i^n] - f_{k,i}^n \right) \right), \\ &:= h_i^{n+1} \tilde{f}_{k,i}^{n+1}, \end{aligned}$$

where $\tilde{f}_{k,i}^{n+1}$ appears to be like an approximation of $f(t_{n+1})$ by an explicit time discretization. This means that our assumption (2.4.15) is also valid at time t_{n+1}. We can of course obtain similar relations for $\boldsymbol{\varrho}_{i,L}^{n+1}$.

In summary, the time splitting scheme is written as follows:

First step (modified and simplified):

$$f_{k,i,R}^{n+\frac{1}{2}} = h_i^{n+1} f_{k,i}^n, \tag{2.4.20}$$

$$\boldsymbol{\varrho}_{i,L}^{n+\frac{1}{2}} = (1 - h_i^{n+1}) \boldsymbol{\varrho}_i^n, \tag{2.4.21}$$

Second step (unchanged):

$$\begin{aligned} f_{k,i,R}^{n+1} = f_{k,i,R}^{n+\frac{1}{2}} &- h_i^{n+1} \frac{\Delta t}{\Delta x} \left(\phi_{i+1/2}(f_{k,R}^{n+\frac{1}{2}}) - \phi_{i-1/2}(f_{k,R}^{n+\frac{1}{2}}) \right) \\ &- h_i^{n+1} \frac{\Delta t}{\Delta x} \left(\phi_{i+1/2}(\mathcal{E}_k[\boldsymbol{\varrho}_L^{n+\frac{1}{2}}]) - \phi_{i-1/2}(\mathcal{E}_k[\boldsymbol{\varrho_L}^{n+\frac{1}{2}}]) \right) \\ &+ h_i^{n+1} \frac{\Delta t}{\tau_i^{n+\frac{1}{2}}} \left(\mathcal{E}_k[\boldsymbol{\varrho}_i^{n+\frac{1}{2}}] - f_{k,i}^{n+\frac{1}{2}} \right), \end{aligned} \tag{2.4.22}$$

$$\boldsymbol{\varrho}_{i,L}^{n+1} = \boldsymbol{\varrho}_{i,L}^{n+\frac{1}{2}} - (1-h_i^{n+1})\frac{\Delta t}{\Delta x}\sum_k \mathbf{m}_k \left(\phi_{i+1/2}(\mathcal{E}_k[\boldsymbol{\varrho}_L^{n+\frac{1}{2}}]) - \phi_{i-1/2}(\mathcal{E}_k[\boldsymbol{\varrho}_L^{n+\frac{1}{2}}])\right)\Delta v$$
$$- (1-h_i^{n+1})\frac{\Delta t}{\Delta x}\sum_k \mathbf{m}_k \left(\phi_{i+1/2}(f_{k,R}^{n+\frac{1}{2}}) - \phi_{i-1/2}(f_{k,R}^{n+\frac{1}{2}})\right)\Delta v. \tag{2.4.23}$$

In this way, at any location in space, according to certain criteria which are detailed below, the scheme can shift from a fluid model to a kinetic one and vice-versa.

2.4.5 An alternative scheme for the fluid equations

Our final goal is a more efficient method for computing rarefied gas dynamics problems than a full microscopic scheme, while maintaining the same accuracy. To this aim a fast numerical scheme for the fluid part of the coupling method, based on the kinetic scheme of Perthame [106] has been implemented. In the last section, we will observed that considerable speedup is obtained using this method compared with the scheme (2.4.10).

In this scheme, the true Maxwellian is replaced by the square-shaped function $M_P[\boldsymbol{\varrho}] = a\chi(v)_{-b\leq v-u\leq b}$, where $\chi(v)$ is a non negative function such that $\chi(v) = 1$ if $u \in [-b, b]$ and 0 elsewhere. The coefficients a and b are computed so that the moment vector of $M_P[\boldsymbol{\varrho}]$ is exactly $\boldsymbol{\varrho}$. Then, the Euler fluxes are approximated by using a kinetic flux vector splitting based on the exact integration of this approximate Maxwellian. This scheme applied to the fluid part of the coupling model then reads:

$$\frac{\boldsymbol{\varrho}_{i,L}^{n+1} - \boldsymbol{\varrho}_{i,L}^{n}}{\Delta t} = -(1-h_i^{n+1})\frac{\left(\mathcal{F}_{i+1/2}(\boldsymbol{\varrho}_L^n) - \mathcal{F}_{i-1/2}(\boldsymbol{\varrho}_L^n)\right)}{\Delta x}$$
$$- \frac{(1-h_i^{n+1})}{\Delta x}\sum_k \mathbf{m}_k \left(\phi_{i+1/2}(f_{k,R}^n) - \phi_{i-1/2}(f_{k,R}^n)\right)\Delta v$$
$$+ \frac{(h_i^{n+1} - h_i^n)}{\Delta t}\boldsymbol{\varrho}_i^n, \tag{2.4.24}$$

where $\mathcal{F}_{i+1/2}(\boldsymbol{\varrho}_L) = \int_{v<0} v\boldsymbol{m}M_P[\boldsymbol{\varrho}_{i+1}]\,dv + \int_{v>0} v\boldsymbol{m}M_P[\boldsymbol{\varrho}_i]\,dv$.

However, for a fair analysis of the behavior of the coupling method, we used the scheme (2.4.10) in almost all the tests cases. Indeed, this scheme is constructed from the discrete moments of the scheme for the kinetic part (we could say that

the schemes for both parts are 'compatible'). In this way, we avoid sources of discrepancies due to a change of the nature of the scheme for the hydrodynamic parts and our observations can really focus on the behaviour of the coupling model.

We have also observed that, although small, some oscillations appear inside the buffer zone when the Perthame scheme is used. To circumvent this problem, we use the Perthame scheme in the pure fluid region (i.e. $h = 0$) and we use the scheme (2.4.10) inside the buffer zone. The transition between the fluid and kinetic models seems to be smoother if the scheme for the fluid part in the buffer zone is compatible (in the above sense) with the scheme for the kinetic part. To better clarify this point observe that, even if the quantity $f_{k,L}$ and $f_{k,R}$ are the same two different schemes leads to two different evaluation of the flux. Thus the flux on the right can be different to the flux on the left even if they have to be the same. Outside the buffer zone, it is possible to shift to any other fluid scheme without noticeable errors.

A different approach to solve this compatibility problem would be to use the alternative coupling method proposed in [39] using a different decomposition of the distribution function f. This investigation is in progress. Investigations, which can possibly solve the above difficulties, on the coupling of the full Boltzmann equation with the fluid equation trough this method are also in progress.

2.5 Moving Buffer and Kinetic zones

We have already mentioned the possibility of dividing the computational domain in different regions with the introduction of several buffer and kinetic zones. Now we need an algorithm for finding the correct locations of the zones and of their motions. To this aim, we must decide where we need the microscopic model. Indeed, shock waves, contact discontinuities or rarefaction waves that are responsible of local discontinuities or sharp gradients do actually move in time. Thus, it is crucial to move the kinetic and buffer regions simultaneously with these waves in order to represent the solution with the appropriate model. Moreover we can achieve considerable computational speedup if we can use narrower kinetic zones (even of width of a few mesh points if the situation permits).

We have experimented different criteria in our simulations. Some of them can be deduced from both the macroscopic and microscopic models while other ones only depend on the microscopic model. Of course the second kind of criteria contain more information but can only be accessed to in the kinetic region.

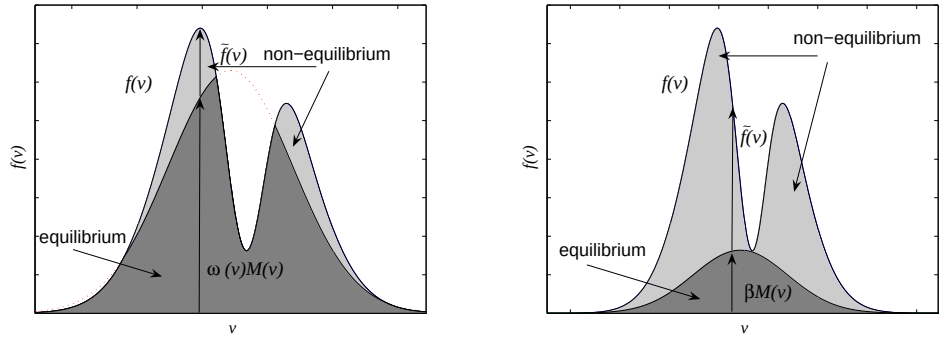

Figure 2.1: Distribution function as a combination of equilibrium and non-equilibrium parts: representation (2.5.1) (left) and representation (2.5.3) (right).

2.5.1 Microscopic Criteria

The most obvious indicator of the degree of rarefaction of a gas (but not of its closedness to the local equilibrium), is the Knudsen number ε which is defined as the ratio of the mean free path of the particles λ to a reference length L:

$$\varepsilon = \lambda / L,$$

where the mean free path is defined by

$$\lambda = \frac{kT}{\sqrt{2}\pi p \sigma_c^2},$$

with k the Boltzmann constant equal to $1.380062 \times 10^{-23} JK^{-1}$, p the pressure and σ_c the collision diameter of molecules. The Knudsen number is determined through macroscopic quantities and can be computed in the whole domain. However, it is well known that when the flow is undisturbed even in a very rarefaction regime, the hydrodynamic approximation is valid. Thus, we need a criterion to locate the discontinuities or sharp gradients inside the domain.

In kinetic regions we can utilize a new indicator, which we will call the equilibrium fraction, and which will tell us if the thermodynamical equilibrium hypothesis is correct or not. The starting point is the following definition [44]:

Definition 2.5.1 *Given a distribution function $f(v)$, and a distribution function*

$M(v)$, called Maxwellian, we define $\omega(v) \in [0,1]$ and $\tilde{f} \geq 0$ in the following way

$$\omega(v) = \begin{cases} \dfrac{f(v)}{M(v)}, & f(v) \leq M(v) \neq 0 \\ 1, & f(v) \geq M(v) \end{cases}$$

and

$$\tilde{f}(v) = f(v) - \omega(v)M(v).$$

Thus $f(v)$ can be represented as (figure 2.1)

$$f(v) = \tilde{f}(v) + \omega(v)M(v). \tag{2.5.1}$$

If we take now

$$\beta = \min_v \{\omega(v)\}, \tag{2.5.2}$$

and

$$\tilde{f}(v) = f(v) - \beta M(v),$$

where $\beta M(v)$ can be seen as the largest Maxwellian smaller than $f(v)$. Thus the distribution function $f(v)$ can be written in the form [16, 17] (figure 2.1).

$$f(v) = \tilde{f}(v) + \beta M(v). \tag{2.5.3}$$

After each time step, once the distribution function has been updated, we proceed to the computation of β, analyze how it has evolved in the kinetic region during this time step and decide accordingly how to move the various zones. For instance in the vicinity of a shock wave, we expect β to be minimal. Thus a possible strategy is to set the kinetic region around this minimum. This strategy will be explored in the numerical tests presented in the last section.

In some cases, the parameter β may provide misleading information. One possible reason for this inaccurate indication comes from the very small values of the distribution function near the artificial boundaries of the velocity domain of the discrete Boltzmann-BGK equation. Thus the computation of the equilibrium fraction near these boundaries is very inaccurate and can lead to values of β much less than 1 which are meaningless.

Another type of inaccuracy occurs when f is very close to the local Maxwellian except in a tiny region of velocity space (see e.g. the situation depicted in figure 2.1 (left)). This very local departure can induce a small value of β while only

a negligible fraction of the particles (in other words, a negligible fraction of the local total mass) are concerned by this departure to equilibrium. In this situation, we can still consider that the distribution function is close to equilibrium and that β provides a misleading information.

One way to circumvent the problem is to take into account the relative weight of the distribution function $f_{i,k}$ with respect to $\sum_k f_{i,k}$. Another strategy is also to measure the global mass of the equilibrium part, and which is given by

$$\varrho_E = \int_{\mathbb{R}^3} \omega(v) M(v) dv,$$

which for the discrete velocity case becomes

$$\varrho_E = \sum_{k \in \mathcal{K}} \omega_k \mathcal{E}_k,$$

and to define a new equilibrium fraction indicator as

$$\beta_M = \frac{\varrho_E}{\varrho}.$$

The parameter β_M gives us the ratio of mass of the equilibrium part to the total mass. It may happen that $\beta \ll 1$ while $\beta_M \approx 1$.

We finally observe that the parameter τ can also give us some useful information. If we split the pure BGK equation in a transport step and in a relaxation step, the latter reads

$$f^{n+\frac{1}{2}} = e^{-\frac{\Delta t}{\tau}} f + (1 - e^{-\frac{\Delta t}{\tau}}) M_f. \tag{2.5.4}$$

Thus, if τ is sufficient small compared to the other parameters, we can suppose that the distribution function relaxes to a local Maxwellian, and the fluid model can be used. On the other hand, the convection term is going to distort the distribution from equilibrium. The strength of the convection term can be estimated by the following quantity:

$$\tau^{'} = v \cdot \frac{\nabla_x f}{f}.$$

However, while τ is a quantity that can be computed from macroscopic quantities, $\tau^{'}$ is not. In order to estimate the magnitude of $\tau^{'}$ using only fluid quantities, we can measure the rates of changes of macroscopic quantities linked to f such as density, momentum and energy. Thus we can compare τ with the following quantities:

$$\frac{\nabla_x \mathcal{F}(\boldsymbol{\varrho})}{\boldsymbol{\varrho}}.$$

The investigation of the validity of these indicators will be the subject of future work.

2.5.2 Macroscopic Criteria

Of course, we cannot use the equilibrium function indicator in the whole domain, because we can only access it in the kinetic region. Thus, we have to find other parameters that can indicate a deviation from the thermodynamical equilibrium. The idea is to make use of smoothness indicators which measure the roughness of the data. We look at the ratio of consecutive gradients for the density

$$\psi(i) = \frac{\varrho(i) - \varrho(i-1)}{\varrho(i+1) - \varrho(i)},$$

and for the velocity

$$\phi(i) = \frac{u(i) - u(i-1)}{u(i+1) - u(i)}.$$

If $\psi(i)$ and $\phi(i)$ are close to 1, then the data are smooth. while if $\psi(i)$ or $\phi(i)$ are far from unity, large variations of these quantities are present. We propose the value of such indicators in order to locate large gradient zones.

If $\psi(i) < 0$ or $\phi(i) < 0$, then slopes at neighboring points have different signs which indicates the existence of maxima or minima. On the other hand, if the gradient varies by a factor 2 between two neighboring points, we suppose that the data become unsmooth. Thus the threshold values which we have chosen for standard conditions are

$$\psi(i) < 0 \text{ or } \psi(i) > 2, \tag{2.5.5}$$

and

$$\phi(i) < 0 \text{ or } \phi(i) > 2, \tag{2.5.6}$$

meaning that if either (2.5.5) or (2.5.6) is satisfied, we must shift (or stay) in the kinetic regime.

In rarefied regimes, a shock waves is not a discontinuity any longer, but rather a region of large gradients. As a consequence, their localization becomes more difficult. The same considerations hold for rarefaction waves and contact discontinuities for which the gradients become smoother as the rarefaction increase. What happens in practice is that the value of the smoothness indicators decrease in magnitude when the Knudsen number increases. Thus we propose to link the value of the smoothness indicators to ε in such a way that, also in the rarefied

regime we can identify a departure from equilibrium. To this aim we propose that if $\varepsilon > 10^{-4}$, the criterion for shifting to the kinetic model becomes

$$\psi(i) < 0.7 \text{ or } \psi(i) > 1.2, \tag{2.5.7}$$

and

$$\phi(i) < 0.7 \text{ or } \phi(i) > 1.2, \tag{2.5.8}$$

Of course, it could be necessary to reduce even more the interval of the fluid regime if the gas is extremely rarefied. The indicator threshold could also be made dependent upon the mesh size and the order of the numerical scheme.

Others indicators that could be used instead of the above defined smoothness indicators are the gradient-length Knudsen numbers

$$\varepsilon_{GL\varrho} = \lambda \frac{|\nabla \varrho|}{\varrho}, \qquad \varepsilon_{GLu} = \lambda \frac{|\nabla u|}{u}.$$

Threshold values for these parameters indicating the transition from continuum to to kinetic regime which have been proposed in [77] and [73] are $\varepsilon_{GL} < 0.05$. It is argued that in this way the error between a macroscopic and a microscopic model is less than 5% [128].

Remark 2.5.1 *In principle, it is possible to use any type of numerical scheme for the solution of the coupling model for both the fluid and kinetic regions. Thus if, for instance, we use high resolution methods such as WENO schemes, we could utilize the smoother indicator defined by measuring the sum of the L^2 norms of all the derivatives of the interpolation polynomial $q_k(x)$ over one cell I_j. The relation reads*

$$IS_k = \sum_{l=1}^{r-1} \int_{x_{j-1/2}}^{x_{j+1/2}} \Delta x^{2l-1} (q_k^{(l)})^2 dx \tag{2.5.9}$$

The value of the weights w_k of the WENO method computed from the indicators IS_k can be used to identify a discontinuity.

2.5.3 Adaptive Kinetic/Fluid Algorithm

We have just listed some macroscopic and microscopic criteria allowing to locate the zones of strong departure to local thermodynamical equilibrium. Using the above criteria the algorithm detailed below permits to move the kinetic regions and to create new kinetic regions during the course of the simulation:

Algorithm for moving Kinetic-Fluid transition region: Assume f^n, f_R^n, $\boldsymbol{\varrho}_L^n$, h^n and h^{n+1} are known.

1. Identify the mesh points at which (2.5.5) or (2.5.6) are satisfied;

2. Check the values of the Knudsen number in the zones around the mesh points found at step 1;

3. if the Knudsen number is greater then 10^{-4}, change the threshold values to (2.5.7) and (2.5.8) and go back to 1;

4. Put a kinetic region around the mesh points at which the smoothness indicators exceed the corrected threshold value (this gives an updated h^{n+1});

5. Advance the coupled system in time by using scheme (2.4.7)–(2.4.10). If a new zone has been created, it is simpler to use the splitting scheme (2.4.20)–(2.4.23). This gives f_R^{n+1}, $\boldsymbol{\varrho}_L^{n+1}$ and f^{n+1}.

6. Measure β and β_M in the kinetic zone;

7. Compute h^{n+2} by using the values of β or β_M. In our tests, we set $h_i^{n+2} = 1$ if β_i or $\beta_{M,i}$ is lower than 0.95 and 0 sufficiently far from this zones. Thus automatically fluid zones are created during the simulation if h becomes zero. Fixed size buffer zones are created to smoothly pass from 1 to 0.

Remark 2.5.2

- *Fluid zones are created sufficiently far from the departures of the thermodynamical equilibrium and wide. Distance from the departures and thickness of the zones are parameters that can be chosen at the beginning of each simulation.*

- *The value of the Knudsen number strongly depends on the choice of the reference length. In our tests, we choose the domain size as reference length. However, this choice of reference length depends on the problem. A more universal Knudsen number can be defined choosing the gradient length defined before as reference length.*

2.6 Numerical tests

2.6.1 General setting

In this section, we present two numerical tests to illustrate the main features of the method. First the performance of the scheme is tested on the unsteady shock test problem for which the very simple structure of the solution makes the analysis easier. The second test problem is the classical Sod shock tube problem, in which the presence of contact discontinuities and rarefaction waves add new difficulties compared to the first problem. Both tests are considered in one space dimension. On each figure, we display the result obtained with the coupling model and with the hydrodynamic model. We do not show the solution of the full kinetic equation because it is very close to that of the coupling system for both tests.

In order to obtain the correct equation of state, we use a one-dimensional velocity space model which is able to account for three-dimensional velocity effects. The model reads

$$\partial_t \begin{pmatrix} F \\ G \end{pmatrix} + v\partial_x \begin{pmatrix} F \\ G \end{pmatrix} = \nu \begin{pmatrix} M_F - F \\ TM_F - G \end{pmatrix}.$$

It is obtained from the full three-dimensional Boltzmann-BGK system by means of a reduction technique [60]. In this model, the fluid energy is given by

$$E = \sum_{k\in\mathcal{K}} \frac{1}{2} v_k^2 F_k + G_k.$$

In this way, we can recover the correct hydrodynamic limit given by the standard Euler system even with a lower dimensional velocity space.

The collision frequency is given by $\nu = \tau^{-1} = (\frac{\mu}{p})^{-1}$ where $\mu = \mu_{ref} \cdot (\theta/\theta_{ref})^{\omega}$ with $\mu_{ref} = 2.117 \times 10^{-5}\ Pa/s$ and $\omega = 0.81$. For our simulation we choose an Argon gas with molecular mass equal to $6.63 \times 10^{-27}\ kg$. This yields a value of the gas constant equal to $R \simeq 208$.

The computational speedup compared with a full kinetic simulation is not very large and mainly corresponds to the possibility of choosing larger timee steps for the hydrodynamic part. This is due to the fact that the hydrodynamic scheme that we use is deduced from the kinetic solver by taking discrete velocity moments. However, the coupling model is not altered if we shift to a more efficient scheme for the hydrodynamic part. In this case, considerable speedup can be achieved. In order to demonstrate this, we have repeated some of the tests with the scheme

described in section 2.4.5. With this scheme, it is possible to achieve a dramatic speedup.

However, we have made most tests using the unefficient scheme described in section 2.4.3 because this scheme is directly deduced from the scheme for the kinetic part by taking discrete velocity moments. In this sense, the schemes for the kinetic and hydrodynamical parts are 'compatible'. Choosing compatible schemes for the two parts allows to focus our observations to the effect of the coupling model, thus reducing the discrepancies which would originate from the choice of the numerical scheme for the hydrodynamic part.

The thickness of the buffer zones is fixed and taken in each test problem equal to $1.5\ m$, while the thickness of the kinetic and fluid regions vary according to the previously described criteria and can shrink to zero.

2.6.2 Unsteady Shock Tests

We consider an unsteady shock that propagates from left to right. The shock is produced by a specular wall at the left boundary $x = -20$. This is performed numerically by introducing an incoming Maxwellian distribution in ghost cell beyond the boundary with parameters ϱ, u, T equal to the $\varrho(1)$, $-u(1)$, $T(1)$ where $(\varrho(1), u(1), T(1))$ are the parameters in the first cell. At the right boundary ($x = 20$), we also add a ghost cell where, at each time step, we impose the macroscopic variables equal to $\varrho(t = 0)$, $u(t = 0)$, $T(t = 0)$ and the distribution function equal to a Maxwellian corresponding to these parameters for the kinetic scheme. The computation is stopped at the final time $t = 0.04$ s. There are 1000 cells in physical space and 140 cells in velocity space. Artificial boundaries in velocity space are put at velocities equal to -3600 m/s and 3600 m/s. The cut-off function h is initialized as $h = 1$ for x ranging from -20 to $-17.5 = a_1$ (kinetic region), $h = \frac{x-b_1}{a_1-b_1}$ with $b_1 = -16$ (buffer zone) and $h = 0$ for $x > -16$ (fluid region).

The initial conditions are such that mass density $\varrho = 5 \times 10^{-7}$ kg/m^3, mean velocity $u = -900$ m/s and temperature $T = 273$ K. The Knudsen number ε at initialization is equal to $\varepsilon \simeq 5.5 \times 10^{-3}$. Since ε is not too small, this suggests us that a kinetic scheme is necessary in some zones of the domain. When the simulation begins, a shock starts to form and a non-equilibrium zone arises. We plot the solution after few time steps $t = 2 \times 10^{-3}$ s for the density (figure 2.2, top) and velocity (figure 2.3, top) to show that the parameters β and β_M are less than 1 near the boundary (figure 2.4, top left). Then, the shock starts to move towards the right and after few time steps, β and β_M near the left boundary tend to return

to their original value 1. Sufficiently far away from the discontinuity, the fluid approximation becomes valid. Thus, the algorithm automatically introduces a second buffer zone $[a_2, b_2]$ (figures 2.2–2.5, middle). On the left-hand side of point a_2, $h = 1$ which means that the fluid equations alone are solved. All regions move according to the value of β computed in the kinetic zone. When β approaches the value 1 then h starts to diminish. We finally plot the results at $t = 0.04$ s at the end of the simulation, for the density (figure 2.2, bottom), mean velocity (figure 2.3, bottom), β and β_M (figure 2.4, bottom left), Knudsen number (figure 2.4, bottom right) and smoothness indicators (figure 2.5, bottom).

We repeat the simulation increasing the initial density to the value $\varrho = 10^{-5}$ kg/m^3. This yields a different initial Knudsen number $\varepsilon \simeq 2.7 \times 10^{-4}$ and gives different results. Now β and more importantly β_M remain close to 1 also in the vicinity of the shock. This means that the fluid equations must produce very similar results as the kinetic equations. After a few time steps, when the shock is formed and starts to move, $\beta \simeq 1$ and $\beta_M \simeq 1$ (figure 2.6, middle left). Then, the scheme automatically sets $h = 0$ and computes the solution entirely with the macroscopic model. We display the density, velocity, Knudsen number, equilibrium fractions β and β_M, smoothness indicators ψ and ϕ when $t = 2 \times 10^{-3}$ s on figure 2.6, and when $t = 0.02$ s on figure 2.7. The final solution ($t = 0.04$) is very close to the solution we can compute with a hydrodynamic scheme. So we do not display it.

We note that as reported in section 2.5.1 the parameter β gives sometimes results that could suggest a strong departure to equilibrium while β_M does not. The parameter β_M seems more accurate in describing the error between a fluid and a kinetic model.

2.6.3 Sod shock tube problem

We consider the classical Sod test with the same number of mesh points in physical and velocity spaces as in the previous test (1000 points in physical space and 140 points in velocity space). We only change the position of the artificial boundaries in velocity space and set it now to the values -2000 m/s and 2000 m/s. The initial value are such that mass density $\varrho_L = 5 \times 10^{-6}$ kg/m^3, mean velocity $u_L = 0$ m/s and temperature $T_L = 273.15$ K if $-20 \leq x \leq 0$, while $\varrho_R = 5 \times 0.125 \times 10^{-6}$ kg/m^3, $u_R = 0$ m/s, $T_R = 218.4$ K if $0 \leq x \leq 20$. The initial data for the kinetic model are taken in thermodynamical equilibrium. The Knudsen numbers at the beginning of the simulation are $\varepsilon_L \simeq 0.6 \times 10^{-3}$ and $\varepsilon_R \simeq 4.5 \times 10^{-3}$ to the left and right hand sides of the discontinuity respectively.

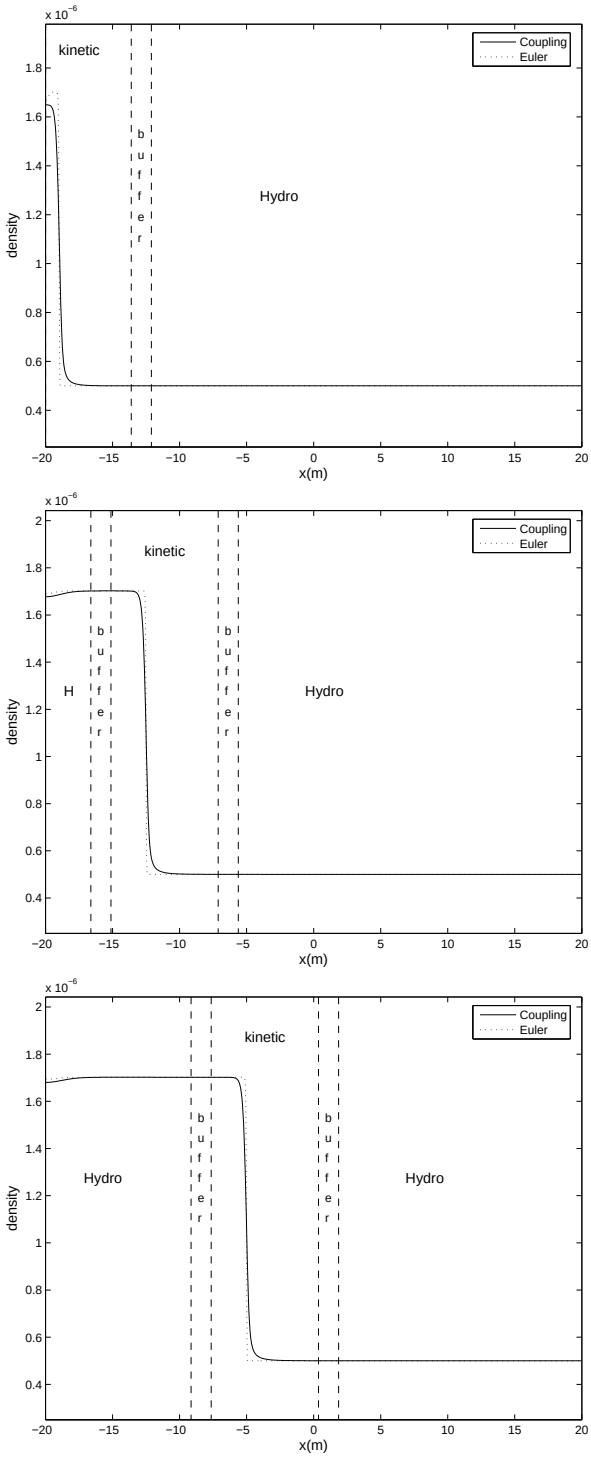

Figure 2.2: Unsteady Shock 1: Density profile at different times $t = 0.002$ (top), $t = 0.02$ (middle), $t = 0.04$ (bottom). The solid line is the solution of the coupling model, the dotted line is that of the Euler system.

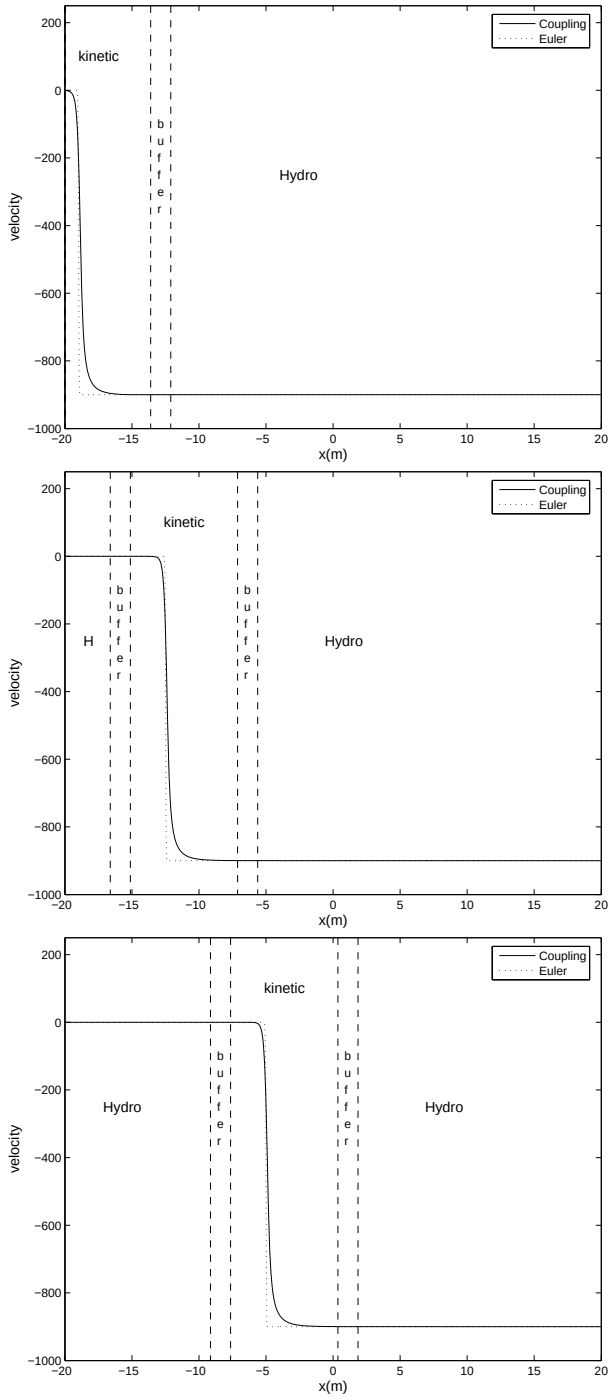

Figure 2.3: Unsteady Shock 1: Velocity profile at different times $t = 0.002$ (top), $t = 0.02$ (middle), $t = 0.04$ (bottom). The solid line is the solution of the coupling model, the dotted line is that of the Euler system.

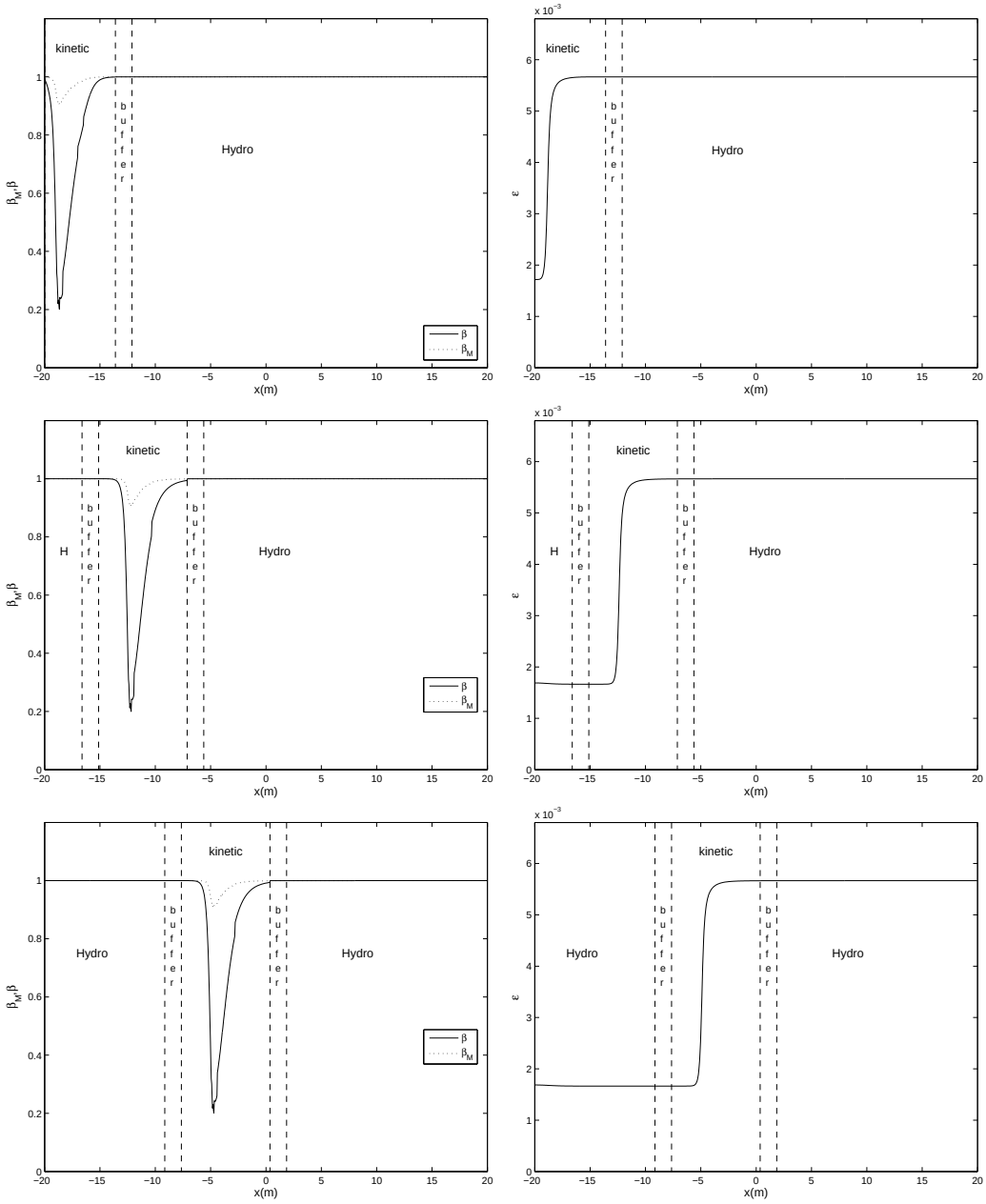

Figure 2.4: Unsteady Shock 1: Equilibrium fraction profile (left), Knudsen number (right) at different times $t = 0.002$ (top), $t = 0.02$ (middle), $t = 0.04$ (bottom).

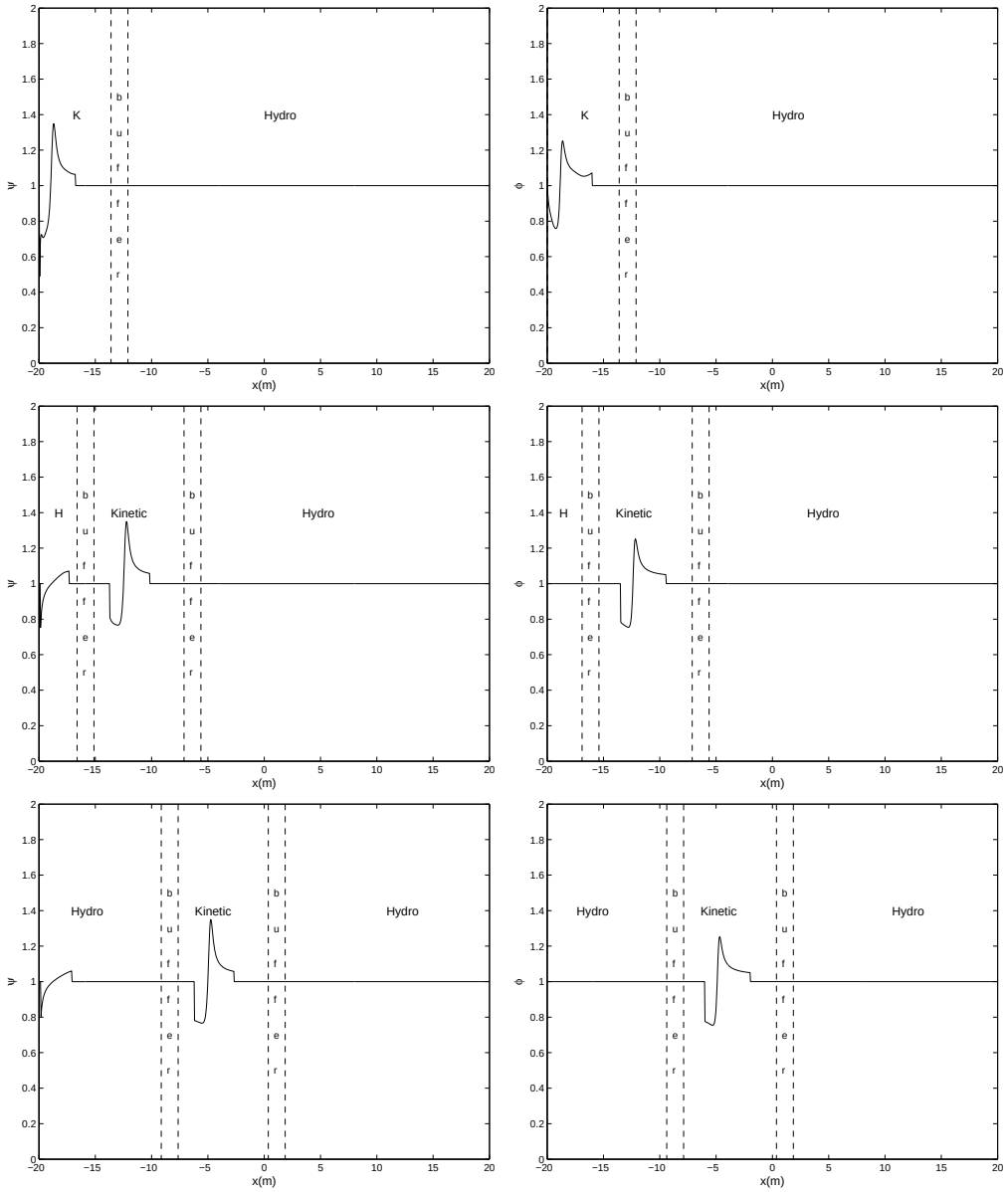

Figure 2.5: Unsteady Shock 1: Smoothness indicators for density (left) and velocity (right) at different times $t = 0.002$ (top), $t = 0.02$ (middle), $t = 0.04$ (bottom)

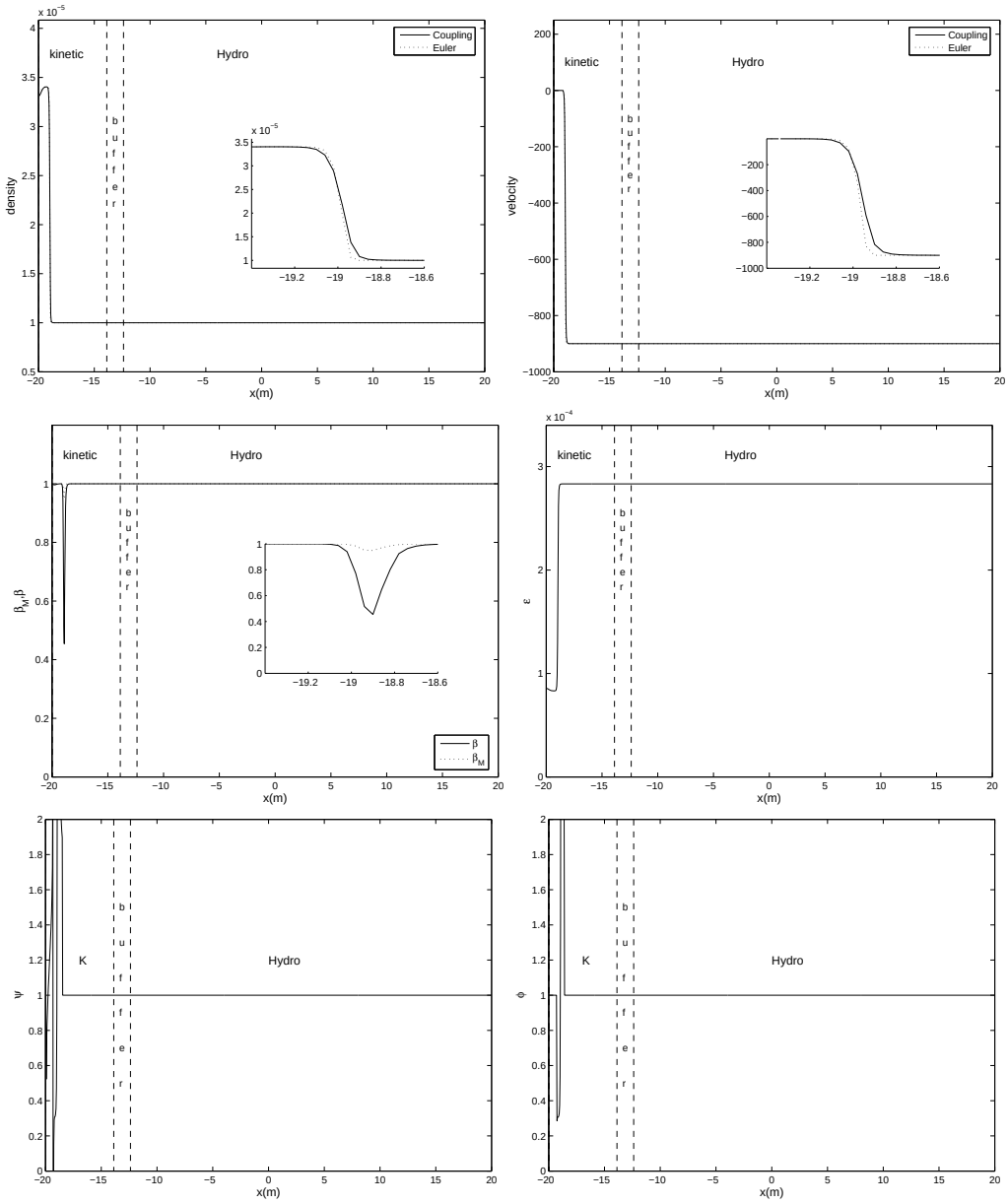

Figure 2.6: Unsteady Shock 2: Solution at $t = 2 \times 10^{-3}$. Density (top left), velocity (top right), equilibrium fraction (middle left), Knudsen number (middle right), density smoothness indicator (bottom left), velocity smoothness indicator (bottom right). The small panels are a magnification of the solution close to the shock.

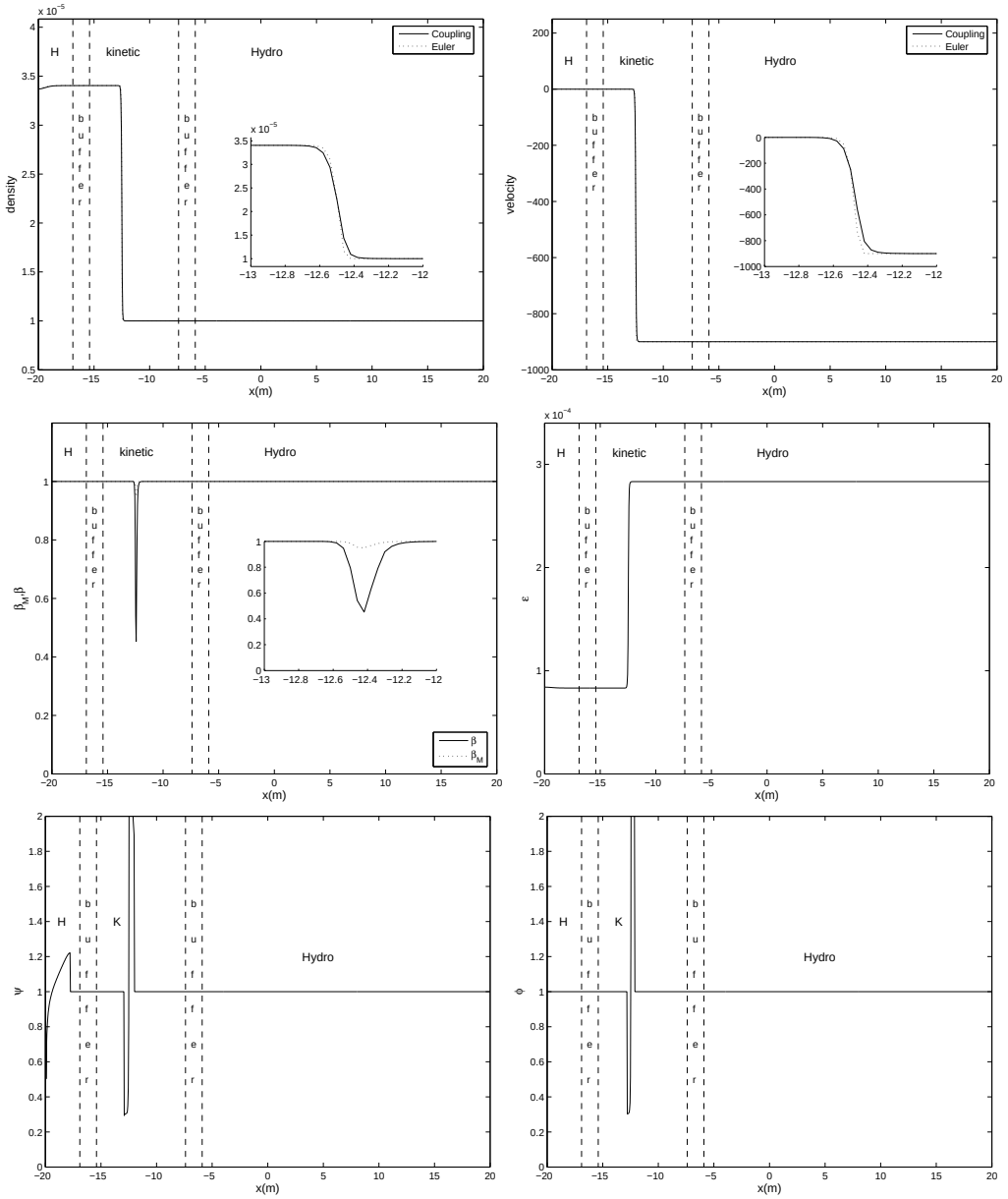

Figure 2.7: Unsteady Shock 2: Solution at $t = 0.02$. Density (top left), velocity (top right), equilibrium fraction (middle left), Knudsen number (middle right), density smoothness indicator (bottom left), velocity smoothness indicator (bottom right). The small panels are a magnification of the solution close to the shock.

We begin by defining a kinetic zone between the initial discontinuity ($h = 1$) and two buffer zones to the right $[a_1, b_1]$ and to the left $[a_2, b_2]$ of it. In the rest of the domain the solution is computed with the macroscopic model that corresponds to $h = 0$. We plot the results in terms of the density (figure 2.8) and mean velocity (figure 2.9). We also display the Knudsen number (figure 2.10 right) and the two equilibrium fractions β and β_M (figure 2.10 left). The smoothness indicators for the density and velocity are shown on figure 2.11. For each variable we plot the solution at three different times: $t = 0.002$ s (top), $t = 0.015$ s (middle) and at $t = 0.03$ s (bottom). During the computation, we notice that the region where $\beta < 1$ (figure 2.10 left, top and middle) grows. The algorithm makes the two buffer zones move accordingly in order to keep this zone inside the kinetic area. The gas is too rarefied and the rarefaction waves as well as the two other waves require the microscopic model (figure 2.8 and 2.9, bottom).

We repeat the simulation with different initial densities: $\varrho_L = 2 \times 10^{-5}$ kg/m^3 and $\varrho_R = 0.25 \times 10^{-5}$ kg/m^3. The two Knudsen numbers are $\varepsilon_L \simeq 0.18 \times 10^{-3}$ and $\varepsilon_R \simeq 1.1 \times 10^{-3}$. This leads to different final results. The initial cut-off function h is chosen as previously, but now the Knudsen numbers are such that the distribution function relaxes more rapidly towards equilibrium and the macroscopic model is sufficiently accurate except in the vicinity of the contact discontinuity and shock wave. Again, we display the density (figure 2.12), mean velocity (figure 2.13), Knudsen number (figure 2.14 right), equilibrium fractions (figure 2.14 left) and smoothness indicators (figure 2.15) at the same instants as in the previous simulation. At the beginning of the simulation, the rarefaction wave lies within the kinetic region (see figures 2.12-2.13 top, middle). As time evolves, the rarefaction wave leaves the kinetic region to end in the fluid region (figures 2.12-2.13 bottom). The error between the macroscopic and the microscopic models in this region is very small. From our tests, we can conclude that the equilibrium parameter β_M seems to be a more precise indicator of local equilibrium than β. Using β_M to characterize equilibrium regions seems a promising strategy for the future developments of the coupling method and application to numerical simulations of transition regimes from rarefied to dense flows.

2.6.4 Use of a different scheme for the fluid-dynamical part

In this section we show how the coupling model behaves when used in conjunction with a different scheme for the fluid-dynamical part. We repeat the computations of the two previous sections, namely the unsteady shock test problem and the Sod shock tube problem. For the unsteady shock test problem, the initial values are

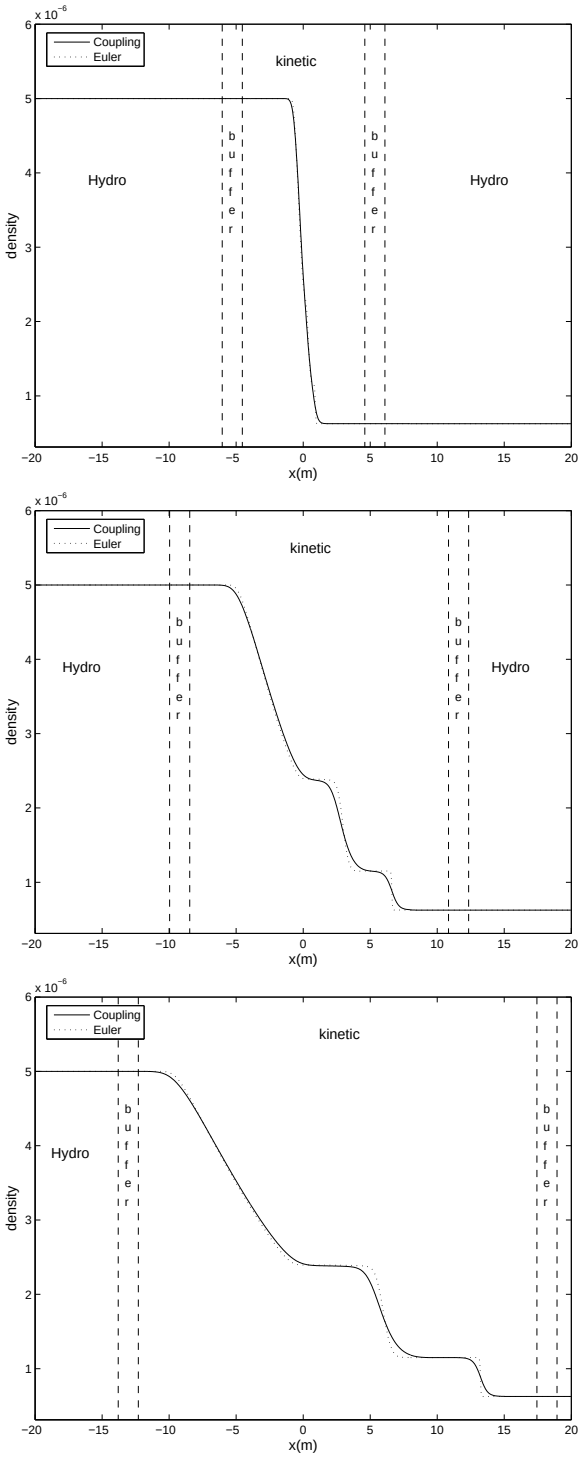

Figure 2.8: Sod test 1: Density profile at different times $t = 0.002$ (top), $t = 0.015$ (middle), $t = 0.03$ (bottom). The solid line is the solution of the coupling model, the dotted line is that of the Euler system.

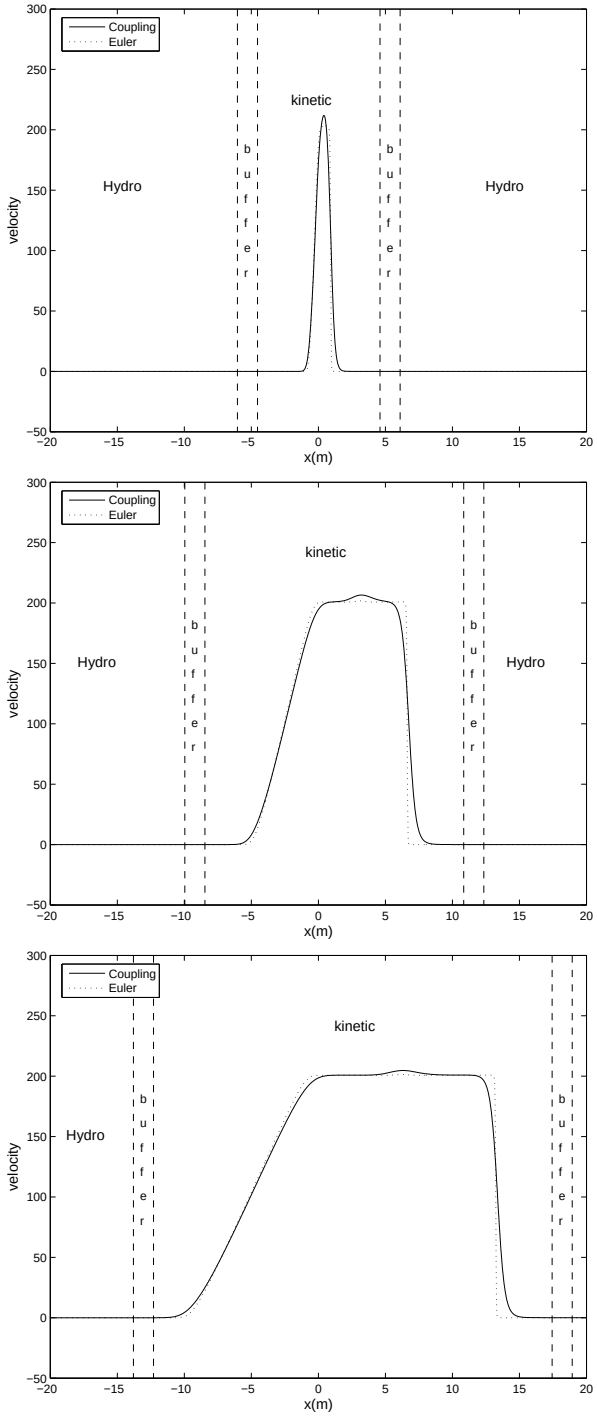

Figure 2.9: Sod test 1: Velocity profile at different times $t = 0.002$ (top), $t = 0.015$ (middle), $t = 0.03$ (bottom). The solid line is the solution of the coupling model, the dotted line is that of the Euler system.

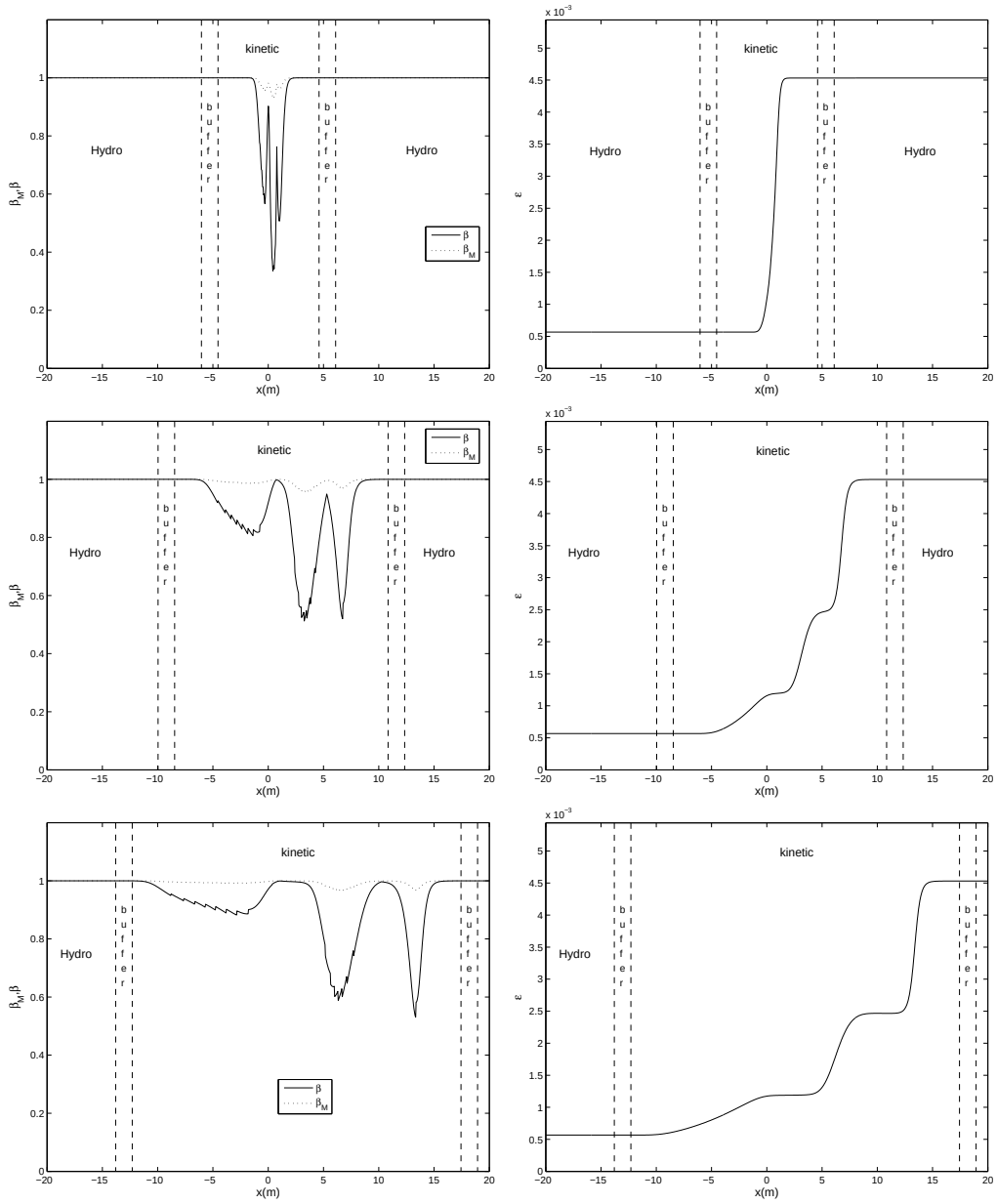

Figure 2.10: Sod test 1: Equilibrium fraction profile (left), Knudsen number (right) at different times $t = 0.002$ (top), $t = 0.015$ (middle), $t = 0.03$ (bottom).

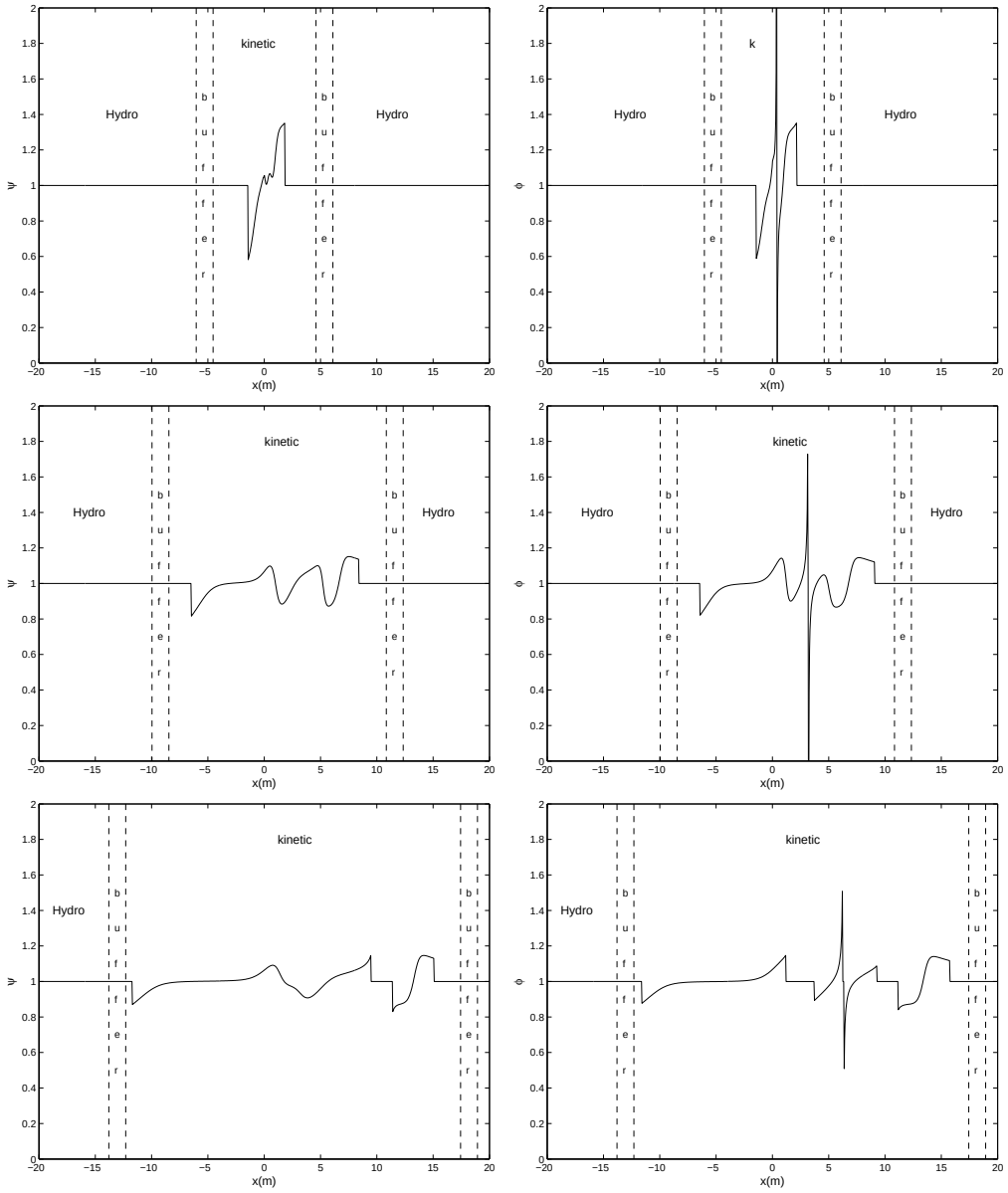

Figure 2.11: Sod test 1: Smoothness indicators for density (left) and velocity (right) at different times $t = 0.002$ (top), $t = 0.015$ (middle), $t = 0.03$ (bottom)

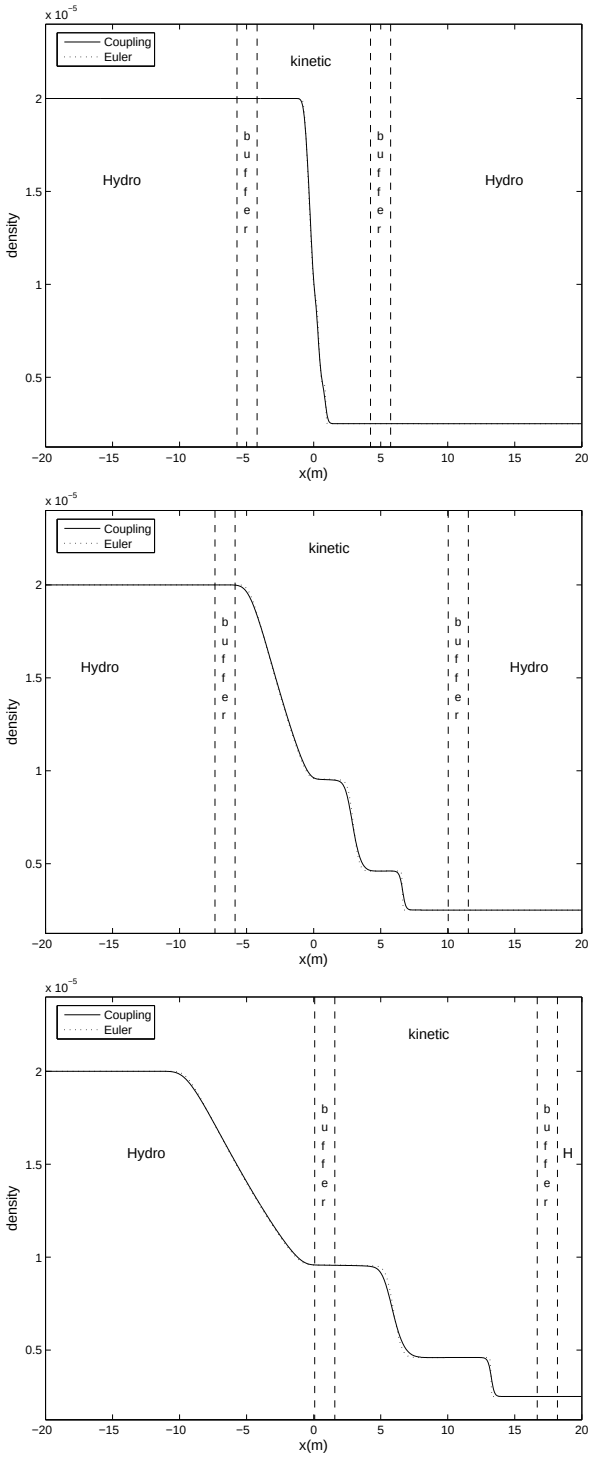

Figure 2.12: Sod test 2: Density profile at different times $t = 0.002$ (top), $t = 0.015$ (middle), $t = 0.03$ (bottom). The solid line is the solution of the coupling model, the dotted line is that of the Euler system.

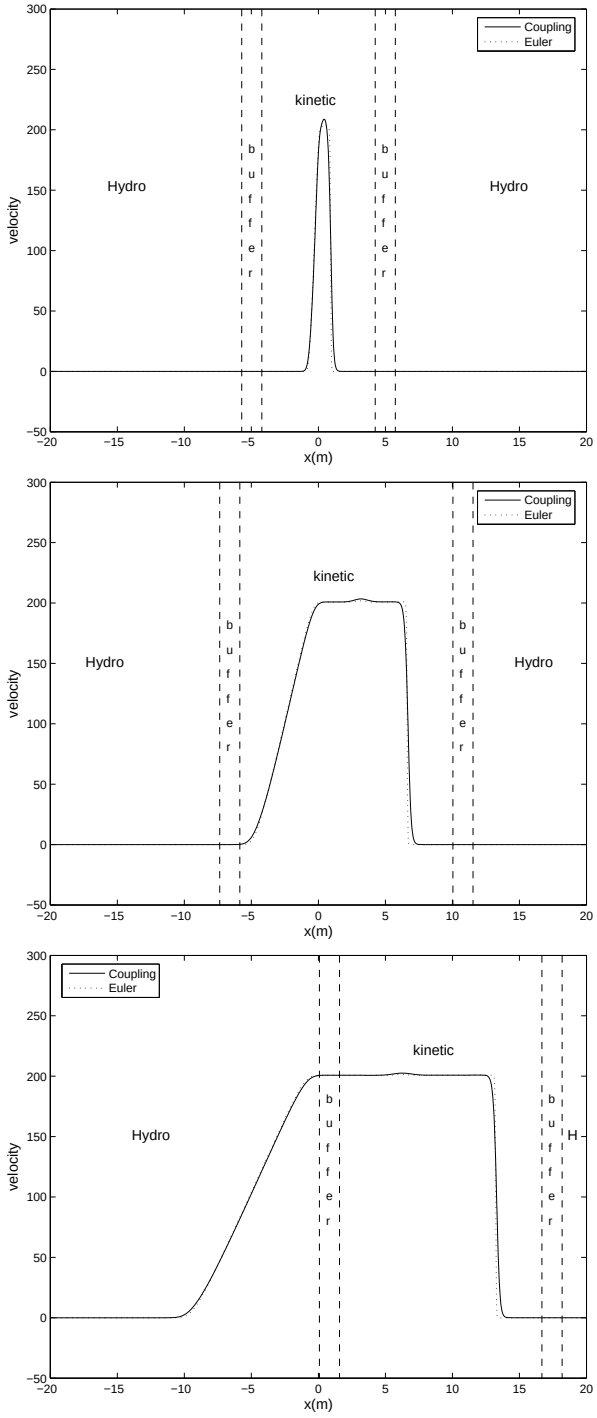

Figure 2.13: Sod test 2: Velocity profile at different times $t = 0.002$ (top), $t = 0.015$ (middle), $t = 0.03$ (bottom). The solid line is the solution of the coupling model, the dotted line is that of the Euler system.

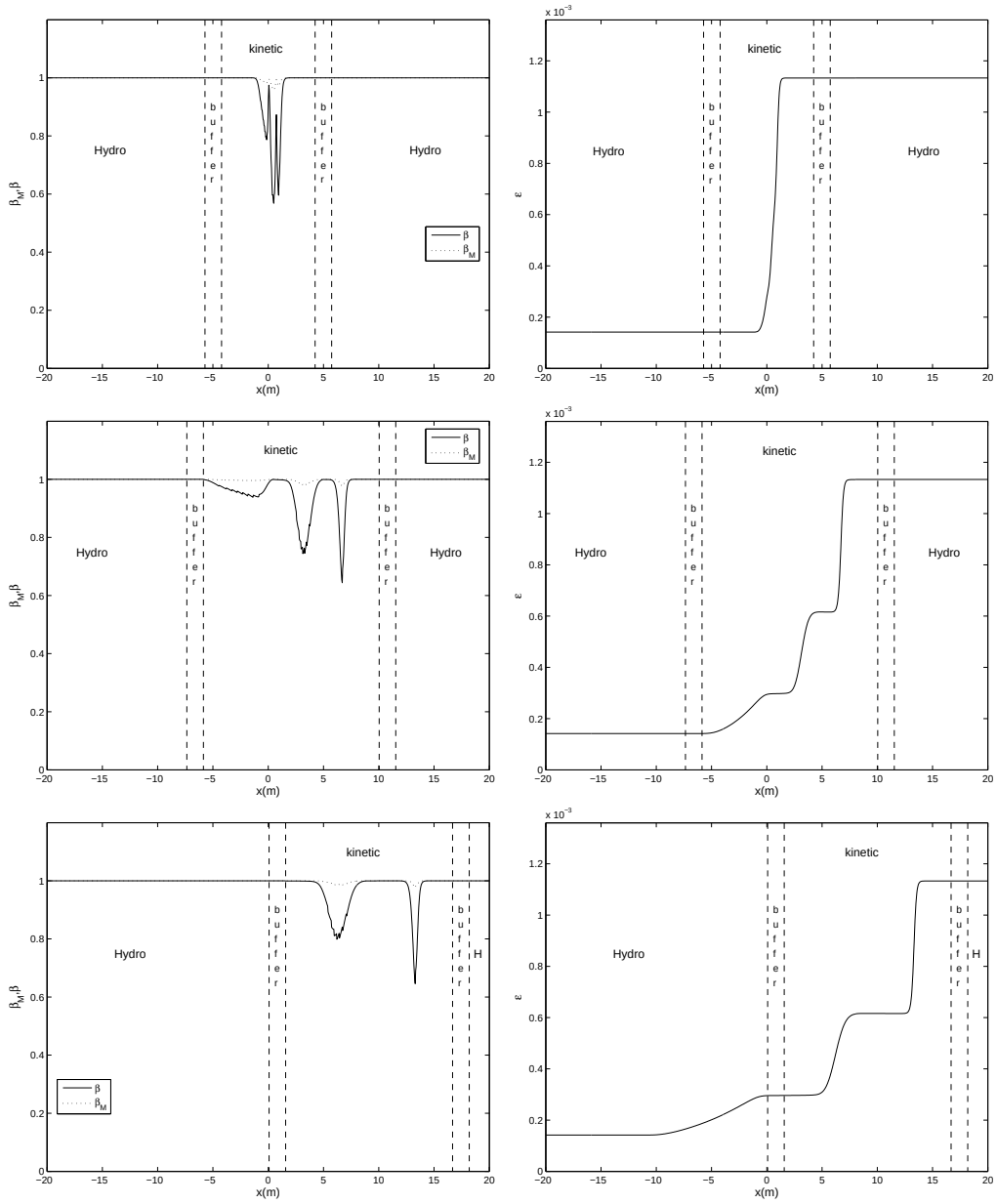

Figure 2.14: Sod test 2: Equilibrium fraction profile (left), Knudsen number (right) at different times $t = 0.002$ (top), $t = 0.015$ (middle), $t = 0.03$ (bottom).

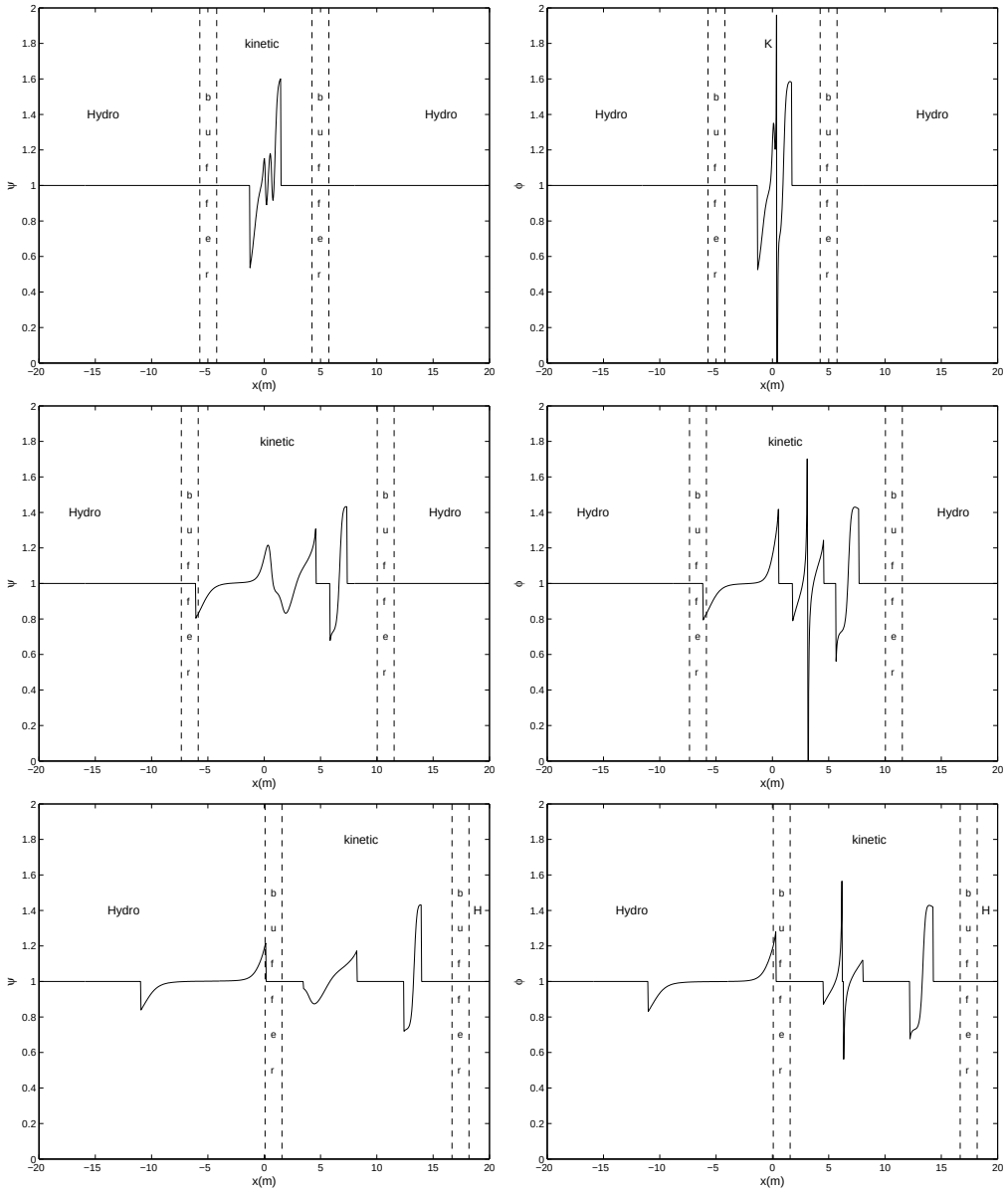

Figure 2.15: Sod test 2: Smoothness indicators for density (left) and velocity (right) at different times $t = 0.002$ (top), $t = 0.015$ (middle), $t = 0.03$ (bottom)

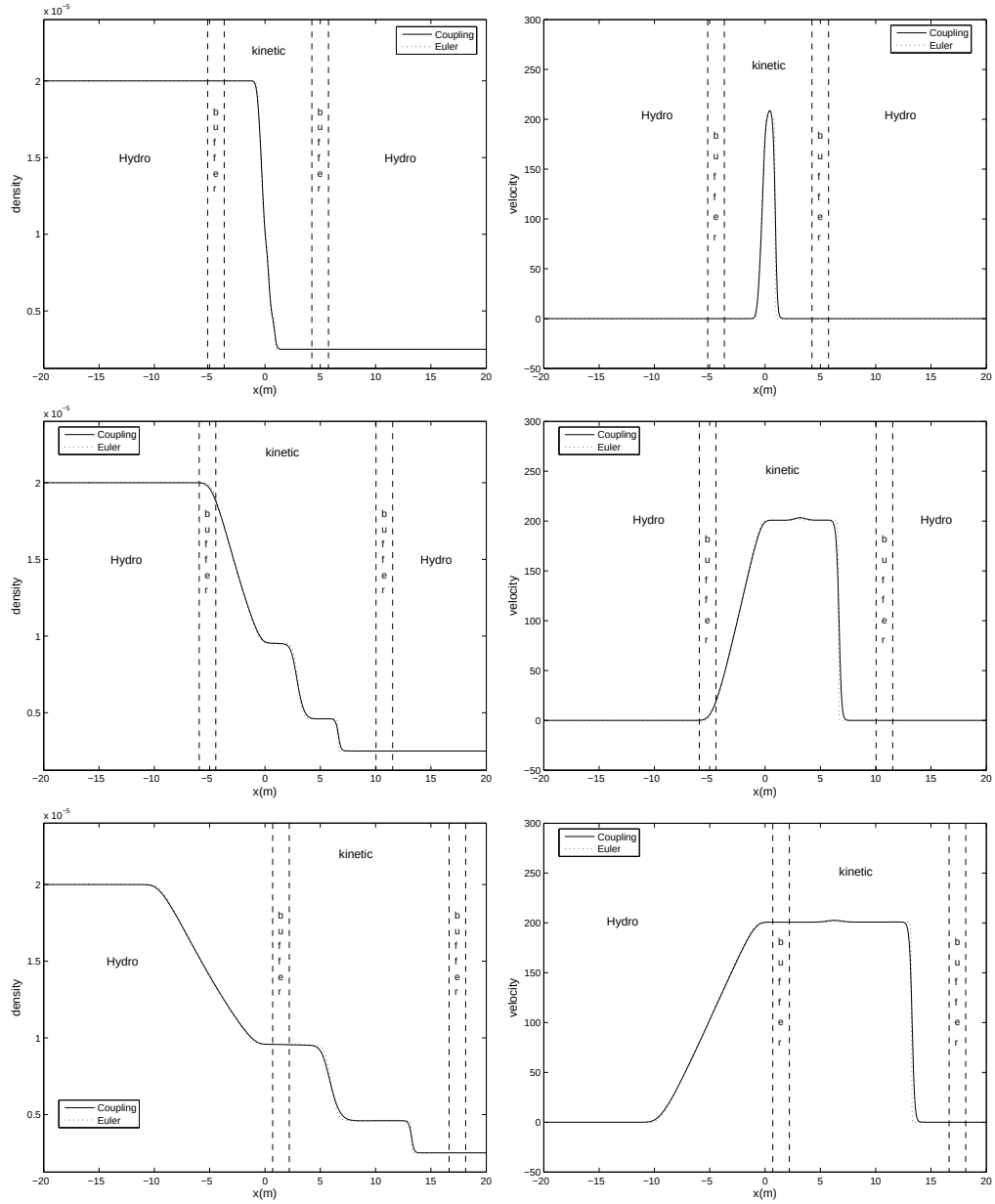

Figure 2.16: Sod Test 3: Density (left), Velocity (right) profiles at different times $t = 0.002$ (top), $t = 0.015$ (middle), $t = 0.03$ (bottom). The solid line is the solution of the coupling model, the dotted line is that of the Euler system.

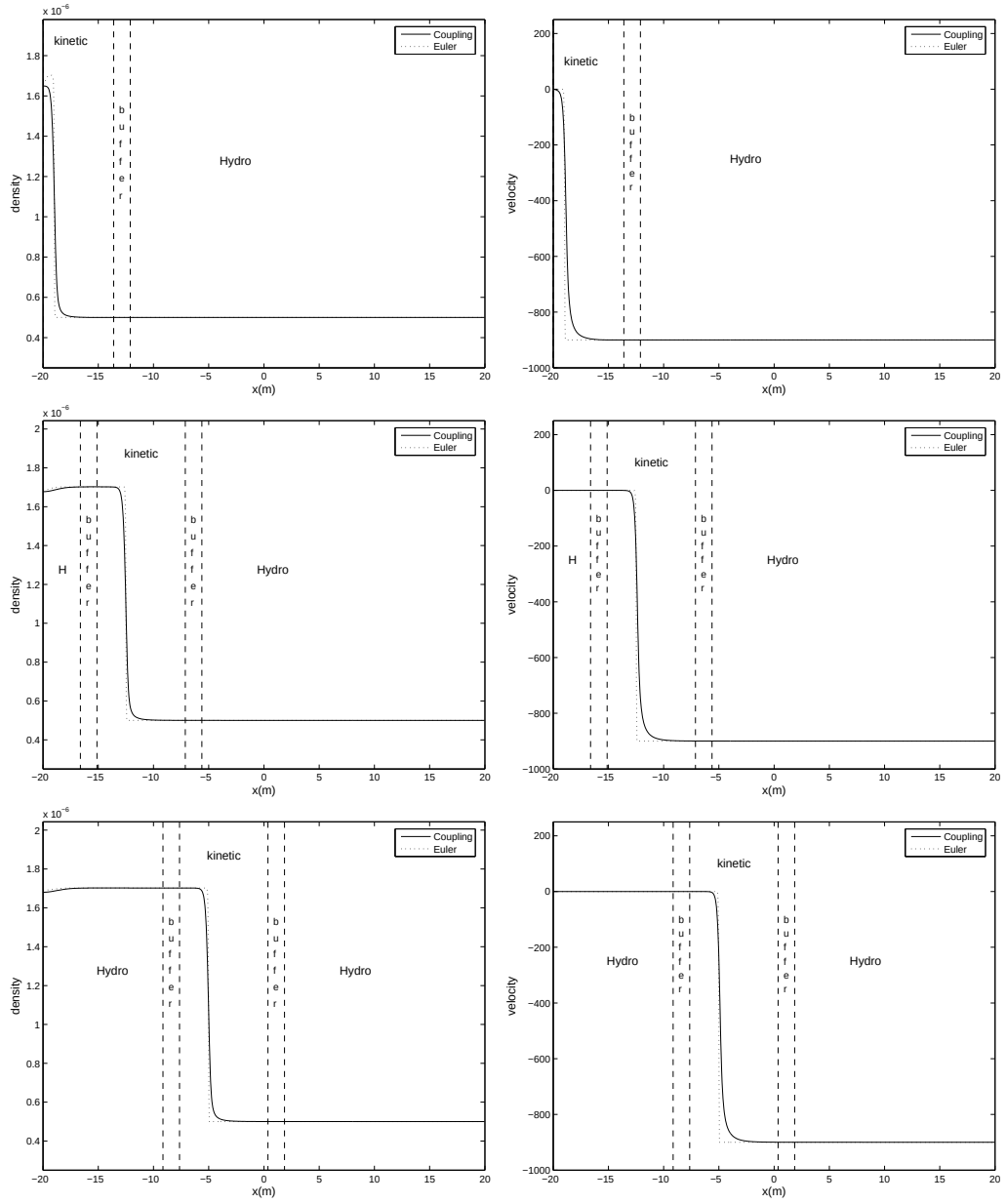

Figure 2.17: Unsteady shock test: Density (left), Velocity (right) profiles at different times $t = 0.002$ (top), $t = 0.02$ (middle), $t = 0.04$ (bottom). The solid line is the solution of the coupling model, the dotted line is that of the Euler system.

$\varrho = 5 \times 10^{-6}$ kg/m^3, mean velocity $u = -900$ m/s and temperature $T = 273$ K, while for the Sod shock test problem, they are $\varrho_L = 2 \times 10^{-5}$ kg/m^3, $u_L = 0$ m/s, $T_L = 273.15$ K and $\varrho_R = 0.25 \times 10^{-5}$ kg/m^3, $u_L = 0$ m/s, $T_L = 273.15$ K. We use the same meshes in physical and velocity spaces as previously. We only plot the results for the density and velocity at different time steps. Figure 2.16 for the Sod shock tube problem and figure 2.17 for the unsteady shock problem show that the solution agrees well with the previous results except for small differences due to the different numerical scheme. The computational time of the two simulations on a 3 Ghz Athlon computer shows a speedup of 65 % for the Sod problem and of 40 % for the unsteady shock problem. This different speedup can be explained by the different sizes of the kinetic regions in the two tests, and also by the different time steps. In the second test, the limitation of the time step due to convection (CFL condition) and that coming from the relaxation are close. Therefore, the simulation times for the macroscopic and microscopic models are closer than in the case of the Sod test. These considerations suggest that the use of such a decomposition technique is very efficient in regimes close to thermodynamical equilibrium in which however, Navier-Stokes or Euler fail to accurately describe the flow. Such regimes are the so-called transitional regimes. Of course, the computational time can be reduced even further for two or three dimensional computations.

2.7 Conclusion

In this work we have proposed a new approach for the solution of rarefied gas dynamics problems through a dynamic coupling of kinetic and fluid equations. This method extends previous works [37] where a static coupling was considered. The main feature of the work is that the two models are coupled in a region in which the full solution is recovered by summing up the two (kinetic and fluid) contributions. One advantage of this technique is that no boundary condition is needed at the boundary of each zone, by contrast to conventional domain decomposition schemes. This makes the method very flexible. In the present work, we have proposed a procedure to dynamically update the location of the different fluid and kinetic regions. This allows a time adaptation of the domain decomposition technique which dramatically increases the efficiency of the method. Another important feature of the method which has been highlighted in the present work is the possibility of creating new kinetic regions (in other words, the topology of the domain decomposition itself can be dynamically updated). The combination of

different criteria both of macroscopic and microscopic nature allows to reliably detect the regions of sharp gradients and discontinuities where the microscopic model must be solved and we can define a priori the approximation tolerance that we decide to accept.

The last part of the paper is devoted to numerical tests in order to compare the performances and results of the coupling method with respect to both the macroscopic and microscopic models. Although only one-dimensional results have been presented, and further tests must be performed to completely validate the method, the results look very encouraging. The algorithm performs well with the two different numerical schemes that have been experimented and significant computational speedup can be achieved without compromising the accuracy of the results. Compared to a steady domain decomposition method, the possibility of dynamically updating the kinetic region allows us to shrink the kinetic zones to the region of interest at any time which results in considerably improved efficiency.

In the future, the numerical tests need to be extended to two dimensional problems. The dynamic domain decomposition strategy will also be adapted to different coupling methods such the localized kinetic upscaling method of Degond, Liu and Mieussens [39], or the hybrid domain decomposition method developed by Dimarco and Pareschi [45] where a Monte Carlo scheme is used to compute the solution of the Boltzmann-BGK equations.

Chapter 3

Hybrid Multiscale Methods II. Kinetic Equations

This Chapter is based on the work [44] published in **SIAM Multiscale Modeling and Simulation Vol 6., No 4,pp. 1169-1197** in collaboration with Prof. Lorenzo Pareschi of the Department of Mathematics and Center for Modeling Computing and Statistics (CMCS) of University of Ferrara.

3.1 Introduction

A broad range of scientific problems involve multiple scales and multi-scale phenomena (material science, chemistry, fluid dynamics, biology...). Examples are microscopic departures from macroscopic neutrality in plasmas, dislocation in plastic deformation, turbulence in fluid or molecular reaction in biology simulations. These phenomena involve different physical laws which govern the processes at different scales. In many situations we are interested only to the macroscopic scale of the problems and we would like to have equations to describe these macroscopic variables ignoring the rest. From the computational point of view, the representation of the solution through the microscopic model has an overwhelming cost. To this aim many numerical methods have been developed which address explicitly the multiscale structure of the solution like wavelet [67], domain decomposition [10, 11, 37, 38, 75] stiff solvers [21, 62, 64, 65] adaptive mesh refinement [22, 105]. In addition coupling techniques of microscopic stochastic model with macroscopic deterministic model for ODE or PDE [48, 49, 50] gave very good results in the nearby past. In the present work we af-

ford in details the problem in the case of multiscale kinetic equations. The Navier-Stokes or the Euler equations, that describe the problem at the macroscopic level, do not give a satisfactory descriptions of the physical system in all situations and a kinetic description through the Boltzmann equation is often required. The development of numerical methods to solve rarefied gas dynamic (RGD) problems is a big challenge due to the presence of different time and/or space scales. As a consequence the dominant methods for the computations are based on probabilistic Monte-Carlo techniques at different levels [7, 89, 93]. They have many advantages in terms of computational cost for problems with high dimensions, simplicity in preserving some physical properties of the underlying problem (typically using a particle interpretation of the statistical sample) and great flexibility when dealing with complicate geometries. On the other hand, particle methods yield low accurate and fluctuating results with respect to deterministic methods and the convergence in general is quite low. Typically, in continuum regions a macroscopic numerical scheme that solves the Euler or the Navier-Stokes equations gives the correct results. Thus it is highly desirable to have a method that combine a Monte Carlo solver in non equilibrium regions with a deterministic solver in equilibrium ones. Domain decomposition techniques are then often used in order to better treat this difficulties and to design suitable numerical schemes. However, this multi-modelling approach, requires the a-priori knowledge of some of the scales, in order to define the different regions where the different models are valid, which are typically hard to know in practice [10, 75, 40].

In this paper we will focus on the BGK-Boltzmann model which is known to be accurate in describing systems close to equilibrium [34]. First we extend the results obtained in [43] for the solution of system of hyperbolic equations with relaxation to the case of kinetic equations. Next, we propose several generalizations to the multiscale hybrid schemes in order to afford the new complications that arise in the simulation of multiscale RGD, like the lack of a compact support for the probability distribution function in velocity space.

The strategy is based on the solution of the full model in the whole computational domain and on the design of the numerical method in such a way that it is capable to take advantage of the model reduction when we approach the thermodynamic equilibrium. This involves the development of heterogeneous numerical methods which hybridize different numerical approaches of probabilistic and deterministic nature.

The main features of the schemes can be summarized as follows

- In regions far from equilibrium, where the solution of the full kinetic equa-

tion is required, the schemes provide a probabilistic Monte Carlo approximation of the solution.

- In thermodynamic equilibrium regions, where the Euler equations are valid, the schemes provide a deterministic finite volume/difference approximation without any time step restrictions induced by the small relaxation rate.

- In intermediate regions, the approximated solution is generated automatically by the schemes as a suitable blending of a nonequilibrium probabilistic component and an equilibrium deterministic one.

The rest of the article is organized as follows. First we introduce the Boltzmann-BGK equations and its main properties. Then we present the hybrid schemes with particular emphasis to the difference between solving the true Boltzmann-BGK equation (which is not compactly supported in velocity space) and a discrete velocity model (for which we need an artificial boundary in velocity space). Next in Section 3.4 we perform several numerical tests in order to compare the different performances of the methods. Some final considerations are reported in the last section.

3.2 Boltzmann-BGK Equation

We consider the Boltzmann-BGK equation

$$\partial_t f + v \cdot \nabla_x f = \frac{1}{\tau}(M_f - f), \tag{3.2.1}$$

with the initial condition

$$f(x, v, t = 0) = f_0(x, v), \tag{3.2.2}$$

Where $f = f(x, v, t)$ is a non negative function describing the time evolution of the distribution of particles which move with velocity $v \in \mathbb{R}^{d_x}$, in the position $x \in \Omega \subset \mathbb{R}^{d_v}$ at time $t > 0$. In most applications $d_x = d_v = 3$ however one-dimensional and two-dimensional models are often used.

The relaxation time τ is defined in the dimensional case as [1]

$$\tau^{-1} = A_c \varrho \tag{3.2.3}$$

Where A_c is a constant and ϱ is the density. In [37] the relaxation parameter is defined as

$$\tau^{-1} = C\varrho T^{1-\omega} \tag{3.2.4}$$

Where T is the temperature, while ω and C are a constant that depend on the gas. In the adimensional case we have

$$\tau^{-1} = \frac{C_1}{\varepsilon} \tag{3.2.5}$$

The parameter $\varepsilon > 0$ is the Knudsen number and is proportional to the mean free path between collison, while C_1 is a constant that we choose equal to one [34], [107]. In the BGK equation the collision are modelled with a relaxation towards the equilibrium M_f called Maxwellian. The local Maxwellian function is defined by

$$M_f(\varrho, u, T)(v) = \frac{\varrho}{(2\pi T)^{3/2}} \exp\left(\frac{-|u-v|^2}{2T}\right), \tag{3.2.6}$$

where ϱ, u, T are the density, mean velocity and temperature of the gas

$$\varrho = \int_{\mathbb{R}^3} f dv,\ u = \int_{\mathbb{R}^3} v f dv,\ T = \frac{1}{3\varrho}\int_{\mathbb{R}^3} |v-u|^2 f dv, \tag{3.2.7}$$

While the energy E is defined as

$$E = \frac{1}{2}\int_{\mathbb{R}^3} |v|^2 f dv, \tag{3.2.8}$$

Finally we define the kinetic entropy of f by

$$H_f = \int_{\mathbb{R}^3} f \log f dv, \tag{3.2.9}$$

Now, if we consider the BGK equation (3.2.1) and multiply it for 1, v, $\frac{1}{2}|v^2|$, the so-called collision invariant, by integrating in v we obtain the first three moments of the distribution function f:

$$\begin{aligned}
&\frac{\partial \varrho}{\partial t} + \sum_{i=1}^{3} \frac{\partial}{x_i}(\varrho u_i) = 0 \\
&\frac{\partial \varrho u_j}{\partial t} + \sum_{i=1}^{3} \frac{\partial}{x_i}(\varrho u_i u_j + p_{ij}) = 0,\ j = 1,2,3 \\
&\frac{\partial}{\partial t}\left(\frac{1}{2}\varrho|u|^2 + \varrho e\right) + \sum_{i=1}^{3} \frac{\partial}{\partial x_i}\left[\varrho u_i\left(\frac{1}{2}|u|^2 + e\right) + \sum_{i=1}^{3} u_i p_{ij} + q_i\right] = 0
\end{aligned} \tag{3.2.10}$$

This equations are the corresponding conservations laws for mass, momentum and energy, in which e represent the internal energy, p the kinetic pressure while q is the third order moment. Furthermore the dissipation of entropy could easily be proved

$$\partial_t \int f \log f dv + \nabla_x \int v f \log f dv \leq 0 \tag{3.2.11}$$

Unfortunately the differential system of equations (3.2.10) is not closed, since it involves higher order moments of the distribution function. Now, it can be seen that M_f is the unique solution of the following entropy minimization problem

$$H_{M_f} = \min\{H_f,\ f \geq 0\ s.t. \int_{\mathbb{R}^3} \mathbf{m} f = \boldsymbol{\varrho}\} \tag{3.2.12}$$

where $\mathbf{m}$ is the vector containing the collision invariants, while $\boldsymbol{\varrho}$ is the vector containing the first three moments of f

$$\mathbf{m}(v) = (1, v, \frac{1}{2}|v|^2),\ \boldsymbol{\varrho} = (\varrho, \varrho u, E) \tag{3.2.13}$$

This is the well-known Boltzmann *H-theorem*, and it means that the local equilibrium state minimizes the entropy of all the possible states leading to the same macroscopic properties. Now formally as $\varepsilon \to 0$ the function f tends to Maxwellian. In this case it is possible to compute f from its moments thus obtaining the closed Euler system of compressible gas dynamics equations

$$\begin{aligned} &\frac{\partial \varrho}{\partial t} + \nabla_x \cdot (\varrho u) = 0 \\ &\frac{\partial \varrho u}{\partial t} + \nabla_x \cdot (\varrho u \otimes u + p) = 0, \\ &\frac{\partial E}{\partial t} + \nabla_x \cdot (Eu + pu) = 0 \\ &p = \varrho T,\ \ E = \frac{3}{2}\varrho T + \frac{1}{2}\varrho |u|^2 \end{aligned} \tag{3.2.14}$$

3.2.1 Boundary Conditions

Typically, equation (3.2.1) is completed with boundary conditions for $x \in \partial\Omega$ and for $v \cdot n \geq 0$ where n denotes the unit normal, pointing inside the domain. The boundary conditions are modelled by

$$|v \cdot n| f(x, v, t) = \int_{v_* \cdot n < 0} |v_* \cdot n| K(v_* \to v, x, t) f(x, v_*, t) dv_* \tag{3.2.15}$$

Where v_* is the velocity after the process. The entering flux is described as a function of the outgoing flux modified by the boundary kernel K. Such definition of the boundary condition preserve the mass if

$$K(v_* \to v, x, t) \geq 0, \int_{v_* \cdot n \geq 0} K(v_* \to v, x, t) dv = 1 \tag{3.2.16}$$

Usually we apply two type of boundary condition absorbing or reflecting, another condition could be a convex combination of the two. From a physical point of view one assume that a fraction of particle (α) is absorbed and re-emitted at a temperature and velocity corresponding to a Maxwellian (with temperature and velocity of the boundary), while the other $(1 - \alpha)$ is specular reflected, this is equivalent to impose for the ingoing velocities

$$f(x, v, t) = (1 - \alpha) * Rf(x, v, t) + \alpha M f(x, v, t), \ v \cdot n(x) \geq 0 \tag{3.2.17}$$

And

$$\begin{aligned} Rf(x, v, t) &= f(x, v - 2n(n \cdot v), t) \\ Mf(x, v, t) &= \mu(x, t) M_\omega(v, t) \end{aligned} \tag{3.2.18}$$

If we denote by T_ω the temperature of the boundary and by u_ω the velocity, M_ω is given by

$$M_\omega(\varrho, u_\omega, T_\omega)(v) = \frac{\varrho}{(2\pi T_w)^{3/2}} \exp\left(\frac{-|u_w - v|^2}{2T_w}\right), \tag{3.2.19}$$

Finally the value of μ is determined by mass conservation

$$\mu(x, t) \int_{v \cdot n \geq 0} M_\omega(v) |v \cdot n| dv = \int_{v \cdot n < 0} f(x, v, t) |v \cdot n| dv \tag{3.2.20}$$

We note that for $\alpha = 0$ (specular reflection) the re-emitted particle have the same flow of mass, temperature and tangential momentum of the incoming molecules, while for $\alpha = 1$ (full accommodation) the re-emitted particle have completely lost memory of the incoming values (only the global mass is conserved).

3.3 Hybrid methods

In the sequel we will restrict for the sake of simplicity to the one dimensional situation $d_x = d_v = 1$, even though our methods apply naturally to the full three

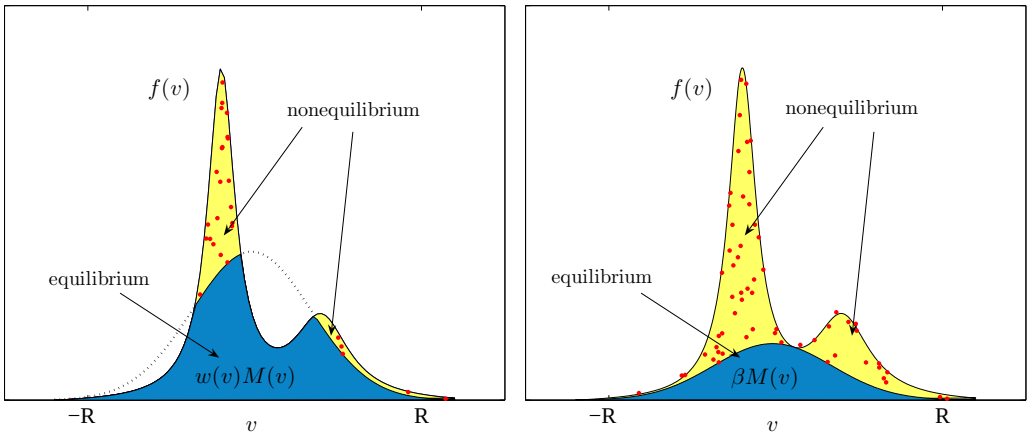

Figure 3.1: Distribution function as a combination of equilibrium and non-equilibrium part representation (3.3.4) left, (3.3.8) right.

dimensional case. Furthermore the dependence on the x and t variables will be omitted in this introductory part.

The starting point in the construction of all the hybrid methods is the interpretation of the distribution function as a probability density,

$$f(v) \geq 0, \ \varrho = \int_{-\infty}^{+\infty} f(v)dv = 1, \tag{3.3.1}$$

and the following definition of hybrid representation

Definition 3.3.1 *Given a probability density $f(v)$, and a probability density $M(v)$, called equilibrium density, we define $w(v) \in [0,1]$ and $\tilde{f} \geq 0$ in the following way*

$$w(v) = \begin{cases} \dfrac{f(v)}{M(v)}, & f(v) \leq M(v) \neq 0 \\ 1, & f(v) \geq M(v) \end{cases} \tag{3.3.2}$$

and

$$\tilde{f}(v) = f(v) - w(v)M(v). \tag{3.3.3}$$

Thus $f(v)$ can be represented as

$$f(v) = \tilde{f}(v) + w(v)M(v). \tag{3.3.4}$$

If we take now

$$\beta = \min_v \{w(v)\}, \tag{3.3.5}$$

and

$$\tilde{f}(v) = f(v) - \beta M(v), \tag{3.3.6}$$

we have

$$\int_v \tilde{f}(v)dv = 1 - \beta. \tag{3.3.7}$$

Let us define for $\beta \neq 1$ the probability density

$$f^p(v) = \frac{\tilde{f}(v)}{1-\beta}.$$

The case $\beta = 1$ is trivial since it implies $f(v) = M(v)$. Thus the probability density $f(v)$, can be written as a convex combination of two probability densities in the form [16, 17]

$$f(v) = (1-\beta)f^p(v) + \beta M(v). \tag{3.3.8}$$

Clearly the above representation is a particular case of (3.3.4).

Remark 3.3.1 *If we define for* $R > 0$

$$w_R(v) = \begin{cases} w(v), & |v| \leq R \\ 0, & |v| > R \end{cases} \tag{3.3.9}$$

and

$$\tilde{f}_R(v) = \begin{cases} \tilde{f}(v), & |v| \leq R \\ f(v), & |v| > R \end{cases} \tag{3.3.10}$$

we have the representation

$$f(v) = \tilde{f}_R(v) + w_R(v)M(v). \tag{3.3.11}$$

In this case taking

$$\beta_R = \min_v \{w_R(v)\} \geq \beta, \tag{3.3.12}$$

and

$$\tilde{f}_R(v) = f(v) - \beta_R E(v), \tag{3.3.13}$$

where $E(v) = M(v)\Psi(|v| \leq R)$ *and* $\Psi(\cdot)$ *is the indicator function, we have*

$$\int_v \tilde{f}_R(v)dv = 1 - \rho_E\beta_R, \qquad \rho_E = \int E(v)dv \leq 1. \tag{3.3.14}$$

Let us define the probability density

$$f_R^p(v) = \frac{\tilde{f}_R(v)}{1 - \rho_E\beta_R}.$$

Again $f(v)$*, can be written as a convex combination of two probability densities in the form*

$$f(v) = (1 - \rho_E\beta_R)f_R^p(v) + \rho_E\beta_R\frac{E(v)}{\rho_E}. \tag{3.3.15}$$

Off course these representations are particularly useful since, as we will see in the sequel, they allow to restrict the deterministic part of the schemes to compactly supported function in velocity space.

For a more general function which depends also on space and time we consider the following representation

$$f(x,v,t) = \underbrace{\tilde{f}(x,v,t)}_{nonequilibrium} + \underbrace{w(x,v,t)M(x,v,t)}_{equilibrium},$$

where $w(x,v,t)$ is a continuum function (which may or may not be compactly supported in v) that characterizes the equilibrium fraction and $\tilde{f}(x,v,t)$ the non equilibrium part of the distribution function. In order to compute the solution we need to discretize the velocity space, thus practically the function $w(x,v,t)$ becomes the approximation $w_k(x,t) = w(x,v_k,t)$, that means we replace our continuous function by piecewise constant function. The general methodology consist in

- Solve the evolution of the perturbation by Monte Carlo methods. Thus $\tilde{f}(x,v,t)$ will be represented by a set of samples in the computational domain.

- Solve the evolution of the equilibrium fraction by deterministic methods. Thus $w(x,v,t)$ $M(x,v,t)$ will be represented on a suitable grid in the computational domain.

In the sequel we will describe the different schemes. In the first part we start from a discrete velocity model (DVM) of the Boltzmann-BGK equation. Thus the velocity space is naturally discretized and bounded by the model itself and the schemes we obtain in this case represent a direct generalization of [43]. In the second part we show how to extend our methodology to the full Boltzmann-BGK equation without any artificial boundary in the velocity space.

3.3.1 Hybrid DVM-BGK Schemes

In order to introduce the reader to the main tools used we first describe briefly a DVM-BGK and how to solve it with fully deterministic and fully Monte Carlo method.

DVM-BGK

We assume that gas particles can attain only a finite set of velocities (see [84] for details about DVM-BGK models). Let $\mathcal{K}$ be a set of N multi-indexes, defined by $\mathcal{K} = \{k = (k^i)_{i=1}^D, k^i \leq K^i\}$, where $D = 1, 2, 3$ is the space dimension and $\{K^i\}$ are given bounds. The set of possible velocities reads

$$\mathcal{V} = \{v_k = k\triangle v + a, k \in \mathcal{K}\} \tag{3.3.16}$$

where a is an arbitrary vector of $\mathbb{R}^D$ and $\triangle v$ is a scalar. We denote the discrete collision invariants by $\mathbf{m}_k = (1, v_k, \frac{1}{2}|v_k|^2)$, and the continuous distribution function becomes a piecewise constant function $f_{\mathcal{K}}(t, x) = (f_k(t, x))_{k\in\mathcal{K}}$, where each component $f_k(t, x)$ is assumed to be an approximation of $f(x, v_k, t)$. The macroscopic quantities are now given by sums on $\mathcal{V}$.

$$\boldsymbol{\varrho}_{\mathcal{K}}(t, x) = \sum_{k\in\mathcal{K}} \mathbf{m}_k f_k(t, x) \tag{3.3.17}$$

$$H_{\mathcal{K}}(t, x) = \sum_{k\in\mathcal{K}} f_k(t, x) \log f_k(t, x) \tag{3.3.18}$$

The solution of the BGK model is reduced to the solution of a set of N equations:

$$\partial_t f_k + v_k \cdot \nabla_x f_k = \frac{1}{\varepsilon}(\mathcal{E}_k - f_k),\ \forall k \in \mathcal{K} \tag{3.3.19}$$

Now the main problem is to define an approximation $\mathcal{E}_{f_{\mathcal{K}}}$ of the Maxwellian equilibrium $M_{f_{\mathcal{K}}}$ such that conservation is preserved (3.2.10) and dissipation of entropy is assured (3.2.11). Notice that the natural approximation $\mathcal{E}_k = M_{f_{\mathcal{K}}}(v_k)$

cannot satisfy this requirements. Let define $\mathcal{E}_\mathcal{K}$ by the minimum of discrete entropy among all the piecewise constant functions, defined on the same support and with the same discretization of the velocity space, that have the same moments of f

$$H_{\mathcal{E}_\mathcal{K}} = \min\{H_g,\ g \geq 0\ s.t. \sum_{k\in\mathcal{K}} \mathbf{m}_k g_k = \boldsymbol{\varrho}_\mathcal{K}\} \tag{3.3.20}$$

It has been proved that the solution for this problem exist, it is unique and has an exponential form [84]. Due to the above results, the computation of $\mathcal{E}_\mathcal{K}$ can be obtained through the solution of the nonlinear set of equations for $\boldsymbol{\alpha}$

$$\sum_{k\in\mathcal{K}} \mathbf{m}_k \exp(\boldsymbol{\alpha}\cdot\mathbf{m}_k) = \boldsymbol{\varrho}_\mathcal{K} \tag{3.3.21}$$

This nonlinear set of equations can be solved, for instance, by a Newton algorithm. The parameters $\boldsymbol{\alpha}$ are function of t and x and can be expressed in terms of the macroscopic variables ϱ, u, T through

$$\boldsymbol{\alpha} = \left(log\left(\frac{\varrho}{(2\pi RT)^{\frac{3}{2}}} - \frac{|u|^2}{2RT}\right), \frac{u}{RT}, -\frac{1}{RT}\right) \tag{3.3.22}$$

Now, let f_0 be a vector of $\mathbb{R}^N$, if the problem (3.3.19) has a solution $f_\mathcal{K}$, then we have

$$f_k(t,x) > 0,\ \forall\, k,t,x \tag{3.3.23}$$

$$\mathcal{E}_k = \exp(\boldsymbol{\alpha}\cdot\mathbf{m}_k),\ \forall k \tag{3.3.24}$$

$$\partial_t \sum_{k\in\mathcal{K}} \mathbf{m}_k f_k + \nabla_x \cdot \sum_{k\in\mathcal{K}} \mathbf{m}_k v_k f_k = 0 \tag{3.3.25}$$

$$\partial_t \sum_{k\in\mathcal{K}} f_k \log f_k + \nabla_x \cdot \sum_{k\in\mathcal{K}} v_k f_k \log f_k \leq 0 \tag{3.3.26}$$

A deterministic numerical scheme for DVM-BGK

We restrict the presentation of the scheme to one spatial dimension and one velocity dimension on a Cartesian grid (see [84] and [107] for details about DVM-BGK deterministic numerical schemes). The equations to be solved are

$$\partial_t f_k + v_k \cdot \nabla_x f_k = \frac{1}{\varepsilon}(\mathcal{E}_k - f_k),\ \forall k \in \mathcal{K} \tag{3.3.27}$$

Consider a spatial Cartesian uniform grid defined by nodes $x_i = (i\triangle x)$ and a time discretization $t_n = n\triangle t$. Thus $f^n_{k,i}$ is an approximation of $f(t_n, x_i, v_k)$ inside the space cell $I =]x_{i-\frac{1}{2}}, x_{i+\frac{1}{2}}[$, the corresponding discrete equilibrium is denoted by $\mathcal{E}^n_i = (\mathcal{E}^n_{k,i})_{k\in\mathcal{K}}$, and is therefore $\mathcal{E}^n_{k,i} = \exp(\boldsymbol{\alpha}^n_i \cdot \mathbf{m}_k)$, where $\boldsymbol{\alpha}^n_i$ is the unique solution of the non linear set of equations

$$\sum_{k\in\mathcal{K}} \mathbf{m}_k \exp(\boldsymbol{\alpha}^{\boldsymbol{n}}_{\boldsymbol{i}} \cdot \mathbf{m}_k) = \boldsymbol{\varrho}^n_i \tag{3.3.28}$$

The computation of $\boldsymbol{\alpha}^{\boldsymbol{n}}_{\boldsymbol{i}}$ is performed through a Newton algorithm with the choice of $\mathcal{E}^n_{k,i} = M_f(x_i, v_k, t_n),\ \forall k \in \mathcal{K}$ as initial value; in the cases tested the convergence of the method is fast, only one iteration is needed very often, however if the choice of the boundary in velocity space is done wisely $\mathcal{E}^n_{k,i}$ approach $M_f(x_i, v_k, t_n)\ \forall k \in \mathcal{K}$.

Now, in order to introduce the hybrid scheme, we split the problem in a relaxation step and a convection step, the transport part is simply the linear convection equation and can be approximated by a standard finite volume scheme, while the relaxation step is represented by a system of stiff ordinary differential equations. The scheme reads

$$f^c_{k,i} = f^n_{k,i} - \frac{\Delta t}{\Delta x}\left(\mathcal{F}^n_{k,i+1/2} - \mathcal{F}^n_{k,i-1/2}\right)\ \forall k \in \mathcal{K} \tag{3.3.29}$$

Where c indicates the intermediate step after the transport. The numerical fluxes are defined by

$$\mathcal{F}^n_{k,i+1/2} = \frac{1}{2}\left(v_k f^n_{k,i+1} + v_k f^n_{k,i} - |v_k|(f^n_{k,i+1} - f^n_{k,i})\right)\ \forall k \in \mathcal{K} \tag{3.3.30}$$

For the relaxation step we utilize the exact solution of the ODE equation

$$f^r_{k,i} = e^{-\frac{\Delta t}{\varepsilon}} f^c_{k,i} + (1 - e^{-\frac{\Delta t}{\varepsilon}})\mathcal{E}^c_{k,i}\ \forall k \in \mathcal{K} \tag{3.3.31}$$

Where $\mathcal{E}^c_{k,i}$ is the discrete equilibrium function computed with the moments found after the convection. The distribution function at the next time step is simply $f^{n+1}_{i,k} = f^r_{i,k}\ \forall k \in \mathcal{K}$. Finally the time step is computed through the relation

$$\Delta t \left(\max_{\mathcal{K}} \left(\frac{|v_k|}{\Delta x}\right)\right) < 1. \tag{3.3.32}$$

A Monte Carlo scheme for DVM-BGK

A Monte Carlo approach to solve the DVM-BGK equations is the next tool we need for the construction of the hybrid schemes. In this model the distribution function is again represented by a piecewise constant function, defined on a compact support. We describe the scheme in one dimension in space and one dimension in space velocity. First we split the equations in two part: a transport and a relaxation stage

$$\partial_t f_k^c(x,t) + v_k \cdot \nabla_x f_k^c(x,t) = 0 \; \forall k \in \mathcal{K} \tag{3.3.33}$$

$$\partial_t f_k^r(x,t) = -\frac{1}{\varepsilon}(f_k^r(x,t) - \mathcal{E}_k^r(x,t)) \; \forall k \in \mathcal{K} \tag{3.3.34}$$

The solution of the relaxation problem can be sought in the form of an evolution of a discrete probability density in each space point

$$p_k(x,t) = \left\{ \begin{array}{l} \dfrac{f_k(x,t)\Delta v}{\varrho(x,t)}, \quad v = v(k), \; \forall k \in \mathcal{K} \end{array} \right. \tag{3.3.35}$$

Thus, with probability $p_k(x,t)$, we assign to a sample velocity v_k. In order to begin the procedure we need to sample from the discrete probability density defined by the initial data $f_k^0(x,t)$. We want to sample N particle for each interval in the discrete space. We use the following strategy: divide the interval [0,1] in K intervals, i-th interval being of length p_k, extract a uniform $[0,1]$ random number ξ, detect the interval k to which ξ belong, give to the sample velocity v_k. We can proceed as follows for each interval:

Algorithm 3.3.1 (Discrete sampling)

1. *compute* $P_k = \sum_{i=1}^{k} p_k, k = 1, .., K, P_0 = 0$
2. *find the integer* k *such that* $P_{k-1} \leq \xi < P_k$*, with* ξ *random number in* $[0,1]$.

Once P has been computed, step 2 can be performed with a binary search, in $O(\ln K)$. Let us define with $\{\nu_1, \nu_2, \ldots, \nu_N\}$ the initial samples from $p_{k,i}^0$ at a given space point x_i. Hence a Monte Carlo method to obtain samples from $p_{k,i}^n$ with n time step and ϱ_i solutions of the transport step is

Algorithm 3.3.2 (Monte Carlo for DVM-BGK equations)

1. *Given N samples ν_k*
   (a) *with probability $e^{-t/\varepsilon}$ the samples are unchanged*
   (b) *with probability $1 - e^{-t/\varepsilon}$ the samples are replaced with equilibrium samples. To extract N equilibrium samples proceed as follows*
      i. *compute $p_{k,i} = \frac{\mathcal{E}^r_{k,i}\Delta v}{\varrho_i}$*
      ii. *use **Algorithm 1***

Where $\mathcal{E}^r_{k,i}$ represent the discrete equilibrium function at point x_i, computed with the moments found after convection. Note that the above procedure requires the exact knowledge of ϱ_i which we can only estimate from the samples at the given point x_i. In practice we need the knowledge of density, mean velocity and temperature at each point x_i to reconstruct the discrete Maxwellian. The simplest method, which produces a piecewise constant reconstruction, is based on evaluating the histogram of the samples on the grid. Given a set of N samples with position $\chi_1, \chi_2, \ldots, \chi_N$ and velocity $\nu_1, \nu_2, \ldots, \nu_N$, we define the discrete probability density at the cell centers

$$p_k(x_i) = \frac{1}{N}\sum_{j=1}^{N} \Psi_{\Delta x}(\chi_j - x_i)\Phi_{\Delta v}(\nu_j - v_k), \quad i,k = \ldots, -2, -1, 0, 1, 2, \ldots \tag{3.3.36}$$

where $\Psi_{\Delta x}(x) = 1$ if $|x| \leq \Delta x/2$ and $\Psi_{\Delta x}(x) = 0$ elsewhere, while $\Phi_{\Delta v}(v) = 1$ if $|v| \equiv 0$ and $\Phi_{\Delta v}(v) = 0$ in other cases.

Let us denote by the index k the sample ν_k and its position χ_k. If we use equations (3.3.36) then ϱ_i is given by the number of samples N_j belonging to the cell I_i

$$\varrho_i = \frac{m}{\Delta x}\sum_{\chi_k \in I_i} 1 = \frac{m}{\Delta x} N_j \tag{3.3.37}$$

where $m = \frac{1}{N}\int \varrho dx$, while the mean velocity and the energy are given by

$$u_i = \frac{1}{N_j}\sum_{\chi_k \in I_i} \nu_k, \; E_i = \frac{1}{2N_j}\frac{m}{\Delta x}\sum_{\chi_k \in I_i} |\nu_k|^2 \tag{3.3.38}$$

We refer the reader to [99] (and the references therein) for an introduction to basic sampling and different reconstruction techniques in Monte Carlo methods.

Finally the transport step does not present any difficulty and can be applied without any need of meshes or reconstructions. In fact, from the exact expression of the solution $f^c_{k,i} = f^r_{k,i}(x - v_k t, t)\ \forall k \in \mathcal{K}$, we simply need to shift the position of the samples accordingly to the law

$$\chi_k = \chi_k + \nu_k t, \quad \forall k. \tag{3.3.39}$$

In the sequel we will use the terminology "particle" to denote the pair (χ_k, ν_k) characterizing the sample ν_k and its position χ_k.

The method described above deserves some remarks.

Remark 3.3.2

- *One important aspect in the method is that we do not need to reconstruct the functions $f_{\mathcal{K}}$ but only the conserved quantity ϱ, u, T.*
- *As for the deterministic DVM-BGK, the Monte Carlo scheme presented needs the computation of a discrete equilibrium function through some iterative solver, such as Newton method.*
- *Note that as $\varepsilon \to 0$ the method becomes a Monte Carlo algorithm for the limiting fluid dynamic equations. This limiting method is the analogue of a kinetic particle method for the compressible Euler equations.*
- *The simple splitting method we have described here is first order in time. Second order Strang splitting can be implemented similarly.*

The hybrid method (HM)

The standard hybrid method is based on the hybrid representation (3.3.8). In the DVM case we consider the hybrid representation for the function $f_{\mathcal{K}}$ instead of f using $\mathcal{E}_{\mathcal{K}}$ instead of $M_{f_{\mathcal{K}}}$. We have two differences respect (3.3.8), the function $f_{\mathcal{K}}$ and $\mathcal{E}_{\mathcal{K}}$ are piecewise constant and defined on a compact support (see figure 3.2 for the representation of $\mathcal{E}(v)$ respect to $M_f(v)$ in the continuous case). Thus we assume that the solution of the relaxation step has the form

$$f^r_k(x,t) \;=\; (1 - \beta^r(x,t)) f^{r,p}_k(x,t) + \beta^r(x,t)\mathcal{E}^r_k(x,t),\ \forall k \in K \tag{3.3.40}$$

From the exact solution of the relaxation step (3.3.31) and the initial data we could obtain the evolution of the unknowns $f^p_{k,i}$ and β^r_i, for the detail of the computations

we remind the reader to [43]

$$f_k^{r,p}(x,t) = f_k^p(x,t=0),\ \forall k \in K \tag{3.3.41}$$
$$\beta^r(x,t) = e^{-t/\varepsilon}\beta(x,t=0) + 1 - e^{-t/\varepsilon}. \tag{3.3.42}$$

Note that $\mathcal{E}_k^r(x,t) = \mathcal{E}_k(x,t=0)$ and that $\beta^r(x,t) \to 1$ as $\varepsilon \to 0$. If we start from $\beta(x,t=0) = 0$ (all particles) at the end of the relaxation a fraction $1-e^{-t/\varepsilon}$ of the particles is discarded by the method as the effect of the relaxation to equilibrium. Thus particles will represent the fractions $(1-\beta^r(x,t))f_k^{r,p}(x,t)$. Moreover the hybrid representation is naturally kept by the relaxation.

After relaxation the exact solution of the transport step reads

$$\begin{aligned} f_k^c(x,t) &= (1-\beta^c(x,t))f_k^{c,p} + \beta^c(x,t)\mathcal{E}_k^c(x,t) = f_k^r(x-v_kt,t) \\ &= (1-\beta^r(x-v_kt,t))f_k^{r,p}(x-v_kt,t) + \\ &+ \beta^r(x-v_kt,t)\mathcal{E}_k^r(x-v_kt,0),\ \forall k \in K. \end{aligned} \tag{3.3.43}$$

To simplify notations let us set

$$f_k^{*,p}(x,t) = (1-\beta^r(x-v_kt,t))f_k^{r,p}(x-v_kt,t),\ \forall k \in K$$
$$\mathcal{E}_k^*(x,t) = \beta^r(x-v_kt,t)\mathcal{E}_k^r(x-v_kt,0),\ \forall k \in K.$$

Unfortunately now the hybrid structure of the solution is not kept since $\mathcal{E}_k^*(x,t)$ are not equilibrium states. For example the above set of equations can be solved taking

$$\beta^c(x,t) = 0, \tag{3.3.44}$$

and

$$f_k^{c,p}(x,t) = f_k^{*,p}(x,t) + \mathcal{E}_k^*(x,t),\ \forall k \in K \tag{3.3.45}$$

The choice (3.3.44) means we completely loose, after the transport, the structure equilibrium non-equilibrium. However, note that we do not need to resample the whole deterministic fraction in fact if we move one step t_1 further in the relaxation using $f_k^c(x,t)$ defined above as initial data we have $\beta^r(x,t+t_1) = 1-e^{-t_1/\varepsilon}$ and

$$f_k^r(x,t+t_1) = e^{-t_1/\varepsilon}(f_k^{*,p} + \mathcal{E}_k^*(x,t)) + (1-e^{-t_1/\varepsilon})\mathcal{E}_k^r(x,t+t_1),\ \forall k \in K \tag{3.3.46}$$

Where $\mathcal{E}_k^r(x,t+t_1) = \mathcal{E}_k^c(x,t)$. Thus, in practice, we can avoid to resample particles after the convection and apply the resampling only on a fraction $e^{-t_1/\varepsilon}$ of the deterministic fraction as needed by the relaxation. More precisely taking cell averages of (3.3.46) as in a standard Monte Carlo method, and using equations (3.3.36) for the reconstruction as shown later, the algorithm to compute the particles that represent the fractions $e^{-t_1/\varepsilon}f_k^c(x,t)$ in each interval reads as follows

Algorithm 3.3.3 (Hybrid Monte Carlo for BGK Discrete Velocity Model)

1. *Given* $m = \dfrac{\Delta x \triangle v}{N} \sum_i \sum_k f^c_{k,i}(t) = m^0 = \dfrac{\Delta x \triangle v}{N^0} \sum_i \sum_k f_{k,i}(t=0)$

2. *for each interval* I_i, $i = \ldots, -2, -1, 0, 1, 2, \ldots$

   (a) *set* $\beta_i = 1 - e^{-t_1/\varepsilon}$

   (b) *set* $N_i = \text{Iround}\left((1-\beta_i) \dfrac{\Delta x \triangle v}{m} \sum_k f^c_{k,i}(t) \right)$

   (c) *set* $P_i = \dfrac{u^*_{p,i}(t)}{u^*_{p,i}(t) + u^*_{\mathcal{E},i}(t)}$,

   with $u^*_{p,i}(t) = \sum_k f^{*,p}_{k,i}(t)$

   and $u^*_{\mathcal{E},i}(t) = \sum_k \mathcal{E}^*_{k,i}(t)$

   (d) *for* $k = 1, \ldots, N_i$
   with probability P_i *take* (ν_j, χ_j) *as one of the advected particles.*
   with probability $1 - P_i$ *take one sample* ν_j *from the deterministic fraction. To extract* $(1-P_i)N_i$ *samples from discrete advected Maxwellian do the following*

   i. *Compute* $p_{k,i} = \frac{\mathcal{E}^*_{k,i} \cdot \Delta v}{\varrho_i}$
   ii. *Compute* $P_{k,i} = \sum_{\mathcal{K}} p_{k,i}, k = 1, .., K, P_{0,i} = 0$
   iii. *Compute a random number* ξ
   iv. *find the integer* k *such that* $P_{k-1,i} \leq \xi < P_{k,i}$
   v. *Give to the sample* ν_j *the velocity* v_{k-1}

After this the hybrid solution is computed simply adding the deterministic terms

$$\beta_i \mathcal{E}^r_{k,i}(t + t_1), \ \forall k \in K$$

to the stochastic terms

$$(1 - \beta_i) f^{r,p}_{k,i}(t + t_1), \ \forall k \in K$$

.

Note that as $\varepsilon \to 0$ we do not perform any resampling at all, and we obtain a relaxation scheme for the limiting Euler equations. We denote with the shorthand

HM the hybrid scheme based on the above algorithm to determine the fraction of solution represented by particles which make use of the choice (3.3.44) after the transport.

Remark 3.3.3

- *The convection part corresponding to $f_k^{*,p}(x,t)$ is solved exactly by transport of particles as in a full Monte Carlo method. At variance the convection part corresponding to $\mathcal{E}_k^*(x,t)$ is solved by finite volumes scheme for DVM.*
- *Note that the effective value of β_i used in the above algorithm differs from $1-e^{-t_1/\varepsilon}$. In fact if N_i^c denotes the number of particles in cell i after the convection step, during the relaxation we keep only an integer approximation N_i^β of $(1-\beta_i)N_i^c$. The effective value of β_i can then be computed at the end of the algorithm as*

$$\beta_i^E = 1 - \frac{N_i^\beta}{N_i^c}.$$

Componentwise hybrid method (CHM)

Another approach consist in finding the maximum value of $\beta^c(x,t) > 0$ in order to maximize the deterministic fraction in equations (3.3.43). To achieve this goal we start from representation (4.3.4) which gives for the relaxation step

$$f_k^r(x,t) \;=\; \tilde{f}_k^r(x,t) + w_k^r(x,t)\mathcal{E}_k^r(x,t),\ \forall k \in K \tag{3.3.47}$$

The evolution for the unknowns $\tilde{f}_k^r(x,t)$, $w_k^r(x,t)$ now are (see [43] for details)

$$\tilde{f}_k^r(x,t) = e^{-t/\varepsilon}\tilde{f}_k(x,t=0), \quad w_k^r(x,t) = e^{-t/\varepsilon}w_k(x,t=0) + 1 - e^{-t/\varepsilon},\ \forall k \in K \tag{3.3.48}$$

As before the hybrid representation is kept by the relaxation process. The only difference with respect to the HM method is that particles are discarded from f_k with different ratios, depending to the local equilibrium degree.

Again the convection destroys the structure of the solution and we get

$$\begin{aligned} f_k^c(x,t) &= \tilde{f}_k^c(x,t) + w_k^c(x,t)\mathcal{E}_k^c(x,t) = f_k^r(x - v_k t, t) \\ &= \tilde{f}_k^r(x - v_k t, t) + w_k^r(x - v_k t, t)\mathcal{E}_k^r(x - v_k t, 0),\ \forall k \in K \end{aligned} \tag{3.3.49}$$

To simplify notations let us set

$$f_k^{*,p}(x,t) = \tilde{f}_k^r(x - v_k t, t), \quad \tilde{\mathcal{E}}_k(x,t) = w_k^r(x - v_k t, t)\mathcal{E}_k^r(x - v_k t, 0),\ \forall k \in K.$$

Here we do not assume $w_k^c(x,t) = 0,\ \forall k \in K$, since we want to take advantage of the componentwise hybrid representation in order to maximize the deterministic fraction of the solution. Thus, starting from the deterministic fractions $\tilde{\mathcal{E}}_k(x,t)$ defined above we construct the new values of $w_k^c(x,t)$, $\tilde{f}_k^c(x,t)$, using Definition 4.3.1 in the case of piecewise constant functions defined on a compact support.

More precisely we define

$$w_k^c(x,t) = \begin{cases} \dfrac{\tilde{\mathcal{E}}_k(x,t)}{\mathcal{E}_k^c(x,t)}, & \tilde{\mathcal{E}}_k(x,t) \leq \mathcal{E}_k^c(x,t) \neq 0 \\ 1, & \tilde{\mathcal{E}}_k(x,t) > \mathcal{E}_k^c(x,t) \end{cases} \qquad \forall k \in K \tag{3.3.50}$$

and

$$\mathcal{E}_k^*(x,t) = \tilde{\mathcal{E}}_k(x,t) - w_k^c(x,t)\mathcal{E}_k^c(x,t),\ \forall k \in K. \tag{3.3.51}$$

In this way we obtain

$$\tilde{f}_k^c(x,t) = f_k^{*,p}(x,t) + \mathcal{E}_k^*(x,t),\ \forall k \in K. \tag{3.3.52}$$

The hybrid method based on the computations of the equilibrium fraction after the transport through (3.3.50) will be called CHM. The next relaxation step then applies as in the HM case, substituting the value $\tilde{f}_k^c(x,t)$ with the relation above

$$\begin{aligned} f_k^r(x,t+t_1) &= \tilde{f}_k^r(x,t+t_1) + w_k^r(x,t+t_1)\mathcal{E}_k^r(x,t+t_1) \\ &= e^{-t_1/\varepsilon} f_k^c(x,t) + (1-e^{-t_1/\varepsilon})\mathcal{E}_k^c(x,t) \\ &= e^{-t_1/\varepsilon}(f_k^{*,p}(x,t) + \mathcal{E}_k^*(x,t) + w_k^c(x,t)\mathcal{E}_k(x,t)) + \\ &+ (1-e^{-t_1/\varepsilon})\mathcal{E}_k(x,t),\ \forall k \in K. \end{aligned} \tag{3.3.53}$$

If we define after the convection step

$$\beta^c(x,t) = \min\{w_k^c(x,t)\},\ \forall k \in K, \tag{3.3.54}$$

we maximize the common value of β^c such that the standard hybrid method applies, that particulary choice leads to another hybrid scheme that will be called HMI. This could be very relevant in applications where it is important that the hybrid decomposition is component independent. For instance if we want to treat the equilibrium part trough a macroscopic scheme we have to adopt this strategy. The independent fluid solver strategy will be the subject of a future work [46].

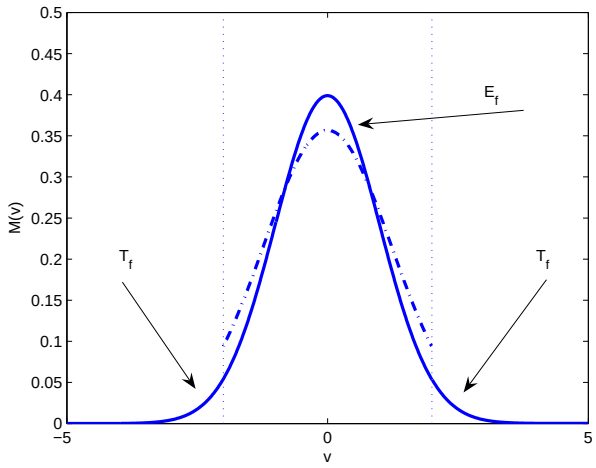

Figure 3.2: Discrete Maxwellian on a truncated velocity domain (dashed lines) and corresponding Maxwellian with same mass, momentum and energy.

3.3.2 Hybrid Boltzmann-BGK Schemes

The use of a discrete velocity model presents several drawbacks. First, since the discrete local Maxwellian equilibrium is needed explicitly, we need a suitable numerical method to solve the non linear system of equations (3.3.21). From the computational side this leads to an increase of computational cost which is especially relevant in higher dimensions. Next, since discrete Maxwellian equilibrium states are compactly supported they differ from Maxwellians of the Boltzmann equation. Thus the corresponding fluid equations may be different from the classical ones (see Figures 3.2 and 3.3), in other words a discrete velocity model cannot describe correctly all possible flows [84]. For this reason it is highly desirable to have a method which is not based on the use of a DVM.

The idea is to split the Maxwellian into two parts

$$M(v) = E_R(v) + T_R(v), \tag{3.3.55}$$

where $E_R(v) = M(v)\Psi(|v| \leq R)$, $R > 0$ represents the central part of the solution and $T_R(v) = M(v)\Psi(|v| > R)$ the tails. The starting point of such schemes is given by representations (3.3.11) and (3.3.15).

Since the schemes follows the same lines of the ones described for the DVM-BGK model we will describe them shortly by emphasizing only the major differ-

ences.

Boltzmann Hybrid Method (BHM)

We start by splitting again our problem into relaxation and transport steps and use representation (3.3.15). The solution of the relaxation now reads

$$f_R^r(x,v,t) = \left(1 - \frac{\rho_E^r(x,t)}{\rho^r(x,t)}\beta_R^r(x,t)\right) f_R^{r,p}(x,v,t) + \beta_R^r(x,t)E_R^r(x,v,t), \tag{3.3.56}$$

where

$$\rho^r(x,t) = \int f_R^r(x,v,t)dv = \int f_R^{r,p}(x,v,t)dv.$$

As before using the exact solution of the relaxation step starting from initial data at $t = 0$ we are able to compute the evolution equations for the unknowns $f_R^{r,p}(x,t)$ and $\beta_R^r(x,t)$. The equation for $\beta_R^r(x,t)$ is the same as in scheme HM

$$\beta_R^r(x,t) = e^{-t/\varepsilon}\beta_R(x,0) + 1 - e^{-t/\varepsilon}. \tag{3.3.57}$$

whereas the equation for the particles distribution now takes into account the changes due to the presence of the tails

$$\begin{aligned} f_R^{r,p}(x,v,t) &= \frac{e^{-t/\varepsilon}\beta_R(x,0) + 1 - e^{-t/\varepsilon}}{a-b} T_R(x,v,0) \\ &+ \frac{1}{a-b}\left(e^{-t/\varepsilon}\left(1 - \frac{\rho_E(x,0)}{\rho(x,0)}\beta_R(x,0)\right)\right) f_R^p(x,v,0), \end{aligned} \tag{3.3.58}$$

where

$$b = (1 - e^{-t/\varepsilon})\left(\frac{\rho_E(x,0)}{\rho(x,0)}\right), \qquad a = \left(1 - \frac{\rho_E(x,0)}{\rho(x,0)}\beta_R(x,0)e^{-t/\varepsilon}\right).$$

The major difference is that as $\varepsilon \to 0$ a fraction $(1 - \rho_E^r(x,t)/\rho^r(x,t))$ of the solution is still represented by particles. After relaxation we transport the particles and the equilibrium part as before to obtain

$$\begin{aligned} f_R^c(x,v,t) &= \left(1 - \frac{\rho_E^c(x,t)}{\rho^c(x,t)}\beta_R^c(x,t)\right) f_R^{c,p}(x,v,t) + \beta_R^c(x,t)E_R^c(x,v,t) \\ &= f_R^{*,p}(x,v,t) + E_R^*(x,v,t). \end{aligned} \tag{3.3.59}$$

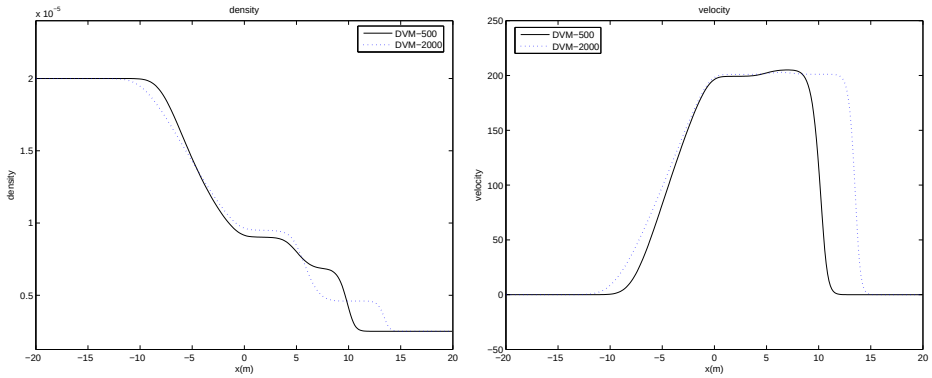

Figure 3.3: Density (left) and velocity (right) profiles for the Sod test, with initial data $\varrho_L = 2 \times 10^{-5}$, $u_L = 0$, $T_L = 273.15$ and $\varrho_R = 0.25 \times 10^{-5}$, $u_R = 0$, $T_R = 273.15$. The limit $\varepsilon \to 0$ for DVM schemes with velocity range $[-2000, 2000]$ and $[-500, 500]$ respectively.

Finally we reproject the solution into the form (3.3.15) by taking $\beta_R^c = 0$ as in scheme HM.

The treatment of the non equilibrium part of the solution has been done using a discrete velocity Monte Carlo scheme for the central part and a general Monte Carlo (i.e. samples can attain any velocity) for the tails. The details of the Boltzmann hybrid method are given in the following algorithm:

Algorithm 3.3.4 (BHM scheme)

1. *Given* $m = \dfrac{\Delta x}{N} \sum_i \varrho_{i,R}^c(t)$, *where* $\varrho_{i,R}^c(t)$ *represent the total mass in each cell at time* t *after convection, that now differs from* $\triangle v \sum_k f_{k,i,R}^c(t)$

2. *for each interval* I_i, $i = \ldots, -2, -1, 0, 1, 2, \ldots$

   (a) *set* $\beta_i = 1 - e^{-t_1/\varepsilon}$

   (b) *set* $N_i = \text{Iround}\left((1-\beta_i)\dfrac{\Delta x}{m}\varrho_i^c(t)\right)$

   (c) *set* $P_i = \dfrac{u_{p,i}^*(t)}{u_{p,i}^*(t) + u_{E,i}^*(t)}$,

with $u^*_{p,i}(t) = \frac{m}{\Delta x}\sum_{\chi_k \in I_i} 1 = \frac{m}{\Delta x} N_j$, *where* N_j *indicate the particles that belong to the cell* I_i

and $u^*_{E,i}(t) = \sum_k E^*_{k,i,R}(t)$

(d) for $k = 1, \ldots, N_i$
with probability P_i *take* (ν_j, χ_j) *as one of the advected particles.*
with probability $1 - P_i$ *take one sample* ν_j *from the deterministic fraction. To extract* $(1-P_i)N_i$ *samples from discrete advected central part of the Maxwellian do the following*

i. Compute $p_{k,i} = \frac{E^*_{k,i,R}\cdot\Delta v}{\varrho_i}$
ii. Compute $P_{k,i} = \sum_{\mathcal{K}} p_{k,i}, k = 1, .., K, P_{0,i} = 0$
iii. Compute a random number ξ
iv. find the integer k *such that* $P_{k-1,i} \leq \xi < P_{k,i}$
v. Give to the sample ν_j *the velocity* v_{k-1}

(e) set $N_i^T = \text{Iround}\left(\beta_i\left(\frac{\Delta x}{m}\varrho^c_{i,R}(t) - \frac{\Delta x \triangle v}{m}\sum_k f^c_{k,i,R}(t)\right)\right)$

(f) for $k = 1, .., N_i^T$ *extract a sample from the tail of the Maxwellian. To extract a sample from the right tail do as following*

i. Compute $r = cos(2 * \pi * \xi_1)$
ii. if $r > 0$ *Compute* $v = \sqrt{-\log(\exp(-R^2) - \xi_2 * \exp(-R^2))}$ *with* ξ_1 ξ_2 *random numbers in* $[0, 1]$.
iii. if $v > R$ *take the sample, else reject the sample.*

As for the HM scheme the final solution is recovered by adding the deterministic term $\beta_i\ E_{k,i,R}(t)$, to the stochastic term.

Boltzmann Componentwise Hybrid Method (BCHM)

The componentwise approach described in the previous section can be adapted to the case of representation (3.3.11). We have

$$f^r(x,v,t) \;=\; \tilde{f}^r_R(x,v,t) + w^r_R(x,v,t)M^r(x,v,t). \tag{3.3.60}$$

The evolution for the unknowns $\tilde{f}^r_R(x,v,t)$, $w^r_R(x,v,t)$ now are

$$\tilde{f}^r_R(x,v,t) \;=\; e^{-t/\varepsilon}\tilde{f}_R(x,v,0) + (1-e^{-t/\varepsilon})T_R(x,v,0), \tag{3.3.61}$$
$$w^r_R(x,v,t) \;=\; e^{-t/\varepsilon}w_R(x,v,0) + (1-e^{-t/\varepsilon})\Psi(|v| \leq R). \tag{3.3.62}$$

Clearly as in scheme BHM as $\varepsilon \to 0$ a fraction of the solution is represented by particles. Again after convection we have

$$f_R^c(x,v,t) = \tilde{f}^c(x,v,t) + w_R^c(x,v,t)M^c(x,v,t) = f_R^{*,p}(x,v,t) + \tilde{M}^r(x,v,t),$$

where $f_R^{*,p}(x,v,t)$ and $\tilde{M}^r(x,v,t)$ represent the advected particles and equilibrium fractions. The value $w_R^c(x,v,t)$ is now computed only in the central part of f, $|v| \leq R$, by

$$w_R^c(x,v,t) = \begin{cases} \dfrac{\tilde{M}^r(x,v,t)}{M^c(x,v,t)}, & \tilde{M}^r(x,v,t) \leq M^c(x,v,t) \neq 0 \\ 1, & \tilde{M}^r(x,v,t) > M^c(x,v,t). \end{cases} \tag{3.3.63}$$

Then we define

$$M^*(x,v,t) = \tilde{M}^r(x,v,t) - w_R^c(x,v,t)M^c(x,v,t)$$

to obtain

$$\tilde{f}^c(x,v,t) = f_R^{*,p}(x,v,t) + M^*(x,v,t). \tag{3.3.64}$$

Finally the same strategy, described in previous section, of taking $\beta_R^c(x,t) = \min_v\{w_R^c(x,v,t)\}$ could be adopted for applications in which the decomposition is component independent. We omit the details.

3.4 Numerical tests

In this section we compare the performance of the Monte Carlo and the Hybrid schemes here presented using two classical tests: a Sod test and an unsteady shock test. We have chosen two unsteady tests because we would like to test the performance of the methods without the effect of averaging the solution in time (typical of Monte Carlo methods for steady problems). Before this, however, we have performed an overall accuracy test of the different schemes.

3.4.1 Accuracy test

We report the total L_1 norm of the errors for the conserved quantity ϱ, u, and T by considering a periodic smooth solution with initial data

$$\varrho(x,0) = 1 + a_\varrho \sin\frac{2\pi x}{L}$$

	$\varepsilon = 10^{-2}$	$\varepsilon = 10^{-3}$	$\varepsilon = 10^{-4}$	$\varepsilon = 10^{-5}$	$\varepsilon = 10^{-6}$
MCM	2.1512	2.3435	2.6886	2.6684	2.6529
HM	2.0234	1.7406	1.2126	0.4020	0.12868
HMI	1.9934	1.600	0.7888	0.2895	0.0961
CHM	1.1704	0.6233	0.2743	0.10938	0.0309
BHM	1.9660	1.9125	1.3499	0.8163	0.7258
BHMI	1.7115	1.4536	0.7517	0.7212	0.6866
BCHM	1.4685	0.9204	0.7000	0.6439	0.6538

Table 3.1: Accuracy test, L_1 norm of the errors for density respect to different value of the Knudsen number ε (in units of 10^{-2}).

	$\varepsilon = 10^{-2}$	$\varepsilon = 10^{-3}$	$\varepsilon = 10^{-4}$	$\varepsilon = 10^{-5}$	$\varepsilon = 10^{-6}$
MCM	2.9320	3.5061	4.8096	4.626	4.6652
HM	2.8686	2.2685	2.1736	0.7182	0.2503
HMI	2.3551	1.9552	1.3733	0.4994	0.1851
CHM	1.3448	0.9139	0.4739	0.1662	0.0527
BHM	3.0944	2.5336	2.4123	1.5215	1.2635
BHMI	2.5098	2.2245	1.4186	1.4417	1.3714
BCHM	1.8727	1.5825	1.4079	1.2246	1.2355

Table 3.2: Accuracy test, L_1 norm of the errors for velocity respect to different value of the Knudsen number ε (in units of 10^{-2}).

$$u(x,0) = 1 + a_u \sin \frac{2\pi x}{L} \tag{3.4.1}$$

$$T(x,0) = 1 + a_T \sin \frac{2\pi x}{L}$$

Where we set

$$a_\varrho = 0.3 \;\; a_u = 0.1 \;\; a_T = 1$$

we use 1500 particles for cell with bounds set at $[-15, 15]$ for the DVM-BGK schemes and bounds set at $[-5, 5]$ for the Boltzmann-BGK schemes, we integrate the equations for $t \in [0, 5 \times 10^{-2}]$ for $\Delta v = 0.16$ and $\Delta x = 0.05$. We compare our hybrid solutions with a reference solution obtained with a fully deterministic DVM-BGK model with the same Δv and Δx but with bound set at $[-20, 20]$ in velocity space.

	$\varepsilon = 10^{-2}$	$\varepsilon = 10^{-3}$	$\varepsilon = 10^{-4}$	$\varepsilon = 10^{-5}$	$\varepsilon = 10^{-6}$
MCM	3.2923	4.4354	6.2404	5.7733	6.1142
HM	2.9520	2.7893	2.6305	0.96996	0.2840
HMI	2.8437	2.5110	1.6132	0.6617	0.2053
CHM	1.8196	1.2004	0.5368	0.1310	0.0651
BHM	3.1869	3.0254	2.8536	2.1430	1.8134
BHMI	2.7132	2.6807	2.3756	2.0148	2.1010
BCHM	2.6210	2.3226	2.1498	1.9315	1.8849

Table 3.3: Accuracy test, L_1 norm of the errors for temperature respect to different value of the Knudsen number ε (in units of 10^{-2}).

We use the shorthand MCM, HM, HMI, CHM, BHM, BHMI, BCHM to denote the Monte Carlo scheme, the DVM-BGK Hybrid Schemes respectively (3.3.44) (3.3.54) (3.3.50) and the Boltzmann-BGK Hybrid Schemes with the same choice of $\beta^c(x,t)$. The results for the relative L_1 errors are reported in Tables 3.1, 3.2, 3.3. The parameters that influence the numerical solution in all the schemes are the number of particles and the number of mesh point in velocity space. Moreover DVM-BGK schemes are influenced by the truncation of the velocity space and by the method we use to solve the nonlinear system (3.3.21), while BHM schemes are influenced by the position of the boundary that divide E_f from T_f, that turns in different number of particles in the domain. The schemes HM, HMI, CHM cause a progressive reduction of fluctuations as the Knudsen number decreases. On the other hand the deterministic computation of the function $\mathcal{E}$ and of the large velocity components are expensive and the hybrid schemes, independently of ε, are computationally more expensive then MCM.

The Boltzmann-BGK solvers are faster since we do not need to compute the solution of a non linear system at each time step for each component of $\mathcal{E}$. They are also faster because the deterministic solver contain less mesh point. However BHM, BHMI, BCHM present more fluctuations with respect HM, HMI, CHM because tails are represented by particles. We report the corresponding computational times for the Boltzmann-BGK schemes with respect to MCM scheme for different Knudsen number in Table 3.4. Note that all these schemes are more accurate and more efficient then MCM. In particular BCHM for $\varepsilon = 10^{-3}$ is about twice time faster and twice time more accurate then MCM.

We remark that no attempt to optimize the truncation parameter in the Boltzmann-BGK schemes has been done in order to obtain the optimum compromise between accuracy and computational time.

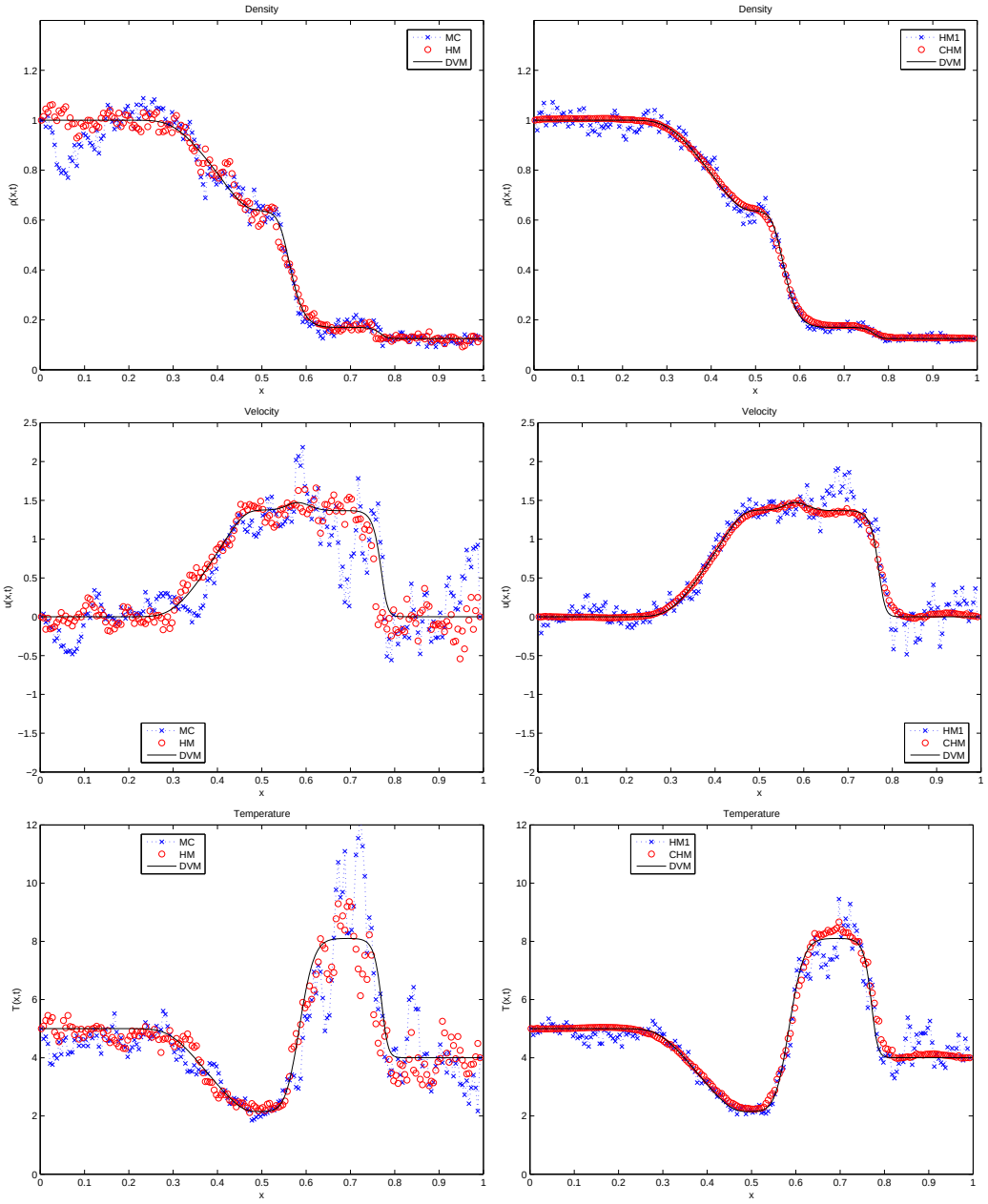

Figure 3.4: Sod test: Solution at $t = 0.05$ with $\varepsilon = 10^{-3}$ for density (top), mean velocity (middle) and temperature (bottom) for MCM and HM (left), HMI and CHM (right), with initial data (3.4.2).

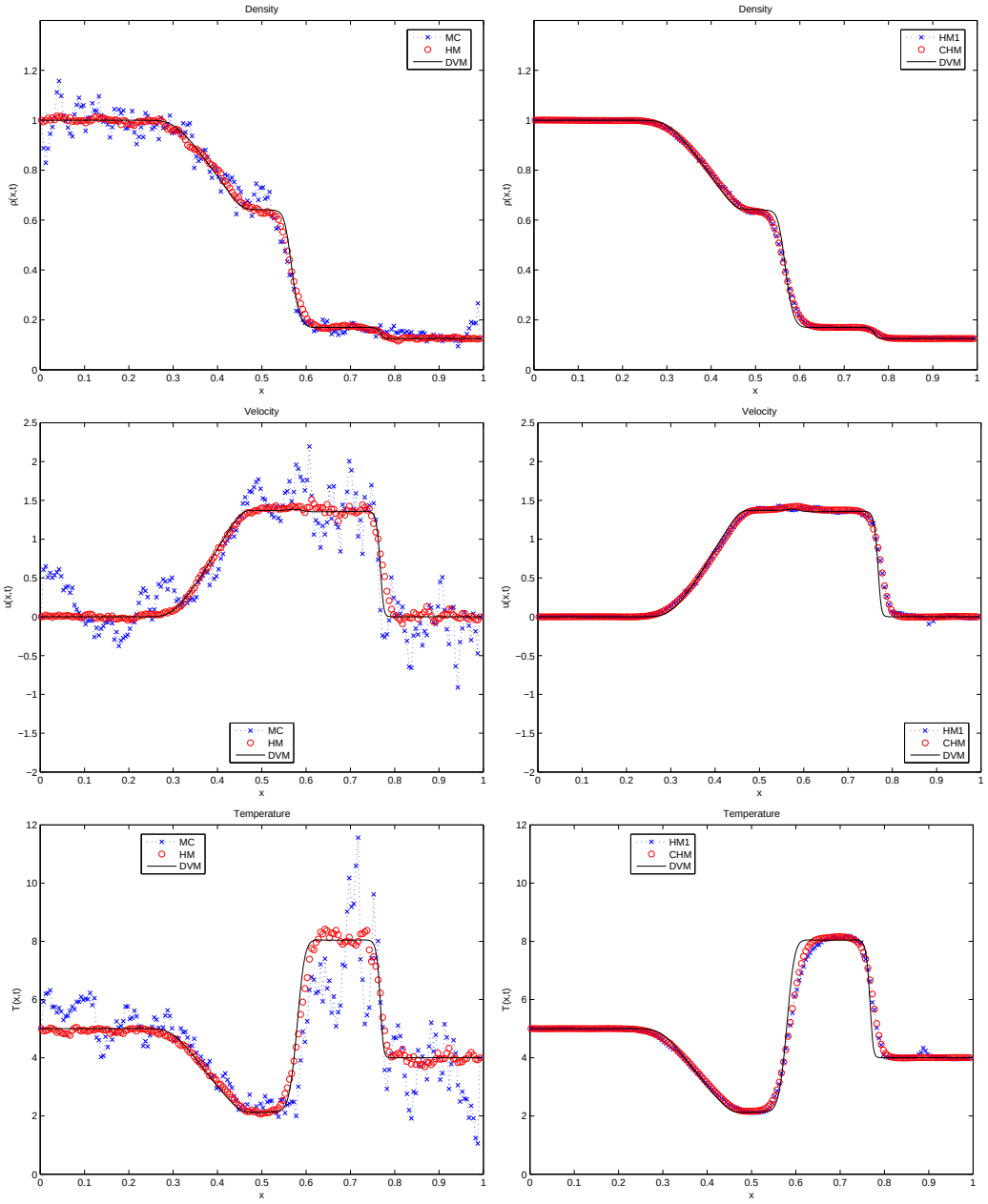

Figure 3.5: Sod test: Solution at $t = 0.05$ with $\varepsilon = 10^{-5}$ for density (top), mean velocity (middle) and temperature (bottom) for MCM and HM (left), HMI and CHM (right), with initial data (3.4.2).

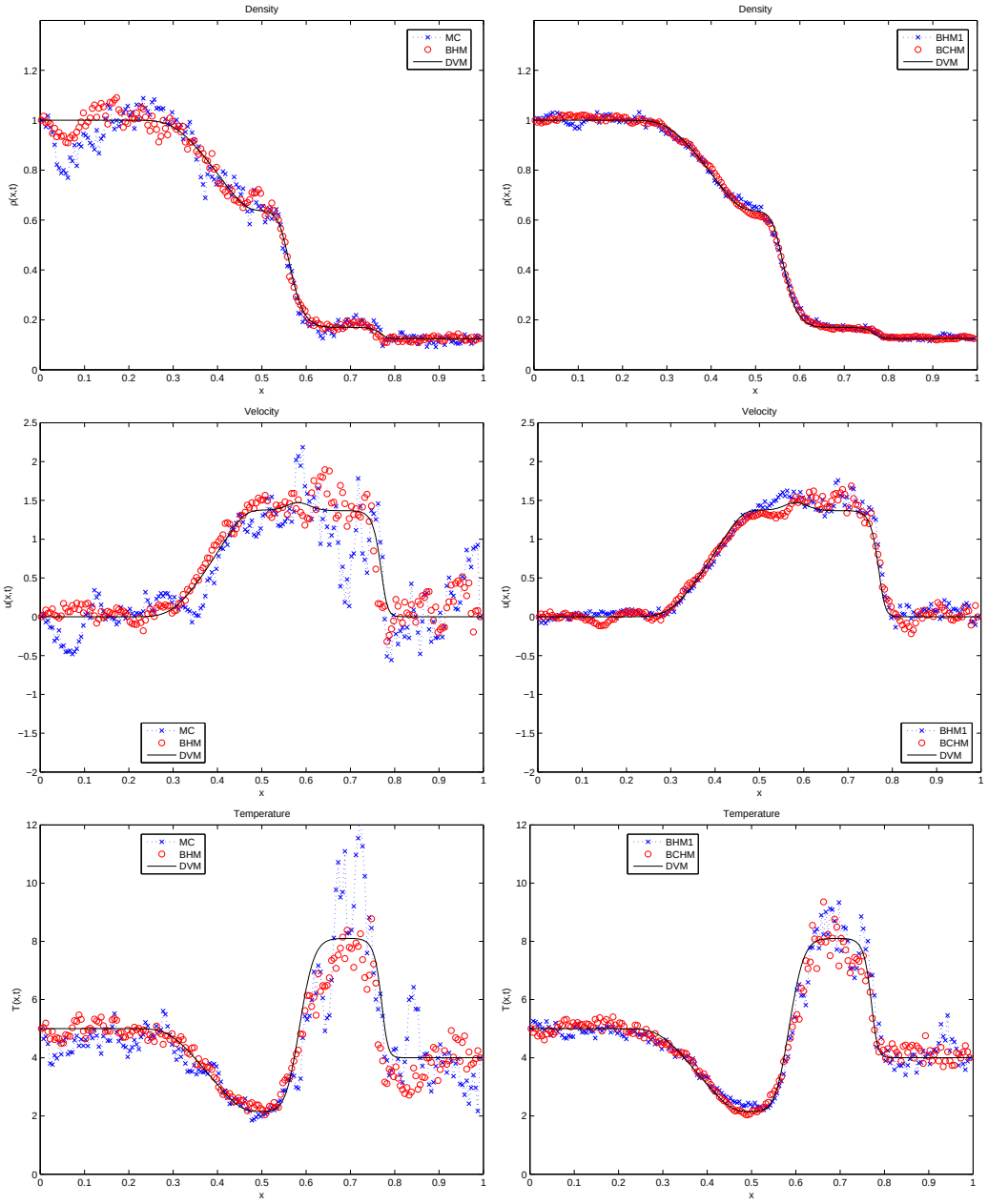

Figure 3.6: Sod test: Solution at $t = 0.05$ with $\varepsilon = 10^{-3}$ for density (top), mean velocity (middle) and temperature (bottom) for MCM and BHM (left), BHMI and BCHM (right), with initial data (3.4.2).

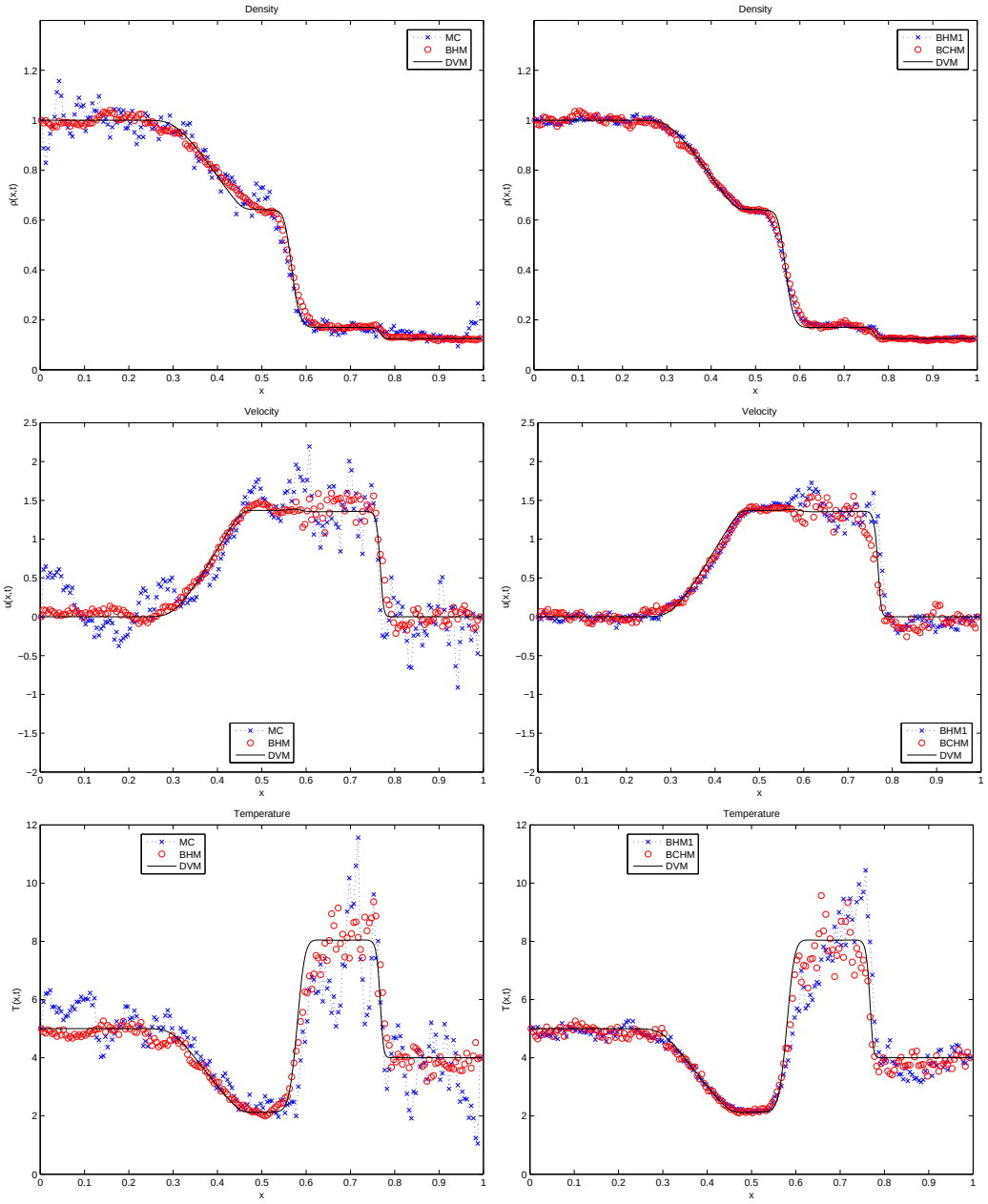

Figure 3.7: Sod test: Solution at $t = 0.05$ with $\varepsilon = 10^{-5}$ for density (top), mean velocity (middle) and temperature (bottom) for MCM and BHM (left), BHMI and BCHM (right), with initial data (3.4.2).

	$\varepsilon = 10^{-2}$	$\varepsilon = 10^{-3}$	$\varepsilon = 10^{-4}$	$\varepsilon = 10^{-5}$	$\varepsilon = 10^{-6}$
MCM	23 sec	25 sec	27 sec	26 sec	27 sec
BHM	35 sec	25 sec	22 sec	22 sec	21 sec
BHMI	34 sec	20 sec	19 sec	20 sec	21 sec
BCHM	15 sec	11 sec	17 sec	21 sec	20 sec

Table 3.4: Computational time test for different value of the Knudsen number ε.

3.4.2 Sod Test

We consider the classical Sod test with initial value

$$\begin{pmatrix} \varrho_L \\ u_L \\ T_L \end{pmatrix} = \begin{pmatrix} 1 \\ 0 \\ 5 \end{pmatrix}, \; if \; 0 \leqq x < 0.5 \quad \begin{pmatrix} \varrho_R \\ u_R \\ T_R \end{pmatrix} = \begin{pmatrix} 0.125 \\ 0 \\ 4 \end{pmatrix}, \; if \; 0.5 \leqq x \leqq 1 \tag{3.4.2}$$

The solution is computed with 200 space points in $[0, 1]$ and the final time is $t = 0.05$. The initial number of particle are 1000 for each space cell, the Knudsen number is $\varepsilon = 10^{-3}$ in one case and $\varepsilon = 10^{-5}$ in the other. In the HM, HMI and CHM schemes the velocity space is bounded at $[-15, 15]$ and discretized with $\Delta v = 0.16$. The bounds between tails and central part of the Maxwellian for BHM, BHMI and BCHM are set to $[-5, 5]$, with the same mesh in velocity. We compare our solutions with a reference solution obtained with a DVM model with 500 space cell and 250 cell in velocity space with bound set at $[-20, 20]$ in velocity. From Figures 3.4, 3.5, 3.6, 3.7 it is clear that all hybrid schemes provide a more accurate solution with less fluctuations with respect to MCM method.

3.4.3 Unsteady shock Test

We consider a unsteady shock that propagates from left to right, the shock is produced introducing a specular wall in the left boundary, this correspond to put an incoming Maxwellian distribution in the ghost cell with parameters ϱ, u, T equal to the parameters $\varrho(1), u(1), T(1)$ in the first cell. At the beginning the flow is uniform with

$$\varrho(x, 0) = 1 \quad u(x, 0) = -1 \quad T(x, 0) = 4 \tag{3.4.3}$$

The computations is stopped when $t = 0.065$, the number of space cells is 200 in $[0, 1]$, the initial number of particle is 1500 for each space cell, the Knudsen

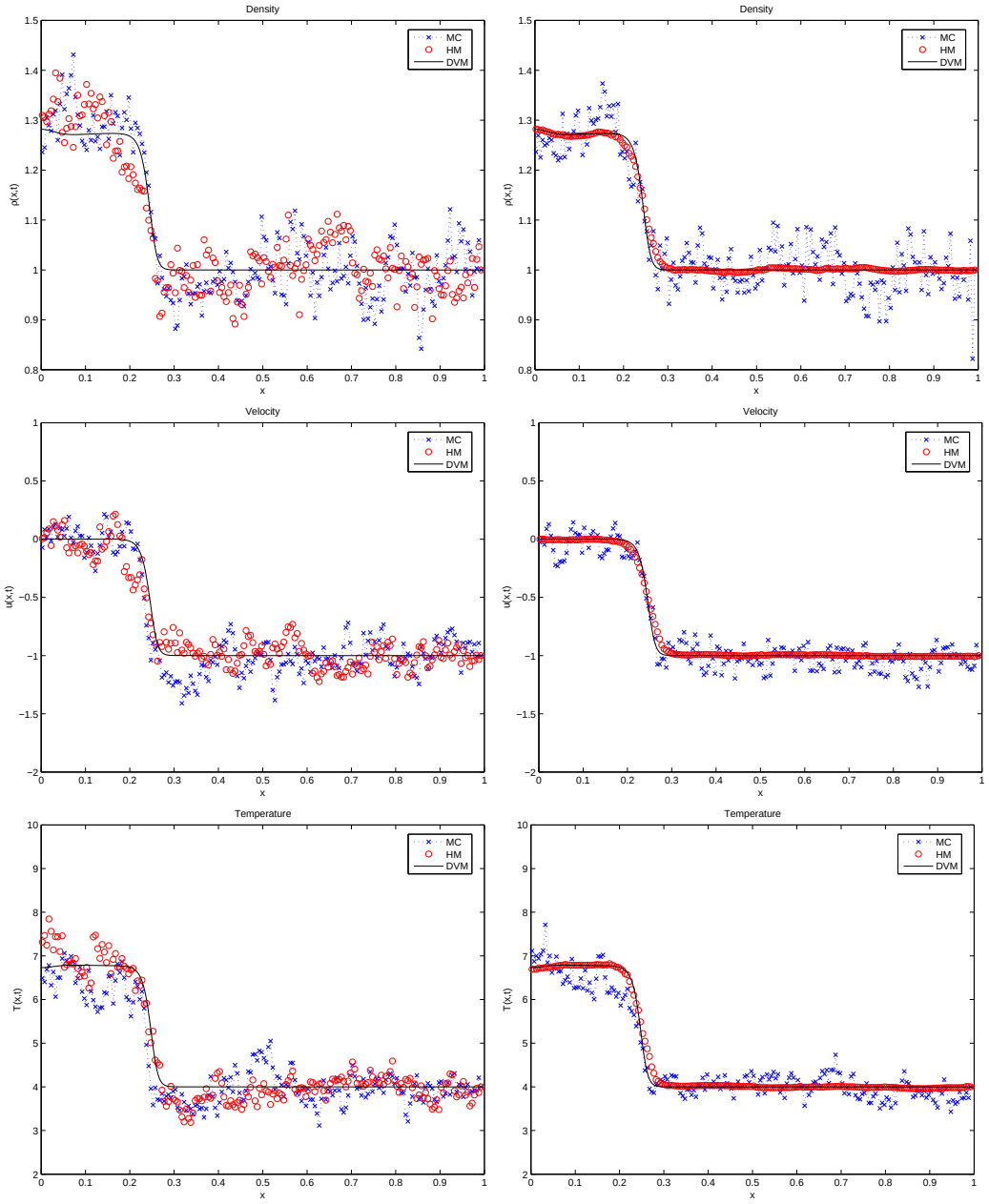

Figure 3.8: Unsteady Shock: Solution at $t = 0.065$ with $\varepsilon = 10^{-3}$ for density (top), mean velocity (middle) and temperature (bottom) for MCM and HM (left), HMI and CHM (right), with initial data (3.4.3).

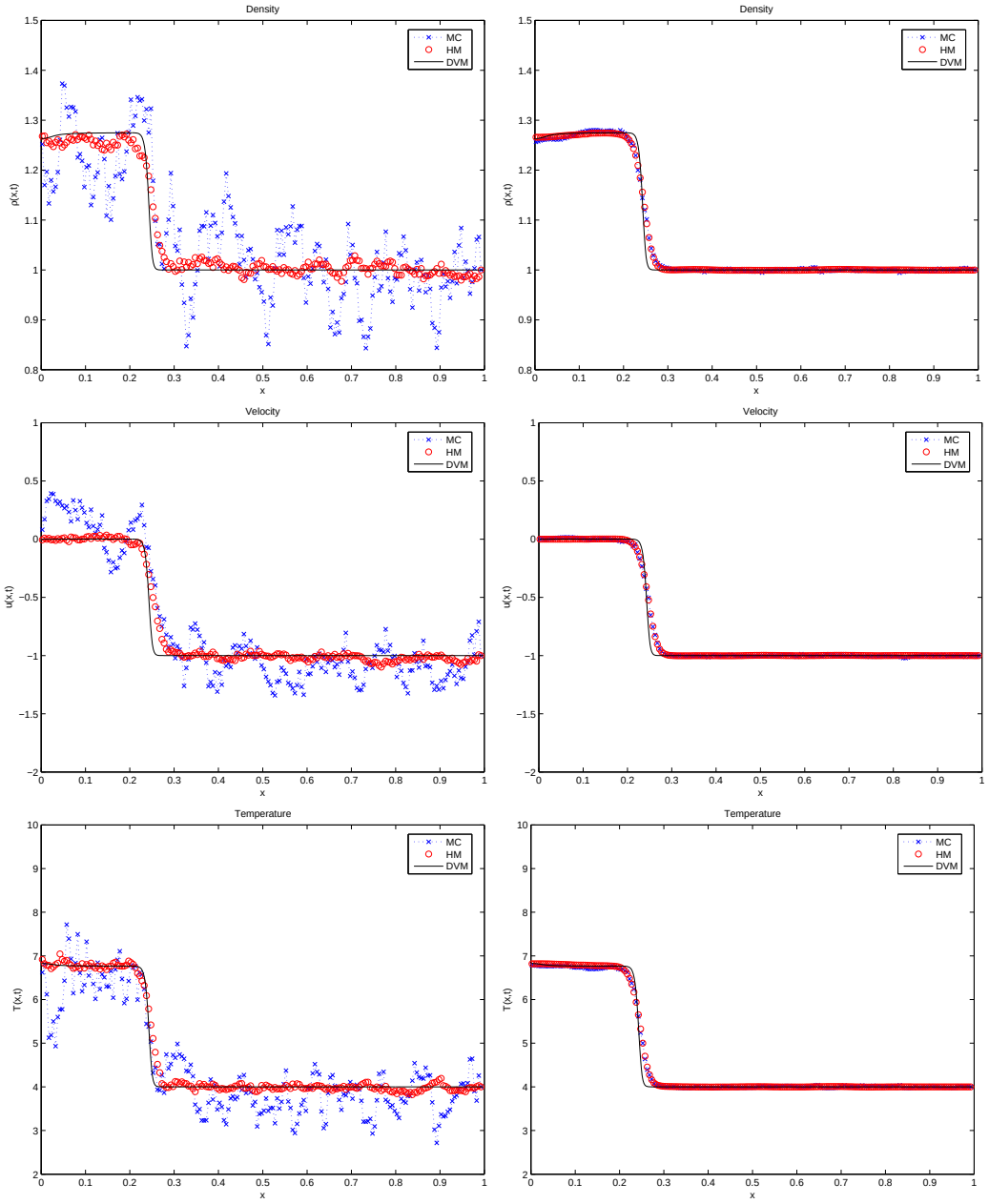

Figure 3.9: Unsteady Shock: Solution at $t = 0.065$ with $\varepsilon = 10^{-5}$ for density (top), mean velocity (middle) and temperature (bottom) for MCM and HM (left), HMI and CHM (right), with initial data (3.4.3).

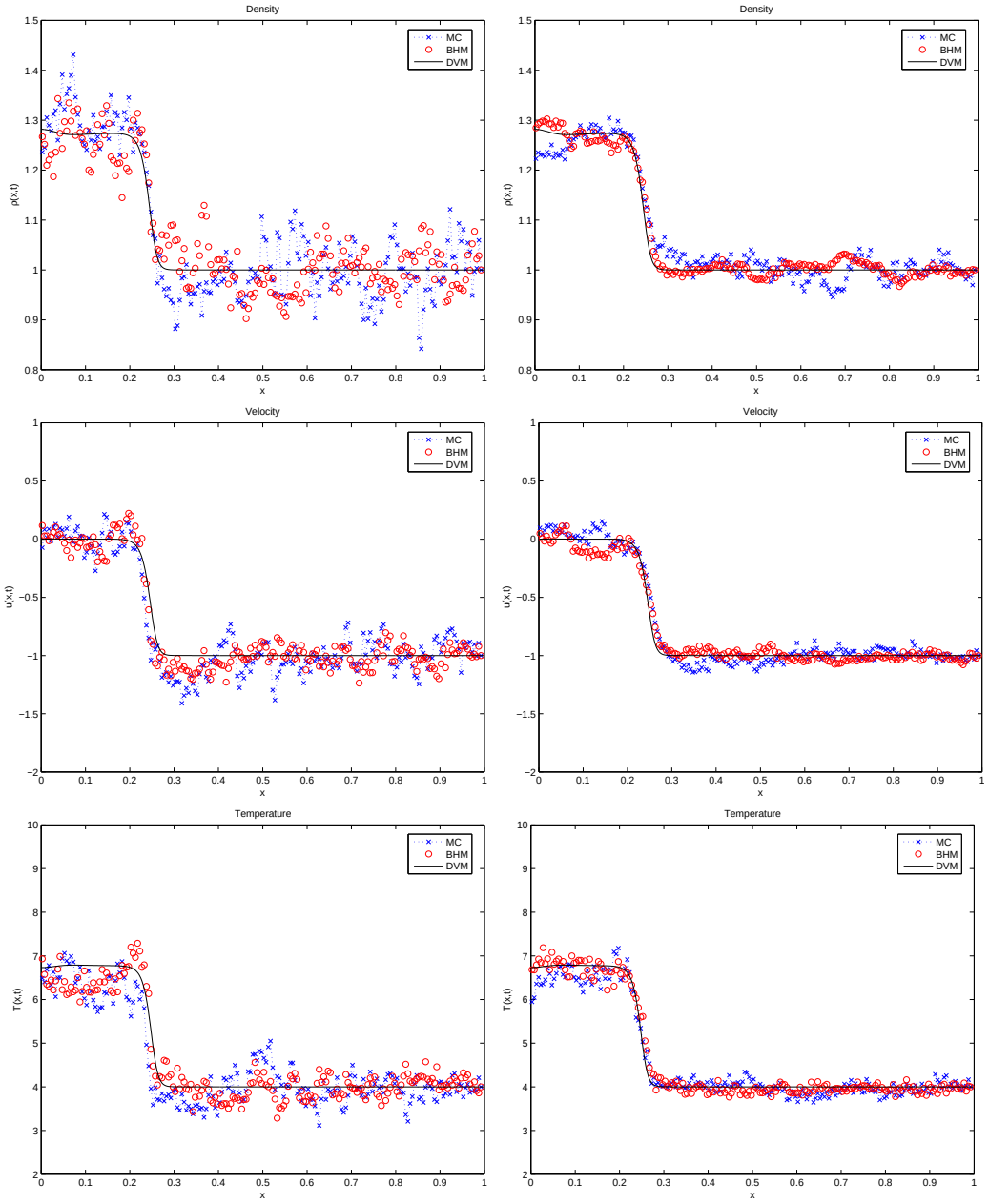

Figure 3.10: Unsteady Shock: Solution at $t = 0.065$ with $\varepsilon = 10^{-3}$ for density (top), mean velocity (middle) and temperature (bottom) for MCM and BHM (left), BHMI and BCHM (right), with initial data (3.4.3).

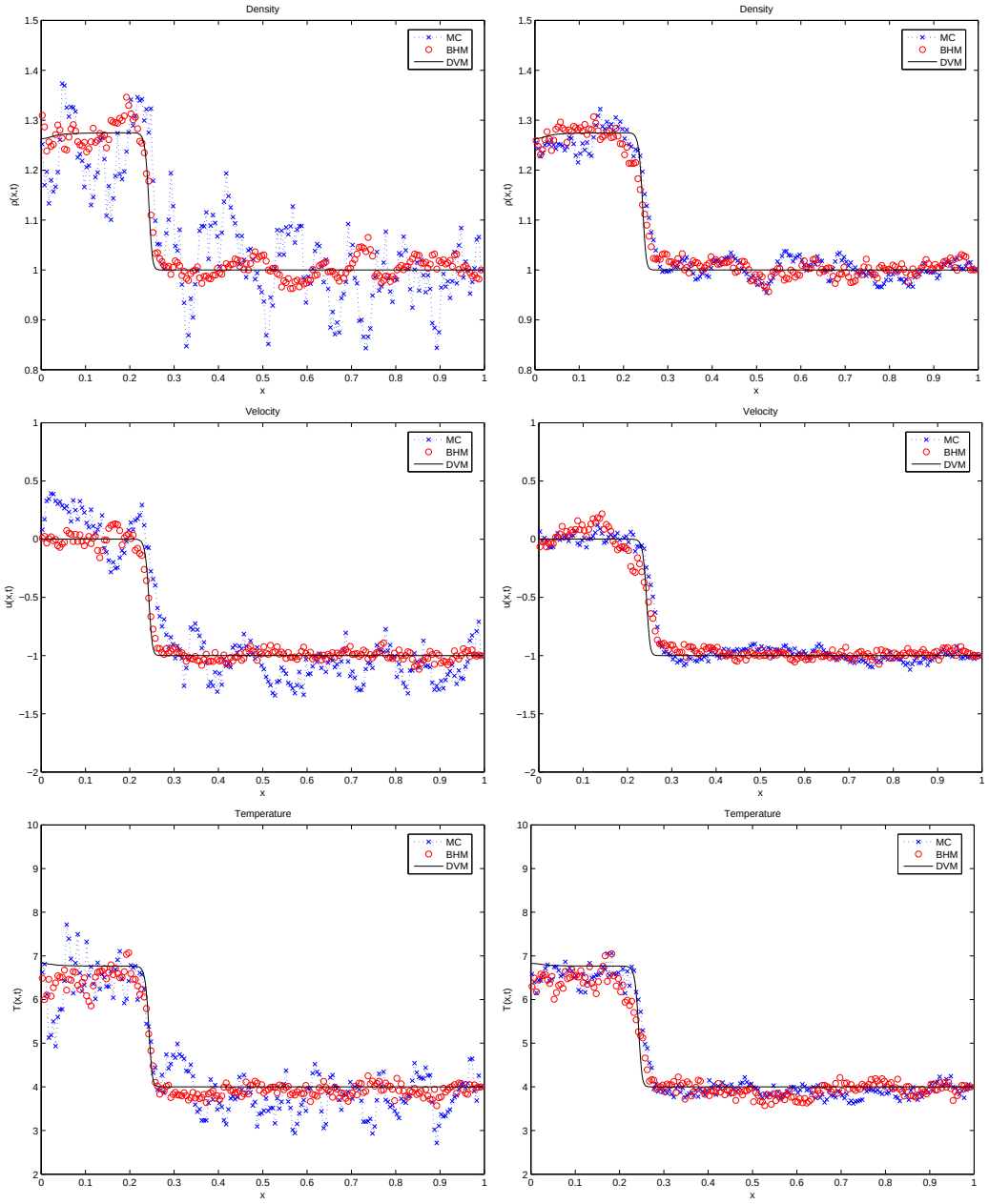

Figure 3.11: Unsteady Shock: Solution at $t = 0.065$ with $\varepsilon = 10^{-5}$ for density (top), mean velocity (middle) and temperature (bottom) for MCM and BHM (left), BHMI and BCHM (right), with initial data (3.4.3).

number is $\varepsilon = 10^{-3}$ in one case and $\varepsilon = 10^{-5}$ in the other. In the HM, HMI and CHM schemes the velocity space is discretized with $\Delta v = 0.16$, the bounds are set at $[-15, 15]$. The bounds between tails and central part of the Maxwellian for BHM, BHMI and BCHM are set to $[-5, 5]$, with the same mesh in velocity. We compare again our solution with a DVM with 500 space cell and 250 cell in velocity space with bound set at $[-20, 20]$. Again the improvement obtained with the hybrid schemes is clear (see Figures 3.8, 3.9, 3.10, 3.11).

3.5 Conclusion

In this work we have considered the development of hybrid methods for kinetic multiscale problems. Although we have described the schemes in the case of Boltzmann-BGK equation our approach can be extended to other kinetic equations. The additional difficulty usually is represented by the structure of the collision operator which requires a specific treatment (see [19, 16, 17] for the case of the full Boltzmann equation).

The hybrid multiscale methods here developed can be used in all cases where a macroscopic description of the phenomena is known but ceases to be valid in some region of the computational domain and the microscopic model has to be used. The necessary condition is that the microscopic variables and the macroscopic conserved variables are linked through an operator that define a local equilibrium.

The general approach consist in a suitable blending of deterministic methods for the equilibrium part and particle methods for the non equilibrium part. Several numerical examples are shown in order to prove the validity and efficiency of the new methods. Off course other tests have to be done to measure the performance of the hybrid methods in real applications.

Acknowledgements. The authors would like to thank Russ Caflisch for the many stimulating discussions.

Chapter 4

A Fluid Solver Independent Hybrid Method and Domain Decomposition Techniques for Multiscale Kinetic equations

This Chapter is based on the work [46] which has to be **submitted in 2008** and on the work [45] published in **Proceedings of the 11th International Conference on Hyperbolic problems: Theory, Numerics, Applications, pp. 457-464** both in collaboration with Prof. Lorenzo Pareschi of the Department of Mathematics and Center for Modeling Computing and Statistics (CMCS) of University of Ferrara.

4.1 Introduction

In this chapter we afford the problem of the simulations of Rarefied Gas Dynamic (RGD) phenomena. However, we want to underline the generality of the formulation of the method presented, which permits to easily extended to other multiscale phenomena the algorithms introduced in the RGD contest. In fact, in order to use the hybrid approach described in the sequel, the only condition which is necessary to satisfy is the possibility to identify a local equilibrium function, which will be defined in details in the case of RGD and known in many cases of practical interest, either analytically or numerically, that originates a model reduction from the microscale to the macroscale formulation. In general, dealing with macroscopic phenomena, permits to ignore the details of microscopic interactions, thus the

model reduction, in terms of equations which describe the system, becomes a natural consequence of the change of scale. The description of a general multiscale hybrid procedure is a subject of a future work.

In fluid dynamic the classical ways to treat problems are Navier-Stokes or Euler equations, however when dealing with large temperature or very low densities, these models are not enough satisfactory in describing the physics and an analysis at mesoscopic level becomes necessary. Thus the well known kinetic approach through the Boltzmann equation [26] is often used instead, besides, the introduction of such a model is closely linked with the introduction of difficulties from the computational point of view. In fact, the system of equation to solve becomes too large, especially in the multidimensional situations, and even with computers of last generation the cost remains too high. To this aim, probabilistic techniques as DSMC are extensively used in real simulations for their great flexibility and low computational cost compared to any type of deterministic scheme for kinetic equations [17], [18], [80], besides the solutions are affected by large fluctuations and, in non stationary situations, the impossibility to average leads to, or low accurate solutions, or high costly simulations. However, even in extremely rarefied regimes the fluid equations still furnish correct solution in regions of the domain in which the gas is not subjected to sharp gradient. The direct consequence is that domain decomposition methods [10], [71], [77], [38] which consider the problem at different scale, fluid or kinetic, in different part of the computational domain, is a practical way to take advantage of the physics without loosing accuracy. We quote also the possibility to improve domain decomposition schemes trough a moving boundary [40, 122], in order to follow discontinuities and sharp gradients inside the domain, methods that are particulary important in the simulation of non stationary problems. However, the exact identification of the non equilibrium zones remains an hard task to accomplish and an open research argument.

Here we propose an alternative algorithm respect to the domain decomposition methods, which represent an effective application of the schemes developed in [44] and which can be used in real simulations. The basic idea consist in solving the kinetic model and the macroscopic model in the entire domain, the first through Monte Carlo(MC) methodologies and the latter through a deterministic scheme and to consider as a solution a suitable merging of the two. Moreover we will show that is not necessary to solve the entire kinetic problem, in fact it is sufficient to describe at a mesoscopic level only the part of the solution which is far from the thermodynamic equilibrium. The immediate result of this observation is a reduction of the number of samples used in the MC solution, and consequently,

of the computational time and fluctuations. These improvements are linked with the diminish of the local Knudsen number, that is a measure of the rarefaction of the gas, thus closer to the fluid regime cost and fluctuations diminish. The implementation of such methodology furnishes results which in general are much more faster than traditional deterministic kinetic schemes and for flow regimes close to fluid, in which the Euler or Navier-Stokes still furnish wrong results, also to DSMC schemes. Moreover the formulation presented already include a domain decomposition technique, which can be obtained forcing the Knudsen number to zero (see [45]) in some part of the domain.

The main features of the scheme can be summarized as follows

- In regions far from equilibrium (i.e. the Knudsen number is big), where the solution of the full kinetic equation is required, the schemes provide a probabilistic Monte Carlo approximation of the solution.
- In thermodynamic equilibrium regions (i.e. the Knudsen number is zero), where the Euler equations are valid, the schemes provide a deterministic finite volume (differences) approximation of the fluid equations.
- In intermediate regions, the approximated solution is generated automatically by the schemes as a suitable blending of a nonequilibrium probabilistic component and an equilibrium deterministic components furnished by the solution of the fluid equations.

The rest of the article is organized as follows. In Section 4.1 we introduce the Boltzmann-BGK equations and his properties. In Section 4.2 we present the fluid solver independent hybrid scheme. In the next section we propose two ways in which is possible to increase the equilibrium fraction of the solution. In Section 4.4 a domain decomposition method based on the hybrid techniques is described. Finally Section 4.5 is devoted to numerical results in one and two-dimension to compare performances respect traditional Monte Carlo and kinetic schemes. Some final considerations and future developments are discussed in the last Section.

4.2 The Boltzmann Equation with BGK Collision Kernel

We will consider in this paper a BGK collision kernel for the Boltzmann equations which is known to be a satisfactory model close to equilibrium regimes, we quote

that extensions to other collision kernel are possible through the use of the Wild's sum [131] and Time Relaxed Methods [94]. The Boltzmann-BGK equation reads

$$\partial_t f(x,v,t) + v \cdot \nabla_x f(x,v,t) = \frac{1}{\tau(x,t)}(M_f(x,v,t) - f(x,v,t)), \tag{4.2.1}$$

with the initial condition

$$f(x,v,t=0) = f_0(x,v), \tag{4.2.2}$$

Where $f(x,v,t)$ is a non negative function describing the time evolution of the distribution of particles with velocity $v \in \mathbb{R}^{d_v}$ and position $x \in \Omega \subset \mathbb{R}^{d_x}$ at time $t > 0$, with d_v and d_x representing the dimension in velocity and physical space respectively. In this simplified model, collisions are mimic by a relaxation towards the equilibrium. In the present work the nondimensional formulations of the Boltzmann equation will be used, in that case τ is defined by

$$\tau(x,t)^{-1} = \frac{C}{\varepsilon(x,t)}, \tag{4.2.3}$$

with the choice $C = 1$ [107, 34] and $\varepsilon(x,t)$ Knudsen number. Others choices for the relaxation time do not change significantly the hybrid algorithm we will describe in next section. Observe anyway that the ratio of deterministic and stochastic component is a function of the relaxation time as explained in details in the next Section.

The local Maxwellian function, representing the local equilibrium, is defined by

$$M_f(\varrho,u,T)(x,v,t) = \frac{\varrho}{(2\pi T)^{d/2}} \exp\left(\frac{-|u-v|^2}{2T}\right), \tag{4.2.4}$$

where ϱ, u, T are the density, mean velocity and temperature of the gas in the x-position and at time t

$$\varrho = \int_{\mathbb{R}^d} f dv,\ u = \int_{\mathbb{R}^d} v f dv,\ T = \frac{1}{d\varrho}\int_{\mathbb{R}^d} |v-u|^2 f dv, \tag{4.2.5}$$

while the energy E is defined as

$$E = \frac{1}{2}\int_{\mathbb{R}^d} |v|^2 f dv, \tag{4.2.6}$$

Consider the BGK equation (4.2.1) and multiply it for 1, v, $\frac{1}{2}|v|^2$, the so-called collision invariant, by integrating in v the above quantities, the equations for the

first three moments of the distribution function f are obtained. They describe respectively the conservations laws for mass, momentum and energy. Unfortunately, the system obtained through the above average in velocity space is not closed since it involves higher order moments of the distribution function.

Observe that, formally from (4.2.1) as $\varepsilon \to 0$, the function f approach the local Maxwellian. In this case it is possible to compute analytically the higher moments of f from ϱ, u and T. Carrying on this computation we obtain the set of compressible Euler equations (see: [27] for details)

$$\begin{aligned} &\frac{\partial \varrho}{\partial t} + \nabla_x \cdot (\varrho u) = 0 \\ &\frac{\partial \varrho u}{\partial t} + \nabla_x \cdot (\varrho u \otimes u + p) = 0, \\ &\frac{\partial E}{\partial t} + \nabla_x \cdot (Eu + pu) = 0 \\ &p = \varrho T, \;\; E = \frac{3}{2}\varrho T + \frac{1}{2}\varrho |u|^2 \end{aligned} \tag{4.2.7}$$

where p is the thermodynamical pressure while $\otimes$ represent a tensor product. Higher order fluid model, like Navier-Stokes, can be derived from the Boltzmann equations. In this case, with some adaptations, is still possible to use the hybrid scheme, we remind to a future work the development of such an hybrid method.

Typically, equation (4.2.1) is completed with boundary conditions for $x \in \partial\Omega$ and for $v \cdot n \geq 0$ where n denotes the unit normal, pointing inside the domain. The boundary conditions are modeled by

$$|v \cdot n| f(x, v, t) = \int_{v_* \cdot n < 0} |v_* \cdot n| K(v_* \to v, x, t) f(x, v_*, t) dv_* \tag{4.2.8}$$

Where v_* represent the velocity value after the boundary process. The entering flux is described as a function of the outgoing flux modified by the boundary kernel K. Such definition of the boundary condition preserve the mass if

$$K(v_* \to v, x, t) \geq 0, \; \int_{v_* \cdot n \geq 0} K(v_* \to v, x, t) dv = 1 \tag{4.2.9}$$

While the simulation of boundaries in open domain is quite simple, the introduction of suitable boundary conditions for gas-surface interaction is an area of research by itself, [28] and reference therein. Two type of conditions absorbing or reflecting are normally applied, another condition could be a convex combination

of the two. From a physical point of view one assume that a fraction of particle (α) is absorbed and re-emitted at a temperature and velocity corresponding to a Maxwellian (with temperature and velocity of the boundary), while the other $(1-\alpha)$ is specular reflected, this is equivalent to impose for the ingoing velocities

$$f(x,v,t) = (1-\alpha) * Rf(x,v,t) + \alpha Mf(x,v,t),\ v \cdot n(x) \geq 0 \tag{4.2.10}$$

and

$$\begin{aligned} Rf(x,v,t) &= f(x, v - 2n(n \cdot v), t) \\ Mf(x,v,t) &= \mu(x,t) M_\omega(v,t) \end{aligned} \tag{4.2.11}$$

If we denote by T_ω the temperature of the boundary and by u_ω the velocity, M_ω is given by

$$M_\omega(\varrho, u_\omega, T_\omega)(v) = \frac{\varrho}{(2\pi T_w)^{3/2}} \exp\left(\frac{-|u_w - v|^2}{2T_w}\right), \tag{4.2.12}$$

Finally the value of μ is determined by mass conservation

$$\mu(x,t) \int_{v\cdot n \geq 0} M_\omega(v)|v \cdot n| dv = \int_{v\cdot n<0} f(x,v,t)|v \cdot n| dv \tag{4.2.13}$$

Concerning inflow and outflow conditions, we set $f(x,v,t) = g(v,t)$ for $x \in \partial\Omega$ and $v \cdot n \geq 0$ where $g(v,t)$ could be any positive function, typically Maxwellian, in the first case, while in the latter case one possibility is to choose $f_x(x,v,t) = 0$ for $x \in \partial\Omega$.

4.3 Hybrid Representation

The scheme described on this paper is based on the hybrid representation defined in [44]. Here we recall only the key points of the methods, for details we remind to it.

In the following description we restrict to 1-D in velocity and physical space, extensions of the methods to the multidimensional case are straightforward. First we need to interpret the distribution function as a probability density, that in the space homogeneous case reads (the x-dependence is omitted in the sequel)

$$f(v,t) \geq 0,\ \varrho = \int_{-\infty}^{+\infty} f(v,t) dv = 1 \tag{4.3.1}$$

and the following definition of hybrid representation:

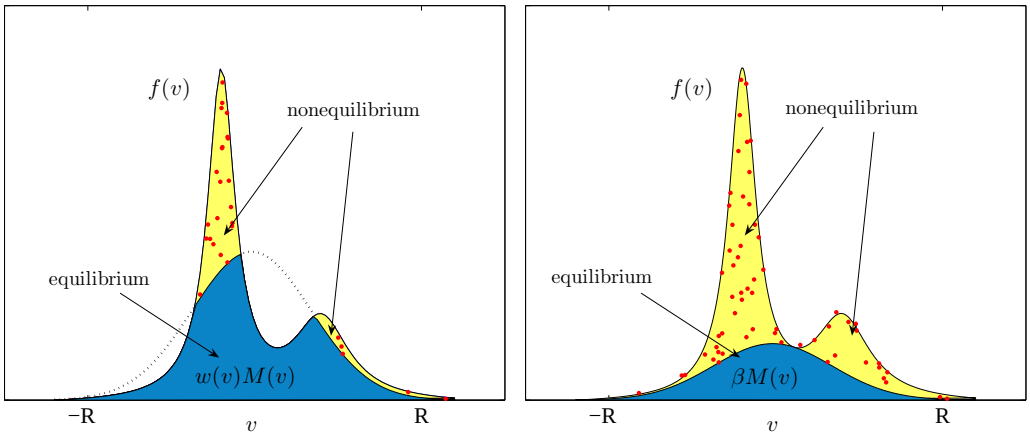

Figure 4.1: Distribution function as a combination of equilibrium and non-equilibrium part representation (4.3.4) left and (4.3.8) right.

Definition 4.3.1 *Given a probability density* $f(v,t)$*, and a probability density* $M(v,t)$*, called equilibrium density, we define* $w(v,t) \in [0,1]$ *and* $\tilde{f}(v,t) \geq 0$ *in the following way*

$$w(v,t) = \begin{cases} \dfrac{f(v,t)}{M(v,t)}, & f(v,t) \leq M(v,t) \neq 0 \\ 1, & f(v,t) \geq M(v,t) \end{cases} \tag{4.3.2}$$

and

$$\tilde{f}(v,t) = f(v,t) - w(v,t)M(v,t). \tag{4.3.3}$$

Thus $f(v,t)$ *can be represented as (Figure 4.1)*

$$f(v,t) = \tilde{f}(v,t) + w(v,t)M(v,t). \tag{4.3.4}$$

If we take now

$$\beta(t) = \min_v\{w(v,t)\}, \tag{4.3.5}$$

and

$$\tilde{f}(v,t) = f(v,t) - \beta(t)M(v,t), \tag{4.3.6}$$

we have

$$\int_v \tilde{f}(v,t)dv = 1 - \beta(t). \tag{4.3.7}$$

Let us define for $\beta(t) \neq 1$ the probability density

$$f(v,t)^p = \frac{\tilde{f}(v,t)}{1-\beta(t)}.$$

The case $\beta(t) = 1$ is trivial since it implies $f(v,t) = M(v,t)$. Thus the probability density $f(v,t)$, can be written as a convex combination of two probability densities in the form [16, 17] (Figure 4.1 right)

$$f(v,t) = (1-\beta(t))f(v,t)^p + \beta(t)M(v,t). \tag{4.3.8}$$

Clearly the above representation is a particular case of (4.3.4). Now we consider the following general representation, including space dependence

$$f(x,v,t) = \underbrace{\tilde{f}(x,v,t)}_{nonequilibrium} + \underbrace{w(x,v,t)M(x,v,t)}_{equilibrium},$$

where $w(x,v,t)$ is in general a continuum function that characterizes the equilibrium fraction and $\tilde{f}(x,v,t)$ the non equilibrium part of the distribution function. The general methodology consist in

- Solve the evolution of the perturbation by Monte Carlo methods. Thus $\tilde{f}(x,v,t)$ will be represented by a set of samples in the computational domain.
- Solve the evolution of the Maxwellian by deterministic methods. Thus $w(x,v,t)M(x,v,t)$ will be represented on a suitable grid in the computational domain.

In the sequel we will describe the Fluid Solver Independent (FSI) scheme, one of the most important difference respect the hybrid kinetic scheme [44] is that a common value for the equilibrium fraction in space velocity has to be chosen $\beta(x,t) = \min_v\{w(x,v,t)\}$ and that it cannot be determined directly, other strategies are necessary, some ideas are explained in the section 4.3.2.

4.3.1 The Fluid Solver Independent Hybrid scheme

FSI is able to take advantage from the solution of the equilibrium part of the distribution function through a macroscopic scheme instead of a kinetic scheme, this leads to a strong reduction of the computational time respect any deterministic

scheme that solve Boltzmann equations. Moreover we stress we could be faster of DSMC (Direct Simulation Monte Carlo) while Knudsen approach zero and moreover more accurate using this methodology. In fact the ratio, between number of particles used in the solution respect number of particles used in a full MC scheme, is equal to the ratio of nonequilibrium portion of the distribution function respect to the entire distribution function. Thanks to that properties we could easily estimate the total computational time as

$$CT_{TOT} = CT_E + \alpha CT_{MC} \tag{4.3.9}$$

where CT_{TOT} is the total computational time, CT_E the time to compute the solution for fluid equations, while CT_{MC} is the time we need to perform a particles simulation for Boltzmann equations, finally α is a scalar function that contains the information related to the equilibrium/nonequilibrium character of the distribution function f.

We now briefly describe a simple MC scheme for the Boltzmann-BGK equation used in the sequel for the hybrid model, the scheme is based on the interpretation of the distribution function as a probability density. First we sample N particles from the initial distribution function $f(x, v, 0)$, subsequently the evolution of $f(x, v, t)$ is given by the evolution of the particles. The second step consists in splitting the equation in a relaxation and transport step

$$\partial_t f^c(x, v, t) + v \cdot \nabla_x f^c(x, v, t) = 0 \tag{4.3.10}$$

$$\partial_t f^r(x, v, t) = -\frac{1}{\varepsilon(x, t)}(f^r(x, v, t) - M^r(x, v, t)) \tag{4.3.11}$$

The first stage is solved through the shifting of the particles according to

$$p_j^{n+1} = p_j^n + \nu_j \Delta t \tag{4.3.12}$$

where p_j^{n+1} and p_j^n represent the position of the sample, before and after the transport, and ν_j its velocity. In order to continue the computation an intermediate step is necessary, in this step the first three moments of the distribution function are reconstructed in each spatial cell starting from samples. They are given by

$$\varrho_i = \frac{m}{\Delta x}\sum_{p_j \in I_i} 1 = \frac{m}{\Delta x} N_i,\ u_i = \frac{1}{N_i}\sum_{p_j \in I_i} \nu_j,\ E_i = \frac{1}{2N_i}\frac{m}{\Delta x}\sum_{p_j \in I_i} |\nu_j|^2 \tag{4.3.13}$$

where $m = \frac{1}{N_t}\int \varrho dx$ represent the mass of a particle, N_i the number of particle inside the space cell I_i and N_t the total initial number of particles, while ϱ_i, u_i, E_i

are respectively the mass the mean velocity and the energy in the cell. For details about reconstruction techniques we refer to [98]. Once the moments are computed it is possible to estimate the local Maxwellian distribution in each spatial cell. Thanks to the above knowledge the second stage of the splitting is solved in the following way: with probability $e^{-(t+t_1)/\varepsilon(x,t)}$ we leave the velocity of the sample unchanged while with probability $1 - e^{-(t+t_1)/\varepsilon(x,t)}$ we substitute the velocity of the sample with one taken from the local Maxwellian. Hence an algorithm for the Monte Carlo BGK model reads

Algorithm 4.3.1 (Monte Carlo for BGK equation)

1. *Compute the initial velocity and position of the particles* $\{\nu_j^0, j = 1, .., N\}$ $\{p_j^0, j = 1, .., N\}$ *by sampling them from initial density* $f_0(x, v)$

2. *Given a spatial discretization* Δx*, and an estimate of the larger sample velocity* $\nu_{max} = 4\sqrt{2T_{max}}$*, with* T_{max} *the maximum temperature in the domain, compute* $\Delta t = \Delta x/\nu_{max}$

3. *While* $t \leq t_f$ *with* t_f *the final chosen time and* t *the actual time.*
   Given the samples values $\{\nu_j^n, j = 1, .., N\}$ *and* $\{p_j^n, j = 1, .., N\}$ *at time* t

   (a) *with probability* $e^{-\Delta t/\varepsilon(x,t)}$ *the samples are unchanged*
   - *set* $\nu_j^{n+1} = \nu_j^n$

   (b) *with probability* $1 - e^{-\Delta t/\varepsilon(x,t)}$ *the samples are replaced with equilibrium samples. To extract one equilibrium samples proceed as follows*

   $$\nu_j^{n+1} = u_i^n + \sqrt{2T_i^n}\rho\cos(\theta), \tag{4.3.14}$$

   with T_i^n *temperature* u_i^n *mean velocity in the cell at time* n *and*

   $$\rho = \sqrt{-\log(\xi_1)},\ \theta = 2\pi\xi_2 \tag{4.3.15}$$

   where ξ_1 *and* ξ_2 *are uniformly distributed random number in* $[0, 1]$.

   (c) *transport the particle*

   $$p_j^{n+1} = p_j^n + \nu_j^{n+1}\triangle t,\ \forall j \tag{4.3.16}$$

   (d) *Compute the updated value of* $\Delta t = \Delta x/\nu_{max}^{n+1}$

(e) Compute the new value of $\varrho_i^{n+1}, u_i^{n+1}, T_i^{n+1}$ *in each cell (this require a loop on the particle vector)*

end for

Note that we do not need to reconstruct the full distribution function at each time step but only the conserved quantities ϱ, u and T(this is computationally advantageous). The simple splitting showed is first order in time, implementation of second order in time scheme through the Strang splitting is possible, however for $\varepsilon \to 0$ second order splitting reduces to first order.

In order to easily describe the FSI method we introduce the projection operator P, the relaxation operator R, and the transport operator T. The projection operator compute from microscopic variable f or M_f the macroscopic variables $U(x,t) = (\varrho(x,t), u(x,t), T(x,t))$, thus $P(f(x,v,t)) = U(x,t)$ and $P(M_f(x,v,t)) = U(x,t)$, since local Maxwellian has the same moments of the distribution function. Given N samples representing the distribution function $f_{MC}(x,v,t)$ at time t, where the subscript MC indicates we are solving the Boltzmann equations through a particle scheme, performing the splitting as in the Monte Carlo case, we could write for the relaxation stage of the microscopic equation

$$R(f_{MC}(x,v,t)) = (1-\beta(x,t))f_{MC}(x,v,t) + \beta(x,t)M_{f,MC}(x,v,t) \quad (4.3.17)$$

where $\beta(x,t) = 1 - e^{\Delta t/\varepsilon(x,t)}$. In our hybrid scheme, the transport step consists of two part, push particles, and compute the solution of Euler equations for $t = t+\Delta t$ given the value of conserved variable $U_E(x,t) = P(\beta(x,t)M_f(x,v,t))$ at time t

$$U_E(x,t+\Delta t) = T(\beta(x,t)P(M_f(x,v,t))) \quad (4.3.18)$$

$$\tilde{f}_{MC}(x,v,t+\Delta t) = T((1-\beta(x,t))f_{MC}(x,v,t)) \quad (4.3.19)$$

where the subscript E indicate we are solving the Euler equations through a deterministic macroscopic scheme. The hybrid solution is recovered at the next time step as

$$U_H(x,t+\Delta t) = P(\tilde{f}_{MC}(x,v,t+\Delta t)) + U_E(x,t+\Delta t) \quad (4.3.20)$$

The new value of the conserved variables $U_H(x,t+\Delta t)$ is used to compute the new local Maxwellian $M_f(x,v,t+\Delta t)$ and continue the computation. Observe now that, at the next time step, the relaxation stage reads

$$\begin{aligned} R(f(x,v,t+\Delta t)) &= (1-\beta(x,t+\Delta t))f_{MC}(x,v,t+\Delta t) + \\ &+ \beta(x,t+\Delta t)M_{f,MC}(x,v,t+\Delta t) \end{aligned} \quad (4.3.21)$$

where

$$f_{MC}(x,v,t+\Delta t) = \tilde{f}_{MC}(x,v,t+\Delta t) + T(\beta(x,t)M_{f,MC}(x,v,t)) \quad (4.3.22)$$

thus we need all the transported distribution function to advance in time. The computational cost of the scheme described at each time step is $CT_{TOT} = CT_E + CT_{MC}$, in fact we are both solving the full Boltzmann equation with MC and the compressible Euler equations. However, we could improve the performances of the above algorithm observing that we do not really need the knowledge of the full distribution function at each time step, besides we need only $(1-\beta(x,t))f(x,v,t)$. We recall

$$\tilde{f}_{MC} = \tilde{f}_{MC}(x,v,t+\Delta t) \quad (4.3.23)$$

$$\beta(x,t)\tilde{M}_f = T(\beta(x,t)M_{f,MC}(x,v,t)) \quad (4.3.24)$$

$$f(t) = f(x,v,t),\ f(t+\Delta t) = f(x,v,t+\Delta t) \quad (4.3.25)$$

$$\beta_1 = \beta(x,t),\ \beta_2 = \beta(x,t+\Delta t) \quad (4.3.26)$$

$$M_{f1} = M_f(x,v,t),\ M_{f2} = M_f(x,v,t+\Delta t) \quad (4.3.27)$$

Considering one space cell and substituting (4.3.22) in (4.3.21), we obtain

$$R(f(t+\Delta t)) = (1-\beta_2)(\tilde{f}_{MC} + \beta_1\tilde{M}_f) + \beta_2 M_{f2} \quad (4.3.28)$$

Thus we need only to sample $(1-\beta_2)\beta_1 M_{f1}$ particles instead of $\beta_1 M_f$, that means when β_1 or β_2 approach one we do not sample any particles. The computational cost of the algorithm, with the above modifications, becomes $CT = CT_E + \alpha CT_{MC}$, where $\alpha = (1-\beta_2)N_p + \beta_1(1-\beta_2)N_M$, with N_p and N_M respectively equal to the number of particles used to describe the non-equilibrium part of the distribution function and the number used for the thermodynamical equilibrium description. The FSI hybrid scheme for the solution of the Boltzmann-BGK equations reads in the simple case in which the Knudsen number remains constant in time and space during the whole simulation

Algorithm 4.3.2 (FSI Hybrid Scheme)

1. *Compute the initial velocity and position of the particles* $\{\nu_j^0, j = 1,..,N\}$ $\{p_j^0, j = 1,..,N\}$ *by sampling them from initial density* $f_0(x,v)$

2. *Given a spatial discretization* Δx*, and an estimate of the larger sample velocity* $\nu_{max} = 4\sqrt{2T_{max}}$*, with* T_{max} *the maximum temperature in the domain, compute* $\Delta t_{MC} = \Delta x/\nu_{max}$

3. *Given the initial value of the moments of the distribution function in each cell ϱ_i, $(\varrho u)_i$, E_i, compute the larger time step allowed by the deterministic macroscopic scheme Δt_D*

4. *Set $\Delta t = min(\Delta t_{MC}, \Delta t_D)$, normally the stronger restriction on the maximum time step is furnished by the microscopic scheme*

5. *While $t \leq t_f$ with t_f the final chosen time and t the actual time.*
   Given the samples values $\{\nu_j^n, j = 1, .., N\}$ and $\{p_j^n, j = 1, .., N\}$ and the moments values $U_i^n = (\varrho_i^n, (\varrho u)_i^n, E_i^n)$ at time t

   (a) *Perform the relaxation step*

      i. *with probability $e^{-\Delta t/\varepsilon}$ the samples are unchanged*
         - *set $\nu_j^{n+1} = \nu_j^n$*

      ii. *with probability $1 - e^{-\Delta t/\varepsilon}$ the samples are replaced with equilibrium samples. Sample* only *$e^{-\Delta t/\varepsilon}(1 - e^{-\Delta t/\varepsilon})$ particles. To extract one equilibrium samples proceed as follows*

$$\nu_j^{n+1} = u_i^n + \sqrt{2T_i^n}\rho\cos(\theta), \tag{4.3.29}$$

      with T_i^n temperature u_i^n mean velocity in the cell at time n and

$$\rho = \sqrt{-\log(\xi_1)},\ \theta_i = 2\pi\xi_2 \tag{4.3.30}$$

      where ξ_1 and ξ_2 are uniformly distributed random number in $[0, 1]$.

      iii. *Compute the effective fraction of equilibrium $\beta_i^E = 1 - \frac{N_i^p}{N_i^t}$ with N_i^p the number of samples which represent the part in non equilibrium and N_i^t the total number of samples inside the cell*

   (b) *Solve the Euler equations for $U_{E,i}^n$ and find $U_{E,i}^{n+1}$ as specified in Eqs. (4.3.18)*

   (c) *Transport particles*

$$p_j^{n+1} = p_j^n + \nu_j^{n+1}\triangle t,\ \forall j, \tag{4.3.31}$$

   (d) *Compute the moments of the non-equilibrium part $P(\tilde{f}_{MC,i})$ using the advected particles that did not change their velocity during the relaxation step*

   (e) *Compute the hybrid solution $U_{H,i}^{n+1} = P(\tilde{f}_{MC,i}) + U_{E,i}^{n+1}$*

(f) Compute the updated value of Δt

(g) Use the new macroscopic value $U_{H,i}^{n+1}$ *to find the new Maxwellian and restart the computation.*

end for

Note that we need to compute and use the effective equilibrium fraction β_i^E which normally is different respect to β_i. In fact given the total number of particles N_i^t in the cell I_i we keep only the integer approximation of $N_i^p = (1 - \beta_i)N_i^t$.

4.3.2 Increasing the Equilibrium Fraction

Observe that the method described does not permit to optimize the equilibrium fraction. In fact at each time step the equilibrium structure is entirely lost and the new fraction of equilibrium is only given by the relaxation step. However, in principle, it is possible to recover some information from the transported local Maxwellian even though we know it through samples rather than analytically. In fact we do not conserve any microscopic information from the solution of the macroscopic equations for the equilibrium part. In the sequel, we will propose two methods to increase the equilibrium fraction after the transport step, leaving a more detailed research on this argument to a future work. We start describing the generalization of the hybrid method once this optimization has been achieved in some way. Finally we will conclude describing an algorithm which can be used with the above method.

We define the equilibrium fraction β^c as the ratio of the transported Maxwellian at time t respect to the new local Maxwellian at time $n + 1$, with notations introduced in eqs. (4.3.23-4.3.27) this function reads

$$\beta^c(x,t) = \min_v \frac{\beta_1 \tilde{M}_f}{M_{f2}} = \min_v \frac{T(\beta(x,t)M_{f,MC}(x,v,t))}{M_f(x,v,t+\Delta t)} \tag{4.3.32}$$

Suppose now, for simplicity, that $\beta^c(x,t) = 0$ at the beginning of our computation, it follows that the hybrid method reads in the same way from equation (4.3.17) to equation (4.3.20). After the transport of the continuous and stochastic part $\beta^c(x, t + \Delta t)$ is computed, thanks to this knowledge the relaxation step in one

space cell at time $n+1$ becomes

$$\begin{aligned} R(f(t+\Delta t)) &= (1-\beta_2)(\tilde{f}_{MC}+\beta_1\tilde{M}_f)+\beta_2 M_{f2} \\ &= (1-\beta_2)(\tilde{f}_{MC}+\beta_2^c M_{f2}+\widehat{M}_f)+\beta_2 M_{f2} \\ &= (1-\beta_2)(\tilde{f}_{MC}+\widehat{M}_f)+((1-\beta_2)\beta_2^c+\beta_2)\,M_{f2} \end{aligned} \tag{4.3.33}$$

where the relation $\beta_1\tilde{M}_f = \widehat{M}_f + \beta_2^c M_{f2}$ with $\beta_2^c = \beta^c(x,t+\Delta t)$ holds. Note that $\widehat{M}_f$ represent the part of the transported Maxwellian which is no more in equilibrium. The possibility of making $\beta^c(x,t)\neq 0$, gives the opportunity to yield independent from the mesh the hybrid method. In fact $\beta(x,t)$, obtained as solution of the relaxation step, is a function of $\varepsilon(x,t)$ and $\triangle t$, it follows that the equilibrium component is a function of the mesh, being $\Delta t \leq \Delta x/\nu_{max}$. However, the ratio of Maxwellian respect to the global distribution function does not depend from the method, instead is intrinsic to the Boltzmann-BGK model. Recovering part of the equilibrium after the transport permits to increase the efficiency of the method without loosing accuracy, thus to extend the use of the scheme to a larger set of problems.

The first and simplest method to estimate $\beta^c(x,t)$ consists in measuring the departure from equilibrium reconstructing the transported Maxwellian from samples. Thus we need a grid in velocity space and a loop over the particles inside each cell. To that aim we consider a cartesian grid of N_v nodes $v_k = k*\Delta v+b$ with k bounded index, Δv the grid step and b the artificial boundary in the unbounded velocity space. Approximating the continuous distribution function $f(x,v,t)$ or $M_f(x,v,t)$ with a discrete velocity model $f(x,v_k,t), M_f(x,v_k,t)$, we are able to identify for each sample the belonging spatial and velocity cell and to measure the quantity

$$w^c(x,v_k,t+\Delta t) = \frac{\beta_1\tilde{M}_f}{M_{f2}} = \frac{T(\beta(x,t)M_{f,MC}(x,v_k,t))}{M_f(x,v_k,t+\Delta t)} \tag{4.3.34}$$

In order to use the method here described with the algorithm of the previous section, we need for each spatial cell one value for the equilibrium fraction, thus we define

$$\beta^c(x,t+\Delta t) = \min_{v_k}\{w^c(x,v_k,t+\Delta t)\} \tag{4.3.35}$$

This method deserves some remarks. The reconstruction of the distribution function from samples increase the computational cost, moreover a small number of particles inside a cell, which is quite common in applications, furnish a large oscillating function, this turns in an imprecise estimate of $\beta^c(x,t)$.

A second way to estimate the equilibrium fraction is still based on the analysis of the transported Maxwellian, we discretize in space and time preserving the velocity space continuous. Consider a time splitting between relaxation and transport part, focusing on the latter

$$\frac{\tilde{M}_i^{n+1}(v) - M_i^n(v)}{\Delta t} + v\frac{M_i^n(v) - M_{i-1}^n(v)}{\Delta x} = 0,\ v \geq 0 \tag{4.3.36}$$

$$\frac{\tilde{M}_i(v)^{n+1} - M_i^n(v)}{\Delta t} + v\frac{M_{i+1}^n(v) - M_i^n(v)}{\Delta x} = 0,\ v < 0 \tag{4.3.37}$$

where $M_i^n(v) \simeq M_f(x, v, t)$, $M_{i+1}^n(v) \simeq M_f(x + \Delta x, v, t)$, $M_{i-1}^n(v) \simeq M_f(x - \Delta x, v, t)$, $\tilde{M}_i^{n+1}(v) \simeq M(x, v, t+\Delta t)$. We put a tilde on the transported Maxwellian to distinguish it respect to the local Maxwellian at time $t+\Delta t$, which is $M_{f,i}^{n+1}(v) \simeq M_f(x, v, t+\Delta t)$. The scheme described above is an upwind method for the Boltzmann equation in the non collisional limit, where of course is necessary to choose a maximum value for the velocity being the Maxwellian function unbounded. Commonly the bound is chosen equal to the larger velocity value of the particles. Solving Eqs. (4.3.36) and (4.3.37)

$$\tilde{M}_i^{n+1}(v) = (1 - \frac{v\Delta t}{\Delta x})M_i^n(v) + \frac{v\Delta t}{\Delta x}M_{i-1}^n(v),\ v \geq 0 \tag{4.3.38}$$

$$\tilde{M}_i^{n+1}(v) = (1 + \frac{v\Delta t}{\Delta x})M_i^n(v) - \frac{v\Delta t}{\Delta x}M_{i+1}^n(v),\ v < 0 \tag{4.3.39}$$

Thus, if $|v|\Delta t \leq \Delta x$, the updated function $\tilde{M}_i^{n+1}(v)$ is a convex combination of the local Maxwellian in the cell i and $i-1$ for positive velocity and in the cell i and $i+1$ for negative velocity. Now in each cell we are looking for the minimum of the ratio

$$\min_v \left(\frac{\beta_1 \tilde{M}_f}{M_{f2}}\right) = \min_v \left(\frac{T(\beta(x,t)M_{f,MC}(x,v,t))}{M_f(x,v,t+\Delta t)}\right) \simeq \min_v \left(\frac{\tilde{M}_i^{n+1}(v)}{M_{f,i}^{n+1}(v)}\right) \tag{4.3.40}$$

In the general case the above computation is not possible with analytic tools. Of course it is always possible to find approximated solutions of (4.3.40), however this operation can be expensive, if it has to be done at each time step in each cell. An alternative and fast way could be to search instead of the minimum an infimum value for (4.3.40) which hopefully results to be close respect the aforementioned

minimum. That value can be estimated observing that

$$\begin{aligned}\min_v\left(\frac{\tilde{M}_i^{n+1}(v)}{M_{f,i}^{n+1}(v)}\right) &\geq \min\left(\min_v\left(\frac{M_i^n(v)}{M_{f,i}^{n+1}(v)}\right),\min_v\left(\frac{M_{i-1}^n(v)}{M_{f,i}^{n+1}(v)}\right)\right)= \\ &= \beta_R^c(x,t+\Delta t),\ v\geq 0 \qquad (4.3.41)\end{aligned}$$

$$\begin{aligned}\min_v\left(\frac{\tilde{M}_i^{n+1}(v)}{M_{f,i}^{n+1}(v)}\right) &\geq \min\left(\min_v\left(\frac{M_i^n(v)}{M_{f,i}^{n+1}(v)}\right),\min_v\left(\frac{M_{i+1}^n(v)}{M_{f,i}^{n+1}(v)}\right)\right)= \\ &= \beta_L^c(x,t+\Delta t),\ v<0 \qquad (4.3.42)\end{aligned}$$

and setting

$$\beta^c(x,t+\Delta t)=\min(\beta_R^c(x,t+\Delta t),\beta_L^c(x,t+\Delta t)) \qquad (4.3.43)$$

where the minimum of the ratios above can be computed exactly, being exponential functions. Moreover (4.3.43) is as close to (4.3.40) as the flow is smooth, it follows that the proposed estimate seems to be good in the whole computational domain except near shocks or sharp gradients.

It is possible to think to other strategies to compute $\beta^c(x,t)$. One strategies could be to compute the moment of the third order, and to compare the results obtained with different value of $\beta^c(x,t)$, the final value of $\beta^c(x,t)$ will be set equal to the maximum value that gives the same moment of $\beta^c(x,t)=0$. The method could be much more faster respect to the reconstruction of the distribution function from samples, we leave the investigation of this aspect to future work.

An algorithm which can be used once $\beta^c(x,t)$ has been computed is the following

Algorithm 4.3.3 (Optimized FSI Hybrid Scheme)

1. *Compute the initial velocity and position of the particles* $\{\nu_{p,j}^0, j=1,..,N_p\}$ $\{p_{p,j}^0, j=1,..,N_p\}$, $\{\nu_{E,j}^0, j=1,..,N_E\}$ $\{p_{E,j}^0, j=1,..,N_E\}$ *by sampling them from initial density* $f_0(x,v)=\tilde{f}(x,v)+\beta^c(x)M_f(x,v)$. N_E *is the number of particles which represent the equilibrium state while* N_p *is the number of particles which represent the non-equilibrium state.*

2. *Points 2-3-4 same as algorithm 2*

3. *While $t \leq t_f$ with t_f the final chosen time and t the actual time. Given the samples values $\{\nu^n_{p,j}, j = 1, .., N_p\}$, $\{p^n_{p,j}, j = 1, .., N_p\}$, $\{\nu^n_{E,j}, j = 1, .., N_E\}$, $\{p^n_{E,j}, j = 1, .., N_E\}$, the moments values $U^n_i = (\varrho^n_i, (\varrho u)^n_i, E^n_i)$ at time t and $\beta^{n,c}_i$ in the cell i. Consider one spatial cell*

   (a) *Perform the relaxation step*

      i. *with probability $e^{-\Delta t/\varepsilon}$ the N_p samples are unchanged, while with probability $e^{-\Delta t/\varepsilon}(1 - \beta^{n,c}_i)$ the N_E samples are unchanged*
         - *set $\nu^{n+1}_{p,j} = \nu^n_{p,j}$*
         - *set $\nu^{n+1}_{p,j} = \nu^n_{E,j}$*

      ii. *with probability $1-e^{-\Delta t/\varepsilon}$ the N_p samples are replaced with equilibrium samples, with probability $(1 - e^{-\Delta t/\varepsilon} + e^{-\Delta t/\varepsilon} * \beta^{n,c}_i)$ the N_E samples are replaced with equilibrium samples. Sample* only *$e^{-\Delta t/\varepsilon}(1 - e^{-\Delta t/\varepsilon})N_p$ and $e^{-\Delta t/\varepsilon}(1 - e^{-\Delta t/\varepsilon} + e^{-\Delta t/\varepsilon} * \beta^{n,c}_i)N_E$ particles.*

      iii. *Compute the effective fraction of equilibrium $\beta^E_i = 1 - \frac{N^{new}_p}{N_T}$ with N^{new}_p the number of samples which represent the non equilibrium state after relaxation and N_T the total number of samples inside the cell*

   (b) *Solve the Euler equations for $U^n_{E,i}$ and find $U^{n+1}_{E,i}$ as specified in Eqs. (4.3.18)*

   (c) *Transport particles*

$$p^{n+1}_{p,j} = p^n_{p,j} + \nu^{n+1}_{p,j} \triangle t, \ \forall j, \tag{4.3.44}$$

$$p^{n+1}_{E,j} = p^n_{E,j} + \nu^{n+1}_{E,j} \triangle t, \ \forall j, \tag{4.3.45}$$

   (d) *Compute the moments of the non-equilibrium part $P(\tilde{f}_{MC})$ using the advected particles that did not change their velocity during the relaxation step*

   (e) *Compute the hybrid solution $U^{n+1}_{H,i} = P(\tilde{f}_{MC}) + U^{n+1}_{E,i}$*

   (f) *Compute the updated value of Δt*

   (g) *Use the new macroscopic value $U^{n+1}_{H,i}$ to find the new Maxwellian*

   (h) *Compute the updated value of $\beta^{n+1,c}_i$ in each cell.*

end for

4.4 Domain decomposition method

We saw that the identification of zones far from the thermodynamical equilibrium is not an easy task to accomplish, domain decomposition techniques are then used in order to better treat these difficulties and to design suitable numerical schemes. In fact we do not need to solve the kinetic equations in the whole computational domain instead it is sufficient to solve the hydrodynamical equations except in small zones where departure from thermodynamical equilibrium like shock waves are present. To this aim we have developed a numerical scheme directly derived from the multiscale hybrid scheme just described, which can be used to obtain a decomposition of the domain, artificially imposing the value of the Knudsen number ε equal to zero, where the thermodynamic profiles provided by Euler equations are sufficiently accurate.

We could view the following domain decomposition technique as a subset of the FSI hybrid scheme. Thus, the scheme becomes a coupling of a Euler solver (by MUSCL scheme) in one part of the domain and a BGK solver in the rest of the domain (by FSI method). In fact, if $\varepsilon \equiv 0$ from the exact solution of the relaxation step we get at each time step

$$f(x, v, t) = M_f(x, v, t). \tag{4.4.1}$$

Thus after transport since we project the entire solution towards the equilibrium, we are no more interested to the form of the distribution function but only by their moments. As a consequence $P(\tilde{f}_{MC}(x, v, t)) \equiv 0$ and the hybrid solution becomes $U^h(x, t) = U_E(x, t)$. In order to divide the domain we need to decide some criteria which permit to detect the zones in thermodynamical equilibrium with respect to the others, this is still an open problem and it will not be addressed in the present work, we quote for instance [40] in which the question is considered in detail. Two consideration about the boundary conditions are necessary

- The deterministic scheme we use to solve the problem in regions where $\varepsilon = 0$, need a value which is supplied by the hybrid scheme. That value contains some statistical fluctuation that could be large, thus the full deterministic model could contain some boundary error given by the fluctuation which propagates in the rest of the domain. In order to avoid the problem a technique could be to make ε a smooth function of x which gently vary

from some fixed value towards zero. For instance we could set ε as

$$\varepsilon(x) = \begin{cases} \varepsilon_F, & \text{for} \quad x \leq a \\ 0, & \text{for} \quad x \geq b \\ \dfrac{x-b}{a-b}\varepsilon_F, & \text{for} \quad x \in [a,b] \end{cases} \tag{4.4.2}$$

Where b represent the boundary of the equilibrium zones, a represent the boundary of the non equilibrium zones in which we use the full hybrid scheme, while ε_F represent the value of the Knudsen number for the hybrid scheme.

- We need also the boundary value for the MC part of the FSI where $\varepsilon \neq 0$, thus at the boundary between $\varepsilon \equiv 0$ and $\varepsilon \neq 0$ we need to sample some particles from the Maxwellian. The number of samples we need is given by $(1-\beta_i)\beta_i U_i^h$, where i indicate the cell, divided for the mass of the particles. However the particles velocity have to be sampled from the local Maxwellian in the cell $(i-1)$, if we are considering the left boundary, or from $i+1$ if the right boundary is considered.

4.5 Implementation and numerical tests

In principle any finite volume or finite difference numerical scheme can be used to solve the compressible Euler equations. We choose a finite volume MUSCL type scheme, which is second order in space, while the time discretization implemented is first order in Δt (see [66] for details). We present the scheme once again in one space dimension, for the sake of simplicity. The system to discretize is (4.2.7), where u now is a scalar and represent the mean velocity in the x direction, while m is equal to ϱu. Let

$$U = \begin{pmatrix} \varrho \\ m \\ E \end{pmatrix}, \quad F(U) = \begin{pmatrix} m \\ \varrho u^2 + p \\ u(E+p) \end{pmatrix}$$

The system (4.2.7) can be written as

$$\frac{\partial}{\partial t}U + \frac{\partial}{\partial x}F(U) = 0 \tag{4.5.1}$$

The spatial discretization reads

$$\frac{\partial}{\partial t}U_i + \frac{1}{h_i}(F_{i+1/2}(U) - F_{i-1/2}(U)) = 0 \tag{4.5.2}$$

with $h_i = x_{i+1/2} - x_{i-1/2}$ and

$$U_i = \frac{1}{h_i}\int_{x_{i-1/2}}^{x_{i+1/2}} U dx \tag{4.5.3}$$

$$\begin{aligned} F^p_{i+1/2} &= \frac{1}{2}(F^p(U_i) + F^p(U_{i+1})) - \frac{1}{2}\sqrt{a}_p(U^p_{i+1} - U^p_i) \\ &+ \frac{1}{4}(h_i\sigma^+_i(U_i) - h_{i+1}\sigma^-_{i+1}(U_i)),\ p = 1,2,3 \end{aligned} \tag{4.5.4}$$

where a^p are positive constant that need to be greater of the square of the eigenvalues of the system to assure the dissipative nature of the solution, and $\sigma^{\pm}_i$ represent the slope in the cell i of the piecewise linear reconstruction

$$\sigma^{\pm}_i = \frac{1}{h_i}(F^p(U_{i+1}) \pm \sqrt{a}_p U^p_{i+1} - F^p(U_i) \mp \sqrt{a}_p U^p_i)\phi(\theta^{\pm}_i) \tag{4.5.5}$$

$$\theta^{\pm}_i = \frac{F^p(U_i) \pm \sqrt{a}_p U^p_i - F^p(U_{i-1}) \mp \sqrt{a}_p U^p_{i-1}}{F^p(U_{i+1}) \pm \sqrt{a}_p U^p_{i+1} - F^p(U_i) \mp \sqrt{a}_p U^p_i} \tag{4.5.6}$$

while the slope limiter chosen, introduced by van Leer [76], is defined by

$$\phi(\theta) = \frac{|\theta| + \theta}{1 + |\theta|} \tag{4.5.7}$$

Finally the integration in time is performed by

$$U^{n+1} = U^n - \frac{\triangle t}{h_i}(F_{i+1/2}(U) - F_{i-1/2}(U)) \tag{4.5.8}$$

where the time step is such that

$$\triangle t \leq \frac{\min_i(h_i)}{\max_p(a_p)} \quad p = 1,2,3 \tag{4.5.9}$$

In the next paragraph we analyze the performances of the Fluid Solver Independent Hybrid scheme and of the domain decomposition scheme in comparison with a classical Monte Carlo scheme. Moreover as reference solution a first order deterministic discrete velocity model (DVM) for the Boltzmann-BGK equation will be used in the 1-D tests. We choose an unsteady shock test in one space dimension for the hybrid method while for the two dimensional case an ellipse embedded in a flow has been implemented with the odmian decomposition method.

	$\varepsilon = 10^{-1}$	$\varepsilon = 10^{-2}$	$\varepsilon = 10^{-3}$	$\varepsilon = 10^{-4}$
MCM	$3.869 * 10^{-2}$	$4.206 * 10^{-2}$	$6.453 * 10^{-2}$	$6.547 * 10^{-2}$
FSI	$3.735 * 10^{-2}$	$4.148 * 10^{-2}$	$3.637 * 10^{-2}$	$2.738 * 10^{-3}$
FSI1	$3.645 * 10^{-2}$	$3.810 * 10^{-2}$	$3.061 * 10^{-2}$	$2.668 * 10^{-3}$

Table 4.1: Ratio of computational times for MCM, FSI and FSI1 respect to DVM scheme for different values of the Knudsen number ε in the unsteady shock test.

In the sequel we report for the DVM scheme only the parameter chosen without describing the algorithm which is expected to be known, we remind to [84] for details on this method. For the two dimensional case only comparisons between Monte Carlo and the hybrid are shown. We recall that our aim is to stress the difference in fluctuations and in computational time that it is possible to obtain using our hybrid method respect to a Monte Carlo method or a deterministic discrete velocity model. For this purpose several cases have been treated varying the Knudsen number value, showing how the time and the fluctuations decrease together with it. We also remark that, while estimate the time differences between the hybrid scheme and a full Monte Carlo is quite easily (in fact our method is based on the same stochastic solver), the same comparison with another kinetic solver are not really straightforward, too many parameters are involved, depending on the precise solver chosen. For that reason we stress that the computational times for the 1-D unsteady shock test, reported in Table 1 are just indicative. However, being undeniable that kinetic deterministic methods are much more expensive that statistical methods specially in multidimensional situations, we observe that the hybrid method here developed is in general equal or faster than a Monte Carlo method. In the sequel we use the shorthand MCM, FSI, FSI1, DDM, DVM and E to denote the Monte Carlo scheme, the FSI method with $\beta^c(x,t) = 0$, the FSI method with $\beta^c(x,t) \neq 0$, the domain decomposition method, the discrete velocity model for Boltzmann-BGK equation and the second order MUSCL Euler solver.

4.5.1 1-D Unsteady shock

We start considering an unsteady shock that propagates from left to right, the shock is produced miming a specular wall on the left boundary, thus for the stochastic component at each time step, particles which escape from the computational domain on the left side are put back in the first cell with opposite veloc-

ity in a random position. On the other side particles are injected with the initial mean velocity and temperature in a number which corresponds to the initial density. For the macroscopic part the usual specular and inflow boundary condition are used. At the beginning the flow is uniform with mass $\varrho = 1$, mean velocity $u = -1$ and energy $E = 2.5$. The computations are stopped when $t = 0.065$, the number of cells are 200 in space, while the initial number of particle are 1000 for each space cell, parameters $a_i,\ i = 1, 2, 3$ are chosen as $a_1 = a_2 = a_3 = \max(\sup(u - c), \sup(u), \sup(u + c)) = 5.045$ for all t and x with c the sound speed. For the DVM method, an explicit Euler discretization for the time derivative and an upwind method for the discretization of the flux has been implemented, the number of cells in space is set to 2000, while the cells in velocity space are such that the distance between two discrete velocities is equal to $\Delta v = 0.4$, with boundary set to $[-20, 20]$. The Knudsen number is respectively equal to $\varepsilon = 10^{-1}$, $\varepsilon = 10^{-2}$, $\varepsilon = 10^{-3}$ and $\varepsilon = 10^{-4}$. In each Figure the solution computed with the Euler scheme and the one computed with the DVM scheme is reported, moreover the FSI, the FSI1 and the MCM are respectively depicted for density, velocity and temperature. We observe that for large Knudsen number FSI, Figure 4.2 left, and MCM, Figure 4.3 furnish the same solution in term of fluctuations, while FSI1, Figure 4.2 right, is similar to the others only in the non-equilibrium region and equal to the Euler solver in the equilibrium region. When ε decrease the non-equilibrium part becomes smaller and both FSI and FSI1 contains less fluctuations than MCM, observe however that the same trend of Figure 4.2 and 4.3 is preserved in Figure 4.5, FSI1 fluctuate only in the non-equilibrium region. Finally for $\varepsilon = 10^{-4}$, Figure 4.6, both the hybrid methods furnish a solution equal to the macroscopic one and at the same computational time. Remarkable is the behavior of the MCM scheme, Figure 4.4 and 4.7, fluctuations increase with the decrease of the Knudsen number, which means that the relaxation is a source of statistical error, observe finally that the DVM scheme, which is first order in space and time, slightly overestimate the shock velocity respect to the other schemes. In Table 1 the ratio of the computational times of the two hybrid methods and of the Monte Carlo method are reported respect to the deterministic discrete velocity scheme, showing how the time dramatically reduce when the Knudsen number goes to zero, to the other part when it is large MCM and hybrid scheme has approximately the same performances.

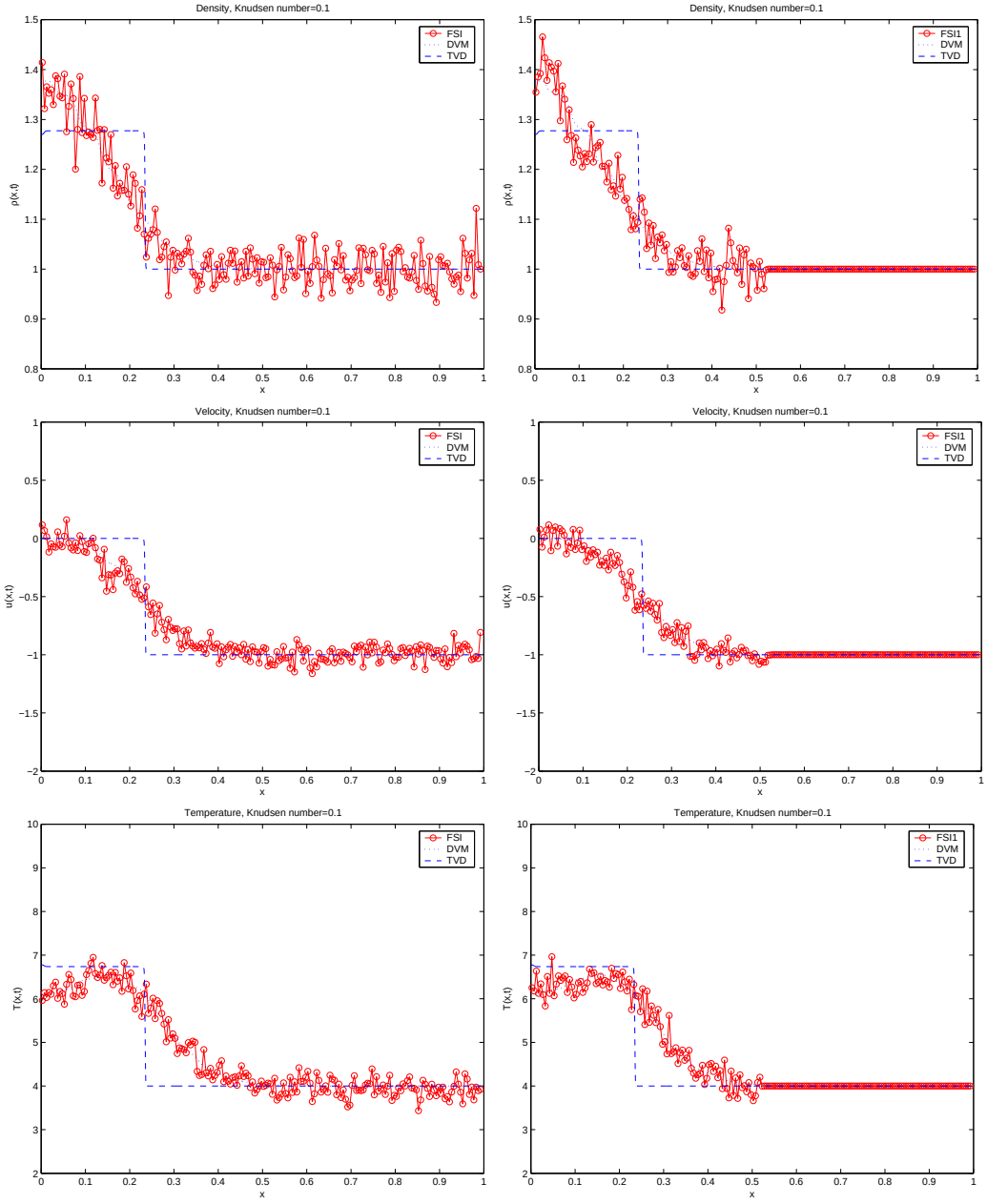

Figure 4.2: Unsteady Shock: Solution at $t = 0.065$ for FSI left, FSI1 right, density top, velocity middle, temperature bottom. Knudsen number $\varepsilon = 10^{-1}$

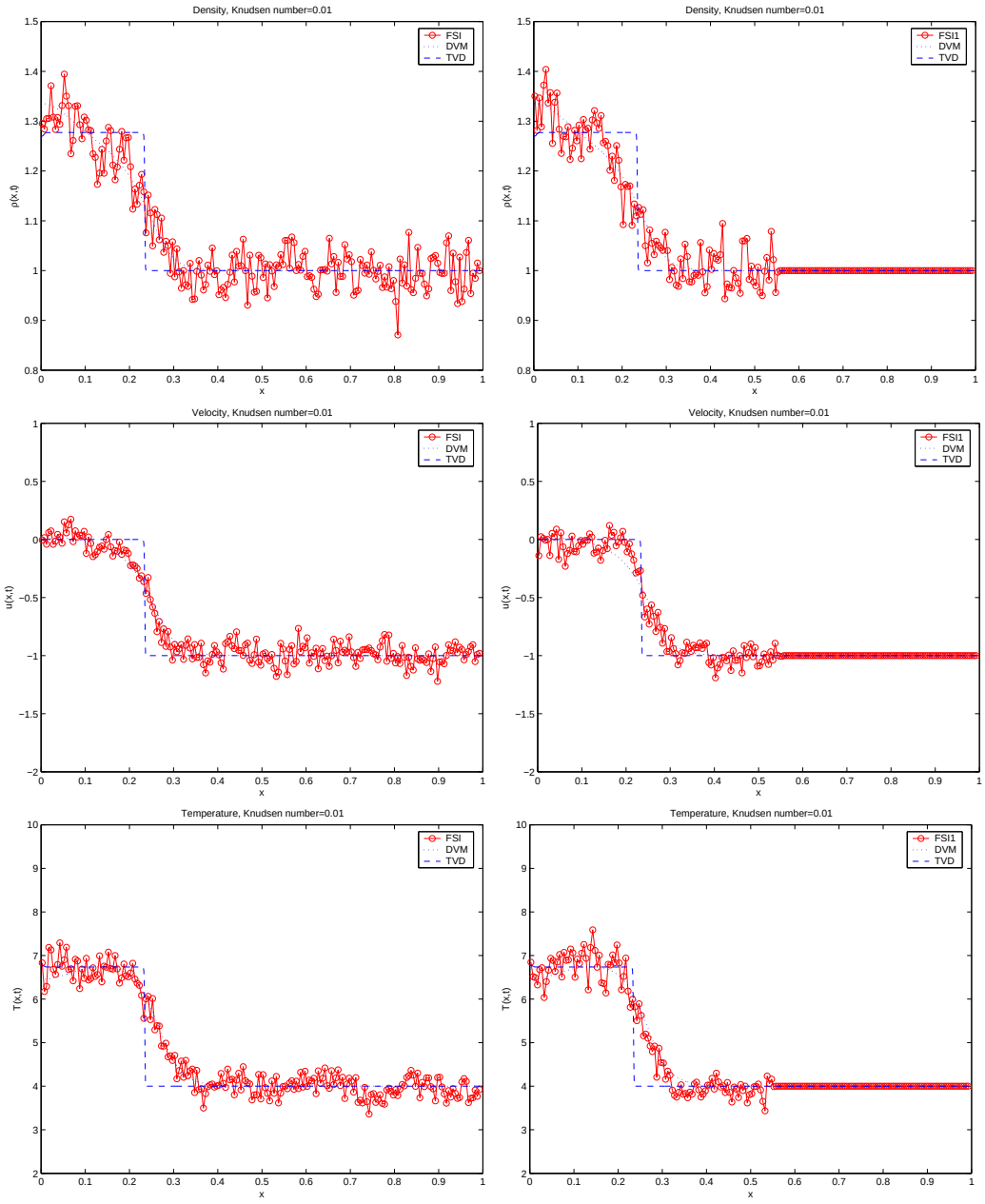

Figure 4.3: Unsteady Shock: Solution at $t = 0.065$ for FSI left, FSI1 right, density top, velocity middle, temperature bottom. Knudsen number $\varepsilon = 10^{-2}$

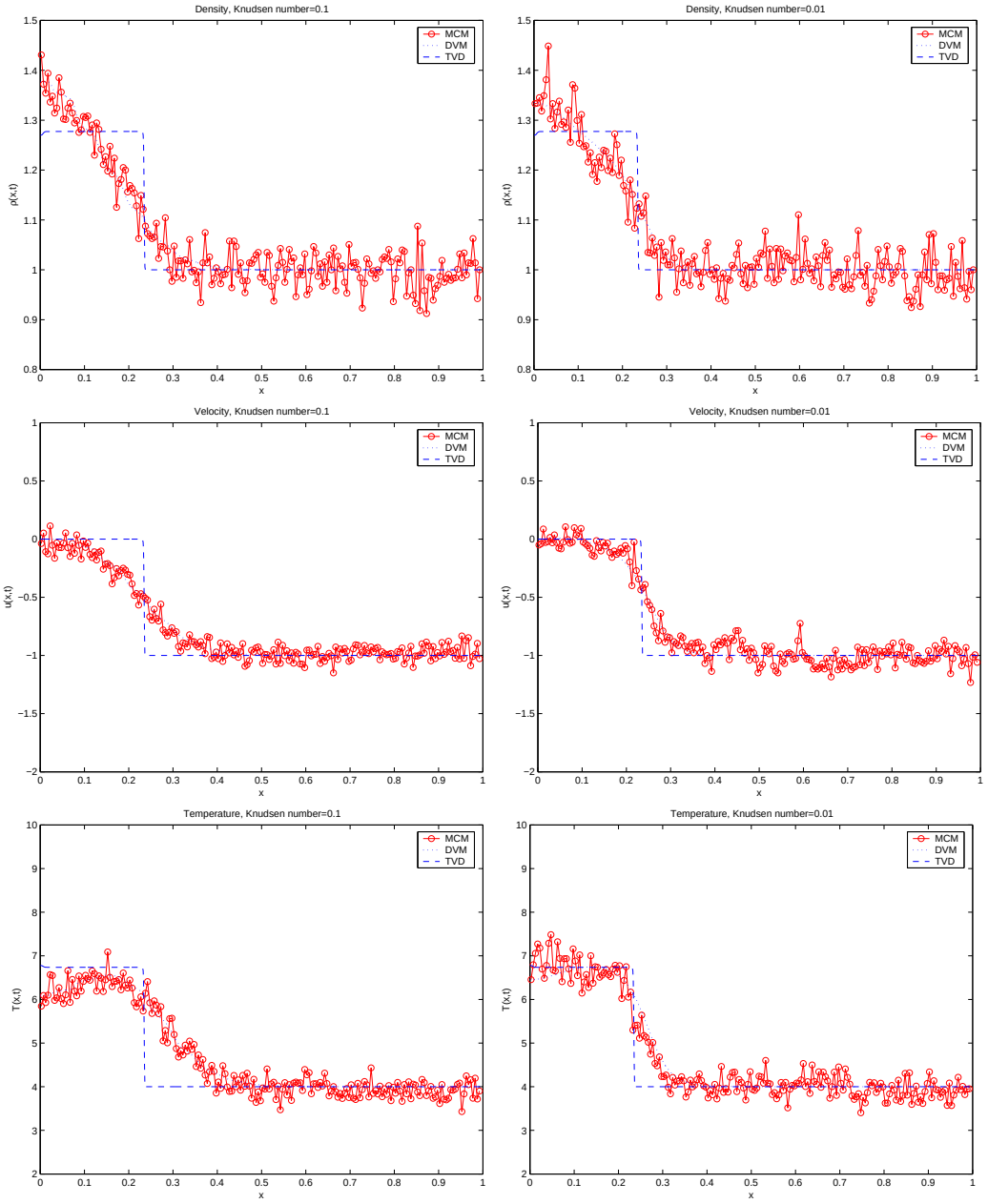

Figure 4.4: Unsteady Shock: Solution at $t = 0.065$ for MCM with Knudsen number $\varepsilon = 10^{-1}$ left, MCM with Knudsen number $\varepsilon = 10^{-2}$ right, density top, velocity middle, temperature bottom.

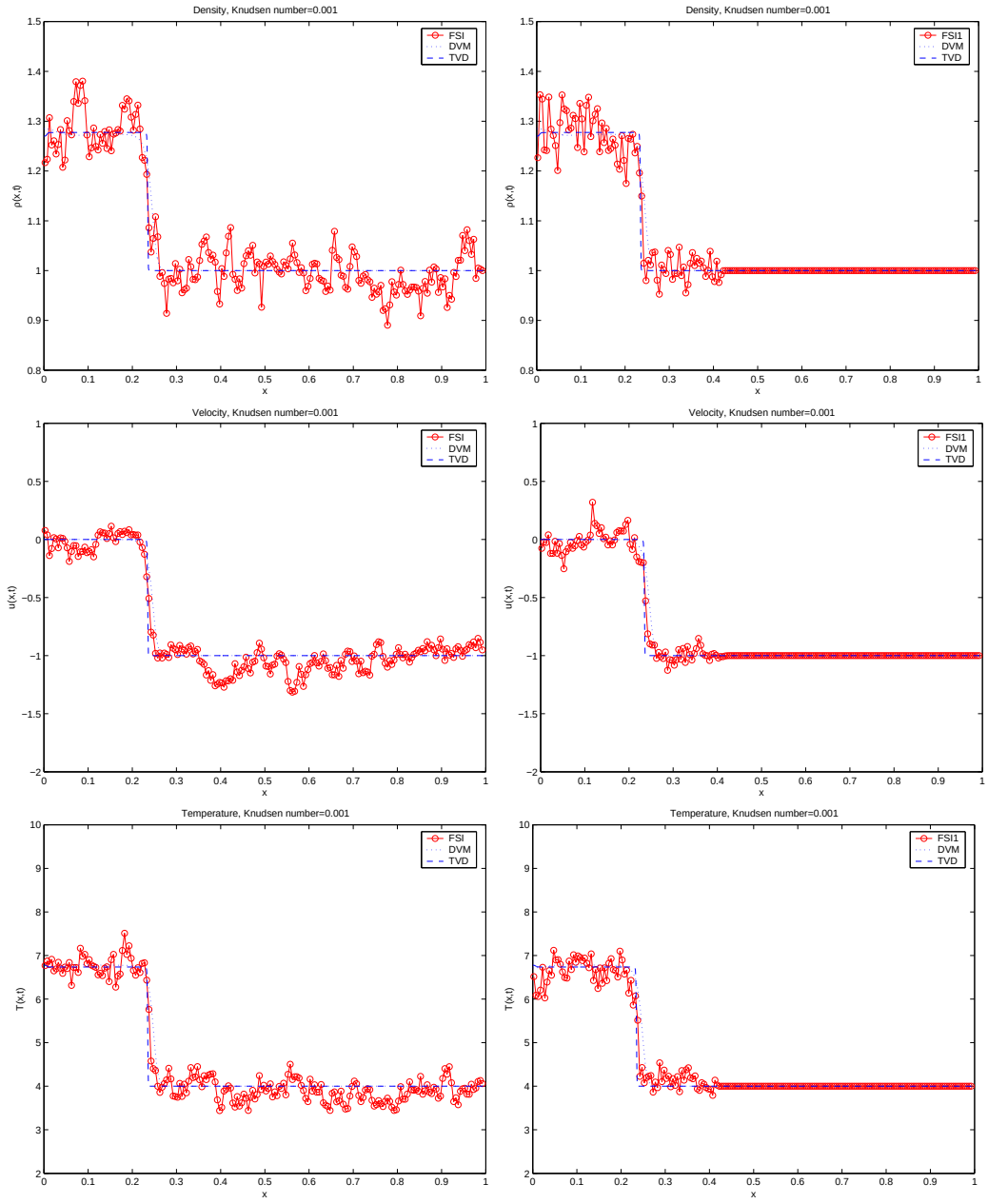

Figure 4.5: Unsteady Shock: Solution at $t = 0.065$ for FSI left, FSI1 right, density top, velocity middle, temperature bottom. Knudsen number $\varepsilon = 10^{-3}$

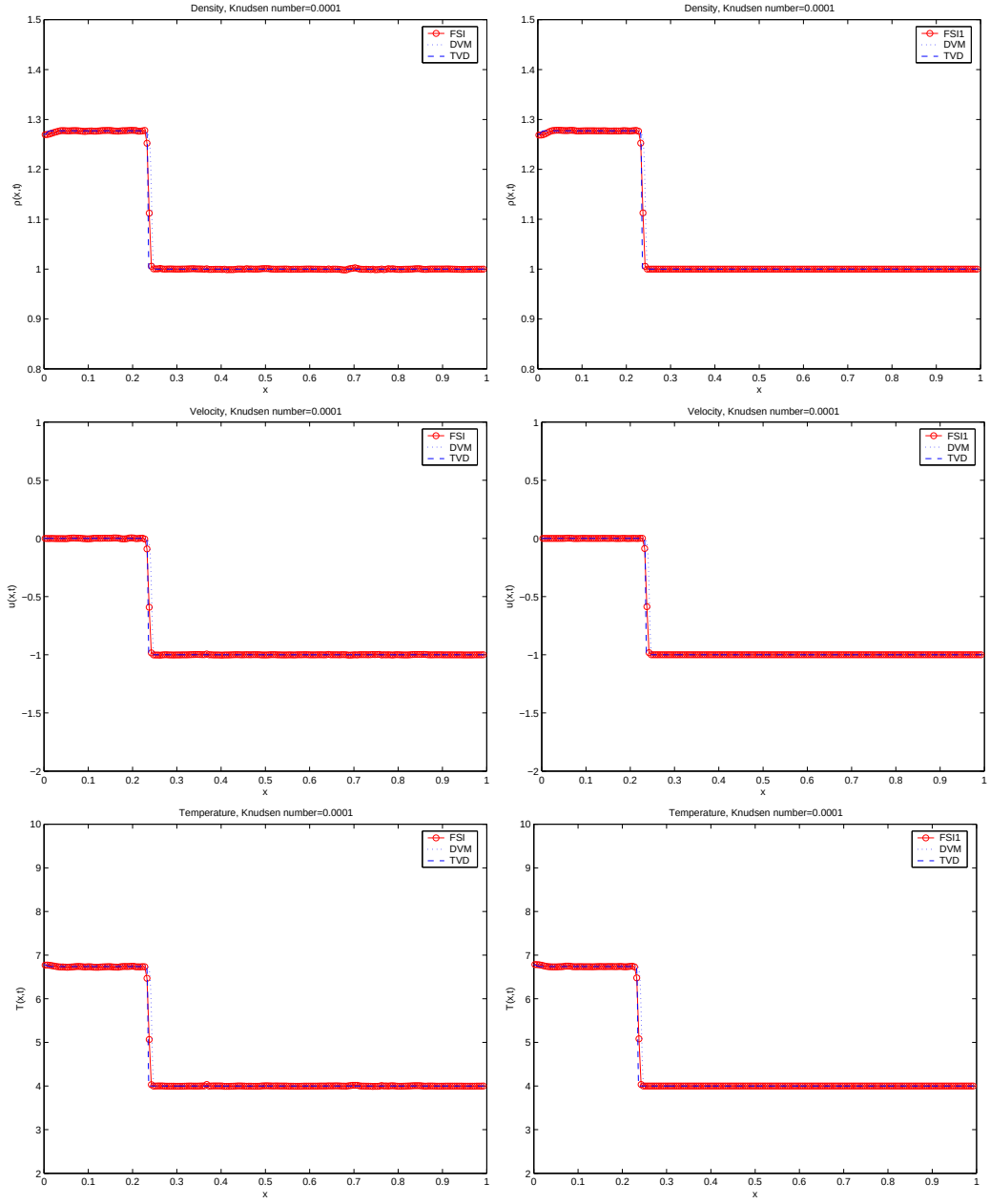

Figure 4.6: Unsteady Shock: Solution at $t = 0.065$ for FSI left, FSI1 right, density top, velocity middle, temperature bottom. Knudsen number $\varepsilon = 10^{-4}$

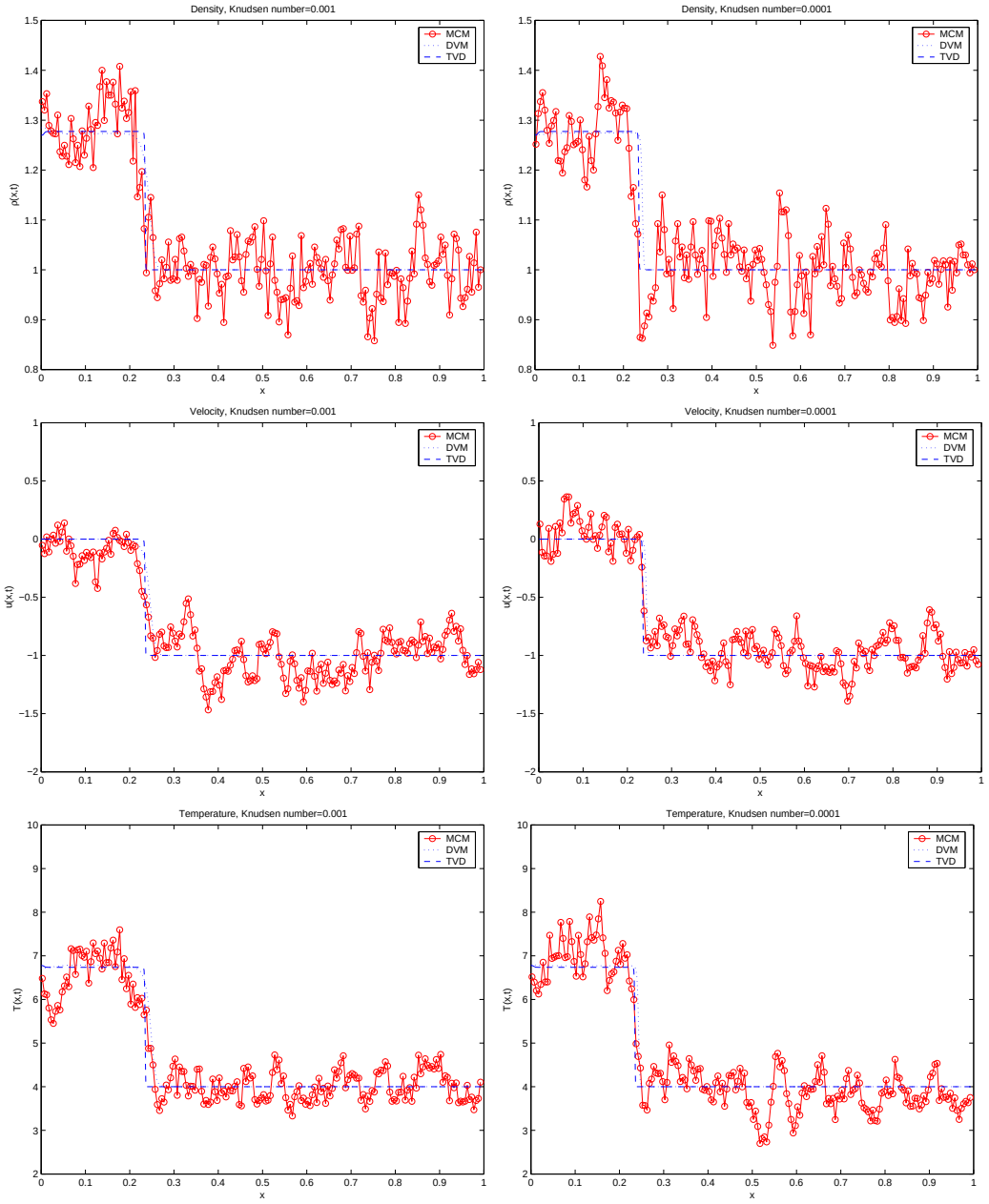

Figure 4.7: Unsteady Shock: Solution at $t = 0.065$ for MCM with Knudsen number $\varepsilon = 10^{-3}$ left, MCM with Knudsen number $\varepsilon = 10^{-4}$ right, density top, velocity middle, temperature bottom.

4.5.2 2D flow past an ellipse

In this section we compare the performance of Monte Carlo schemes and of DDM . We consider an ellipse embedded in a flow with the following characteristic

$$\varrho = 1, \;\; T = 5, \;\; M = 10 \tag{4.5.10}$$

Where M indicates the Mach number, we choose full accommodation boundary condition with temperature $T_E = 10$. The Knudsen number is $\varepsilon = 10^{-4}$ that correspond to $\beta = 0.75$ if $((x-2)/1.8)^2 + (y-1)^2 < 0.8$ while $\varepsilon = 0$ if $((x-2)/1.9)^2 + (y-1)^2 > 0.8$ that correspond of course to $\beta = 1$. The value of the Knudsen number shift from the two reported value while we move from one region towards the other as shown in Figure 4.9. The number of space cell are 200×200, the number of particles are 40 for cell. Since we are computing a stationary solution we could after some fixed time strongly diminish the fluctuation by averaging in time the solution, however we want to stress the difference of fluctuations and computational time of our hybrid scheme with respect to Monte Carlo, for this reason the solution is not averaged. What we could see is the better accuracy and performance we obtain respect a Monte carlo scheme. In the test presented we have a computational gain of about 40% which clearly increases in simulations in which we approach the hydrodynamic limit. In fact if $\varepsilon \to 0$ particles and fluctuations completely disappear and the time we need to perform the solution is the same of a solver for the compressible gas dynamic equations.

4.6 Conclusion

In this chapter we have considered the extension of the hybrid kinetic methods to the case of a general solver, microscopic or macroscopic, for the Maxwellian component, moreover we showed how to construct a domain decomposition technique starting from that idea. The simplified BGK collision kernel has been used in this work, however extension to the full Boltzmann kernel it is possible through the use of time relaxed method [94].

We showed the really encouraging results of this strategies in terms of computational performances respect to traditional methods for kinetic equations like discrete velocity model or spectral schemes. In addition this algorithm permits to obtain less fluctuations respect direct simulation Monte Carlo, in relation to the equilibrium/non equilibrium character of the solution and when the Knudsen number is sufficiently small, it also permits to compute results faster.

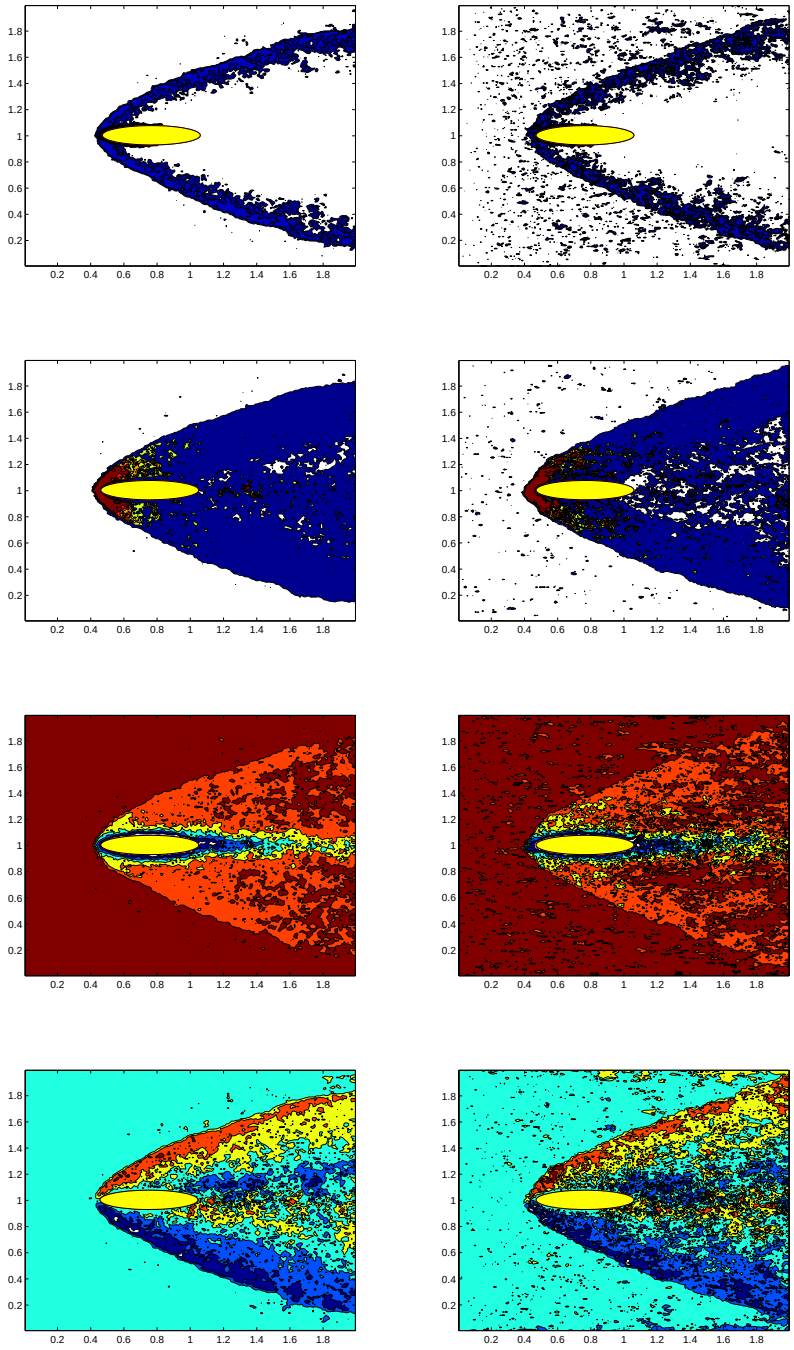

Figure 4.8: 2D flow: Domain Decomposition Hybrid scheme(left) Monte Carlo (right). Density (top), temperature (middle), velocity x- direction (middle) and velocity y-direction (bottom).

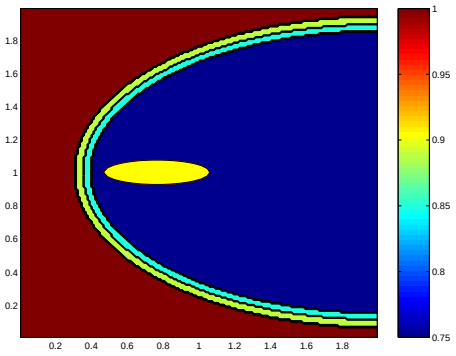

Figure 4.9: Degree of equilibrium in different regions of the domain (β).

Some open questions remain about how to increase the fraction of equilibrium in order to give a larger improvement to the performances. In any case, it is possible to round on that problem forcing the Knudsen number to zero in regions in which it is known that macroscale and microscale models furnish the same results. It is also interesting, and it is the subject of future work, to measure the response of the above methods to many others situations from the rarefied gas dynamic to nanosystem or plasma physics problems.

Acknowledgements. The authors would like to thank Russ Caflisch for the many stimulating discussions.

Part III

Multiscale Plasma Modeling and Simulation

Chapter 5

Direct Simulation Monte Carlo schemes for Coulomb Interactions

This Chapter is based on the work [14] which has to be **submitted in 2008**, in collaboration with Prof. Russell Caflisch of the Department of Mathematics of UCLA CA and Prof. Lorenzo Pareschi of the Department of Mathematics and Center for Modeling Computing and Statistics (CMCS) of University of Ferrara.

5.1 Introduction

When a gas is far from the thermodynamical equilibrium, the description of the system through the fluid equation is not satisfactory and its fundamentals properties depend upon the interactions of the particles. Collisional phenomena can be distinguished in to long-range interactions and short-range interactions. The literature on numerical schemes for short-range forces is wide ([3], [7], [16], [17]) and many efficient methods has been developed for these problems. To the other part, how to deal with long-range interactions like the Coulomb potential field it is still not clear. The present work is a contribution in this direction.

In the case of Coulomb interactions the field of each particle interact simultaneously with a large number of other particles, thus multiple collisions phenomena are involved adding difficulties to the numerical description. However, this multiple interactions can be seen as a number of simultaneous binary collisions, where each of these gives a small contribution to the relaxation process through a small angle scattering between particles.

The Landau-Fokker-Planck equation seems to be a valid substitute respect to

the Boltzmann operator (and can be derived from it, see for instance [42]) to describe this type of system, which is simply its asymptotic form in the case of Coulomb potential field, in which the large angle deflection of a charged particle, in a multiple Coulomb interaction, is considered as a series of consecutive weak binary collisions. The classic Boltzmann collision integral is still able to describe the interactions, but the typical time between two consecutive collisions prohibits to construct efficient explicit schemes, the resulting time step will be in these cases too small and an excessive use of the computational resources is needed. Moreover due to the small effect of a single interaction such detailed analysis is unnecessary.

In the present work, starting from the approximation derived by Bobylev for the Boltzmann collision operator, we generalize his approach constructing a series of direct Monte Carlo methods, showing how the scheme developed can be inserted in a larger class of numerical schemes, in the same spirit of Monte Carlo schemes for rarefied gas dynamic. Moreover, keeping separated the discretization of the time derivative and the approximation of the collision operator, we perform a series of numerical convergence tests for the approximated collision operator in order to show that the effective rate coincide with the one hypothesized in [9], once the time steps is chosen sufficiently small.

The rest of the chapter is organized as follow. In Section 5.2, we introduce the Boltzmann and Fokker-Planck equations and their properties. In Section 5.3, we show the approximated Boltzmann operator and the limiting case in which, for small angle scattering, it converges to an approximated operator for the Landau-Fokker-Planck equation. Section 5.4 shows direct simulation Monte Carlo methods for the Coulomb interactions. Several test problems which demonstrate the capabilities of the method, difference and analogies with BN (Bobylev-Nanbu scheme), and convergence tests are presented in Section 5.5. Some final considerations are discussed in Section 5.6.

5.2 The Boltzmann and the Fokker-Planck equations

Consider the Boltzmann equation

$$\frac{\partial f(x,v,t)}{\partial t} + v \cdot \nabla_x f(x,v,t) + a \cdot \nabla_v f(x,v,t) = Q(f,f) \tag{5.2.1}$$

with the initial condition

$$f(x,v,t=0) = f_0(x,v), \tag{5.2.2}$$

where $f = f(x, v, t)$ is a non negative function describing the time evolution of the distribution of particles which move with velocity $v \in \mathbb{R}^3$ in the position $x \in \Omega \subset \mathbb{R}^3$ at time $t > 0$. The vector a represent the acceleration due to the force acting on particles such as gravity, electric field or magnetic field. In the sequel the dependence on the variables for the distribution function will be omitted when it appears to be clear. The bilinear operator $Q(f, f)$ describes the binary collisions between particles and is given by

$$Q(f,f) = \int_{\mathbb{R}^3} \int_{S^2} B\left(|q|, \frac{q \cdot n}{|q|}\right) [f(v')f(v'_*) - f(v)f(v_*)] dn dv_* \tag{5.2.3}$$

where S^2 is the unit sphere in $\mathbb{R}^3$, $q = v - v_*$, $n \in S^2$ the unit normal. The post collisional velocity are computed by

$$v' = \frac{1}{2}(v + v_* + |q|n), \; v'_* = \frac{1}{2}(v + v_* - |q|n) \tag{5.2.4}$$

The collision kernel $B(|q|, q \cdot n/|q|)$, which characterize the detail of the interaction, is defined as

$$B(|q|, \cos\theta) = |q|\sigma(|q|, \theta), \; (0 \leq \theta \leq \pi) \tag{5.2.5}$$

Here $\cos\theta = q \cdot n/|q|$ and $\sigma(q, \theta)$ is the collision cross section at the scattering angle θ, that correspond to the number of particles scattered per unit time, per unit of incident flux and per unit of solid angle. We introduce also the total scattering cross section and the momentum scattering cross section that will be used in the remainder of the paper

$$\sigma_{tot}(|q|) = 2\pi \int_0^\pi \sigma(|q|, \theta) \sin\theta d\theta \tag{5.2.6}$$

$$\sigma_m(|q|) = 2\pi \int_0^\pi \sigma(|q|, \theta) \sin\theta (1 - \cos\theta) d\theta \tag{5.2.7}$$

In the case of hard sphere molecules the cross section and the collision kernel takes the form

$$\sigma(q, \theta) = \frac{d^2}{4}, \; B(|q|, \theta) = \frac{d^2}{4}|v - v_*| \tag{5.2.8}$$

while in the variable hard sphere case we have

$$\sigma(q, \theta) = C_\alpha |v - v_*|^{\alpha - 1}, \; B(|q|, \theta) = C_\alpha |v - v_*|^\alpha \tag{5.2.9}$$

with C_α and α positive constants. The case $\alpha = 1$ is referred as Maxwellian gas while for $\alpha = 1$ we recover the hard sphere model. In the case of Coulomb interactions the Rutherford formula holds

$$\sigma(|q|, \theta) = \frac{b_0^2}{4\sin^4(\theta/2)} \tag{5.2.10}$$

where $b_0 = e^2/(4\pi\epsilon_0 m_r |v - v_*|^2)$, with e the charge of the particle, ϵ_0 the vacuum permittivity and m_r the reduced mass, which corresponds to $m/2$, if the particles are of the same species, with m equal to the mass. Observe that from the above formula follows that the scattering cross section tends to infinity as the angle θ tends to zero. In order to obtain finite and meaningful values for the total and the momentum cross section is necessary to introduce a cut-off value for the impact parameter. The cut-off value is justified by the shielding effect phenomena, leading to the following values for the total cross section and the momentum cross section

$$\sigma_{tot}(|q|) = \pi\lambda_d^2 \tag{5.2.11}$$

$$\sigma_m(|q|) = 4\pi b_0^2 \log\Lambda \tag{5.2.12}$$

with $\lambda_d = (\frac{\epsilon_0 kT}{ne^2})^{1/2}$ the Debye length and $\Lambda = \frac{1}{\sin(\theta^{min}/2)}$.

In the case of grazing collisions it is possible to derive from the Boltzmann operator the Landau-Fokker-Planck operator (see [42] for details)

$$Q^L(f,f) = \frac{1}{8}\frac{\partial}{\partial v_i}\int_{\mathbb{R}^3} |q|\sigma_m(|q|)((|q|^2)\delta_{ij} - q_i q_j) \times \left(\frac{\partial}{\partial v_j} - \frac{\partial}{\partial v_{*j}}\right) f(v) f(v_*) dv_* \tag{5.2.13}$$

In the next section we will see how it is possible to construct numerical schemes starting from the Boltzmann equation which approximate the Landau operator.

5.3 The approximated Boltzmann equation

From now on, we will focus on the space homogeneous equation without force fields. Once the collision term is solved, the solution of the full Boltzmann equation can recovered computing the transport and the force term through a time splitting.

Although the divergence of the collision integral has been solved with the cut-off of the scattering cross section, the simulation of the Boltzmann equation for Coulomb interactions still represent a big trouble, due to the too high computational cost which is necessary to directly simulate the equations with time explicit

schemes. In fact rewriting Eq. (5.2.1) in the space homogenous case pointing out the gain and loss term

$$\frac{\partial f}{\partial t} = Q^+(f,f) - f(v)L[f](v),\ L[f](v) = \sigma_{tot}(|q|)\int_{\mathbb{R}^3}|q|f(v_*)dv_* \tag{5.3.1}$$

$$Q^+(f,f) = \int_{\mathbb{R}^3}\int_{S^2} B\left(|q|, \frac{q\cdot n}{|q|}\right) f(v')f(v'_*)dndv_* \tag{5.3.2}$$

it is easy to observe that the large value of the total collision cross section forces the time step to be small, thus too many steps become necessary to compute the final solution, yielding this schemes useless. In fact discretizing the time derivative we obtain

$$f(v,t+\Delta t) = \Delta t Q^+(f,f) + f(v,t)\left(1 - \Delta t\sigma_{tot}(|q|)\int_{\mathbb{R}^3}|q|f(v_*)dv_*\right) \tag{5.3.3}$$

now if we want to preserve a probabilistic interpretation we need the coefficients to be positive, thus Δt has to be extremely small if $\sigma_{tot}(|q|)$ is very large.

Recently an approximated Boltzmann operator has been developed by Bobylev and Nanbu ([9]), which permits to use larger time steps during the simulation even in the case of Coulomb collisions. Here we try to generalize this approach in order to construct Direct Monte Carlo schemes for small particles interactions.

Rewrite equation (5.2.1) in the homogenous case in the following form

$$\frac{\partial f}{\partial t} = \int_{\mathbb{R}^3} JF(U,q)dv_* \tag{5.3.4}$$

where $U = (v+v_*)/2$ denotes the center of mass velocity, and

$$F(U,q) \equiv f(U+q/2)f(U-q/2) = f(v)f(v_*) \tag{5.3.5}$$

while the operator J is defined as

$$JF(U,|q|\omega) = \int_{S^2} B(|q|,\omega\cdot n)[F(U,|q|n) - F(U,|q|\omega)]dn \tag{5.3.6}$$

with $\omega = q/|q|$. If we approximate the operator J in equation (5.3.4) by

$$J = \frac{1}{\tau}(\exp(\tau J) - \widehat{I}) \tag{5.3.7}$$

where $\widehat{I}$ is the identity operator and τ are assumed to be small, the equation reads

$$\frac{\partial f}{\partial t} = \frac{1}{\tau}\int_{\mathbb{R}^3}(\exp(\tau J) - \widehat{I})F(U,q)dv_* = \frac{1}{\tau}(P_\tau(f,f) - \varrho f) \tag{5.3.8}$$

with

$$P_\tau(f,f) = \int_{\mathbb{R}^3}\exp(\tau J)f(v)f(v_*)dv_* \tag{5.3.9}$$

The operator $\exp(\tau J)$ can be written as

$$\exp(\tau J)\psi(\omega) = \int_{S^2} B_\tau(\omega\cdot n, |q|)\psi(n)dn \tag{5.3.10}$$

where $\psi(\omega)$ is an arbitrary function and

$$B_\tau(\omega\cdot n, |q|) = \sum_{l=0}^{\infty}\frac{2l+1}{4\pi}\exp(-\lambda_l(|q|)\tau)P_l(\omega\cdot n) \tag{5.3.11}$$

is the Green function, with $P_l(\omega\cdot n)$ the Legendre polynomial and $\lambda_l(|q|)$ equal to

$$\lambda_l(|q|) = 2\pi\int_{-1}^{1}B(\mu,|q|)(1-P_l(\mu))d\mu \tag{5.3.12}$$

where $\mu = \omega\cdot n,\ -1\le\mu\le 1$ Using the above expression we obtain

$$P_\tau(f,f) = \int_{\mathbb{R}^3\times S^2} B_\tau(|q|, \frac{q\cdot n}{|q|})f(v')f(v'_*)dndv_* \tag{5.3.13}$$

Note that

$$\int_{S^2} B_\tau(\omega\cdot n,|q|) = 1 \tag{5.3.14}$$

5.3.1 A first order approximation for the Landau-Fokker-Planck equation

Assume now that the scattering cross section $\sigma(|q|,\theta)$ is concentrated at small angle near $\theta\approx 0$, thus $B_\tau(|q|,\mu)$ is concentrated near $\mu = 1$. In that situation it is possible to derive the following formal approximation

$$\lambda_l(u) \simeq 2\pi\int_{-1}^{1}B_\tau(|q|,\mu)(1-P_l(1)+(1-\mu)P_l'(1))d\mu = \pi l(l+1)\int_{-1}^{1}B_\tau(|q|,\mu)(1-\mu)d\mu \tag{5.3.15}$$

where $P_l'(1) = l(l+1)/2$. The approximate Green function reads

$$B_\tau(\mu, |q|) \simeq B_\tau^L(\mu, |q|) = \sum_{l=0}^{\infty} \frac{2l+1}{4\pi} P_l(\mu) \exp\left(-\frac{l(l+1)}{2}|q|\sigma_m(|q|)\tau\right) \tag{5.3.16}$$

The superscript L in equation (5.3.16) means that equation (5.3.8) with the above kernel approximate the Landau-Fokker-Planck equation. For a formal proof we refer to the paper of Nanbu and Bobylev ([9]).

Consider now the case of a Coulomb potential field in a single component gas or plasma. This choice, with the cut-off of the scattering angle introduced in the previous section, leads to the following approximated equation of order $0(\tau)$

$$\frac{\partial f}{\partial t} = \frac{1}{\tau}\left(\int_{\mathbb{R}^3\times S^2} D\left(\frac{q\cdot n}{|q|}, \frac{\tau}{2\varrho\tau_1}\right) f(v',t) f(v_*',t) dn dv_* - \varrho f(v,t)\right) \tag{5.3.17}$$

where

$$\frac{1}{\tau_1} = 4\pi \left(\frac{e^2}{4\pi\epsilon_0 m_r}\right)^2 \frac{\varrho \ln\Lambda}{|q|^3} \tag{5.3.18}$$

and

$$D(\mu, \tau_0) = \sum_{l=0}^{\infty} \frac{2l+1}{4\pi} P_l(\mu) \exp(-l(l+1)\tau_0) \tag{5.3.19}$$

5.4 DSMC schemes for Coulomb Interactions

Note that is not necessary to work with the collisional kernel $D(\mu, \tau_0)$ computed above, instead a simpler function $D^*(\mu, \tau_0)$ can be used, preserving the same accuracy $0(\tau)$, if the following condition remain satisfied

$$D^*(\mu, \tau_0) \geq 0,\ 2\pi \int_{-1}^{1} D^*(\mu, \tau_0) d\mu = 1 \tag{5.4.1}$$

$$\lim_{\tau_0 \to 0} D^*(\mu, \tau_0) = \frac{1}{2\pi}\delta(1-\mu) \tag{5.4.2}$$

$$\lim_{\tau_0 \to 0} \frac{2\pi}{\tau_0} \int_{-1}^{1} [D^*(\mu, \tau_0) - D(\mu, \tau_0)] P_l(\mu) d\mu = 0 \tag{5.4.3}$$

One possible substitution is represented by

$$D^*(\mu, \tau_0) = \frac{A}{4\pi \sinh A} \exp(\mu A) \tag{5.4.4}$$

where $A = A(\tau)$ satisfy

$$\coth A - \frac{1}{A} = \exp^{-\frac{\tau}{\varrho\tau_1}} \tag{5.4.5}$$

It is now clear that it is possible to apply slightly modified versions of the standard direct Monte Carlo algorithms for Maxwell molecules to the equation

$$\frac{\partial f}{\partial t} = \frac{1}{\tau}(P_\tau^*(f,f) - \varrho f) \tag{5.4.6}$$

with

$$P_\tau^*(f,f) = \int_{\mathbb{R}^3\times S^2} D^*\left(\frac{q\cdot n}{|q|}, \frac{\tau}{2\varrho\tau_1}\right) f(v',t) f(v_*',t) dn dv_* \tag{5.4.7}$$

The only difference is the way the angle is sampled. In the standard DSMC is sampled uniformly over the sphere, while here is sampled accordingly to $D^*(\mu, \tau_0)$. Let us discretize the time and denote $f^n(v)$ the approximation of $f(v, n\Delta t)$, the forward Euler scheme can be used to solve Eq. (5.4.6)

$$f^{n+1} = \left(1 - \frac{\varrho\Delta t}{\tau}\right) f^n + \frac{\varrho\Delta t}{\tau} P_\tau^*(f,f) \tag{5.4.8}$$

This equation has the following probabilistic interpretation: a particle with velocity v_i will not collide with probability $(1 - \varrho\Delta t/\tau)$ and it will collide with probability $\varrho\Delta t/\tau$ accordingly to the collision law described by $P_\tau^*(f,f)$. Observe that the probabilistic interpretation holds till $\varrho\Delta t \leq \tau$, otherwise the coefficient in front of f^n becomes negative. Note that taking the limit of the above relation,$\varrho\Delta t = \tau$, leads to the scheme of Nanbu and Bobylev. The possibility to take different values of $\Delta t \leq \tau/\varrho$ permits to reduce the statistical fluctuations and to reduce the error due to the time discretization at no additional cost since at variance with the Variable Hard sphere case, here no acceptance-rejection procedure is present.

Hence a Monte Carlo algorithm for the solution of the approximated space homogeneous Landau-Fokker-Planck equations reads as following:

Algorithm 5.4.1 (Nanbu-Babovsky (NB) for Coulomb Interactions)

1. *Given N samples v_k^0 with $k = 1, 2, .., N$ computed from the initial distribution function $f(v, t = 0)$*

2. *DO* $n = 1$ *to* n_{TOT} *with* $n_{TOT} = t_{final}/\Delta t$

   Given $\{v_k^n, k = 1, ..., N\}$

   (a) *Set* $N_c = round(\varrho N \Delta t/2\tau)$*, where the* $round$ *is statistical*

   (b) *Select* N_c *pairs* (i, j) *uniformly among all possible pairs*

   (c) *Perform the collision between* i *and* j *particles according to the following collision law*

      i. *Compute the cumulative scattering angle* $\cos\theta$ *as*

$$\cos\theta = \frac{1}{A}\ln(\exp^{-A} + 2U\sinh A) \tag{5.4.9}$$

      where U *is a random number and* $A = A(\tau)$ *is computed trough the solution of the non linear equation*

$$\coth A - \frac{1}{A} = \exp^{-\frac{\tau}{\varrho\tau_1}} \tag{5.4.10}$$

      ii. *With the above value of* $\cos\theta$ *perform the collision between* i *and* j *and compute the post collisional velocity according to*

$$v_i' = v_i - \frac{1}{2}(q(1 - \cos\theta) + h\sin\theta) \tag{5.4.11}$$

$$v_j' = v_j + \frac{1}{2}(q(1 - \cos\theta) + h\sin\theta) \tag{5.4.12}$$

      where $q = v_i - v_j$*, while h is defined as*

$$h_x = q_\perp \cos\epsilon$$

$$h_y = -(q_y q_x \cos\epsilon + q q_z \sin\epsilon)/q_\perp$$

$$h_z = -(q_z q_x \cos\epsilon - q q_y \sin\epsilon)/q_\perp$$

      where $q_\perp = (q_y^2 + q_z^2)^{1/2}$ *and* $\epsilon = 2\pi U_1$ *with* U_1 *a random number*

      iii. *set* $v_i^{n+1} = v_i'$ *and* $v_j^{n+1} = v_j'$

   (d) *Set* $v_i^{n+1} = v_i$ *for the particles that have not been selected*

END DO

We noticed the structure of the approximate operator analyzed in the previous section is similar to the structure of the classical Boltzmann collision integral. Thus is possible to construct, in the same spirit of Maxwell molecules for rarefied gas dynamic, a Monte Carlo scheme based on the classical Bird method.

From the inspection of the approximated Landau operator, it follows that the average number of significant collisions in a time step Δt is given by

$$N_c = \frac{N}{2}\frac{\varrho \Delta t}{\tau} \tag{5.4.13}$$

which means that the average time between two collisions is given by

$$\frac{\Delta t}{N_c} = \frac{2\tau}{\varrho N} \tag{5.4.14}$$

The Bird method, in the case of Maxwell molecules, can be seen as a NB scheme in which the smallest possible time step $\Delta t_1 = \Delta t / N_c$ is used, in fact only one pair collide each Δt_1

$$f^{n+1} = \left(1 - \frac{\varrho \Delta t_1}{\tau}\right) f^n + \frac{\varrho \Delta t_1}{\tau} P_\tau^*(f,f) = \left(1 - \frac{2}{N}\right) f^n + \frac{2}{N} P_\tau^*(f,f) \tag{5.4.15}$$

Hence the Bird algorithm for the approximated Landau-Fokker-Planck equation reads

Algorithm 5.4.2 (Bird for Coulomb Interactions)

1. *Given N samples v_k^0 with $k = 1, 2, .., N$ computed from the initial distribution function $f(v, t = 0)$*
2. *set time counter $t_c = 0$*
3. *set $\Delta t_c = 2\tau / \varrho N$*
4. *DO $n = 1$ to n_{TOT} with $n_{TOT} = t_{final}/\Delta t$*
   (a) *repeat*
      i. *Select a random pair (i, j) uniformly within all possible pairs*
      ii. *perform the collision accordingly to the collision law defined in the first algorithm and produce $v_i^{'}$ and $v_j^{'}$*
      iii. *Set $\tilde{v}_i = v_i^{'}$ and $\tilde{v}_j = v_j^{'}$*

iv. update the time counter $tc = tc - \Delta t_c \log(\xi)$ *until* $t_c \geq (n+1)\Delta t$

(b) Set $v_i^{n+1} = \tilde{v}_i, i = 1, ..., N$

END DO

The main difference respect to the previous algorithm is that multiple collisions between particles are allowed in Δt. Moreover in this case the CFL condition can be violated and τ can be grater than $\varrho\Delta t$. Thus, as the number of samples increase to infinity, the Nanbu-Babovsky scheme converge in probability to the discretized approximated Boltzmann equation. At variance the Bird scheme converge to the solution of the approximated Boltzmann equation increasing the number of samples, in fact Δt_1 approach zero. Thus for $\tau \to 0$ the first converge to the discretized Landau-Fokker-Planck equation and the second to the exact solution of the equation.

Remark 5.4.1 *Observe that, although in the schemes τ function as the Knudsen number in rarefied gas dynamic, at variance it has not a clear physical meaning. Mathematically the parameter in front of the collision operator is measure the goodness of the approximation. Once it is fixed it furnish a model for the interactions between particles which is so close to the Landau operator as τ is close to zero. That is, for every value of the above parameter, we solve a different model for interactions.*

Remark 5.4.2 *From the above observation it follows that, again from the mathematical point of view, given the approximated equation in the form (5.4.6), the Bird scheme (5.4.15), in which not all the particles collide in one time step Δt, furnish a better solution to the problem. It still remains not clear if the method is also a good physical approximation for system in which particles encounter many contemporary collisions.*

5.5 Numerical Tests

where the Coulomb logarithm value is fixed to $\log \Lambda = 0.5$. The simulations are run for most of the relaxation process, because all the schemes reach the same final equilibrium state and start from the same initial data, our interest is to analyze the different behaviors of the methods when particles are both far from these two situations. Thus, fixing $t_f = 40$ with the values above reported we obtain $\Delta T_f / \Delta T_0 \simeq 0.2$ for the analytic solution, in the rest of the equilibrium process

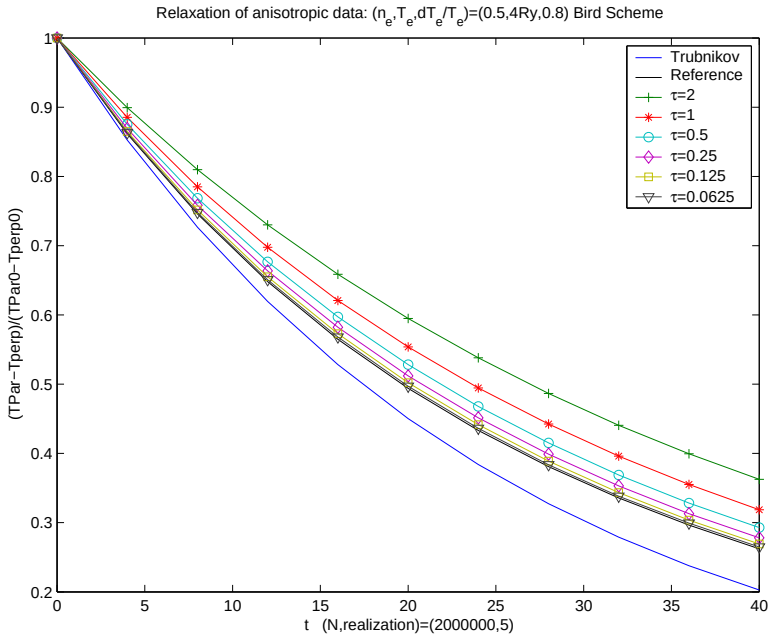

Figure 5.1: Relaxation of the velocity distribution function with anisotropic initial data for different values of τ. Bird scheme.

5.5.1 Test case

The behavior of the DSMC schemes is illustrated through a series of tests in which the relaxation of the velocity distribution function with anisotropic temperature is considered. Thus the initial distribution results to be ellipsoidal with $T_x \neq T_y = T_z$. The initial values for temperature and density are set to

$$T = 4 * R, \ \varrho = 0.5 \tag{5.5.1}$$

where R is the Rydberg constant. The initial difference in the temperature is fixed to $\Delta T_0 = 0.8$. The approximate analytic solution of the Fokker-Planck equation, in the case of small temperature difference, for $\Delta T = T_x - T_y$ is given by [123]

$$\Delta T = \Delta T_0 \exp^{-\frac{8}{5\sqrt{2\pi}}\frac{t}{\tau_T}} \tag{5.5.2}$$

the relaxation time τ_T corresponds to

$$\frac{1}{\tau_T} = \frac{\varrho e^4 \log \Lambda}{\pi\sqrt{2}\epsilon_0^2 m^{1/2}(kT)^{3/2}} \tag{5.5.3}$$

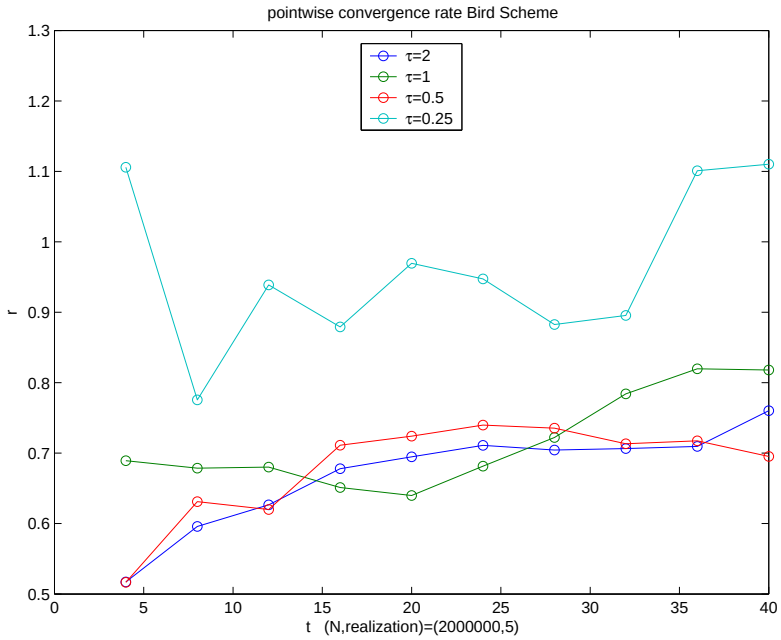

Figure 5.2: Pointwise order of accuracy $r(\tau) = \log 2(R(\tau))$ for the Bird scheme for decreasing values of the parameter τ.

the schemes and the analytic solution become closer till they coincide. We remark that although analytic, the solution is still obtained through approximations and valid for ranges in which ΔT_0 is small. This is made more clear by the Figures at the end of the section, even for very small τ the schemes do not relax at the same rate of the approximate formula (5.5.2).

5.5.2 Simulations

Our aim is to perform comparisons between the Bird scheme and the Bobylev-Nanbu (BN) scheme. The curves which describes the behavior of the Nanbu-Babovsky (NB) scheme with different choices of the time step lie between this two extremely cases. In the sequel we will analyze

- The deterministic error.
- The statistical fluctuations of the two schemes.

The sources of errors for the methods are due to

- The approximation of the Boltzmann operator
- The finite number of particles
- The discretization of the time derivative
- The conservative algorithm used for collisions

In order to make a fair comparison of the methods and to stress the capacity to describe the relaxation phenomena we try to eliminate the common sources of errors. First we compute the deterministic error due to the substitution of the original collision operator with its approximation and to the discretization of the time derivative. To that aim we increase the number of samples and average the solution of M independent realization removing statistical fluctuations

$$\overline{u}(t) = \frac{1}{M}\sum_{i=1}^{M} u_i(t) \tag{5.5.4}$$

where $\overline{u}(t)$ indicates the average solution at time t and

$$u_i(t) = \frac{T_i(t)_x - T_i(t)_y}{T(0)_x - T(0)_y} \tag{5.5.5}$$

with i the realization number. The number of samples used in the convergence analysis test for each realization is N=$2 * 10^6$ while the realizations are 5. Observe however that, using the Bird method together with a large number of particles for each realization, leads to a very accurate discretization of the time derivative (the effective time step is a function of 1/N), while with the Babovsky-Nanbu scheme the increase of the samples number does not effect the treatment of the time derivative, moreover the two methods has approximately the same computational time, at the contrary of the rarefied gas dynamic case for variable hard sphere. The choice of many samples and few realizations, is due to the will to avoid effects of finite particles number in conservative Monte Carlo methods ([47]).

This behavior can be cleared noticing that while $\tau \to 0$ also the time step $\Delta t \to 0$ thus the error introduced by the BN scheme in the discretization of the time derivative disappear. It is also easily noticeable from Figure 5.5 that the BN scheme lies closer to the analytic solution respect Bird, which means the error introduced by the discretization of the time derivative, overrelax the solution

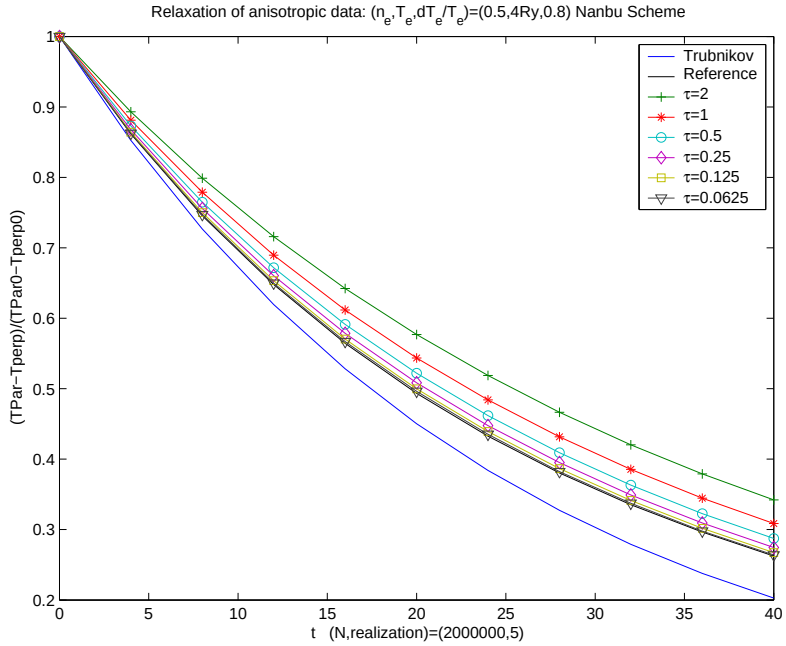

Figure 5.3: Relaxation of the velocity distribution function with anisotropic initial data for different values of τ. Bobylev-Nanbu scheme.

Summarizing the first test tries to catch the deterministic error measuring the order of accuracy of the two methods, we expect that for the Bird scheme this is due only to the approximate collision operator while for BN the error is due both to the approximation of the operator and to the discretization of the time derivative. The order of accuracy r at time t is computed as

$$r(\tau) = \log_2 R(\tau),\ R(\tau) = \frac{|\overline{u}(4\tau) - \overline{u}(2\tau)|}{|\overline{u}(2\tau) - \overline{u}(\tau)|} \tag{5.5.6}$$

with R the error ratio. Our second purpose is to measure the stochastic fluctuations of the two methods. We compare the two variances defined as

$$\Sigma^2(\tau, N) = \frac{1}{M}\sum_{i=1}^{M}(u_i - \overline{u})^2 \tag{5.5.7}$$

Fixing the parameter τ, i.e. the approximation of the Boltzmann operator, the variances of the two methods are compared for increasing number of samples starting from $N = 100$ to $N = 3200$ each measure is obtained doubling N.

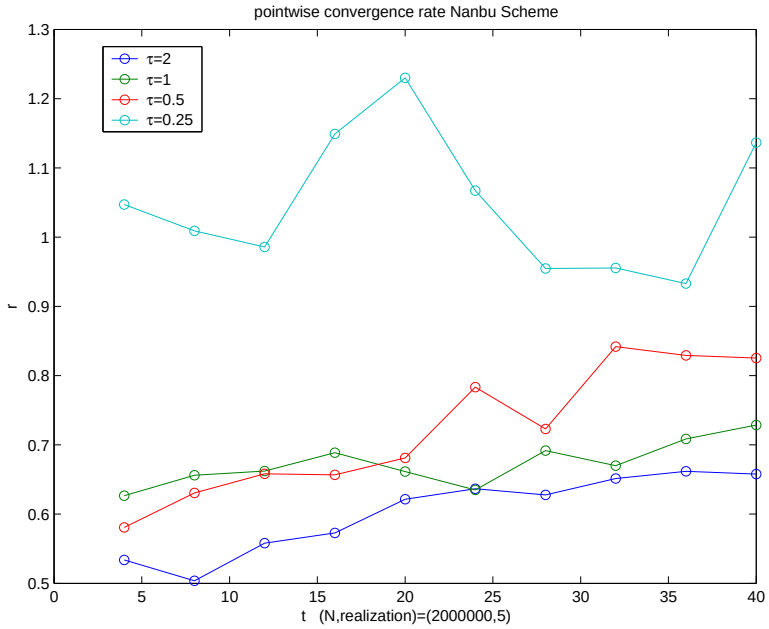

Figure 5.4: Pointwise order of accuracy $r(\tau) = \log 2(R(\tau))$ for the Bobylev-Nanbu scheme for decreasing values of the parameter τ.

In this test the number of realization is chosen equal to $M = 1500$. We expect the Bird scheme to have less fluctuations respect to the BN scheme.

5.5.3 Results

Here we report the solution of the tests described in the previous Section. In Figure 5.1 the solution for the relaxation of temperature in the different directions is showed for the Bird method, while in Figure 5.3 for the BN method. The behavior of the schemes has been analyzed using six different values for the parameter τ

$$\tau = 2 \; \tau = 1 \; \tau = 0.5 \; \tau = 0.25 \; \tau = 0.125 \; \tau = 0.0625 \tag{5.5.8}$$

Moreover the solution with $\tau = 0.03125$ with $N = 2 * 10^6$ and $M = 10$ realizations has been computed as a reference solution. In both Figures the analytic and approximated solution is reported (blue line) showing a discrepancy with the computed solution even with the more accurate one.

The time step used in the BN scheme is chosen in order to satisfy the relation $\varrho\Delta t/\tau = 1$. In Figures 5.2 and 5.4 the convergence rate r is plotted for respectively Bird and BN. Both the schemes approach the value 1 when $\tau \to 0$ as expected from the theory. Anyway it is possible to observe from Figure 5.5, in which the solution of the two methods for the same values of τ (respectively $\tau = 2$, $\tau = 1$, $\tau = 0.5$ and $\tau = 0.25$) has been compared, that the two algorithms furnish a different relaxation rate for large values of the approximation parameter of the collision operator, while for small values the two methods in practice coincide.

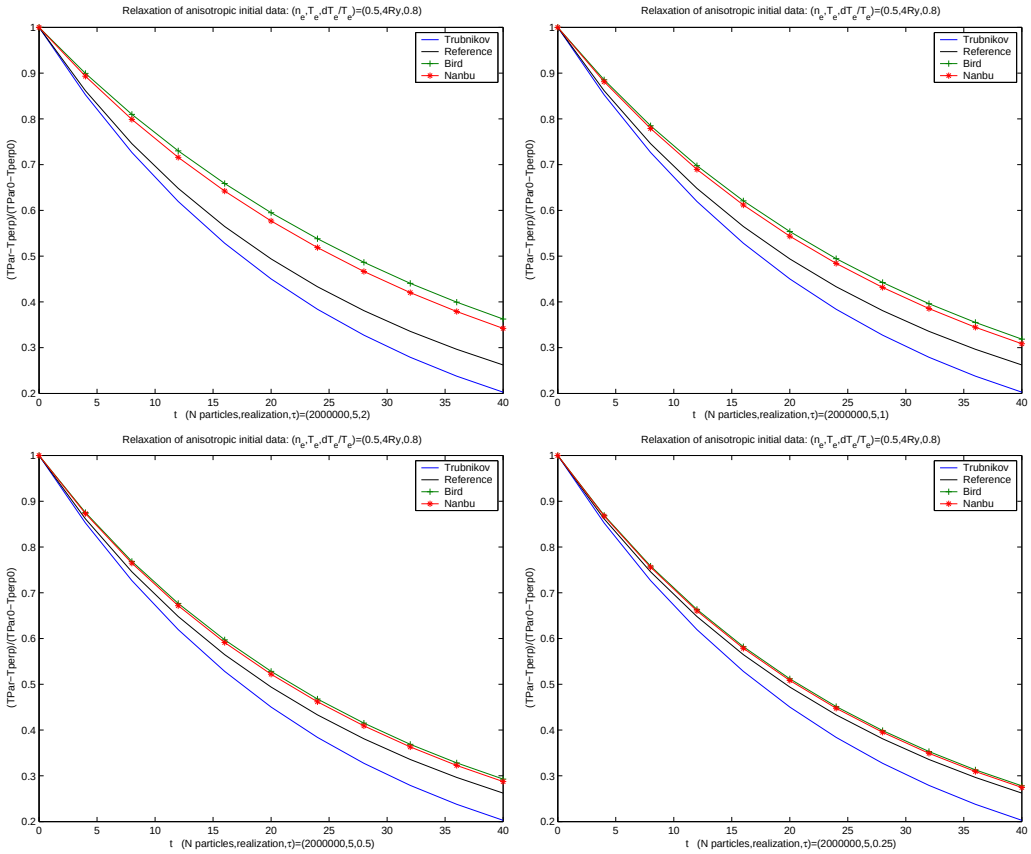

Figure 5.5: Comparison of the Bird and Bobylev-Nanbu method for $\tau = 2$ top left, $\tau = 1$ top right, $\tau = 0.5$ bottom left, $\tau = 0.25$ bottom right. In each Figure the Trubnikov (blue line) and the reference solution (black line) are depicted.

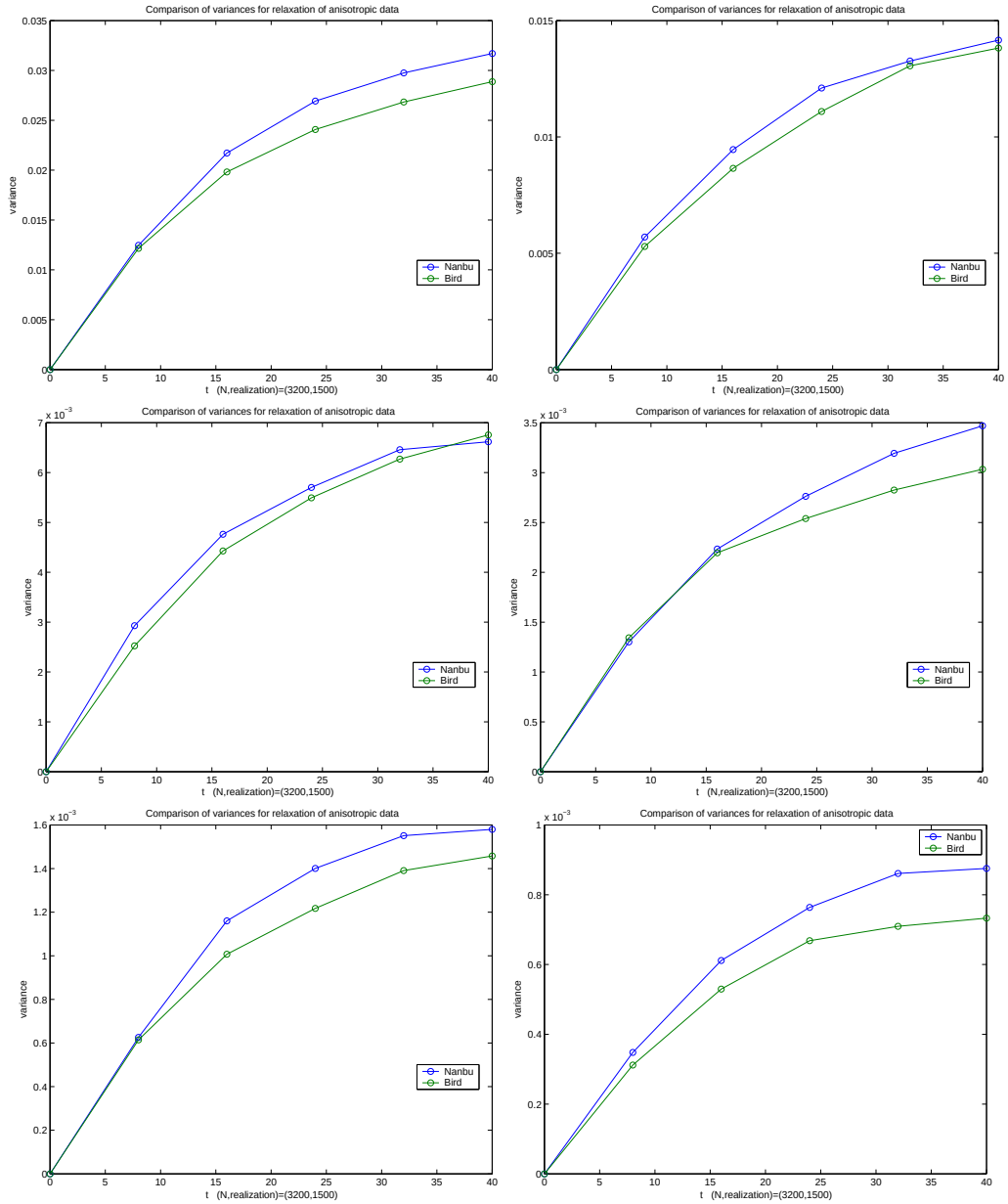

Figure 5.6: Comparison of the Bird and Bobylev-Nanbu variance for $\tau = 1$ and $N = 100$ top left $N = 200$ top right $N = 400$ middle left $N = 800$ middle right $N = 1600$ bottom left $N = 3200$ bottom right with $M = 1500$ realizations.

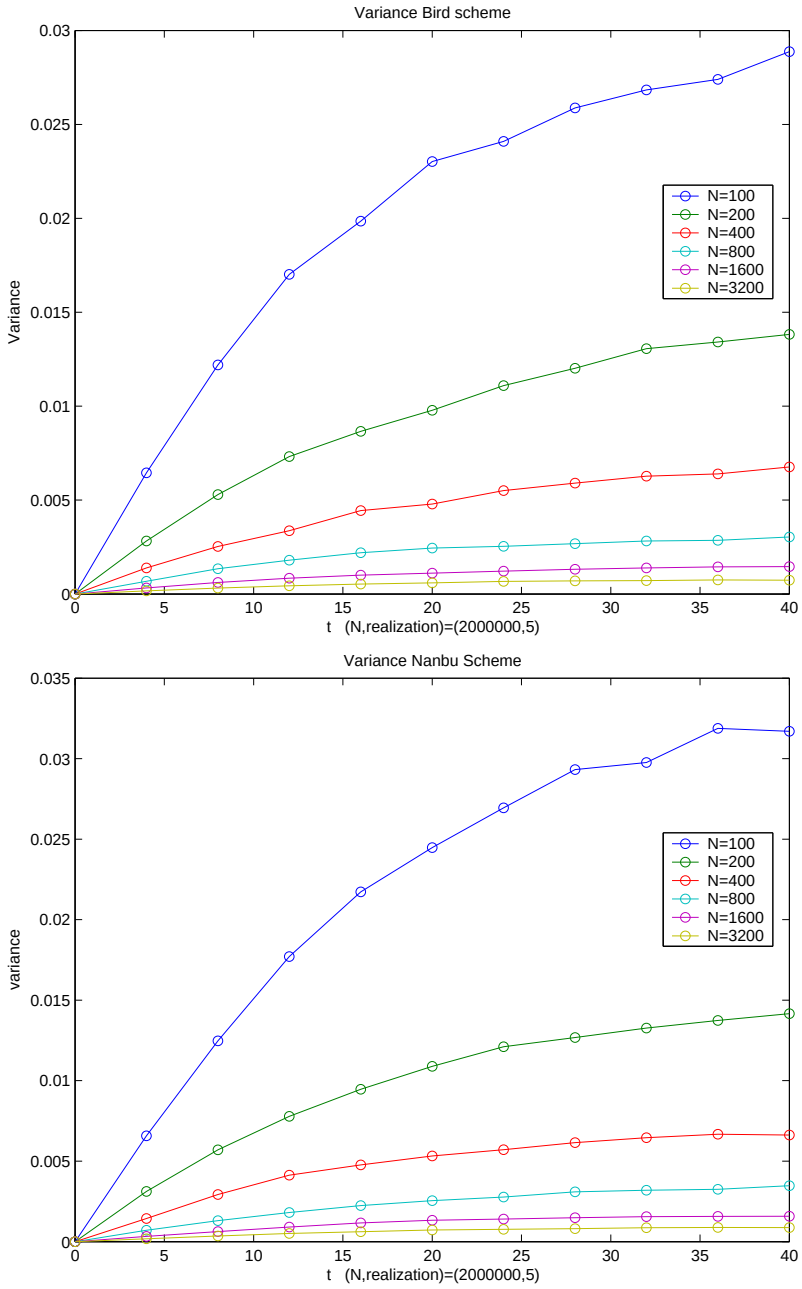

Figure 5.7: Bird (top) and Bobylev-Nanbu (bottom) variance for $\tau = 1$ and N increasing from 100 to 3200 with $M = 1500$ realizations. Here the reference solution $\overline{u}$ is computed with a fine application of the Bird scheme for the Figure on the top and of the Bobylev-Nanbu scheme for the Figure on the bottom.

respect the one furnished by the exact solution of the model (each τ define a different model for particles interactions, when τ is small this model is close to the Landau model).

In order to show the different performance in terms of statistical fluctuations we fixed the parameter $\tau = 1$ and perform several simulations increasing the number of samples N. In Figure 5.6 a comparison between the two variances, obtained with Bird and BN, has been plotted. The statistical fluctuations of the two method are approximately the same for all the initial choices of N, anyway it is possible to see how the Bird scheme oscillates slightly less respect to the BN scheme for all the values. This behavior is mainly due to the fact that we compare the solution of the BN scheme with a fine solution obtained with the Bird scheme. This is because, in the Bird scheme, the error due to the discretization of the time derivative is negligible, moreover increasing the number of particles also the statistical error disappear, making the solution close to the exact one. Thus, if we compare the BN scheme with a fine solution obtained with the same scheme with the fixed value $\tau = 1$ and $\Delta t = \tau/\rho$, the same behavior of the Bird scheme is recovered (Figure 5.7 bottom). If, instead of choosing a large value for τ we keep it small, the variance of the two methods become practically coincide, in fact if we want a fine approximation of the collision operator with the Bobylev-Nanbu method, also the time step has to be small, which means we are approaching the Bird method.

5.6 Conclusion

In this work we have proposed a generalization of the Monte Carlo scheme proposed by Bobylev and Nanbu for the solution of plasma physics problems in which the predominant collisions are of the Coulomb type [9]. The extension is achieved through the use of classic algorithm for the rarefied gas dynamic (see: [7], for instance) to the plasma physics phenomena. The main feature of the work is given by the possibility to obtain a better approximation of the time derivative of the distribution function without increasing the computational time for the DSMC case respect the original algorithm of Nanbu. Thus, although non intuitive, an algorithm in which not all particles collide at each time step and some particles collide more than once, furnish a better solution of the approximate Boltzmann operator, which has been shown to be an approximation, under some hypothesis of small angle-scattering between particles, of the Landau-Fokker-Planck operator. From the physical point of view this results propose something different respect to the

past, in fact, any other model in literature about Coulomb interactions, provides at least one collision for any particle present inside the computational domain.

The second part of the paper is centered on the numerical tests in order to compare performances and results of the methods proposed. In the tests it has been shown the convergence rate to be of order 1 both for Bird and Bobylev-Nanbu, while the variance much smaller for the first, with a computational cost of the same order for the methods. Moreover we could say, although they have not been showed, that the DSMC schemes perform well with different initial data for the same test case, but some comparisons with a deterministic scheme for the Landau equations have to be done in future to better appreciate their behaviors in different situations.

In future we hope to extend the methods described in [94] for rarefied gas dynamics to Coulomb interactions, then if the successful use of time relaxed Monte Carlo methods can be showed, it will open others interesting future development. In fact it could become possible to extend the hybrid methods developed in [17, 44] to plasma physics problems which are close to the thermodynamic equilibrium. In this methods part of the distribution function (the one in non-equilibrium) is solved by stochastic methods and part (the part in equilibrium) by deterministic methods, allowing strong reduction of computational time together with a reduction of the fluctuations, which are typical of particles simulations.

Chapter 6

A Hybrid Method for Accelerated Simulation of Coulomb Collisions in a Plasma

This Chapter is based on the work [15] which is **accepted with minor revisions in SIAM Multiscale Modeling and Simulation**, in collaboration with Prof. Russell Caflisch and Dott. Richard Wang of the Department of Mathematics of UCLA CA and Prof. Bruce Cohen and Dott. Andris Dimits of the Lawrence Livermore National Laboratory, Livermore CA, USA.

6.1 Introduction

In many plasma systems, the principal interactions between charged particles are Coulombic. For inter-particle distance d larger than the Debye length λ_D, Coulomb interactions are mediated through electro-magnetic fields governed by a Vlasov equation. On the other hand, if $d < \lambda_D$, these interactions can be described as Coulomb collisions, governed by the Fokker-Planck equation.

The Fokker-Planck equation has a time scale t_{FP}, defined by the rate of change of the particle velocity vector angle. If the characteristic time t_0 of interest is large compared to t_{FP}, then Coulomb interactions will drive the velocity distribution $f(\mathbf{v})$ to its equilibrium, given by a Maxwellian distribution M, with density n_M, velocity $\mathbf{u}_M$ and temperature T_M. Further evolution of the system can be described by continuum equations for n_M, $\mathbf{u}_M$ and T_M. At the other extreme if $t_0 << t_{FP}$, the plasma can be described as collisionless. In the intermediate

regime with t_0 and t_{FP} of comparable size, then the kinetics of Coulomb collisions are significant for the evolution of the velocity distribution function for the plasma.

This paper is concerned with Monte Carlo particle methods for simulation of Coulomb collisions in a plasma using binary collisions. One of the earliest and most influential Monte Carlo binary collision models was proposed by T. Takizuka & H. Abe (TA) in 1977 [120] and modified by Nanbu in 1997 [88]. In subsequent work, Bobylev and Nanbu [9] derived a general time-explicit formulation for the approximation of the Fokker-Planck equation by a binary collision model. Wang et al. [127] performed a numerical convergence study for the methods of TA and Nanbu.

The two methods proposed by TA [120] and Nanbu [88] have been widely used in the plasma physics community. Simulation of Coulomb collisions can be a computational bottleneck, however, since the collision times are often very disparate from the characteristic times of interest. This difficulty is compounded by the wide range of collision rates for many problems. For example, consider a velocity distribution in the form of a bump-on-tail; i.e., a near-equilibrium distribution at low velocity with an isolated spike far out on its tail (the "bump"). The rate of collisions between two particles of velocity $\mathbf{v}_1$ and $\mathbf{v}_2$ is proportional to u^{-3} for $u = |\mathbf{v}_1 - \mathbf{v}_2|$. The average rate of collisions between the particles in the central distribution $f \approx M$ is of size $T_M^{-3/2}$ in which T_M is the temperature of the Maxwellian distribution M. The bump may be concentrated at a velocity difference u_B from the center of M with $u_B >> T_M^{1/2}$, so that its rate of interaction with M is of size $u_B^{-3} << T_M^{-3/2}$. Direct simulation of the Coulomb collisions for a bump-on-tail distribution is dominated by collisions between M and itself, which preserve M but do not affect the evolution of f, and the important interactions of the bump with M will be rare events. This shows that direct simulation of this problem is highly inefficient.

The purpose of this paper is to present a hybrid method for accelerating the simulation of Coulomb collisions. It represents the distribution function as a combination of a thermal component m (a Maxwellian distribution) and kinetic component k (numerically represented as a set of particles). Evolution of the thermal component m is performed using continuum methods based on conservation principles; while evolution of the kinetic component k is performed by Monte Carlo simulation of binary collisions using the method of TA or Nanbu. An interaction between m and k is performed by sampling a particle from m and selecting a particle from k, then treating the interaction as a particle collision. In addition, ther-

malization (particles moved from k to m) and dethermalization (particles moved from m to k) are performed with probabilities p_T and p_D respectively.

This hybrid method is motivated by a similar hybrid method for rarefied gas dynamics (RGD) developed by Pareschi & Caflisch [16]. In the RGD application, the division between Maxwellian and particle components is performed solely in physical space x; e.g., the probabilities p_T and p_D are functions only of x. For Coulomb collisions, however, the division between the two components must be performed in phase space $(x, \mathbf{v})$, and p_T and p_D are functions of x and $\mathbf{v}$.

The remainder of this paper is organized as follows: The Monte Carlo binary collision methods of TA [120] and Nanbu [88], as well as the general formulation of Bobylev and Nanbu [9], are presented in Section 6.2, and the hybrid method is formulated in Section 6.3. Determination of p_T and p_D is performed in Section 6.4 through a detailed balance requirement and the use of Nanbu's s parameter. Computational results are presented in Section 6.5, following by conclusions in Section 6.6.

6.2 Monte Carlo Simulation of Coulomb Collisions

We first introduce the governing equation for the physical process, and describe the TA and Nanbu Monte Carlo binary collision models for a spatially homogeneous plasma. We consider collisions between N particles consisting of $N/2$ particles from each of two species α and β.

6.2.1 Governing equation

Coulomb collisions in a plasma can be treated as the simulation of many continuous small-angle binary collisions [118]. The time evolution of the particle distribution in a spatially homogeneous, non-equilibrium plasma is described by the Fokker-Planck equation:

$$\frac{\partial f_\alpha}{\partial t} = (\frac{\delta f_\alpha}{\delta t})_c \tag{6.2.1}$$

in which f_α is the distribution function of the α species and $(\frac{\delta f}{\delta t})_c$ is the collision operator defined as (MKS units)

$$(\frac{\delta f_\alpha}{\delta t})_c = -\sum_\beta \frac{\partial}{\partial v_j} \frac{e_\alpha^2 e_\beta^2 \log\Lambda}{8\pi\epsilon_0^2 m_\alpha} \int dv' [\frac{\delta_{jk}}{u} - \frac{u_j u_k}{u^3}][\frac{f_\alpha}{m_\beta}\frac{\partial f_\beta'}{\partial v_k'} - \frac{f_\beta'}{m_\alpha}\frac{\partial f_\alpha}{\partial v_k}]. \tag{6.2.2}$$

in which we use the notation $\mathbf{u} = \mathbf{v}_\alpha - \mathbf{v}_\beta$, $u = |\mathbf{u}|$ and $f'_\beta = f_\beta(\mathbf{v}')$. The equation for f_β is similar.

Bobylev and Nanbu [9] derived a general formulation for a binary collision model that approximates the solution of (6.2.1) over a time step Δt. The resulting equation (see [9] for further details and definitions) is

$$f_\alpha(\mathbf{v}, t + \Delta t) = \sum_{\beta=1}^{n} \pi_{\alpha\beta} \int_{R^3 \times S^2} d\mathbf{v}_\beta d\mathbf{n} D_{\alpha\beta}(\frac{\mathbf{g} \cdot \mathbf{n}}{g}, A_{\alpha\beta}\frac{\Delta t}{g^3}) f_\alpha(\mathbf{v}'_\alpha, t) f_\beta(\mathbf{v}'_\beta, t). \tag{6.2.3}$$

They also found a set of conditions on the kernel $D_{\alpha\beta}$ which ensure that f is an approximate solution of (6.2.1), with error of size $O(\Delta t)$. As described in the following, the TA and Nanbu collision models each correspond to Monte Carlo simulation of the integral (6.2.3) for a specific choice of $D_{\alpha\beta}$.

6.2.2 The Collision Model of Takizuka and Abe

Although the TA model was not analyzed in [9], we show that the collision model of TA corresponds to the following formula for D:

$$D_{TA}(\mu, \tau) = (2\pi)^{-1}(2\pi\tau)^{-1/2} e^{-\zeta^2/2\tau} (d\zeta/d\mu) \tag{6.2.4}$$

in which

$$\tau = < \zeta^2 > = (\frac{e_\alpha^2 e_\beta^2 n_L \log\Lambda}{8\pi\epsilon_0^2 m_{\alpha\beta}^2 u^3})\Delta t \tag{6.2.5}$$

and the scattering angle θ in the frame of the relative velocity is defined by

$$\begin{aligned} \theta &= 2\arctan\zeta \\ \mu &= \cos\theta. \end{aligned} \tag{6.2.6}$$

Also e_α and e_β are electric charges for the species α and β, n_L is the smaller density of the particle species α and β, Λ is the Coulomb logarithm, $u = |\mathbf{v}_\alpha - \mathbf{v}_\beta|$ is the relative speed, Δt is the time step , and $m_{\alpha\beta} = m_\alpha m_\beta/(m_\alpha + m_\beta)$ is the reduced mass. With the choice $D = D_{TA}$, the convergence criteria of Bobylev and Nanbu in [9] is satisfied, as shown in Appendix 6.7.1.

A Monte Carlo algorithm for simulation of the integral (6.2.3) with the kernel (6.2.4) over a single time interval Δt consists of performing the following steps $N/2$ times:

1. Randomly select two particles with velocity $\mathbf{v}_\alpha$ and $\mathbf{v}_\beta$ from the distributions f_α and f_β. This is done by exclusive sampling, so that no particle is selected more than once. This corresponds to the term $f_\alpha f_\beta$ in (6.2.3).

2. Sample a value of $\mu = \cos(2\arctan\zeta)$, in which ζ is a Gaussian random variable with mean 0 and variance $\tau =< \zeta^2 >$ and τ is defined by (6.2.5) using $u = |\mathbf{v}_\alpha - \mathbf{v}_\beta|$. Define θ by $\theta = 2\arctan\zeta$. This corresponds to the factor $(2\pi\tau)^{-1/2}e^{-\zeta^2/2\tau}(d\zeta/d\mu)$ in D_{TA}.

3. Choose the azimuthal angle ϕ randomly and uniformly from the interval $[0, 2\pi]$. This corresponds to the remaining factor $(2\pi)^{-1}$ in D_{TA}.

4. The new velocities are $\mathbf{v}_\alpha^{'}$ and $\mathbf{v}_\beta^{'}$ defined by

$$\begin{aligned} \mathbf{v}_\alpha^{'} &= \mathbf{v}_\alpha + \frac{m_{\alpha\beta}}{m_\alpha}\Delta\mathbf{u} \\ \mathbf{v}_\beta^{'} &= \mathbf{v}_\beta - \frac{m_{\alpha\beta}}{m_\beta}\Delta\mathbf{u} \end{aligned} \tag{6.2.7}$$

   in which

$$\begin{aligned} \Delta u_x &= (u_x/u_\perp)u_z\sin\theta\cos\phi - (u_y/u_\perp)u\sin\theta\sin\phi - u_x(1-\cos\theta) \\ \Delta u_y &= (u_y/u_\perp)u_z\sin\theta\cos\phi + (u_x/u_\perp)u\sin\theta\sin\phi - u_y(1-\cos\theta) \\ \Delta u_z &= -u_\perp\sin\theta\cos\phi - u_z(1-\cos\theta) \\ \mathbf{u} &= \mathbf{v}_\alpha - \mathbf{v}_\beta. \\ u_\perp &= \sqrt{u_x^2 + u_y^2}. \end{aligned} \tag{6.2.8}$$

5. Replace the velocities $\mathbf{v}_\alpha$ and $\mathbf{v}_\beta$ by $\mathbf{v}'_\alpha$ and $\mathbf{v}'_\beta$. This corresponds to the appearance of $\mathbf{v}'_\alpha$ and $\mathbf{v}'_\beta$ as the arguments of f_α and f_β in (6.2.3).

These are exactly the steps of the algorithm described in the work of TA [120]. Note that in this algorithm, as well as in the algorithm of Nanbu and the general formulation of [9], every particle collides exactly once in each time interval.

6.2.3 Nanbu's Collision Model

As described in [9], the collision model of Nanbu corresponds to the following formula for D:

$$D_{Nanbu}(\mu,\tau) = \frac{A}{4\pi\sinh A}\exp\mu A. \tag{6.2.9}$$

Monte Carlo simulation using this kernel over a single time interval Δt consists of performing the following steps $N/2$ times:

1. Randomly select two particles with velocity $\mathbf{v}_\alpha$ and $\mathbf{v}_\beta$ from the distribution f. This is done by exclusive sampling, so that no particle is selected more than once.

2. Calculate the quantities s and A solving

$$s = 2\tau \tag{6.2.10}$$

$$\coth A - A^{-1} = e^{-s} \tag{6.2.11}$$

   with τ defined by (6.2.5), using $u = |\mathbf{v}_\alpha - \mathbf{v}_\beta|$ in the definition (6.2.5) of τ.

3. Sample a value of the random variable μ from the interval $[-1, 1]$ with probability density

$$f(\mu) = 2\pi D_{Nanbu} = A(2\sinh A)^{-1} e^{A\mu} \tag{6.2.12}$$

   and define θ by $\mu = \cos(\theta)$.

4. Choose the azimuthal angle ϕ randomly and uniformly from the interval $[0, 2\pi]$.

5. The new velocities are $\mathbf{v}_\alpha^{'}$ and $\mathbf{v}_\beta^{'}$ are defined as in (6.2.7) and (6.2.8).

6. Replace the velocities $\mathbf{v}_\alpha$ and $\mathbf{v}_\beta$ by $\mathbf{v}'_\alpha$ and $\mathbf{v}'_\beta$.

These are exactly the steps of the algorithm described in the work of Nanbu [120], with some minor changes in notation, for consistency with the TA method.

In the remainder of the paper, the collisions are assumed to be between particles from a single species so that the subscripts α and β are dropped. In addition, the distribution function will be assumed to be spatially homogeneous, so that particle position can be neglected.

6.3 The Hybrid Method

The hybrid method is based on representation of the velocity distribution function f as a combination of a thermal component m and a kinetic component k; i.e.,

$$f(\mathbf{v}) = m(\mathbf{v}) + k(\mathbf{v}). \tag{6.3.1}$$

The thermal component is a Maxwellian distribution

$$m(\mathbf{v}) = n_m(2\pi T_m)^{-3/2} \exp\left(-|\mathbf{v} - \mathbf{u}_m|^2/2T_m\right). \tag{6.3.2}$$

Because of the (expected) slow interaction of the thermal component m with the kinetic component k, the average density, velocity and temperature n_m, $\mathbf{u}_m$ and T_m of m are not assumed to be those of the full distribution f. This explains the difference between the notation m and M, since M is assumed to density, velocity and temperature that are equal to those of f.

Denote n_m and n_k to be the effective number of particles in the thermal and kinetic components, respectively, of f. At present these numbers will be kept to be even integers. The kinetic component will be simulated using a set of discrete particles; i.e.,

$$g(\mathbf{v}) = \sum_{i=1}^{n_k} \delta(\mathbf{v} - \mathbf{v}_i). \tag{6.3.3}$$

In each time interval, the simulation steps are the following:

1. Determine the number of collisions of each type; i.e.,
   - $n_{mm} = n_m^2/2(n_k + n_m)$ is the number of collisions between 2 m particles.
   - $n_{kk} = n_k^2/2(n_k+n_m)$ is the number of collisions between 2 k particles.
   - $n_{mk} = n_m n_k/(n_k + n_m)$ is the number of collisions between an m particle and a k particle.
2. Perform the collisions.
   - The $m - m$ collisions do not change the distribution m, so they do not need to be performed.
   - For each $k-k$ collision, select two particles $\mathbf{v}_1$ and $\mathbf{v}_2$ from k. Perform a collision between them, as in the method of TA or Nanbu, to get new velocities $\mathbf{v}_1'$ and $\mathbf{v}_2'$. In k, replace $\mathbf{v}_1$ and $\mathbf{v}_2$ by $\mathbf{v}_1'$ and $\mathbf{v}_2'$.
   - For each $m - k$ collisions, sample a particle $\mathbf{v}_m$ from m and select a particle $\mathbf{v}_k$ from k. Perform a collision between them, as in the method of TA or Nanbu, to get new velocities $\mathbf{v}_m'$ and $\mathbf{v}_k'$. The postcollision velocity $\mathbf{v}_k'$ replaces $\mathbf{v}_k$ in k.
3. Apply thermalization and dethermalization.

- For each post-collision particle $\mathbf{v}'$ (i.e., $\mathbf{v}'_1$, $\mathbf{v}'_2$ or $\mathbf{v}'_k$ from the previous step), thermalize $\mathbf{v}'$ with probability $p_T(\mathbf{v}')$. This is done by removing $\mathbf{v}'$ from k (in the next step its number, momentum and energy will be added to m).
- For each post-collision particle $\mathbf{v}'_m$, dethermalize $\mathbf{v}'_m$ with probability $p_D(\mathbf{v}'_m)$. This is done by adding $\mathbf{v}'_m$ to k (in the next step its number, momentum and energy will be subtracted from m).

4. Apply conservation.

   - Adjust the number n_k of particles in k, due to thermalization and dethermalization.
   - Adjust the number, momentum and energy of m, due to thermalization and dethermalization. This is most easily performed by requiring that the total number, momentum and energy of $f = m + k$ be the same before and after the collisions.

A possible problem with this algorithm is that sampling velocities $\mathbf{v}_m$ from m may remove too much energy from m. This can be avoided by conservative sampling. First sample all n_{mk} velocities from m and then shift and scale these so that the average momentum and energy of the sampled particles is the same as the average momentum and energy of m.

6.4 Choice of p_D and p_T

6.4.1 Detailed Balance Condition

Consider an equilibrium distribution M represented as

$$M = m + k = f \tag{6.4.1}$$

in which m is the continuum component and k is the kinetic component. Note that m is an equilibrium, but m is not necessarily equal to M. In Appendix 6.7.2, detailed balance is used to derive conditions on p_D and p_T, starting from the scattering integral of (6.2.3) with the inclusion of thermalization/dethermalization. Although this is the theoretically correct approach, it does not lead to explicit conditions on p_D and p_T.

In this section, we adopt a simpler approach by requiring that thermalization/dethermalization applied to all of $f = m + k$ does not change m and k, if $f = M$ is a Maxwellian. This is performed as follows: Apply thermalization to k with probability p_T and dethermalization to m with probability p_D. Also define a projection Π_M onto equilibria, i.e., $\Pi_M f$ is the Maxwellian with same $(\rho, \mathbf{u}, T)$ as f. The resulting distribution is

$$f' = \Pi_M((1 - p_D)m + p_T k) + p_D m + (1 - p_T)k. \tag{6.4.2}$$

Now assume that $f = m + k = M$ and require that the form of f is conserved; i.e.,

$$\begin{aligned} m &= \Pi_M((1 - p_D)m + p_T k) \qquad (6.4.3)\\ k &= p_D m + (1 - p_T)k. \end{aligned}$$

It follows that

$$\begin{aligned} k &= (p_D/p_T)m \qquad (6.4.4)\\ M &= (1 + p_D/p_T)m. \qquad (6.4.5) \end{aligned}$$

Denote

$$\gamma = M/m. \tag{6.4.6}$$

For simplicity assume that

$$\mathbf{u}_M = \mathbf{u}_m = 0 \tag{6.4.7}$$

or more generally that $\mathbf{u}_M = \mathbf{u}_m$. This is not generally true, but is a reasonable assumption if $f = M$. Then look for

$$\gamma(\mathbf{v}) = ce^{|\mathbf{v}|^2/2\tau} \tag{6.4.8}$$

in which

$$\begin{aligned} c &= (n_M/n_m)(T_m/T_M)^{3/2} \qquad (6.4.9)\\ \tau^{-1} &= T_m^{-1} - T_M^{-1}. \qquad (6.4.10) \end{aligned}$$

Note that $m < M$ for all $\mathbf{v}$, so that

$$T_m < T_M. \tag{6.4.11}$$

Insertion of (6.4.10) into (6.4.4), shows that the detailed balance requirement for p_D and p_T is

$$1 + p_D/p_T = ce^{|\mathbf{v}|^2/2\tau}. \tag{6.4.12}$$

6.4.2 Velocity-based choice of p_D and p_T

Look for p_T, p_D to satisfy

$$\begin{aligned} p_T &= 1 \qquad \text{for } |\mathbf{v}| < v_1 \\ p_D &= 1 \qquad \text{for } |\mathbf{v}| > v_2. \end{aligned} \tag{6.4.13}$$

in which v_1 and v_2 are constants with $v_1 < v_2$. Define

$$\begin{aligned} p_D &= \sqrt{\alpha(\gamma-1)} \\ p_T &= \sqrt{\alpha/(\gamma-1)} \end{aligned} \tag{6.4.14}$$

which automatically satisfies (6.4.12). For a given choice of v_1, v_2, set

$$\begin{aligned} c &= 1 \\ \tau &= (4\log 2)^{-1}(v_1^2+v_2^2) \\ \gamma_1 &= \gamma(v_1) = e^{v_1^2/2\tau} \\ \gamma_2 &= \gamma(v_2) = e^{v_2^2/2\tau} \\ \alpha_1 &= \alpha(v_1) = (\gamma_1 - 1) \\ \alpha_2 &= \alpha(v_2) = (\gamma_2 - 1)^{-1}. \end{aligned} \tag{6.4.15}$$

The choice of τ was made so that

$$0 < \alpha_1 < 1, \;\; 0 < \alpha_2 < 1 \tag{6.4.16}$$

i.e.

$$v_1^2/2\tau < \log 2 < v_2^2/2\tau. \tag{6.4.17}$$

Since $p_D(v_1) = \alpha_1$ and $p_T(v_2) = \alpha_2$, the construction below will ensure that $0 \le p_D \le 1$ and $0 \le p_T \le 1$.

Equations (6.4.13) and (6.4.14) determine α for $|\mathbf{v}| < v_1$ (i.e., for $\gamma < \gamma_1$) and $|\mathbf{v}| > v_2$ (i.e., for $\gamma > \gamma_2$). Define α in the interval $\gamma_1 < \gamma < \gamma_2$ by interpolation with respect to γ to get

$$\alpha = \begin{cases} (\gamma-1) & \text{for } |\mathbf{v}| < v_1 \\ \alpha_1 + \frac{(\gamma-\gamma_1)}{\gamma_2-\gamma_1}(\alpha_2-\alpha_1) & \text{for } v_1 < |\mathbf{v}| < v_2 \\ (\gamma-1)^{-1} & \text{for } v_2 < |\mathbf{v}|. \end{cases} \tag{6.4.18}$$

Figure 6.1 shows a typical graph of the probabilities p_T and p_D as functions of v.

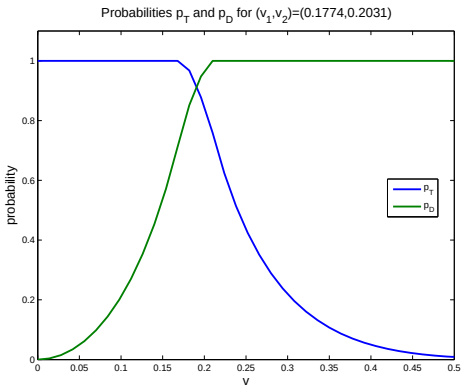

Figure 6.1: Probabilities p_T and p_D for thermalization and dethermalization as functions of $v = |\mathbf{v}|$, in which $v_1 = 0.1774$ and $v_2 = 0.2031$.

Note that the choice $c = 1$, along with (6.4.9) determines the mass of the Maxwellian component of m to be

$$n_m = n_M (T_m / T_M)^{3/2}. \tag{6.4.19}$$

In addition, the values of p_T for $|\mathbf{v}| < v_1$ and p_D for $v_2 < |\mathbf{v}|$ could be set to values $\bar{p}_T$ and $\bar{p}_D$ that are different than 1 and the formulas above could be modified to accommodate this change.

6.4.3 s-Based Method

In order to correctly incorporate the time step Δt into the hybrid method, we base the thermalization/dethermalization probabilities p_T and p_D on Nanbu's parameter s rather than $\mathbf{v}$. Choose values of s_1 and s_2 with $s_1 > s_2 > 0$. For each value of Δt, determine values of v_1 and v_2 so that $s(v_1, \Delta t) = s_1$ and $s(v_2, \Delta t) = s_2$. Then use the method in Section 6.4.2 with these values of v_1 and v_2.

The choice of p_T and p_D described above is somewhat arbitrary; optimizing this choice subject to the condition (6.4.12) (or some improvement on this condition, as in Appendix 6.7.2) could lead to an improved hybrid method.

6.5 Computational Results

6.5.1 Bump-on-Tail and Maxwellian Initial Data

As a test of the hybrid method, we performed a series of computations for initial data that is a bump-on-tail. As discussed in Section 6.1, this problem involves two widely separated time scales for Coulomb interactions, so that it is well suited for the hybrid method: a fast time scale for collisions between particles within the central Maxwellian and a slower time scale for those between particles from the central Maxwellian and the bump. We also performed computation for initial data that is Maxwellian, in order to test the consistency of the hybrid method.

The bump-on-tail initial distribution $f_0(\mathbf{v})$ is specified to be a combination of a Max-
wellian $M_0(\mathbf{v})$ and a bump $g_0(\mathbf{v})$. The bump is specified to be approximately a δ-function containing 10% of the mass of the distribution and centered at $\mathbf{v} = (v_b, 0, 0)$ with $v_b = a\sqrt{T_e/m_e}$. The Maxwellian M_0 is centered and scaled so that the average velocity is 0 and the temperature is T_e. The examples presented here are for two different choices of a: $a = 4$ in problem BOT4 and $a = 3$ in problem BOT3.

The computation is performed in a dimensionless formulation in which the electron mass is $m_e = 1$, and the electron density n_e and temperature T_e were chosen to be $n_e = 0.1$ and $T_e = 0.05065776$. For a characteristic time for the collision process, we use

$$\begin{aligned} t_c &= u_{th}^3 \left(\frac{q_e^2}{\epsilon_0 m_e/2} \right)^{-2} \left(\frac{n_e \log \Lambda_e/2}{4\pi} \right)^{-2} \\ u_{th} &= \sqrt{6T_e/m_e} \end{aligned} \tag{6.5.1}$$

which has value $t_c = 5.348275$. Unless otherwise state, the number of particles is $N = 128,000$.

Note that in all the simulation examples reported here, the plasma is spatially homogeneous so that there are no electromagnetic fields and no convection.

6.5.2 Consistency Tests

As a consistency test, we first performed computations for Maxwellian initial data $M(\mathbf{v})$, with density $n_e = 0.1$, temperature $T_e = 0.05065776$ and zero average velocity, as stated above.

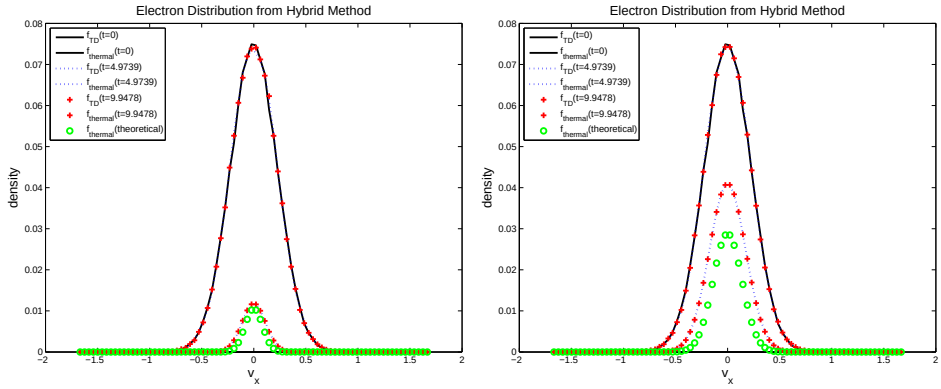

Figure 6.2: Comparison of the hybrid method for Maxwellian (equilibrium) initial data at three different times ($t = 0$, $t = 8.8t_c$, $t = 18.5t_c$). The plots show the full distribution function $f(v_x)$ (upper curves) and the thermal component $m(v_x)$ (lower curves), as well as the thermal component (circles) predicted from the theory of Section 6.4.1. The hybrid method parameters are $(s_1, s_2) = (2, 1)$ (left) and $(s_1, s_2) = (1, 0.5)$ (right).

Figure 6.2 shows the result of simulation using the hybrid method with this initial data for two different values of the hybrid parameters s_1 and s_2. The hybrid method parameters are $(s_1, s_2) = (2, 1)$ on the left and $(s_1, s_2) = (1, 0.5)$ on the right; the time step is $\Delta t = t_c/100$. The total distribution $f = m + k$ (upper curves) and the thermal component m (lower curves) of the distribution are shown as a function of the x-velocity v_x at three times $t = 0$, $t = 8.8t_c$, $t = 18.5t_c$. The initial data consists of all particles; i.e., $k = M$ and $m = 0$ for $t = 0$. The total distribution f is the same for all t, which is consistent with its Maxwellian initial data. Although it starts at 0, by time $t = 8.8t_c$ (i.e. after an initial transient), the thermal component m has reached a nonzero steady state which is the same as its value at $t = 18.5t_c$. This demonstrates the success of the detailed balance condition (6.4.12). Also shown is the thermal component $m_{theoretical}$ predicted from the choice $c = 1$ for which the density is given by (6.4.9). Although the theoretical prediction is correct for the hybrid simulation on the left, it is incorrect for the simulation on the right. A better theory (better than that of Section 6.4.1) could help to improve the formulation of the hybrid method.

Next we perform a comparison of the s-based and v-based hybrid methods on the bump-on-tail problem BOT4. Set $(s_1, s_2) = (3, 2)$ and $\Delta t = t_c/10$. The corre-

sponding values of v_1 and v_2, satisfying $s = 2\tau$ from (6.2.10) with $\tau = \tau(v, \Delta t)$ defined by (6.2.5), are $(v_1, v_2) = (0.1774, 0.2031)$. The top row of graphs in Figure 6.3 shows the results for the v-based method (upper left) and the s-based method (upper right) with these parameters. Each graph shows a comparison of results from the hybrid (blue dashed line) and Nanbu (red solid line) methods at time at time $t = 1.3t_c$. These graphs are identical (and show good agreement between the hybrid and Nanbu methods) since the values of (v_1, v_2) were chosen to be in agreement with the values of (s_1, s_2).

Now keep the same values of (v_1, v_2) and (s_1, s_2), but change the time step to $\Delta t = t_c/1000$. The results (on the lower graphs of Figure 6.3) show that the accuracy of the v-based method (lower left) deteriorates as the time step is decreased; whereas the accuracy of the s-based method (lower right) improves. In addition, the thermal component (green dotted line) for the s-based method decreases with smaller time step, so that the efficiency of the s-based method decreases. This gain in accuracy but loss of efficiency for the s-based method is acceptable dependence on Δt; while the loss of accuracy with decreased Δt for the v-based method is not acceptable.

The reason for this dependence on time step is easily understood. For the v-based method, the probability of thermalization is independent of the time step Δt, so that for small Δt the thermalization is too strong. On the other hand, for the s-based method, the thermalization per time step decreases as Δt decreases, and the function $s(\Delta t)$ has the correct dependence on Δt, as well as on density and temperature.

6.5.3 Simulation for the Evolution of a Bump-on-Tail

Figures 6.4 and 6.5 show a comparison of the solutions computed by the hybrid (blue dashed line) and Nanbu (red solid line) methods for bump-on-tail problems BOT4 and BOT3, respectively, at various times between the initial time and a final time $T = 7.2t_c$. For the hybrid method the parameters are $(s_1, s_2) = (3, 2)$ and $\Delta t = t_c/10$. The thermal component of the hybrid representation (6.3.1) (green dotted line) is also plotted. Both figures show very agreement between the hybrid and Nanbu curves, providing a measure of validation for the hybrid method.

For problem BOT4 in Figure 6.4 the parameters are $\Delta t = t_c/10$ and $(s_1, s_2) = (3, 2)$. The thermal component of the hybrid representation (6.3.1), which contains about $1/3$ of the particles.

For problem BOT3 in Figure 6.5 the parameters are $\Delta t = t_c/100$ and $(s_1, s_2) = (1, 0.5)$. In this problem, the thermal component of the hybrid representation con-

tains about $1/7$ of the particles.

6.5.4 Variation of Parameters Δt, s_1 and s_2

In order to understand the effect of the parameters Δt, s_1 and s_2 on the solution of the hybrid method, we performed computation for the bump-on-tail problem BOT4 of Figure 6.4 with different parameter values. Figures 6.6 and 6.7 show the solution of BOT4 at $t = 1.2t_c$ and $t = 3.6t_c$, respectively. In each figure, the time step is $\Delta t = t_c/10$ for the graphs in the left column and $\Delta t = t_c/100$ for those in the right column. Also, the values of (s_1, s_2) are $(s_1, s_2) = (1, 0.5)$ for the graphs in top row, $(s_1, s_2) = (2, 1)$ for the middle row and $(s_1, s_2) = (3, 2)$ for the bottom row.

A scatter plot of these values of γ_{eff} and γ_{acc} in the graph on the left in Figure 6.9. This graph shows that these values collapse onto a single curve, so that γ_{acc} is a single-valued function of γ_{eff}. This shows that for any level of accuracy there is a resulting level of efficiency. Further variation of the parameters (s_1, s_2) does not change performance of the method. This conclusion holds only within the context of specific choice of p_D and p_T. The relationship between accuracy and efficiency could be changed by considering a wider class of functions p_D and p_T. In the graph on the left in Figure 6.9, the values of accuracy γ_{acc} appear to taper off to a finite nonzero value.

The graph on the right in Figure 6.9 shows that statistical fluctuations due to the finite value N of particles contribute importantly to this residual error. There may be an additional significant contribution to the total error due to finite Δt effects. This graph shows a plot of γ_{acc} versus γ_{eff} for three values of N: $N = 32,000$, $N = 128,000$ and $N = 512,000$. The values of (s_1, s_2) are $4 < s_2 < 6.2$ and $s_1 = s_2 + 2$, which are larger than those in Figure 6.8 and the graph on the left of Figure 6.9.

Comparison of the results for $N = 32,000$, $N = 128,000$ and $N = 512,000$ in this graph shows the errors γ_{acc} are smaller for larger values of N. More specifically, for larger values of N, the linear decrease of γ_{acc} continues for smaller values of γ_{eff}, and the remaining residual value of γ_{acc} is smaller.

6.6 Conclusions

The hybrid method developed above combines continuum and particle descriptions for the evolution of a velocity distribution function through Coulomb inter-

In Figure 6.6 at an early time, the bump is still distinct but is shifted and diffused from its original position and shape. In Figure 6.7 at a later time, the bump is no longer a distinct peak but has been reduced to a shelf in the distribution function. Comparison of the figures shows that for larger Δt or smaller s_1 and s_2 the bump is overthermalized, with the result that it is shifted too far toward the center and becomes too wide. As Δt is decreased and s_1 and s_2 are increased, the accuracy of the computation dramatically improves.

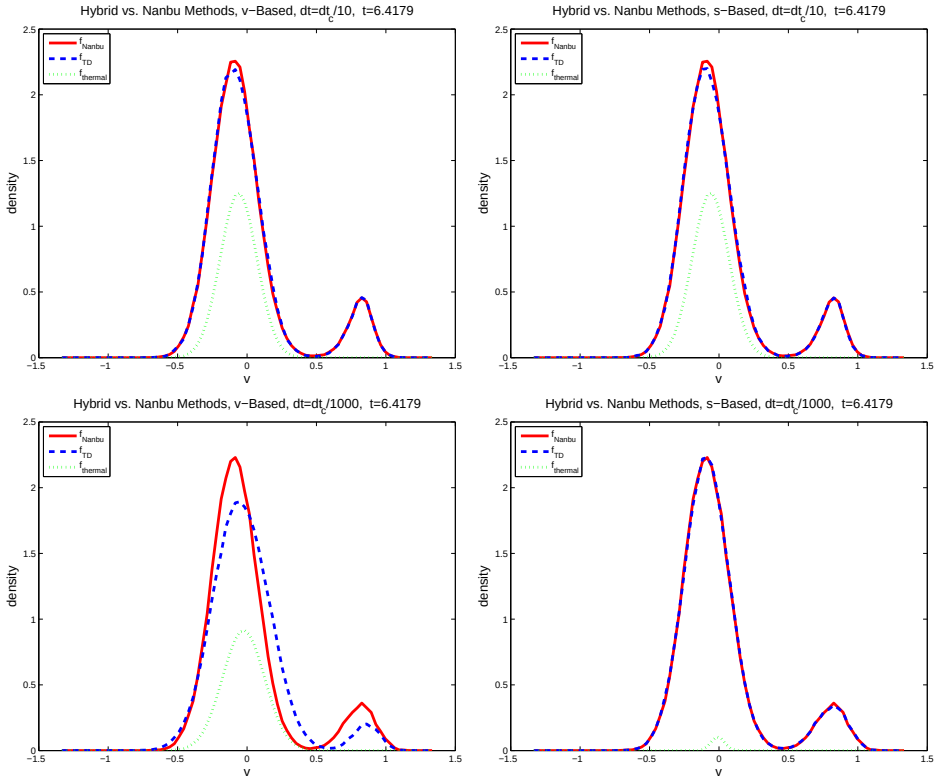

Figure 6.3: Comparison of the v-based and s-based versions of the hybrid method for different time steps Δt. The plots show the velocity distribution function from the hybrid (blue dashed line) and Nanbu (red solid line) method, as well as the thermal component for the hybrid method (green dotted line), for problem BOT4 at time $t = 1.3t_c$. The time step is $\Delta t = t_c/10$ for the top row and $\Delta t = t_c/1000$ for the bottom row. The left column comes from the v-based method with $(v_1, v_2) = (0.1774, 0.2031)$, while the right column comes from the s-based method with $(s_1, s_2) = (3, 2)$.

On the other hand, the size of the thermal component, which determines the efficiency of the hybrid method, is larger for larger values of Δt and smaller values of s_1 and s_2. This shows a trade-off between efficiency and accuracy of the hybrid method.

6.5.5 Accuracy and Efficiency for the Hybrid Method

In order to measure the performance of the hybrid method, we first define quantities γ_{eff} and γ_{acc} that measure the efficiency and accuracy of the computations, as

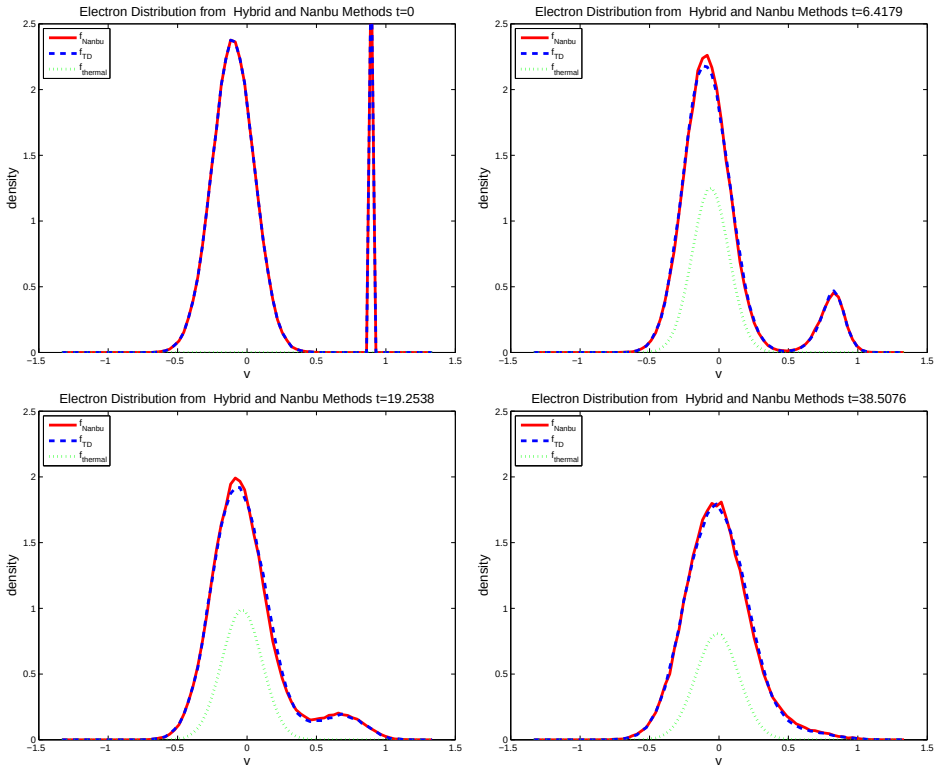

Figure 6.4: Comparison of the hybrid (blue dashed line) and Nanbu (red solid line) solutions at different times $t = 0$ (upper left), $t = 1.2t_c$ (upper right), $t = 3.6t_c$ (lower left) and $t = 7.2t_c$ (lower right). The computations use $\Delta t = t_c/10$ and $(s_1, s_2) = (3, 2)$ for the problem BOT4.

$$\gamma_{eff} = \frac{1}{Tn_f}\int_0^T n_m dt \tag{6.5.2}$$

$$\gamma_{acc} = \frac{1}{Tn_f}\int\int_0^T |f - f_H| dt dv. \tag{6.5.3}$$

Efficiency of the method is meant to be the ratio between the computational savings of the hybrid method and the computational cost of the standard method. Since the computational effort is roughly proportional to the number of particles in the simulation, the efficiency measure γ_{eff} is the ratio of n_m and n_f in which n_m and n_f are the number of particles in the Maxwellian component m and the total number of particles in f.

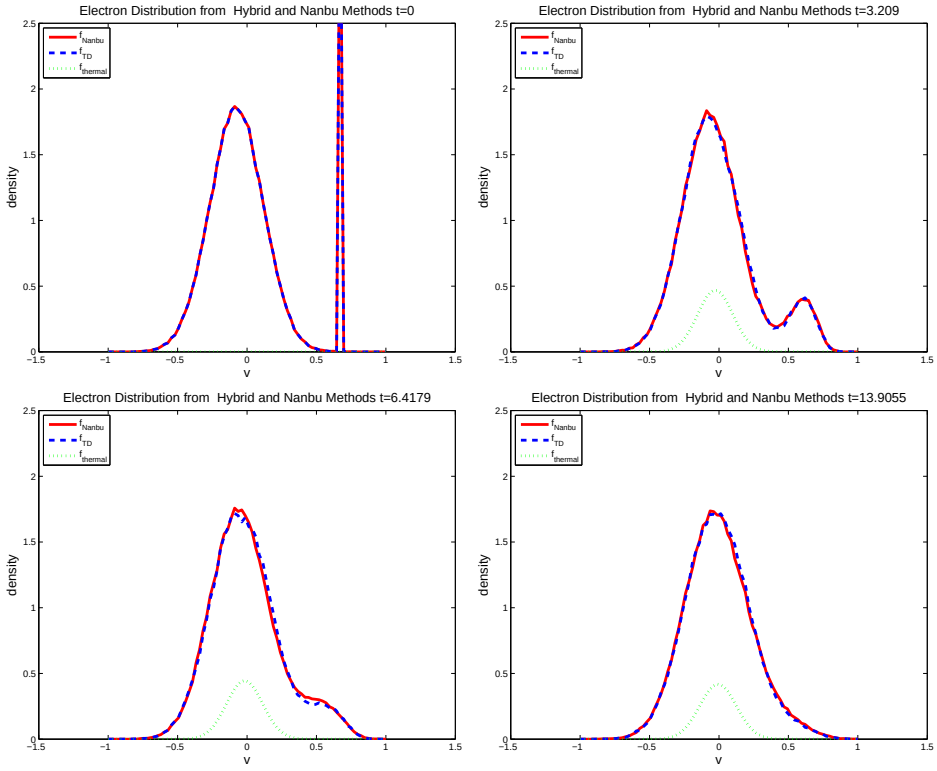

Figure 6.5: Comparison of the hybrid (blue dashed line) and Nanbu (red solid line) solutions at different times $t = 0$ (upper left), $t = 0.6t_c$ (upper right), $t = 1.2t_c$ (lower left) and $t = 2.6t_c$ (lower right). The computations use $\Delta t = t_c/100$ and $(s_1, s_2) = (1, 0.5)$ for the problem BOT3.

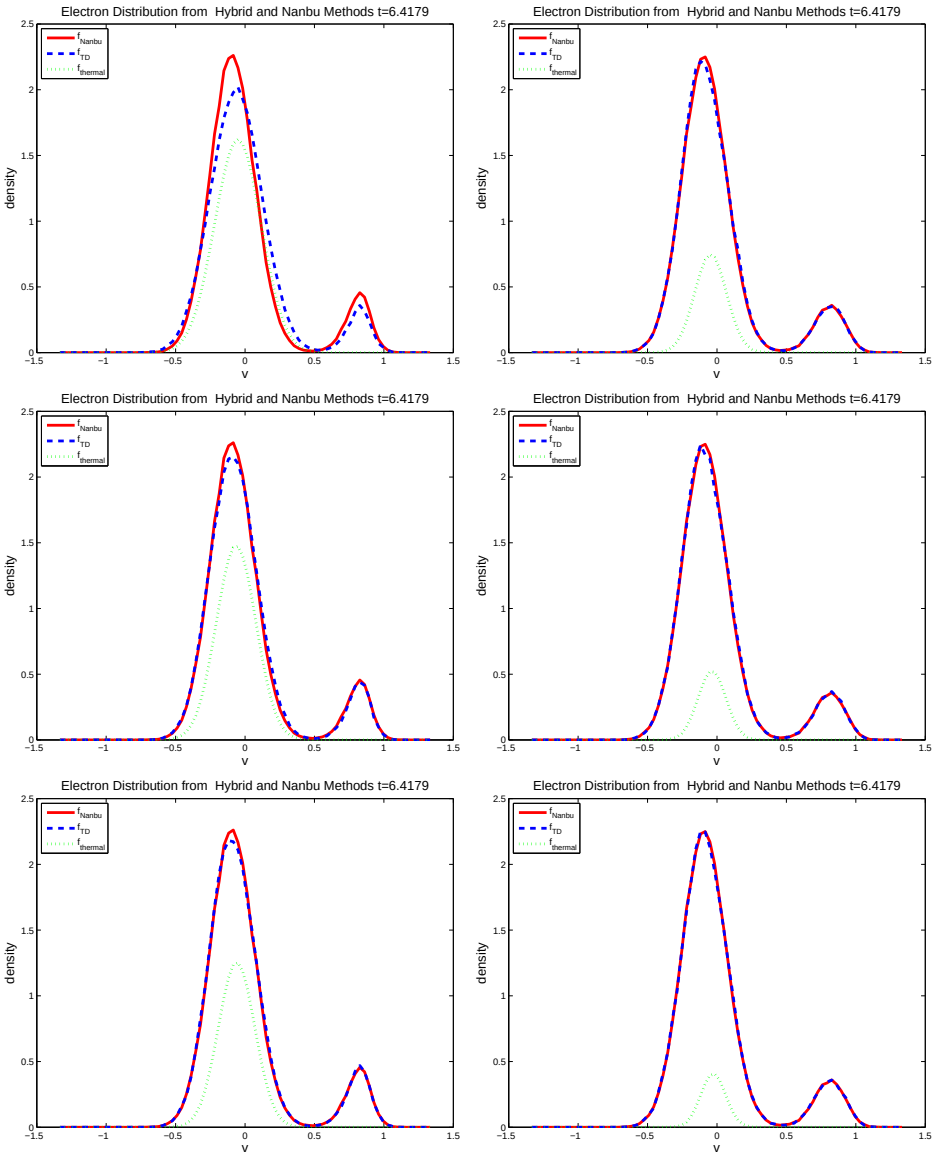

Figure 6.6: Comparison of the hybrid (blue dashed line) and Nanbu (red solid line) solutions for different values of the parameters Δt, s_1 and s_2. The values of Δt are $t_c/10$ for the left column and $t_c/100$ for the right column. The values of (s_1, s_2) are $(1, 0.5)$ for the top row, $(2, 1)$ for the middle row and $(3, 2)$ for the bottom row. These simulations are for problem BOT4 of Figure 6.4 at time $t = 1.2t_c$.

As a measure of accuracy, γ_{acc} is the relative size of L^1 norm (in v and t) of the error. We performed a series of computations for parameters in the range $0.2 \leq s_2 \leq 2$ and $0.2 \leq s_1 - s_2 \leq 2$, and for time step $\Delta t = t_c/10$ and final time $T = 74t_c$. The resulting values of γ_{eff} and γ_{acc} are presented in contour plots in Figure 6.8, which shows them to be constant along (nearly) linear curves in the (s_1, s_2) plane.

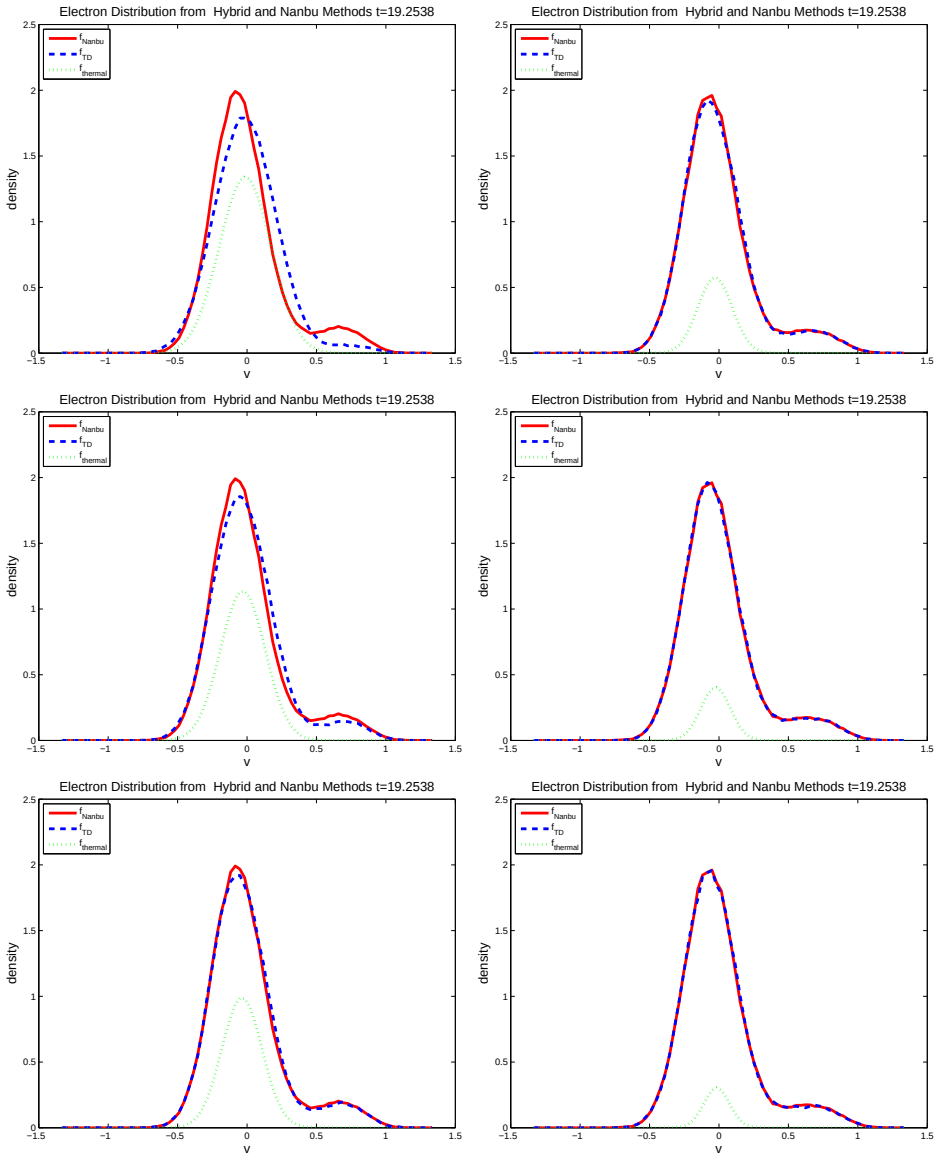

Figure 6.7: Same as Figure 6.6 but at later time $t = 3.6t_c$.

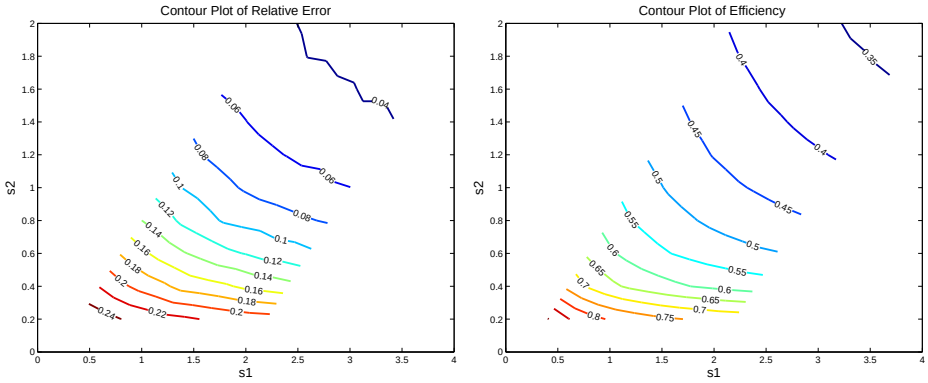

Figure 6.8: Error (left) and Efficiency (right) for the hybrid method applied to the problem BOT4 of Figure 6.4, as functions of the parameters s_1 and s_2.

actions. The method includes particle interactions, but since the examples here are spatially homogeneous, the continuum description is just an equilibrium Maxwellian distribution.

Because of the variation of the interaction rate as a function of particle velocity, the division of f between particles and continuum must be performed as a function of velocity. In the hybrid method of this paper, the velocity dependence is effected through velocity dependence of the thermalization and dethermalization probabilities $p_T(v)$ and $p_D(v)$.

The specific choice of $p_T(v)$ and $p_D(v)$ is ad hoc and formulated in terms of two parameters s_1 and s_2 (or v_1 and v_2) as well as Δt. The simulations show that for this method the efficiency is a single-valued function of the accuracy of the method. Therefore the method provides a certain level of efficiency (acceleration) for prescribed accuracy of the hybrid approximation.

Further development of the hybrid method could include development of alternative formulations and optimization of $p_T(v)$ and $p_D(v)$, modification of the method so that that the distribution is completely thermalized as $t \to \infty$ (i.e., $m \to M$ and $k \to 0$), development of a mathematical foundation for this method, and improved analysis of the detailed balance properties of the method. Applications of the method will be carried out for spatially inhomogeneous problems, especially those having the character of a bump-on-tail.

Acknowledgements. This work performed under the auspices of the U.S. Department of Energy by the University of California, Los Angeles, under grant DE-FG02-05ER25710, and by Lawrence Livermore National Laboratory under

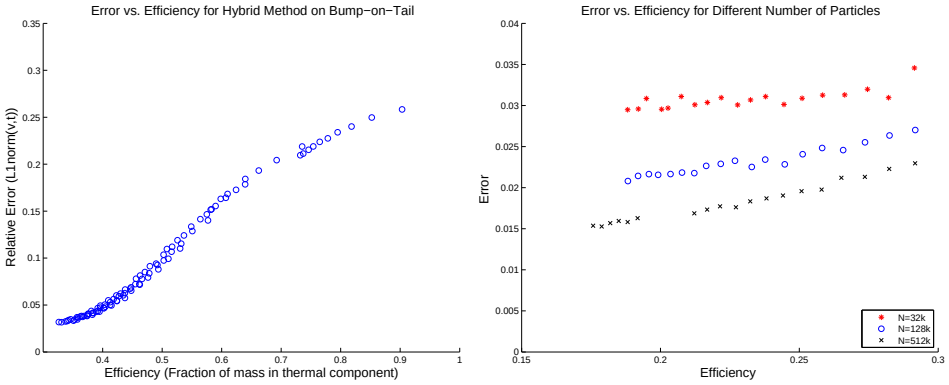

Figure 6.9: Error vs. efficiency for the bump-on-tail problem of Figure 6.4. The graph on the left is a scatter plot of the values of error and efficiency from Figure 6.8. The graph at right shows a continuation of error and efficiency for larger values of s_1 and s_2 and for values of N given by $32,000$ (stars), $128,000$ (circles) and $512,000$ (x's).

Contract DE-AC52-07NA27344. The work was supported by the Office of Advanced Scientific Computing Research, DOE Office of Science, under the Multiscale Initiative program.

6.7 appendix

6.7.1 Analysis of the Scattering Kernel D for the Takizuka & Abe Method

The convergence criteria from Bobylev and Nanbu (equations (48a)-(48c) in [9]) are that

$$D(\mu,\tau) \geq 0 \tag{6.7.1}$$

$$2\pi \int_{-1}^{1} d\mu D(\mu,\tau) = 1 \tag{6.7.2}$$

$$\lim_{\tau\to 0} D(\mu,\tau) = (2\pi)^{-1}\delta(1-\mu) \tag{6.7.3}$$

$$\lim_{\tau\to 0}(2\pi/\tau)\int_{-1}^{1} d\mu D(\mu,\tau)[1-P_\ell(\mu)] = \ell(\ell+1) \tag{6.7.4}$$

in which P_ℓ is the Legendre polynomial for positive integers ℓ.

As written in (6.2.4), the kernel for the TA method is

$$D_{TA}(\mu,\tau) = (2\pi)^{-1}(2\pi\tau)^{-1/2}e^{-\zeta^2/2\tau}(d\zeta/d\mu). \tag{6.7.5}$$

The analysis of this kernel is similar to the analysis of the kernel for the Nanbu method presented in [9]. Conditions (6.7.1)-(6.7.3) are easily verified.

To verify (6.7.4), use $\mu = \cos\theta$ and $\zeta = \tan(\theta/2)$ to calculate for small τ

$$\begin{aligned}
\frac{2\pi}{\tau}\int_{-1}^{1} d\mu D_{TA}(\mu,\tau)[1-P_\ell(\mu)] &= \frac{1}{\tau}\int_0^\infty \frac{e^{-\zeta^2/2\tau}}{(2\pi\tau)^{1/2}}[1-P_\ell(\cos(2\arctan\zeta))]d\zeta \\
&= \frac{1}{\tau}\int_0^\infty \frac{e^{-\xi^2/2}}{(2\pi)^{1/2}}[1-P_\ell(\cos(2\arctan\sqrt{\tau}\xi))]d\xi \\
&\approx \frac{1}{\tau(2\pi)^{1/2}}\int_0^\infty \frac{e^{-\xi^2/2}}{(2\pi)^{1/2}}\tau\xi^2\ell(\ell+1)d\xi \\
&\approx \ell(\ell+1).
\end{aligned} \tag{6.7.6}$$

These calculations use the expansion $P_\ell(\cos(2\arctan\sqrt{\tau}\xi)) \approx 1 - 2\tau\xi^2 P'_\ell(1)$ for small τ and $P'_\ell(1) = \ell(\ell+1)$.

6.7.2 Detailed Balance for Binary Collisions with Thermalization/Dethermalization

For collisions between particles of a single species, omit the subscripts α and β in (6.2.3) to obtain

$$f(\mathbf{v}) = \int_{R^3\times S^2} d\mathbf{w}d\mathbf{n}D(\frac{\mathbf{g}\cdot\mathbf{n}}{g}, \Lambda\frac{\Delta t}{g^3})f(\mathbf{v}',t)f(\mathbf{w}',t). \tag{6.7.7}$$

Using the requirement [9] that $\int_{S^2} d\mathbf{n}D = 1$ equation (6.7.7) can be written as the following equation for the change Δf in time Δt

$$\Delta f(\mathbf{v}) = \int_{R^3\times S^2} d\mathbf{w}d\mathbf{n}D(\frac{\mathbf{g}\cdot\mathbf{n}}{g}, \Lambda\frac{\Delta t}{g^3})\left\{f(\mathbf{v}',t)f(\mathbf{w}',t) - f(\mathbf{v},t)f(\mathbf{w},t)\right\} \tag{6.7.8}$$

which will be used in the formulation of detailed balance conditions.

The equation (6.7.7) can be rewritten to include thermalization and dethermalization. Since it is an equation for $f(\mathbf{v})$, the thermalization/dethermalization

is only applied to the terms $f(\mathbf{v})$ and $f(\mathbf{v}')$ inside the integral. Using the representation $f = m + k$, the integral on the right side of (6.2.3) becomes

$$\int_{R^3\times S^2} d\mathbf{w}d\mathbf{n}D\left\{\left[m(\mathbf{v}^{'})m(\mathbf{w}^{'}) + (1-p_D)m(\mathbf{v}^{'})k(\mathbf{w}^{'}) + p_T k(\mathbf{v}^{'})f(\mathbf{w}^{'})\right]\right.$$
$$\left. + \left[p_D m(\mathbf{v}^{'})k(\mathbf{w}^{'}) + (1-p_T)k(\mathbf{v}^{'})f(\mathbf{w}^{'})\right]\right\} \quad (6.7.9)$$

in which

$$D = D(\frac{\mathbf{g}\cdot\mathbf{n}}{g}, \Lambda\frac{\Delta t}{g^3}). \quad (6.7.10)$$

Note that dethermalization is not applied to the term $m(\mathbf{v}^{'})m(\mathbf{w}^{'})$. In the integral (6.7.9) and in all of the formulas below p_D and p_T are evaluated at $\mathbf{v}$, since the thermalization/dethermalization is applied after the collision. The terms in the first set of square brackets are the terms that contribute to the thermal component; while those in the second set of square brackets are the terms that contribute to the kinetic component. The contributions to the thermal component are projected onto a Maxwellian, so that

$$m(\mathbf{v}, t+\Delta t) = \Pi_M \int_{R^3\times S^2} d\mathbf{w}d\mathbf{n}D\left[m(\mathbf{v}^{'})m(\mathbf{w}^{'}) + (1-p_D)m(\mathbf{v}^{'})k(\mathbf{w}^{'})\right.$$
$$\left. + p_T k(\mathbf{v}^{'})f(\mathbf{w}^{'})\right] \quad (6.7.11)$$

$$k(\mathbf{v}, t+\Delta t) = \int_{R^3\times S^2} d\mathbf{w}d\mathbf{n}D\left[p_D m(\mathbf{v}^{'})k(\mathbf{w}^{'}) + (1-p_T)k(\mathbf{v}^{'})f(\mathbf{w}^{'})\right] \quad (6.7.12)$$

The projection in (6.7.11) is equivalent to the following equations for n_m, $\mathbf{u}_m$ and T_m

$$(n_m, n_m\mathbf{u}_m, n_m T_m)(t+\Delta t) = \int_{R^3\times R^3\times S^2} d\mathbf{v}d\mathbf{w}d\mathbf{n}D\left(1, \mathbf{v}', |\mathbf{v}'-\mathbf{u}_m|^2/2\right)$$
$$\left[m(\mathbf{v}^{'})m(\mathbf{w}^{'}) + (1-p_D)m(\mathbf{v}^{'})k(\mathbf{w}^{'}) + p_T k(\mathbf{v}^{'})f(\mathbf{w}^{'})\right] \quad (6.7.13)$$

As in equation (6.7.8), these can be rewritten as equations for the change in k and in n_m, $\mathbf{u}_m$ and T_m; i.e.,

$$\begin{aligned}
&(\Delta n_m, \Delta(n_m\mathbf{u}_m),\ \Delta(n_m T_m)) \\
&= \int_{R^3\times R^3\times S^2} d\mathbf{v}d\mathbf{w}d\mathbf{n}D\left\{\left(1, \mathbf{v}', |\mathbf{v}'-\mathbf{u}_m|^2/2\right)\left[m(\mathbf{v}^{'})m(\mathbf{w}^{'}) + \right.\right. \\
&\left.(1-p_D)m(\mathbf{v}^{'})k(\mathbf{w}^{'}) + p_T k(\mathbf{v}^{'})f(\mathbf{w}^{'})\right] \\
&\left. - \left(1, \mathbf{v}, |\mathbf{v}-\mathbf{u}_m|^2/2\right)m(\mathbf{v})f(\mathbf{w})\right\} \quad (6.7.14)
\end{aligned}$$

$$\Delta k(\mathbf{v}) = \int_{R^3 \times S^2} d\mathbf{w} d\mathbf{n} D\{p_D m(\mathbf{v}^{'}) k(\mathbf{w}^{'}) + (1 - p_T) k(\mathbf{v}^{'}) f(\mathbf{w}^{'}) - k(\mathbf{v}) f(\mathbf{w})\}. \quad (6.7.15)$$

The detailed balance condition says that in equilibrium ($f = m + k = M$), each process and the reverse process exactly cancel. For equations (6.7.14) and (6.7.15), this says that

$$\begin{aligned} 0 &= \left(1, \mathbf{v}', |\mathbf{v}'|^2\right) \left[m(\mathbf{v}^{'}) m(\mathbf{w}^{'}) + (1 - p_D) m(\mathbf{v}^{'}) k(\mathbf{w}^{'}) + p_T k(\mathbf{v}^{'}) f(\mathbf{w}^{'})\right] \\ &- \left(1, \mathbf{v}, |\mathbf{v}|^2\right) m(\mathbf{v}) f(\mathbf{w}) \quad (6.7.16) \\ 0 &= \left[p_D m(\mathbf{v}^{'}) k(\mathbf{w}^{'}) + (1 - p_T) k(\mathbf{v}^{'}) f(\mathbf{w}^{'})\right] - k(\mathbf{v}) f(\mathbf{w}) \quad (6.7.17) \end{aligned}$$

so that the thermalization and dethermalization conserve particle number, momentum, and kinetic energy. Although these conditions are not used in the hybrid method formulated above, they may be useful for improving the current hybrid method.

Appendix A

A remark on the finite number of particles effect in Monte Carlo methods for kinetic equations

This Appendix is based on the work [47] published in **Submitted to Proceedings of the 6th International Congress on Industrial and Applied Mathematics** in collaboration with Prof. Lorenzo Pareschi and Dott. Piero Foscari of the Department of Mathematics and Center for Modeling Computing and Statistics (CMCS) of University of Ferrara.

A.1 Introduction

The numerical solution of kinetic equations is usually performed through statistical simulation methods such as Monte Carlo [28]. The reason for this is twofold, on the one hand probabilistic techniques provide an efficient toolbox for the simulation due to the reduced computational cost when compared with deterministic schemes, on the other hand the evolution of the statistical samples follows the microscopic binary interaction dynamics thus providing all the relevant physical properties of the system. Traditionally the methods are considered extremely efficient when dealing with stationary problems. In such case, in fact, fluctuations can be eliminated by taking subsequent averages of the solution after then a certain "stationary time" has been reached. Here we show, with the help of a simple one-dimensional system, that this averaging procedure does not guarantee convergence towards the correct steady state due to finite number of particles correlations

introduced by the microscopic conservation laws. Similar analysis for rarefied gas dynamics have been done in [115, 102].

A.1.1 The model equation

We will consider a simple one–dimensional kinetic model, where the binary interaction between particles obey to the law

$$v' = v\cos\theta - w\sin\theta, \qquad w' = v\sin\theta + w\cos\theta, \tag{A.1.1}$$

where $\theta \in [-\pi, \pi]$ is a collision parameter. The microscopic energy after the binary interaction rule is conserved

$$(v')^2 + (w')^2 = v^2 + w^2, \tag{A.1.2}$$

whereas momentum is not.

Let $f(v,t)$ denote the distribution of particles with velocity $v \in \mathbb{R}$ at time $t \geq 0$. The kinetic model can be easily derived by standard methods of kinetic theory, considering that the change in time of $f(v,t)$ depends on a balance between the gain and loss of particles with velocity v due to binary collisions. This leads to the following integro-differential equation of Boltzmann type [68],

$$\frac{\partial f}{\partial t} = \int_{\mathbb{R}}\int_{-\pi}^{\pi} \frac{1}{2\pi}\left(f(v')f(w') - f(v)f(w)\right) d\theta\, dw. \tag{A.1.3}$$

As a consequence of the binary interaction the second momentum of the solution is conserved in time, whereas the first momentum is preserved only if initially it is equal to zero. For this model one can show that the stationary solution $f_\infty(v)$ is the Maxwell density

$$f_\infty(v) = \frac{1}{\sqrt{2\pi}} e^{-v^2/2}. \tag{A.1.4}$$

A standard Monte Carlo method for this equation can be easily derived using either Bird's or Nanbu's algorithm for Maxwell molecules [7, 89]. The two algorithms differ mainly in the way the time discretization is treated, but not in the way collisions (sampling from the collision integral operator) are performed. Our results do not differ for the two methods.

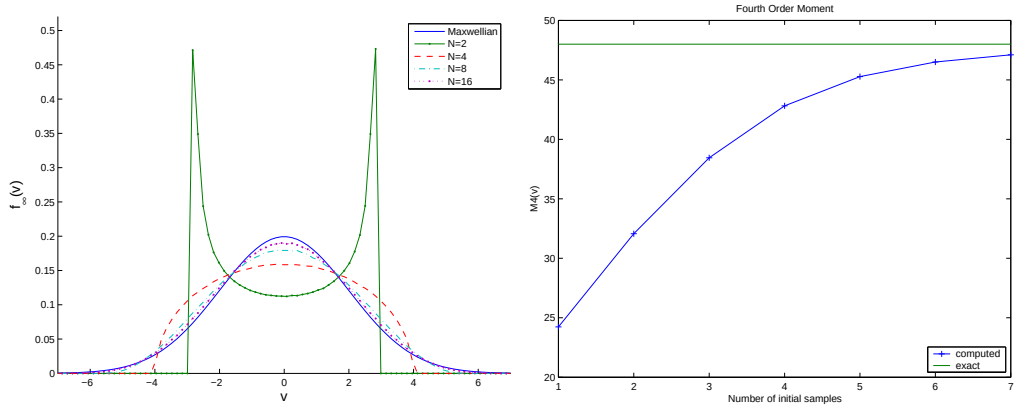

Figure A.1: Equilibrium states for different finite sets of particles vs Maxwellian (left) and equilibrium value of the fourth order moment for the different finite sets of particles.

A.2 Numerical results

The problem we consider here is related to the effect of the finite number of particles in Monte Carlo simulations. Note that given a set of particles $v_1, v_2, \ldots, v_N$ with energy $E = \frac{1}{2}\sum_{i=1}^{N} v_i^2$, we have the inequality

$$|v_i| \leq R_N = \sqrt{2EN}. \tag{A.2.1}$$

As a consequence of this, any particle dynamic, namely any transformation of the type

$$v_i' = \phi_i(v_1, \ldots, v_N), \quad i = 1, \ldots, N, \tag{A.2.2}$$

that preserves exactly energy is such that the particle solution remains compactly supported in $[-R_N, R_N]$ at any time. This implies that the distribution of such particles cannot be Maxwellian (or any other non compactly supported statistics) unless the particles number goes to infinity. This is exactly what happens if we use the so-called Nanbu-Babovsky [3] strategy of performing collisions by pairs so that the Monte Carlo methods are exactly conservative and not conservative in the mean. We report in Figure 1 (left) the numerical distribution of the finite sets of particles in the case of the one-dimensional Maxwell model (A.1.3). The results have been obtained taking initially Maxwellian samples with zero mean and energy 4 and then averaging in time over the Monte Carlo solutions to the equation.

For very small numbers of particles it is remarkable that the computed distribution differ considerably from the expected Maxwellian. The different fourth order moments of the corresponding steady solutions are then plotted in Figure 1 (right) against the exact fourth order moment of the Maxwellian. We point out that such small particle numbers can be present is some cells when one consider fully non homogeneous rarefied gas flow simulations and thus, even if the transport part can affect the nature of these correlations, a particular care has to be taken when averaging over such small numbers. Similar conclusion are valid also for different kinetic models where the steady state statistics is not compactly supported like in granular gases, plasma physics, quantum kinetic theory, traffic flows and economic models.

Bibliography

[1] K. AOKI, Y. SONE, AND T. YAMADA, *Numerical analysis of gas ows condensing on its plane condensed phase on the basis of kinetic theory*, Physics of Fluids A, vol. 2 (1990), pp. 1867–1878.

[2] O. AKTAS, AND N.R. ALURU, *A combined continuum/DSMC technique for multiscale analysis of microfluidic filters*. J. Comp. Phys., vol.178, (2002) pp. 342–72.

[3] H. BABOVSKY, *On a simulation scheme for the Boltzmann equation*, Math. Methods Appl. Sci., 8 (1986), pp. 223–233.

[4] L. L. L. BAKER, N. G. HADJICONSTANTINOU, *Variance Reduction for Monte Carlo solutions of the Boltzmann equation*, Physics of Fluids, 17 (2005)

[5] H. BABOVSKY AND R. ILLNER, *A convergence proof for Nanbu's simulation method for the full Boltzmann equation*, SIAM J. Numer. Anal., 26 (1989), pp. 45–65.

[6] N. BELLOMO AND A.BELLOUQUID, *From a class of kinetic models to the macroscopic equations for multicellular systems in biology.* Mathematical models in cancer (Nashville, TN, 2002). Discrete Contin. Dyn. Syst. Ser. B 4 (2004), pp. 5980

[7] G. A. BIRD, *Molecular gas dynamics and direct simulation of gas flows*, Clarendon Press, Oxford (1994).

[8] J. A. BITTENCOURT *Fundamentals of plasma physics*, Springer (2004).

[9] A. V. BOBYLEV AND K. NANBU *Theory of collision algorithms for gases and plasmas based on the Boltzmann equation and the Landau-Fokker-Planck equation*, Physical Review E, Vol. 61 $N^{\circ}4$ (2000).

[10] J. F. BOURGAT, P. LETALLEC, B. PERTHAME, AND Y. QIU, *Coupling Boltzmann and Euler equations without overlapping*, in Domain Decomposition Methods in Science and Engineering, Contemp. Math. 157, AMS, Providence, RI, (1994), pp. 377–398.

[11] J. F. BOURGAT, P. LETALLEC, M.D. TIDRIRI, *Coupling Boltzmann and Navier-Stokes equations by friction*. J. Comput. Phys. 127, 2, (1996), pag. 227–245.

[12] M. BRIANI, R. NATALINI, G. RUSSO, *Implicit-Explicit Numerical Schemes for Jump-Diffusion Processes,* IAC Report N.38 (4/2004).

[13] J.E. BROADWELL, *Shock structure in a simple discrete velocity gas,* Phys. Fluids, 7 (1964), pp. 1013–1037.

[14] R. E. CAFLISCH, G. DIMARCO, L. PARESCHI, *Direct Simulation Monte Carlo schemes for Coulomb Interactions,* Preprint 2008.

[15] R. E. CAFLISCH, C. WANG, G. DIMARCO, B. COHEN, A. DIMITS, *A Hybrid Method for Accelerated Simulation of Coulomb Collisions in a Plasma*, Accepted with minor revisions in SIAM Multiscale Modeling and Simulation.

[16] R. E. CAFLISCH AND L. PARESCHI, *Implicit Monte Carlo methods for rarefied gas dynamics I: The space homogeneous case*, J. Comput. Phys., 154 (1999), pp. 90–116.

[17] R. E. CAFLISCH AND L. PARESCHI, *Towards a hybrid method for rarefied gas dynamics*, IMA Vol. App. Math. 135, (2004), pp. 57–73.

[18] R. E. CAFLISCH, *Monte Carlo and Quasi-Monte Carlo Methods*, Acta Numerica (1998) pp. 1–49.

[19] R. E. CAFLISCH, H. CHEN, E. LUO AND L. PARESCHI, *A hybrid method that interpolates between DSMC and CFD*, AIAA Proceedings (submitted).

[20] R. E. CAFLISCH, *The fluid dynamical limit of the nonlinear Boltzmann equation,* Commun. Pure Appl. Math., 33, (1980) pp. 651-666.

[21] R. E. CAFLISCH, S. JIN, AND G. RUSSO, *Uniformly accurate schemes for hyperbolic systems with relaxation*, SIAM J. Numer. Anal., 34 (1997), pp. 246–281.

[22] CALHOUN AND R. J. LEVEQUE, *An accuracy study of mesh refinement on mapped grids*, Proceedings of the Chicago Workshop on Adaptive Mesh Refinement Methods, Lecture Notes in Computational Science and Engineering, Vol. 41 (2003) pp. 91-102.

[23] E. A. CARLEN, M. C. CARVALHO, AND E. GABETTA, *Central limit theorem for Maxwellian molecules and truncation of the Wild expansion*, Comm. Pure Appl. Math., 53 (2000), pp. 370–397.

[24] E. A. CARLEN, F. SALVARANI, *On the optimal choice of coefficients in a truncated Wild sum and approximate solutions for the Kac equation*, J. Statist. Phys. 109 (2002), no. 1-2, pp. 261–277.

[25] CCERES, M. J.; CARRILLO, J. A.; GAMBA, I. M.; MAJORANA, A.; SHU, C.-W., *Deterministic kinetic solvers for charged particle transport in semiconductor devices.*, Transport phenomena and kinetic theory, 151–171, Model. Simul. Sci. Eng. Technol., Birkhuser Boston, Boston, MA, 2007.

[26] C. CERCIGNANI, *The Boltzmann Equation and Its Applications*, Springer-Verlag, New York, (1988).

[27] C. CERCIGNANI, R. ILLNER, M. PULVIRENTI, *The mathematical theory of dilute gases*. Springer-Verlag, New York, (1995).

[28] C. Cercignani, *Rarefied Gas Dynamics: From Basic Concepts to Actual Calculations*, Cambridge Texts in Applied Mathematics, Cambridge University Press, Cambridge (2000).

[29] F. CHALUB, P.A. MARKOWICH, B. PERTHAME, C. SCHMEISER, *Kinetic models for chemotaxis and their drift-diffusion limits* Monatsh. Math. 142 (2004), pp. 123–141.

[30] G. Q. CHEN, D. LEVERMORE AND T. P. LIU, *Hyperbolic conservation laws with stiff relaxation terms and entropy*, Comm. Pure Appl. Math., vol. 47 (1994), pp. 787–830.

[31] P. COLELLA, A. MAJDA, V. ROYTBURD *Theoretical and Numerical structures for reacting shock waves*. SIAM J. Sci. Stat. Comp., 7, (1986), pp. 1059–1080.

[32] S.CORDIER, L.PARESCHI AND G.TOSCANI, *On a kinetic model for a simple market economy*, J. Stat. Phys. (to appear).

[33] F. CORON, B. PERTHAME *Numerical passage from kinetic to fluid equations*. SIAM J. Numer. Anal., 28, (1991), pp. 26–42.

[34] F. CORON AND B. PERTHAME, *Numerical passage from kinetic to uid equations*, SIAM J. Numer. Anal., vol. 28 (1991), pp. 26–42.

[35] N. CROUSEILLES, P. DEGOND, M. LEMOU, *A hybrid kinetic-fluid model for solving the gas-dynamics Boltzmann BGK equation*, Journal of Computational Physics, vol. 199 (2004), pp. 776-808.

[36] N. CROUSEILLES, P. DEGOND, M. LEMOU, *A hybrid kinetic-fluid model for solving the Vlasov-BGK equation*, Journal of Computational Physics 203 (2005) 572-601.

[37] P. DEGOND, S. JIN, L. MIEUSSENS, *A Smooth Transition Between Kinetic and Hydrodynamic Equations* , Journal of Computational Physics, vol. 209 (2005), pp. 665-694.

[38] P. DEGOND, S. JIN, *A Smooth Transition Between Kinetic and Diffusion Equations*, SIAM Journal of Numerical Analysis, vol. 42 n° 6 (2004), pp. 2671–2687.

[39] P. DEGOND, J.G. LIU, L. MIEUSSENS, *Macroscopic Fluid Model with Localized Kinetic Upscaling Effects*, MMS 5(3), 940–979 (2006)

[40] P. DEGOND, G. DIMARCO, L. MIEUSSENS, *A moving interface method for dynamic kinetic-fluid coupling*, Journal of Computational Physics Vol. 227, pp. 1176-1208.

[41] S. DESHPANDE, *A second order accurate kinetic theory based method for inviscid compressible flow*. Journal of Computational Physics, (1979).

[42] L. DESVILLETTS, *On Asymptotics of the Boltzmann Equation when the Collisions Become Grazing*, Transp. Th. Stat. Phys., 21, 259–276 (2002).

[43] G. DIMARCO AND L. PARESCHI, *Hybrid multiscale methods I. Hyperbolic Relaxation Problems*, Comm. Math. Sci., 1, (2006), pp. 155-177.

[44] G. DIMARCO AND L. PARESCHI, *Hybrid multiscale methods II. Kinetic equations*, SIAM Multiscale Modeling and Simulation Vol 6., No 4,pp. 1169-1197.

[45] G. DIMARCO AND L. PARESCHI, *Domain decomposition techniques and hybrid multiscale methods for kinetic equations*, Proceedings of the 11th International Conference on Hyperbolic problems: Theory, Numerics, Applications, pp. 457-464.

[46] G. DIMARCO AND L. PARESCHI, *A Fluid Solver Indipendent Hybrid Method for Multiscale Kinetic equations*, Preprint 2008.

[47] G. DIMARCO, P. FOSCARI, L. PARESCHI, *A remark on the finite number of particles effect in Monte Carlo methods for kinetic equations*, Submitted to Proceedings in Applied Mathematics and Mechanics (2007). pp. 2.

[48] W. E AND B. ENGQUIST, *The heterogeneous multiscale methods*, Comm. Math. Sci., 1, (2003), pp. 87-133.

[49] W. E AND B. ENGQUIST, *The heterogeneous multiscale method for homogenization problems*, Lect. Notes Comput. Sci. Eng., 44 (2005), pp 89–110.

[50] W. E AND B. ENGQUIST, *Multiscale Modeling and Computation*, Notices of the AMS, 50(9), (2003), pp. 1062–1070.

[51] B. ENGQUIST, T. YEN-HSI, *Heterogeneous multiscale methods for stiff ordinary differential equations* Math. Comp. 74 (2005), no. 252, pp. 1707–1742.

[52] F. FILBET, E. SONNENDRÜCKER AND P. BERTRAND, *Conservative Numerical schemes for the Vlasov equation.* J. Comput. Phys. 172, (1989) pp. 177–186.

[53] G. GLIMM, *The continuous structure of discontinuities* Let. Notes in Phys. 344, (2001) pp. 166–187.

[54] J.A. FLECK JR., J.D. CUMMINGS, *An implicit Monte Carlo scheme for calculating time and frequency dependent nonlinear radiation transport*. Journal of Computational Physics, 8, (1971), pp. 313–342, .

[55] E. GABETTA, L. PARESCHI, AND G. TOSCANI, *Relaxation schemes for nonlinear kinetic equations*, SIAM J. Numer. Anal., 34 (1997), pp. 2168–2194.

[56] E. HAIRER AND G. WANNER, *Solving Ordinary Differential Equations* II: Stiff and Differential-Algebraic Problems, Springer-Verlag, New York, (1987).

[57] D.B. HASH AND H.A. HASSAN, *Assessment of schemes for coupling Monte Carlo and Navier-Stokes solution methods* J. Thermophys. Heat Transf., 10, (1996), pp. 242–249.

[58] R.W. HOCKNEY, J.W. EASTWOOD, *Computer simulation using particles*, Mc-Graw Hill International Book Co., (1981).

[59] T. M. M. HOMOLLE, N. G. HADJICONSTANTINOU, *Low-variance deviational simulation Monte Carlo*, Physics of Fluids, 19 (2007)

[60] A. B. HUANG AND P. F. HWANG, *Test of statistical models for gases with and without internal energy states*, Physics of Fluids, 16(4):466475, 1973.

[61] S. JIN, *Runge-Kutta methods for hyperbolic conservation laws with stiff relaxation terms*, J. Comput. Phys., 122 (1995), pp. 51–67.

[62] S. JIN, C. D. LEVERMORE, *Numerical Schemes for hyperbolic conservation laws with stiff relaxation terms*, J. Comp. Physics, 126 (1996), pp. 449–467.

[63] S. JIN, AND L. PARESCHI, *Discretization of the multiscale semiconductor Boltzmann equation by diffusive relaxation schemes*, J. Comp. Phys., 161, (2000), pp. 312–330.

[64] S. JIN, L. PARESCHI, AND G. TOSCANI, *Diffusive relaxation schemes for multiscale discrete-velocity kinetic equations*, SIAM J. Numer. Anal., 35 (1998), pp. 2405–2439.

[65] S. JIN, L. PARESCHI, AND G. TOSCANI, *Uniformly accurate diffusive relaxation schemes for multiscale transport equations*, SIAM J. Numer. Anal., 35 (1998), pp. 2405–2439.

[66] S. JIN AND Z. P. XIN, *Relaxation schemes for systems of conservation laws in arbitrary space dimensions*, Comm. Pure Appl. Math., 48 (1995), pp. 235–276.

[67] M. JANSEN, R. BARANIUK, AND S. LAVU, *Multiscale Approximation of Piecewise Smooth Two-Dimensional Functions using Normal Triangulated Meshes*, Appl. Comp. Harm. Anal., vol. 19(1) (2005), pp 92–130.

[68] M. Kac, *Probability and Related Topics in Physical Sciences*, Lectures in Appl. Math., Interscience Publishers, London, New York, 1959.

[69] M.H. KALOS, P.A. WHITLOCK, *Monte Carlo Methods, Volume I: Basics*, John Wiley & Sons, New York, (1986).

[70] A. KLAR AND R. WEGENER, *Enskog-like kinetic models for vehicular traffic*, J. Stat. Phys., 87 (1997), pp. 91114.

[71] M.A. KATSOULAKIS, A.J. MAJDA AND A. SOPASAKIS, *Multiscale Couplings In Prototype Hybrid Deterministic/Stochastic Systems: Part I, Deterministic Closures*, Comm. Math. Sci., Vol. 2, No. 2, (2004), pp. 255-294

[72] M.A. KATSOULAKIS, A.J. MAJDA AND A. SOPASAKIS, *Multiscale couplings in prototype hybrid deterministic/stochastic systems. II. Stochastic closures*, Commun. Math. Sci., vol. 3 (2005), pp. 453–478.

[73] V.I. KOLOBOV, R.R. ARSLANBEKOV,V.V. ARISTOV, A.A. FROLOVA, S.A. ZABELOK, *Unified Solver for Rarefied and Continuum Flows with Adaptive Mesh and Algorithm Refinement*, Journal of Computational Physics Vol. 223 No. 2, pp. 589–608 (2007).

[74] B. E. LAUNDER AND N. SHIMA, *Second moment closure for the near wall sublayer: Development and application* AIAA J., 27, (1989) pp. 1319–1325.

[75] P. LETALLEC AND F. MALLINGER, *Coupling Boltzmann and Navier-Stokes by half fluxes* Journal of Computational Physics, 136, (1997) pp. 51–67.

[76] R. J. LEVEQUE, *Numerical Methods for Conservation Laws*, Lectures in Mathematics, Birkhauser Verlag, Basel (1992).

[77] D. LEVERMORE, W.J. MOROKOFF, B.T. NADIGA, *Moment realizability and the validity of the NavierStokes equations for rarefied gas dynamics*, Physics of Fluids, Vol. 10, No. 12, (1998).

[78] C. D. LEVERMORE, *Moment Closure Hierarchies for Kinetic Theories*, J. Stat. Phys., 83, (1996) pp. 1021-1065.

[79] Z.-H. LI AND H.-X. ZHANG, Numerical investigation from rarefied flow to continuum by solving the Boltzmann model equation *International Journal for Numerical Methods in Fluids Volume*, 42, 4, (2003) pp. 361–382.

[80] S. LIU, *Monte Carlo strategies in scientific computing*, Springer, (2004).

[81] T.-P. LIU, *Hyperbolic conservation laws with relaxation*, Commun. Math. Phys., 108 (1987), pp. 153–175.

[82] T.-P. LIU AND S.-H. YU, *Boltzmann Equation: Micro-Macro Decompositions and Positivity of Shock Profiles*, Commun. Math. Phys. 246, (2004) pp. 133-179.

[83] P.A.MARKOWICH AND L.PARESCHI, *Fast conservative and entropic numerical methods for the boson Boltzmann equation*, Num. Math., 99, (2005), pp. 509-532.

[84] L. MIEUSSENS, *Discrete Velocity Model and Implicit Scheme for the BGK Equation of Rarefied Gas Dynamic* ,Mathematical Models and Methods in Applied Sciences, Vol 10 No. 8 (2000) 1121-1149.

[85] L. MIEUSSENS, *Discrete Velocity Model and numerical schemes for the Boltzmann-BGK equation in plane and axisymmetric geometries*, J. Comput. Phys., Vol. 162, 429-466, 2000.

[86] L. MIEUSSENS, *Convergence of a discrete-velocity model for the Boltzmann-BGK equation.* Comput. Math. Appl., 41(1-2):83–96, 2001.

[87] J.C. MANDAL, AND S.M. DESHPANDE, *Kinetic flux vector splitting for Euler equations*, Computers & Fluids, vol.23, (1994), pp. 447–78.

[88] K. NANBU *Theory of cumulative small-angle collision in plasmas*, Physical Review E, Vol. 55 $N°4$ (1997).

[89] K. NANBU, *Direct simulation scheme derived from the Boltzmann equation*, J. Phys. Soc. Japan, 49 (1980), pp. 2042–2049.

[90] G. NALDI AND L. PARESCHI, *Numerical schemes for hyperbolic systems of conservation laws with stiff diffusive relaxation*, SIAM J. Numer. Anal., 37 (2000), pp. 1246–1270.

[91] R. NATALINI, *Convergence to equilibrium for relaxation approximations of conservation laws*. Comm. Pure Appl. Math., vol. 49 (1996) pp. 795–823

[92] T. NISHIDA, *Fluid dynamical limit of the nonlinear Boltzmann equation at the level of the compressible Euler equations,* Commun. Math. Phys., 61, (1978) pp. 119148.

[93] L. PARESCHI, S. TRAZZI, *Numerical Solution of the Boltzmann equation by time relaxed Monte Carlo (TRMC) methods*, International Journal for Numerical Methods in Fluids, vol. 48 (2005), pp. 947-983.

[94] L. PARESCHI, AND G. RUSSO, *Time Relaxed Monte Carlo methods for the Boltzmann equation*, SIAM J. Sci. Comput. 23 (2001), pp. 1253–1273.

[95] L. PARESCHI, *Central differencing based numerical schemes for hyperbolic conservation laws with stiff relaxation terms*, SIAM J. Num. Anal., vol. 39 (2001), pp. 1395–1417.

[96] L. PARESCHI, AND G. RUSSO, *Asymptotic preserving Monte Carlo methods for the Boltzmann equation*, Transport Theory Statist. Phys., 29 (2000), pp. 415–430.

[97] L. PARESCHI, G. RUSSO AND G. TOSCANI, *Fast Spectral Methods for the Fokker-Planc-Landau Operator*, J. Comp. Phys. 165, pp. 216-236, (2000).

[98] L. PARESCHI, G. RUSSO, *An introduction to the numerical analysis of the Boltzmann equation*, Lecture Notes at M&KT 2004, Riv. Mat. Univ. Parma (7) 4 (2005), 145–250.

[99] L. PARESCHI, *Hybrid multiscale methods for hyperbolic and kinetic problems*, Esaim Proceedings Vol. 15, EDP Sciences, SMAI (2005) pp. 87–120.

[100] L. PARESCHI, AND M.SEAID, *A New Monte Carlo Approach for Conservation Laws and Relaxation Systems*, Lecture Notes in Computer Science, Vol. 3037, pp. 281–288, (2004).

[101] L. PARESCHI, AND B. WENNBERG, *A recursive Monte Carlo method for the Boltzmann equation in the Maxwellian case*, Monte Carlo Methods Appl., 7 (2001), pp. 349–358.

[102] L. Pareschi, G. Russo, S. Trazzi, A. Shevryn, Ye. Bondar, M. Ivanov, *Comparison betweenTime Relaxed Monte Carlo Method and Majorant Frequency Scheme methods for the space homogeneous Boltzmann equation,* RAREFIED GAS DYNAMICS: 24th International Symposium on Rarefied Gas Dynamics, AIP Conference Proceedings, 762, (2005), pp. 571–576.

[103] L. Pareschi, G. Toscani, *Self-similarity and power-like tails in nonconservative kinetic models*, J.Stat. Phys., 124, (2006), 747–779.

[104] L.Pareschi, G.Toscani, *Modelling and numerical methods for granular gases,* Chapter 9, Modeling and computational methods for kinetic equations, Series: Modeling and Simulation in Science, Engineering and Technology, Birkhauser (2004), pp.259-286.

[105] PEMBER, R.B., BELL, J.B., COLELLA, P., CRUTCHFIELD, W.Y., *An Adaptive Cartesian Grid Method for Unsteady Compressible Flow in Irregular Regions*, J. Comp. Phys., Vol.120, No.2 (1995), pp. 278-304.

[106] B. PERTHAME, *Boltzmann type schemes for gas dynamics and the entropy property*, SIAM J. Num. Anal., vol. 27, (1990), pp. 1405.

[107] S. PIERACCINI, G. PUPPO, *Implicit-explicit schemes for BGK kinetic equations*, J. Sci. Comput. 32 (2007), no. 1, 1–28.

[108] D. I. PULLIN, *Direct simulation methods for compressible inviscid ideal gas flow*, J. Comput. Phys., 34 (1980), pp. 231–244.

[109] D. I. PULLIN, *Generation of normal variates with given sample*, J. Statist. Comput. Simulation, 9 (1979), pp. 303–309.

[110] A. QUARTERONI, A. VENEZIANI. *Analysis of a geometrical multiscale model based on the coupling of PDE's and ODE's for Blood Flow Simulations*, SIAM J. on MMS, Vol.1, No. 2, (2003), pp. 173–195.

[111] M. Renardy, W. Hrusa, and J. Nehel, *Mathematical problems in viscoelasticity* Pitman Monographs and Surveys in Pure and App. Math. 35, Longman Sci. Tech., New York (1987).

[112] M. N. Rosenbluth, W. M. MacDonald, and D. L. Judd, *Relaxation of a System of Particles with Coulomb Interactions* Phys. Rev. 107, 1 (1957).

[113] R. ROVEDA, D.B. GOLDSTEIN, AND P.L. VARGHESE, *Hybrid Euler/Particle Approach for Continuum/ Rarefied Flows*, AIAA J. Spacecraft Rockets 35, (1998), pp. 258–265.

[114] R. ROVEDA, D.B. GOLDSTEIN, AND P.L. VARGHESE, *Hybrid Euler/Direct Simulation Monte Carlo Calculation of Unsteady Slit Flow*, AIAA J. Spacecraft Rockets 37, (2000), pp. 753-760.

[115] V. Ya. Rudyak, *Correlations in a finite number of particles system simulating a rarefied gas*, Fluid Dynamics, 26, (1991), pp. 909–914.

[116] G. RUSSO, AND R. E. CAFLISCH, *Implicit methods for kinetic equations*, in Rarefied Gas Dynamics: Theory and Simulations, Progress in Aeronautics and Astronautics 159, AIAA, New York, (1992), pp. 344–352.

[117] T. SCHULZE, P. SMEREKA AND W. E, *Coupling kinetic Monte-Carlo and continuum models with application to epitaxial growth*, J. Comput. Phys., 189, (2003), pp. 197–211.

[118] L. Spitzer, Jr., *Physics of Fully Ionized Gases,* 2nd ed. Interscience, New York, 1967.

[119] G. STRANG, *On the construction and the comparison of difference schemes*. SIAM J. Numer. Anal., 5 (1968), pp. 506–517.

[120] T. TAKIZUKA AND H. ABE , *A binary collision model for plasma simulation with a particle code*, Journal of Computational Physics, Vol. 25, pag. 205–219 (1977).

[121] S. TIWARI, AND A. KLAR, *An adaptive domain decomposition procedure for Boltzmann and Euler equations*. J. Comp. Appl. Math., vol.90, (1998) pp. 223–37.

[122] S. TIWARI, *Coupling of the Boltzmann and Euler equations with automatic domain decomposition*, J. Comput. Phys., vol. 144, 1998, 710–726.

[123] B. A. TRUBNIKOV *Review of Plasma Physics*, Consultant Bureau, New York, 1965, Vol.1.

[124] C. TRUESDELL, AND R. G. MUNCASTER, *Fundamentals of Maxwell Kinetic Theory of a Simple Monatomic Gas*, Academic Press, New York, (1980).

[125] W. VINCENTI AND C. KRUGER, *Introduction to physical gas dynamics*, Krieger Melbourne (1982).

[126] W. X. WANG, M. OKAMOTO, N. NAKAJIMA AND S. MURAKAMI, *Vector Implementation of Nonlinear Monte Carlo Coulomb Collisions*, Journal of Computational Physics, Vol. 128, 209–222 (1996).

[127] C. WANG, T. LIN, R. E. CAFLISCH, B. COHEN AND A. DIMITS, *Particle Simulation of Coulomb Collisions: Comparing the methods of Takizuka & Abe and Nanbu*, under review (2006).

[128] W.-L. WANG AND I. D. BOYD, *Predicting Continuum breakdown in Hypersonic Viscous Flows*, Physics of Fluids, Vol. 15, 2003, pp 91-100.

[129] W.L.WANG, Q. SUN, AND I.D. BOYD, *Towards development of a hybrid DSMC-CFD method for simulating hypersonic interacting flows*, AIAA 2002-3099.

[130] G. B. WHITHAM, Linear and Nonlinear Waves, Wiley-Interscience, New York, (1974).

[131] E. WILD, *On Boltzmann's equation in the kinetic theory of gases*, Proc. Cambridge Philos. Soc., 47 (1951), pp. 602–609.

[132] K. XU, L. MARTINELLI, AND A. JAMESON, *Gas-kinetic finite volume methods, flux-vector splitting, and artificial diffusion*. J. Comp. Phys., vol.120, (1995) pp. 48–65